

T 305

VEGETABLE OIL BASED HYPERBRANCHED POLY(ESTER AMIDE) NANOCOMPOSITES

**A thesis submitted in partial fulfillment of the requirements for
the award of the degree of
Doctor of Philosophy**

By

Sujata Pramanik

Registration Number TZ121483 of 2012



**School of Sciences
Department of Chemical Sciences
Tezpur University
Napaam, Tezpur- 784028
July 2014**

ABSTRACT

Hyperbranched poly(ester amide) (HBPEA) with the enchainment of ester and amide moieties in the polymeric backbone coalesces the properties of both polyesters and polyamides together with bringing revolutionary advances in the realm of multifaceted materials. The use of non-edible vegetable oils in the fabrication of HBPEA fits in the current quest for sustainable bioresource apart from meeting the 7th postulate of the twelve Green Chemistry principles. The performance of HBPEA remained a stumbling block owing to their poor performance and absence of special properties like electrical, antimicrobial and so on, until the breakthrough came about with the advent of nanotechnology in the domain of HBPEA. The unison of high aspect ratio and surface energy of the nanomaterials along with the unique architecture of HBPEA in the nanocomposites proved effective in circumvention of performance trade-offs of the pristine HBPEA.

Toward this vision, the thesis entitled “Vegetable oil based hyperbranched poly(ester amide) nanocomposites” is focused on fabrication of castor oil based HBPEA nanocomposites for multimodal applications across the domains. The thesis is compiled into seven chapters. Starting on with a comprehensive introduction on HBPEA and its nanocomposites in Chapter 1, the remaining scopes in this endeavor were analyzed and objectives set priori to implementation of the present work. Based on the technical plans, Chapter 2 described the synthesis of castor oil based HBPEA and justified in establishing its supremacy over its linear analog. Quantitative yield of diethanol fatty amide (DEFA) of the oil was obtained for the first time amongst all other literatures documented till date. The desirable performance of 10 wt% A'A₂ monomer (diethanol amine) containing HBPEA forwarded it as a biodegradable thin film material and confirmed its potentiality as the matrix for the preparation of different nanocomposites. The research on bio-based HBPEA nanocomposites has a strong background to look into, particularly in the quest for advanced engineering materials. In this perspective, the thesis deals with the preparation of HBPEA nanocomposites using different nanomaterials such as polyaniline (PAni) nanofiber, PAni nanofiber modified montmorillonite (MMT), functionalized multi-walled carbon nanotubes (MWCNT) and silver nanoparticles decorated MWCNT in Chapters 3, 4, 5 and 6 respectively. Chapter 3 highlighted the role of PAni nanofiber, complemented by the templating facet of the hyperbranched framework in imparting significant impact on the

mechanical, thermal and antistatic properties of HBPEA/PAni nanofiber nanocomposites. Chapter 4 dealt with the judicious modification of MMT using potent antimicrobial PAni nanofiber, and incorporation of the same into HBPEA to obtain an advanced antimicrobial coating material. These nanocomposites possessing potent efficacy against Gram positive bacteria, antifungal activity and antialgal activity against an algal consortium proved to be effective in addressing microbial infections using nano-biotechnology. Chapter 5 focused on exploiting green chemistry tools of microwave irradiation and ultrasonication for the functionalization of MWCNT. The covalent-noncovalently functionalized MWCNT/HBPEA nanocomposites described in subchapter 5A, were found to be biocompatible substrates for *in vitro* adhesion and proliferation of peripheral blood mononuclear cells possessing antibacterial efficacy against Gram positive and acid fast bacterial strains and, biodegradability in phosphate buffer saline. The above findings open up promising avenue of these multifunctional nanocomposites as antibacterial dressing materials for infected burn wounds. Although these HBPEA nanocomposites established their utility in biomedical domains, an important property of the nanotubes *viz.*, the electrical property could not be exploited in context to antistatic materials owing to the low content of the nanotubes in the nanocomposites. To this end, the subchapter 5B discussed the noncovalent functionalization of the nanotubes by concomitant use of DEFA and greener tool of ultrasonication. DEFA functionalized nanotubes were thereafter used as a reactive component for *in-situ* polycondensation reaction to form HBPEA nanocomposites. The noncovalently functionalized MWCNT/HBPEA nanocomposites exhibited pronounced thermostability, antistatic property and selective antibacterial efficacy against Gram positive bacterial strains. In the endeavor to widen the antibacterial spectrum and enhance the low tensile strength of the noncovalently functionalized MWCNT/HBPEA nanocomposites, the unique properties of MWCNT were coalesced with silver nanoparticles in Chapter 6. The templating attributes of DEFA was exploited for imparting 'green capping' to silver nanoparticles, apart from noncovalent functionalization of the nanotubes. The widened antibacterial activity against both Gram positive and Gram negative bacterial strains, pronounced sheet resistance, performance and thermal stability of these nanocomposites excels them as potent antibacterial, thermostable and antistatic sustainable materials for different advanced applications including coatings, textiles, biomedical electronics and so on. The thesis ends with the concluding remarks highlighting the major achievements and future perspectives of the reported works in Chapter 7.

DECLARATION

I do hereby declare that the thesis entitled “**Vegetable oil based hyperbranched poly(ester amide) nanocomposites**”, submitted to the Department of Chemical Sciences, Tezpur University under the School of Sciences, in partial fulfillment for the award of the **Degree of Doctor of Philosophy in Science**, is a record of the original research work carried out by me.

All sources of assistance have been assigned due acknowledgment.

I also declare that neither this work as a whole nor a part of it has been submitted to any other University or Institute for any other degree, diploma or award.

Place: Tezpur University

Sujata Pramanik
(Sujata Pramanik)

Date: 28-07-14



TEZPUR UNIVERSITY

(A Central University established by an Act of Parliament)

Napaam, Tezpur-784028

District: Sonitpur, Assam, India

Ph.: 03712-267009

Fax: 03712-267005, 03712-26706

E-mail: nkarak@tezu.ernet.in

CERTIFICATE

This is to certify that the thesis entitled “**Vegetable oil based hyperbranched poly(ester amide) nanocomposites**” submitted to the School of Sciences, Tezpur University in part fulfillment for the award of the degree of **Doctor of Philosophy in Science**, is a record of research work carried out by **Ms. Sujata Pramanik** under my supervision and guidance.

All helps received by her from various sources have been duly acknowledged.

No part of this thesis has been reproduced elsewhere for award of any other degree.

Place: Tezpur University

Date: 28/02/2014

(Prof. Niranjana Karak)

School of Sciences

Department of Chemical Sciences



TEZPUR UNIVERSITY

(A Central University established by an Act of Parliament)

Napaam, Tezpur-784028

District: Sonitpur, Assam, India

CERTIFICATE

This is to certify that the thesis entitled “**Vegetable oil based hyperbranched poly(ester amide) nanocomposites**” submitted to the School of Sciences, Tezpur University in part fulfillment for the award of the degree of **Doctor of Philosophy in Science**, has been examined by us on and found to be satisfactory.

The committee recommends for the award of the degree of **Doctor of Philosophy**.

Principal Supervisor

Date:

External Examiner

Date:

PREFACE

The biomimetic approach of unlocking the 'three-dimensional dendritic' pervasive topologies of nature in the fabrication of 'hyperbranched poly(ester amide)' (HBPEA), amalgamating the properties of both polyesters and polyamides, add a whole new perspective in the realm of multifunctional materials. The design of HBPEA using biorenewables, albeit logical detours, but guarantees to shift the society into a new paradigm to address a cocktail of problems ranging from sustainability to environmental footprints. The advent of nanotechnology in the arena of HBPEA improves their performance in addition to bringing in special properties in the same. The existence of HBPEA in polymer industry under the commercial trade name of Hybrane[®] is well proven. However the quest for bio-based HBPEA nanocomposites combining the afore-mentioned advantages is of prime concern in the current scenario of sustainability together with meeting the industrial requisites.

Thus the main objective of this thesis remained to fabricate bio-based HBPEA nanocomposites for advanced multimodal applications. In the light of above discussion, castor oil based HBPEA was synthesized using $A_2+B_2+A'A_2$ approach and its supremacy over the linear analog was established in terms of performance and rheological behavior. The impetus was laid on use of greener approaches including ultrasonication and microwave irradiation tools for both the functionalization of the nanomaterials and fabrication of HBPEA nanocomposites. The nanocomposites of HBPEA using polyaniline (PAni) nanofiber modified montmorillonite and covalent-noncovalent functionalized multi-walled carbon nanotubes (MWCNT) exhibited pronounced antimicrobial activity along with their desired performance. The interfacial interactions of benzenoid-quinoid moieties of PAni nanofiber, noncovalently functionalized MWCNT and silver nanoparticles decorated MWCNT with HBPEA resulted in improved mechanical property and thermostability together with the antistatic properties. Amongst these, the fabrication of multifaceted silver nanoparticles decorated MWCNT/HBPEA nanocomposites possessing antistatic, thermostable and wider antibacterial activity for different advanced applications in coatings, textiles, biomedical electronics and so on forms the major achievement of the present research work. Thus the prepared nanocomposites exhibited galore of applicability from biomedical to antistatic domains.

ACKNOWLEDGEMENT

The voyage from the state of innocence through dreams of youthful adventure to Ph.D. wouldn't have been complete without acknowledging all those people around who have tangibly contributed in realizing the same.

Above all my sincere thanks go to my Ph.D. supervisor, Prof. Niranjan Karak, Department of Chemical Sciences, Tezpur University, for investing his full effort in guiding me in achieve my goals. Starting on with experimental hands-on training to questioning thoughts and expressing ideas, his heuristic teaching would remain as mnemonic throughout my life. His words '*aachenar anando*' (meaning unknown happiness) echoed in my ears every other day and undoubtedly inspired me to move ahead and take up new challenges during my Ph.D. endeavor. A line dedicated to Sir, 'Arjun couldn't realize his potentials unless he had Krishna with him'. Although I may not turn out to be Arjun but yes you were always like Krishna to me. Hope I can keep these roots alive throughout my life. Thank you Sir!

I would like to extend my thanks to my doctoral committee members, Prof. R.C. Deka and Prof. T.K. Maji, Department of Chemical Sciences, Tezpur University for their advice and constant monitoring of my progress. I owe a great deal of gratitude to the Head of the Department (HoD) of Chemical Sciences for providing me the opportunity to carry out my research work. I would like to acknowledge with much appreciation the crucial role of the other faculty members and staff of Department of Chemical Sciences, Tezpur University for their kind helps during my Ph.D. tenure. The research scholars and student friends are also acknowledged for the in-built of sportive and competitive environment.

I am thankful to Prof. A. Kumar, Department of Physics and Prof. A.K. Buragohain, Vice Chancellor, Dibrugarh University for their critical advice in carrying out the multidisciplinary studies related to my objectives. I express my gratitude to the administrative of Tezpur University for helping me carry out my research work. I am grateful for the financial assistance given by Defense Research Laboratory (DRL), Tezpur and UGC.

I acknowledge Prof. M.K. Chaudhuri, Vice Chancellor, Tezpur University for his intellectual stimulation and inspiration to become a stalwart and earn one of the top global posts, taking Indra Nooyi as an example.

I would take the opportunity to sincerely acknowledge Industrial Green Chemistry World (IGCW) for selecting me for Green Chemistry Innovation Award in the student's category in the year 2013.

SAIF, NEHU, Shillong is acknowledged for their help in availing HRTEM facility.

Thanks to all my friends who willingly and selflessly helped me throughout my stay in the University. Special thanks goes to my APNL labmates for providing me as stimulating and fun-filled environment for carrying out my research works. I would also like to express my heartfelt gratitude to Pradeep dada, IIT Bombay for his constant effort in making me understand the hedonic adaptation of life and remain happy in whatever the situation is. He conceptualized the same as a 'threadmill' wherein people try in maintaining a baseline level of happiness despite of fluctuations in demographic circumstances.

Last but not the least, I place a deep sense of gratitude to my family members who have constantly been my role models, strength in the form of cheerleading squad and source of inspiration throughout my life. I owe everything to them for lifting me uphill to this phase of life. Thank you Ma, Baba and Bhai!!

Place: Tezpur University

Date: 28-07-14

Sujata Pramanik
(Sujata Pramanik)

CONTENT OF THE THESIS

Content	Page No.
Abstract	i
Declaration	iii
Certificate from Supervisor	iv
Certificate from Examiners	v
Preface	vi
Acknowledgement	vii
Contents	ix
List of Abbreviations and Symbols	xvi
List of Tables	xx
List of Figures	xxii
List of Schemes	xxvi

Chapter 1

General introduction

Highlights	1.1
1.1. Introduction	1.2
1.2 Historical background	1.5
1.3. Materials and methods	1.6
1.3.1. Raw materials	1.6
1.3.1.1. Hyperbranched poly(ester amide) (HBPEA)	1.7
1.3.1.2. Nanomaterials	1.10
1.3.2. Methods	1.17
1.3.2.1. Synthesis of HBPEA	1.17
1.3.2.2. Preparative methods of HBPEA nanocomposites	1.25
1.4. Characterization	1.27
1.4.1. Analytical techniques	1.27
1.4.2. Spectroscopic techniques	1.29
1.4.3. X-ray diffraction	1.30

1.4.4. Microscopic techniques	1.31
1.4.5. Testing and analysis	1.32
1.4.5.1. Mechanical and rheological	1.32
1.4.5.2. Thermal	1.32
1.4.5.3. Chemical resistance	1.32
1.4.5.4. Electrical	1.33
1.4.5.5. Biological	1.33
1.5. Properties	1.34
1.6. Applications	1.38
1.7. Scopes of investigation	1.42
1.8. Objectives of the present work	1.43
1.9. Plans of the present work	1.43
References	1.45

Chapter 2

Castor oil based hyperbranched poly(ester amide) resin

Highlights	2.1
2.1. Introduction	2.2
2.2. Experimental	2.3
2.2.1. Materials	2.3
2.2.1.1. Chemicals	2.3
2.2.1.2. Microbial strains and enzyme	2.5
2.2.2. Methods	2.6
2.2.2.1. Preparation of 'super dry' methanol and sodium methoxide	2.6
2.2.2.2. Preparation of methyl ester of castor oil	2.6
2.2.2.3. Preparation of diethanol fatty amide of castor oil	2.6
2.2.2.4. Synthesis of linear and hyperbranched resins	2.7
2.2.2.5. Curing of resins	2.7
2.2.3. Instrumentation	2.8
2.2.4. Biodegradation study	2.9
2.3. Results and discussion	2.10
2.3.1. Synthesis of resins	2.10
2.3.2. Physical properties of resins	2.11
2.3.3. FTIR study	2.12

2.3.4. NMR study	2.13
2.3.5. Rheological study	2.16
2.3.6. Curing study	2.18
2.3.7. Physico-mechanical performance study	2.21
2.3.8. Thermal study	2.23
2.3.9. Biodegradation study	2.23
2.4. Conclusion	2.26
References	2.27

Chapter 3

Hyperbranched poly(ester amide)/polyaniline nanofiber nanocomposites

Highlights	3.1
3.1. Introduction	3.2
3.2. Experimental	3.3
3.2.1. Materials	3.3
3.2.2. Methods	3.4
3.2.2.1. Preparation of PANi nanofiber	3.4
3.2.2.2. Preparation of nanocomposites	3.4
3.2.3. Instrumentation	3.4
3.3. Results and discussion	3.5
3.3.1. Preparation of PANi nanofiber	3.5
3.3.2. Preparation of nanocomposites	3.6
3.3.3. FTIR study	3.6
3.3.4. Rheological study	3.7
3.3.5. TEM study	3.9
3.3.6. XRD study	3.9
3.3.7. Physico-mechanical performance study	3.11
3.3.8. Thermal study	3.13
3.3.9. Antistatic property	3.13
3.4. Conclusion	3.16
References	3.17

Chapter 4

Hyperbranched poly(ester amide)/polyaniline nanofiber modified montmorillonite nanocomposites

Highlights	4.1
4.1. Introduction	4.2
4.2. Experimental	4.3
4.2.1. Materials	4.3
4.2.1.1. Chemicals	4.3
4.2.1.2. Microbial strains	4.4
4.2.2. Methods	4.4
4.2.2.1. Preparation of PANi nanofiber modified MMT	4.4
4.2.2.2. <i>Ex-situ</i> preparation of nanocomposites	4.4
4.2.3. Instrumentation	4.5
4.2.4. Antimicrobial activity	4.5
4.2.4.1. Antibacterial and antifungal activities	4.5
4.2.4.2. Antialgal activity	4.6
4.3. Results and discussion	4.6
4.3.1. Preparation of nanohybrid	4.6
4.3.2. Preparation of nanocomposites	4.7
4.3.3. FTIR study	4.8
4.3.4. Morphological study	4.10
4.3.5. XRD study	4.10
4.3.6. Physico-mechanical performance study	4.12
4.3.7. Thermal study	4.12
4.3.8. Antimicrobial activity	4.13
4.4. Conclusion	4.17
References	4.18

Chapter 5

Hyperbranched poly(ester amide)/functionalized multi-walled carbon nanotube nanocomposites

Highlights	5.1
------------	-----

5A. Covalent-noncovalent functionalized multi-walled carbon nanotube/hyperbranched poly(ester amide) nanocomposites

5A.1. Introduction	5.2
5A.2. Experimental	5.3
5A.2.1. Materials	5.3
5A.2.1.1. Chemicals	5.3
5A.2.1.2. Microbial strains and peripheral blood mononuclear cells	5.3
5A.2.2. Methods	5.4
5A.2.2.1. Functionalization of MWCNT	5.4
5A.2.2.2. <i>Ex-situ</i> preparation of nanocomposites	5.5
5A.2.3. Instrumentation	5.5
5A.2.4. Antibacterial activity	5.6
5A.2.5. <i>In vitro</i> biocompatibility assay	5.6
5A.2.5.1. Isolation and culturing of peripheral blood mononuclear cells	5.6
5A.2.5.2. MTT assay	5.7
5A.2.5.3. <i>In-vitro</i> cell response	5.7
5A.2.6. Reactive oxygen species study	5.7
5A.2.7. Biodegradation study	5.7
5A.3. Results and discussion	5.8
5A.3.1. Functionalization of MWCNT	5.8
5A.3.1.1. FTIR study	5.9
5A.3.1.2. XRD study	5.10
5A.3.1.3. Raman study	5.10
5A.3.1.4. HRTEM study	5.11
5A.3.2. Preparation of nanocomposites	5.12
5A.3.2.1. FTIR study	5.12
5A.3.2.2. HRTEM study	5.12
5A.3.2.3. XRD study	5.14
5A.3.2.4. Physico-mechanical performance study	5.14
5A.3.2.5. Thermal study	5.15
5A.3.2.6. Antibacterial activity	5.17
5A.3.2.7. <i>In vitro</i> biocompatibility study	5.18
5A.3.2.8. ROS study	5.20
5A.3.2.9. Biodegradation study	5.20
5A.4. Conclusion	5.22

5B. Noncovalent functionalized multi-walled carbon nanotube / hyperbranched poly(ester amide) nanocomposites

5B.1. Introduction	5.23
5B.2. Experimental	5.24
5B.2.1. Materials	5.24
5B.2.1.1. Chemicals	5.24
5B.2.1.2. Microbial strains	5.24
5B.2.2. Methods	5.24
5B.2.2.1. Noncovalent functionalization of MWCNT	5.24
5B.2.2.2. <i>In-situ</i> preparation of nanocomposites	5.24
5B.2.3. Instrumentation	5.25
5B.2.4. Thermal degradation kinetics study	5.25
5B.2.5. Antibacterial activity	5.26
5B.3. Results and discussion	5.26
5B.3.1. Preparation of nanoconjugate	5.26
5B.3.2. Preparation of nanocomposites	5.27
5B.3.3. FTIR study	5.28
5B.3.4. XRD study	5.29
5B.3.5. HRTEM study	5.29
5B.3.6. Physico-mechanical performance study	5.30
5B.3.7. Antibacterial activity	5.32
5B3.8: Thermal degradation kinetic study	5.34
5B.3.9. Antistatic property	5.35
5B.4. Conclusion	5.38
References	5.39

Chapter 6

Hyperbranched poly(ester amide)/silver nanoparticles decorated multi-walled carbon nanotube nanocomposites

Highlights	6.1
6.1. Introduction	6.2
6.2. Experimental	6.2
6.2.1. Materials	6.3
6.2.1.1. Chemicals	6.3

6.2.1.2. Microbial strains	6.3
6.2.2. Methods	6.3
6.2.2.1. Preparation of silver nanoparticles decorated MWCNT	6.3
6.2.2.3. <i>In-situ</i> preparation of nanocomposites	6.3
6.2.3. Instrumentation	6.3
6.2.4. Antibacterial activity	6.4
6.3. Results and discussion	6.4
6.3.1. Preparation of silver nanoparticles decorated MWCNT	6.4
6.3.2. Preparation of nanocomposites	6.5
6.3.3. FTIR study	6.5
6.3.4. HRTEM study	6.6
6.3.5. UV-visible study	6.6
6.3.6. XRD study	6.8
6.3.7. EDX study	6.9
6.3.8. Physico-mechanical performance study	6.9
6.3.9. Thermal study	6.9
6.3.10. Antistatic property	6.10
6.3.11. Antibacterial activity	6.10
6.4. Conclusion	6.12
References	6.13

Chapter 7

Conclusions and future scopes

Highlights	7.1
7.1. Concluding remarks and outlook	7.2
7.2. Future scopes	7.6

List of Publications

In Journals	P1
From thesis	P1
Other related publications	P2
In conference/seminar/workshop proceedings	P2

LIST OF ABBREVIATIONS AND SYMBOLS

AA	adipic acid
AEPO	2-amino-2-ethyl-1,3-propanediol
AgNP	silver nanoparticle(s)
AIBN	2,2'-azobis(2-methylpropionitrile)
APS	ammonium peroxydisulphate
BA	benzoic acid
BSA	bovine serum albumin
CEC	cation exchange capacity
CFU	colony forming unit
cm	centimetre
CMM	couple monomer methodology
CNT	carbon nanotube(s)
cPs	centipoise
DB	degree of branching(s)
DEFA	N,N-bis(2-hydroxyethyl)fatty amides/diethanol fatty amides of castor oil
DiEA	diethanol amine
DiPA	diisopropanol amine
dL/g	decilitre per gram
DMAc	N,N-dimethylacetamide
DMEM	dulbecco's modified eagle medium
DMF	dimethylformamide
DMM	double monomer methodology
DMSO	dimethyl sulphoxide
DNA	deoxyribonucleic acid
dPAn	2,2'-diphenic anhydride
DSC	differential scanning calorimetry
E _a	activation energy
EB	elongation at break
EDX	electron dispersive X-ray

FESEM	field emission scanning electron microscopy/microscope
FTIR	Fourier transform infrared spectroscopy
FWHM	full width at half maximum
g/cm ³	gram per cubic centimeter
g/mL	gram per milliliter
g/mol	gram per mole
G'	storage modulus
G''	loss modulus
GAn	glutaric anhydride
GMA	glycidyl methacrylate
GPC	gel permeation chromatography
H-bonding	hydrogen bonding
HBPEA	hyperbranched poly(ester amide)(s)
HPhAn	cis-hexahydrophthalic anhydride
HRTEM	high resolution transmission electron microscopy/microscope
HSAB	hard-soft acid base
Hz	hertz
IA	itaconic acid
I _B /I _Q	intensity ratio of benzenoid is to quinoid
I _D /I _G	intensity ratio of D-band is to G-band
I _{ester} /I _{amide}	intensity ratio of ester is to amide band
IMPA	3,3'-iminobis(N,N-dimethylpropyl amine)
IPhA	isophthalic acid
kg	kilogram
kN	kilo Newton
MAAn	maleic anhydride
MECO	methyl ester of castor oil
mequiv/100g	milliequivalent per 100 gram
mgKOH/g	milligram of KOH per gram
MIC	minimum inhibitory concentration
mm/min	millimeter per min
mmol	millimole
MMT	montmorillonite

MPa	megapascal
mPa·s	millipascal second
MTT	3-(4,5-dimethylthiazol-2-yl)-2,5-diphenyltetrazolium bromide
M_w	weight average molecular weight
MWCNT	multi-walled carbon nanotube(s)
nm	nanometre
NMR	nuclear magnetic resonance spectroscopy
PAni	polyaniline
pBdA	<i>p</i> -benzene dicarboxylic acid
PBMC	peripheral blood mononuclear cells
PBS	phosphate buffer saline
PDI	polydispersity index
PEA	poly(ester amide)(s)
PET	polyethylene terephthalate
PETL	pentaerythritol
PGMA	poly(glycidyl methacrylate)
PhAn	phthalic anhydride
PLA	poly(L-lactide)
PP	polypropylene
R	gas constant
SAED	selected area electron diffraction
SbA	sebacic acid
ScA	succinic acid
ScAn	succinic anhydride
SEM	scanning electron microscopy/microscope
SMM	single monomer methodology
SPR	surface plasmon resonance
SWCNT	single-walled carbon nanotube(s)
t	time
T	absolute temperature
TEM	transmission electron microscopy/microscope
T_g	glass transition temperature
TGA	thermogravimetric analyzer/analysis

THF	tetrahydrofuran
TOC	total organic carbon content
TPa	terapascal
TPTZ	2,4,6-tris(2-pyridyl)-s-triazine
TS	tensile strength
UTM	universal testing machine
UV	ultraviolet
v/v	volume by volume
W	watt
W/mK	watts per metre Kelvin
wt%	weight percent
XRD	X-ray diffraction
α	degree of conversion
β	heating rate
η_{inh}	inherent viscosity
θ	scattering angle
μL	microlitre
Ω/sq	ohm(s) per square
$^{\circ}\text{C}$	degree centigrade

LIST OF TABLES

Table No.	Table Legend
Table 1.1	Dihydroxyalkyl amines and secondary amines used in synthesis and tuning of end functional groups of HBPEA
Table 1.2	Different vegetable oils and their major fatty acid profiles used in synthesis of HBPEA
Table 1.3	Dibasic acids/anhydrides used in synthesis of HBPEA
Table 1.4	Typical functionalization methodologies of CNT and their salient features
Table 1.5	Key milestones in the development of HBPEA chemistry
Table 1.6	List of patents retrieved from SciFinder® for the search queries 'hyperbranched poly(ester amide)' and 'hyperbranched polyesteramide' in the period 2001-2013
Table 2.1	Physical characterization of castor oil, MECO, DEFA and resins
Table 2.2	Physico-mechanical performance of thermosets
Table 2.3	Weight changes of thermosets in different chemical media
Table 2.4	Degradation temperatures of thermosets
Table 3.1	Physical properties of organic solvents and induction time for the formation of PANi nanofiber
Table 3.2	Domain length, <i>d</i> -spacing and strain of PANi nanofiber
Table 3.3	Physico-mechanical performance of thermosetting HBPEA/PAni nanofiber nanocomposites
Table 3.4	Weight changes of thermosetting HBPEA/PAni nanofiber nanocomposites in different chemical media
Table 4.1	Physico-mechanical performance of thermosetting nanocomposites of HBPEA/nanohybrid
Table 4.2	Antimicrobial activity of HBPEA and nanocomposites of HBPEA/nanohybrid
Table 5A.1	Benzenoid and quinoid bands and their intensity ratios for P4 and M3
Table 5A.2	Position, FWHM and intensity ratios of D- and G- bands for M1 and M2
Table 5A.3	Performance and domain length of thermosetting covalent-noncovalent

functionalized MWCNT/HBPEA nanocomposites

Table 5A.4 Ratio of intensity of ester and amide bands of HBPEA and HPMWNT5

Table 5B.1 Physico-mechanical performance of thermosetting noncovalent functionalized MWCNT/HBPEA nanocomposites

Table 6.1 Physico-mechanical performance of thermosetting AgCNT/HBPEA nanocomposites

LIST OF FIGURES

Figure no.	Figure legend
Fig. 1.1	Histogram showing the number of publications in the period 1994-2013 retrieved from SciFinder®
Fig. 1.2	Different strategies for functionalization of CNT
Fig. 1.3	Mechanism of MMT modification (a), trans (b) and gauche (c) conformations of modifier chains intercalated in MMT
Fig. 1.4	Schematic representation of HBPEA (at the centre) and its diverse spectrum of applications (peripheral images)
Fig. 2.1	FTIR spectra of (A): castor oil (a), MECO (b), DEFA (c), PEA resin (d), PEA1 (before curing) (e) and PEA2 (before curing) (f); and (B): HBPEA5 (a), HBPEA (b) and HBPEA15 (c) resins
Fig. 2.2	¹ H NMR spectra of MECO (a), DEFA (b) and PEA resin (c)
Fig. 2.3	¹ H NMR spectra of HBPEA5 (a), HBPEA10 (b) and HBPEA15 (c) resins
Fig. 2.4	¹³ C NMR spectra of MECO (a), DEFA (b) and PEA resin (c)
Fig. 2.5	¹³ C NMR spectra of HBPEA5 (a), HBPEA10 (b) and HBPEA15 (c) resins
Fig. 2.6	Variation of viscosity as a function of time
Fig. 2.7	Variation of viscosity with (A) shear rate; and (B) temperature
Fig. 2.8	TG thermograms of (A): PEA1 (a), and PEA2 (b); and (B) HBPEA5, HBPEA10 and HBPEA15 thermosets
Fig. 2.9	Weight loss profile of PEA (a) and hyperbranched (b) thermosets, SEM micrographs of: HBPEA5(c), <i>P. aeruginosa</i> degraded HBPEA5 (d), HBPEA10 (e) and HBPEA15 (f) thermosets
Fig. 2.10	Weight loss profile (a) and TOC measurements (b) of thermosets post enzyme inoculation, SEM micrographs of enzymatically degraded thermosets (with surface plots as the inserts) of HBPEA5 (c), HBPEA10 (d) and HBPEA15 (e)
Fig. 3.1	FTIR spectra of (A): PAni nanofiber; and (B): HBPEA (a), HBPEAP5

- (b), HBPEAP7.5 (c), HBPEAP10 (d) and HBPEAP12.5 (e)
- Fig. 3.2 Variations of (A) G' ; and (B) G'' with time
- Fig. 3.3 Variations of (A) G' ; and (B) G'' with frequency
- Fig. 3.4 Variations of (A) G' ; and (B) G'' with temperature
- Fig. 3.5 TEM micrographs of HBPEA (a), PAni nanofiber (b), HBPEAP5 (c), HBPEAP7.5 (d), HBPEAP10 (e) and HBPEAP12.5 (f)
- Fig. 3.6 (A) XRD patterns; and (B) deconvolution of (110) diffraction peak of PAni nanofiber
- Fig. 3.7 XRD patterns of HBPEA (a), HBPEAP5 (b), HBPEAP7.5 (c), HBPEAP10 (d) and HBPEAP12.5 (e)
- Fig. 3.8 (A) TG thermograms; and (B) sheet of HBPEA and HBPEA/PAni nanofiber nanocomposites
- Fig. 4.1 Dispersion stability of nanohybrid in different organic solvents
- Fig. 4.2 FTIR spectra of (A): nanohybrid (a) and MMT (b); and (B): HBPEA (a), HBPEAC1 (b), HBPEAC2.5 (c) and HBPEAC5 (d)
- Fig. 4.3 FESEM micrographs of MMT with inset of EDX (a) and nanohybrid at time: 10 min (b), 2 h (c) and 5 h with inset of EDX (d)
- Fig. 4.4 HRTEM micrographs of HBPEAC1 (a) and (b), HBPEAC2.5 (c) and (d), and HBPEAC5 (e) and (f), at magnification scale bar of 200 nm and 50 nm respectively
- Fig. 4.5 XRD patterns of (A): nanohybrid (a) and MMT (b); and (B): HBPEA (a), HBPEAC1 (b), HBPEAC2.5 (c) and HBPEAC5 (d)
- Fig. 4.6 Possible interactions during curing of nanocomposite
- Fig. 4.7 TG thermograms of MMT, nanohybrid and thermosetting nanocomposites of HBPEA/nanohybrid
- Fig. 4.8 Representative culture plates showing antibacterial activity of (A) HBPEA; (B) HBPEAC1; (C) HBPEAC2.5; and (D) HBPEAC5 against *P. aeruginosa* (a), *E. coli* (b), *B. subtilis* (c) and *S. aureus* (d)
- Fig. 4.9 Representative culture plates showing antifungal activity of HBPEA and nanocomposites of HBPEA/nanohybrid against *A. niger* (a), *F. oxysporium* (b) and *C. capcii* (c)
- Fig. 5A.1 (A) Dispersion stability of M2 and M3; (B) FTIR spectra with the inset of deconvoluted peaks for benzenoid and quinoid rings; (C) XRD

- patterns; and (D) Raman spectra with the inset of deconvoluted peaks for D- and G- bands of M1 and M2
- Fig. 5A.2 HRTEM micrographs of: M1(a), P4 (b), M2 (c), and M3 with the inset of tendrillar morphology (d)
- Fig. 5A.3 (A) FTIR spectra; (B) HRTEM micrograph of HPMWNT1; (C) XRD diffractograms; and (D) TG thermograms of HBPEA and covalent-noncovalent functionalized MWCNT/HBPEA nanocomposites
- Fig. 5A.4 (A) CFU count; and (B) protein content
- Fig. 5A.5 (A) MTT assay; (B) SEM micrograph of porous film; SEM micrographs of PBMC adhesion and proliferation upon seeding onto: (C) HBPEA; (D) HPMWNT1; (E) HPMWNT2.5; and (F) HPMWNT5
- Fig. 5A.6 (A) ROS kinetics; (B) weight loss profile; (C) and (D) deconvoluted $I_{\text{ester}}/I_{\text{amide}}$ of HBPEA and HPMWNT5
- Fig. 5B.1 (A) FTIR spectra; (B) deconvoluted FTIR peak of CH_b of nanoconjugate; (C) deconvoluted FTIR peak of CH_b of HPFCNT1; and (D) FTIR spectra of polymer showing the formation of ester linkage
- Fig. 5B.2 XRD patterns of HBPEA and noncovalent functionalized MWCNT/HBPEA nanocomposites
- Fig. 5B.3 HRTEM micrographs of: (A) M1; (B) nanoconjugate; (C) coiled geometry of the nanoconjugate; and (D) surface roughness of nanoconjugate; (E) HPFCNT0.25; and (F) HPFCNT0.5
- Fig. 5B.4 HRTEM micrographs of HPFCNT1; (B) coherency map; (C) HRTEM micrograph (for calculation of coherency coefficient); (D) HSB-color coded map; and SAED pattern of: (E) M1; and (F) HPFCNT1
- Fig. 5B.5 Antibacterial activity in terms of (A) CFU count; and (B) protein content
- Fig. 5B.6 TG thermograms of HBPEA and noncovalent functionalized MWCNT/HBPEA nanocomposites
- Fig. 5B.7 Plots of $\ln \beta$ versus $1000/T$ for first step of degradation at different ' α ' of: (A) HBPEA; (B) HPFCNT0.25; (C) HPFCNT0.5; and (D) HPFCNT1
- Fig. 5B.8 Plots of $\ln \beta$ versus $1000/T$ for second step of degradation at different ' α ' of: (A) HBPEA; (B) HPFCNT0.25; (C) HPFCNT0.5; and (D)

HPFCNT1

- Fig. 5B.9 (A) Plots of E_a versus ' α ' for first and second decomposition steps; and (B) sheet resistance of HBPEA and noncovalent functionalized MWCNT/HBPEA nanocomposites
- Fig. 6.1 FTIR spectra of DEFA functionalized AgCNT: immediately after mixing (a), and after sonication (b), HPAgCNT0.25 (c), HPAgCNT0.5 (d) and HPAgCNT1 (e)
- Fig. 6.2 HRTEM micrographs of HPAgCNT1 at magnification scale of (A) 100 nm and (B) 50 nm; (C) SAED pattern; and (D) silver nanoparticles size distribution histogram
- Fig. 6.3 (A) UV-visible spectra; (B) XRD patterns; (C) EDX of HPAgCNT0.25; and (D) TG thermograms of thermosetting HBPEA and AgCNT/HBPEA nanocomposites
- Fig. 6.4 (A) Sheet resistance; and (B) antibacterial activity of HBPEA and AgCNT/HBPEA nanocomposites
-

LIST OF SCHEMES

Scheme No.	Scheme legend
Scheme 1.1	Reaction mechanism of (a) cyclic anhydride with dihydroxy amine, (b) esterification of N,N-bis(2-hydroxyalkyl) amide and, (c) internal acyl shift rearrangement
Scheme 2.1	Synthesis of resins
Scheme 2.2	Possible crosslinking mechanism for formation of PEA1 and PEA2
Scheme 3.1	Preparative protocol for HBPEA/PAni nanofiber nanocomposite
Scheme 4.1	Preparative protocol for nanohybrid
Scheme 4.2	Preparative protocol for nanocomposite of HBPEA/nanohybrid
Scheme 5A.1	Schematic representation for functionalization of MWCNT
Scheme 5A.2	Preparative protocol for covalent-noncovalent functionalized MWCNT/HBPEA nanocomposite
Scheme 5B.1	(A) Schematic representation for coupled action of sonication and DEFA in noncovalent functionalization of MWCNT; and (B) proposed mechanism for formation of noncovalently functionalized MWCNT/HBPEA nanocomposite
Scheme 6.1	Plausible mechanism of the formation of DEFA functionalized AgCNT and its polymerization to yield nanocomposite

Chapter 1

General introduction

Highlights

This chapter presents a comprehensive overview on hyperbranched poly(ester amide) (HBPEA) and their nanocomposites. The technological progress in the synthesis of HBPEA is surveyed over the past few decades with emphasis on the hunt of appropriate raw materials. HBPEA nanocomposites are highlighted in context of achieving material's property for advanced engineering applications. Starting off with the study of different nanomaterials, the chapter explores the suitable preparative protocols for the fabrication of HBPEA nanocomposites. The chapter moves ahead with the characterization tools and testing methods to comprehend the bio-physico-chemical attributes of HBPEA and its nanocomposites. The properties of the same are critically discussed for leveraging their ample potential in diversified domains of material and biomedical sciences. An archive of the multihued diorama of these advanced materials is presented together with pointing out the scopes, which forms the basis of the objectives for the present research work.

1.1. Introduction

'Three dimensional dendritic' architecture is the most ubiquitous topology amidst all others encountered in the nature. This biomimetic interest, exemplified splendidly in enzymatic systems, elicits significant innovations in the arena of three-dimensional architectural macromolecules. The multifaceted materials possessing ample potential are in great demand in various spheres of scientific community. In this context, the focus on the hyperbranched polymers- one of the frontier macromolecules, evolved since the latter part of 20th century.^{1,2} The close scaling of such pervasive morphologies present in a repertoire of biomolecules, testified by amylopectin, glycogen, proteoglycans, and vascular and respiratory vessels in mammals with various hyperbranched polymers is inspiring. Hyperbranched polymers are novel and versatile because of their unique three-dimensional tendrillar structure emanating from a focal point and ending with multitude of end group functionalities with a gamut of properties like high reactivity, compatibilizing ability, nanoscale templating, scaffolding and so on.³ The hallmark features like low melt and solution viscosity as well as variation of packing density from focal point to the surface generated from the unique architectural geometry of hyperbranched polymers add a whole new perspective in the realm of multifunctional materials.⁴ They are regarded as economically feasible counterparts of dendrimers in the novel class of dendritic polymers because of the one-pot synthesis, control over the molar mass and branching density of the former, without much compromising in the properties of the latter.¹ The competitive reaction in the one-pot synthesis of hyperbranched polymers leads to the formation of both linear and branching chain segments and consequently results in imperfect structure as compared to dendrimers.¹ They, however, outshine their linear analogs of the equivalent molar mass in terms of high solubility, low viscosity and presence of multitude of active functionalities.¹ The paramountcy of hyperbranched polymers in the perspective of commercial and technological applications is exemplified by their utility in colossal domains ranging from reactive component in the coating formulations to drug-delivery systems.⁵⁻⁷

Following Berzelius prophesy of the formation of a highly branched polyester resin using tartaric acid (a tetrafunctional monomer of A₂B₂ type) and glycerol (a trifunctional monomer of B₃ type), Kim and Webster reported the synthesis of hyperbranched polyphenylene in 1988.⁸ Since then, there has been an ongoing effort to synthesize a number of hyperbranched polymers including hyperbranched polyamides, hyperbranched

polycarbonates and so on.⁹⁻¹⁵ Amongst all others, hyperbranched polyesters have galore of utilities as commodity materials including coating formulations.¹⁶ The poor alkali resistance, long curing time (in case of thermosets) and relatively low strength of the same restrict their practical applications, which in turn instigates the inclusion of other functional groups to conquer this limitation.¹⁷⁻²⁰ Hyperbranched polyamides, on the other hand possesses good mechanical properties but low flexibility.²⁰ Further the design of degradable hyperbranched polymers with tailored properties to meet demands in the emerging technologies including biomedical, packaging and so forth is an ongoing challenge for the researchers across the globe.¹⁸ In this vein, the unison of ester with amide as the repeating linkage in the main chain together with the added facet of hyperbranched architectural attributes seemed promising. The strong alkali resistance, adequate flexibility, toughness, dimensional stability and degradability merit special mention in hyperbranched poly(ester amide) (HBPEA).²⁰ In addition to the above, the transformation of these HBPEA to thermosetting one is envisaged to impart improvement of the desired properties along with better curing characteristics over hyperbranched polyesters and flexibility over the brittle hyperbranched polyamides. HBPEA, thus, carves a unique niche of its own owing to the modulations of ester and amide functionalities to achieve the combination of favourable properties (including degradability and mechanical properties) for applications in the domain of material and biomedical sciences.²¹

Hitherto, the use of petroleum-based resources has pre-dominated the synthesis of HBPEA. In view of the foreseen catastrophe of these major conventional resources tramping towards the verge of extinction, the renewable bio-based resources proved to be one of the promising materials of choice of 20th century.²² In accord with the green synthetic pathways, focus remained on the use of greener feedstocks for the synthesis of HBPEA. The hunt for the use of vegetable oils as starting materials for the same is based on numerous advantages including low toxicity, biodegradability, versatility in the structure and properties, aptitude to facile modification, ready availability and environmentally benign.²³ To this end, a drive to switch over from edible to non-edible vegetable oils based HBPEA has a great potential in the arena of industrial uses of such novel polymers. However a number of bio-based poly(ester amide) (PEA) are documented in literature, but there are no reports on the use of same for the synthesis of HBPEA, though they hold many advantages over the former.

However, the highly branched and non-entangled architecture of HBPEA results in

poor mechanical properties (low moduli and strength) for their uses in advanced engineering applications.²⁴ The poor thermal, barrier and electrical properties, chemical resistance, flame-retardancy, antimicrobial activity and so on also add to drawbacks of the pristine HBPEA. In this milieu, developments are striving for materials with multifaceted properties, and compounding seems to be a promising technique to ameliorate the drawbacks of pristine polymers.²⁵ Traditionally, the use of HBPEA filled or composite systems requires compromise between the performance and processibility as high amount of reinforcing agents are incorporated for attaining the desired properties.⁴ In addition such systems also suffer from maintaining the light weight characteristic and retaining of transparency (in case of transparent polymers) of the parent polymer. The trend of the new era of continuous miniaturization using nanotechnology has forced to address the aforementioned problems.²⁶ In the lines with the international effort to design high performance materials, today focus remains on the ‘emerging nanotechnology’ for plethora of applications, which paves way to the subsequent industrial revolution.²⁷ The nanomaterials possess remarkable properties intrinsically associated with high aspect-ratio (surface/volume), surface energy and reduced lattice constants compared to their macro-scaled counterparts.²⁸ The unique synergies of ‘nano-effect’ (nanoscale dimensions) and hyperbranched architecture of PEA proved effective in circumvention of performance trade-offs of the conventionally filled and composite systems, and achieving enhanced properties at low loading of the nanomaterials.²⁶ The multifunctional features of HBPEA nanocomposites involve improved mechanical, thermal and barrier properties, chemical resistance and biodegradability in comparison to that of pristine HBPEA. Thus the importance of HBPEA nanocomposites lies in imparting value-added properties which are absent in pristine HBPEA, without comprising the processability and other properties including low density. The HBPEA nanocomposites are the ‘radical alternatives’ to these traditional HBPEA systems having reinforcement is in the nanoscale regime. In essence, these multifunctional materials can thus be associated epithet of so-called “ultimate scientific frontiers” due to their intriguing physico-chemical properties and their potential applications in spectrum of domains.

The various publications and patents in this regard over the two decades usher the diverse spectrum of HBPEA and its nanocomposites, which are discussed in the subsequent sections. A web search using scientific database, SciFinder[®] returned 135 references for the search query consisting of two keywords ‘hyperbranched poly(ester amide)’ and

'hyperbranched polyesteramide' on 21th September, 2013. The year-wise publications over the last two decades are shown in Fig. 1.1. However a set of only 3 references could be traced by the search engine for the search query 'hyperbranched polyesteramide nanocomposites'. Thus this may form the basis as one of the promising areas of research.

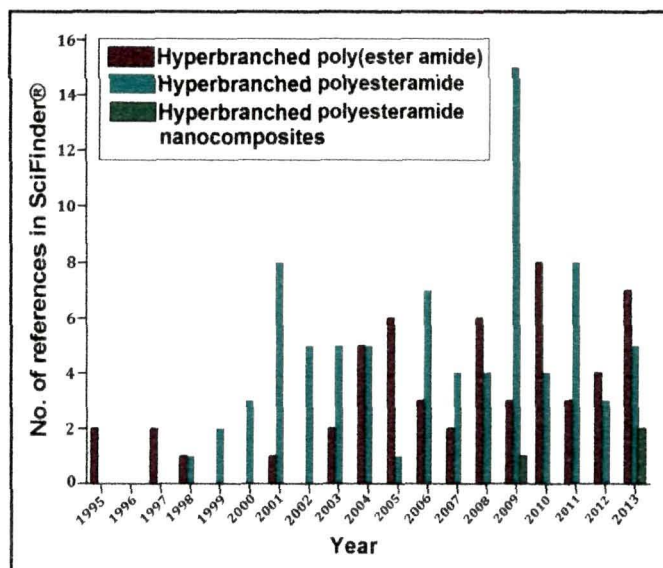


Fig. 1.1 Histogram showing the number of publications in the period 1994-2013 retrieved from SciFinder®

1.2. Historical background

The genesis of PEA dates back to the report of Du Pont researcher, R.E. Christ in early 1944 using a amino alcohol, dibasic carboxylic acid and dihydric alcohol.¹⁹ The first report on the synthesis of HBPEA documented by Krischeldorf et al. in 1995 was based on the bulk silyl-activated polycondensation of 3,5-bis(3-acetoxybenzamido)benzoic acid.²⁹ However the industrial application of the prepared HBPEA was not possible due to the iterative protocol involving a number of acylation and silylation reactions and use of hazardous chemicals like pyridine.^{29,30} However HBPEA like any other hyperbranched polymers can be synthesized by single-monomer methodology (SMM) and double-monomer methodology (DMM), being divided into two subclasses namely A_x+B_y (where A, B are different functional groups and $x,y \geq 2$) approach and couple-monomer methodology (CMM).⁴ The non-availability of suitable AB_x monomer ($x \geq 2$) as well as the occurrence of crosslinking reactions encountered in bulk polymerization both in SMM and A_x+B_y approach forwards CMM to be a potent technique in addressing the aforementioned challenges. In the

endeavor to scrutinize an alternative cost-effective and industrially convenient strategy, Stanssens and his group reported the preparation of β -dihydroxyalkyl amides using diethanol amine (DiEA) and dicarboxylic acids/anhydrides.³¹ The polycondensation reaction of this AB₂ type monomer, however, resulted in a partially crosslinked gel product.³² In this regard, the DSM's coatings research team led by van Benthem at Geleen in 1996 heralded a breakthrough in the field of HBPEA and replaced DiEA with diisopropanol amine (DiPA).³²⁻³⁴ This helped avert the above problem of gelation because of the diminished reactivity of the secondary -OH group of DiPA as compared to the primary one of DiEA.³² Since then a number of attempts have been made by different researchers in context of preparing industrially viable HBPEA without gelation.³⁵⁻⁴³

The first report on HBPEA nanocomposites comprising of poly(L-lactide) (PLA) with silica using HBPEA as a compatibilizer was documented by Wen et al. wherein HBPEA improved the miscibility and interfacial interaction between inorganic silica and PLA matrix in the ternary nanocomposites.⁴⁴ However the first intercalated binary nanocomposite of HBPEA and montmorillonite (MMT) nanocomposite was reported by Amin et al in 2013 only.⁴⁵ The researchers reported a handful of pioneering works^{46,47} thereafter using MMT and gold nanoparticles, but the domicile of HBPEA nanocomposites is yet to expand. The literature too remains silent in context of bio-based HBPEA nanocomposites.

1.3. Materials and methods

The fabrication of multifunctional macroscopic engineered materials by selection of appropriate nanomaterials remains the focal point of research.⁴⁸ HBPEA nanocomposites are prepared using nanomaterials like silica, MMT and gold nanoparticles with HBPEA as the matrix by employing different techniques.⁴⁵⁻⁴⁷ Thus in this section brief descriptions on various important nanomaterials and different HBPEA are presented. As the study of diverse nanomaterials becomes a mammoth task, so the subsequent section is streamlined according to a few representative nanomaterials of the three distinct classes of nanomaterials.

1.3.1. Raw materials

The choice of suitable monomers or monomer pair is the utmost crucial factor governing the molecular design of a hyperbranched polymer. A range of raw materials are used in the synthesis of HBPEA for obtaining optimal versatility in structure and concomitant properties. The β -dihydroxyalkyl groups containing secondary amine and dicarboxylic acids

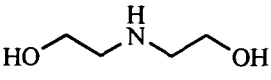
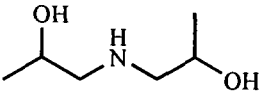
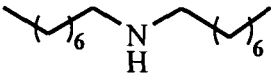
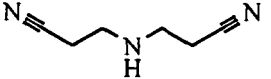
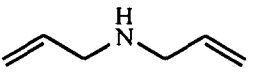
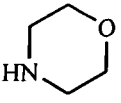
/anhydrides are used as the building blocks for the synthesis of HBPEA.³²

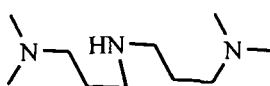
1.3.1.1. Hyperbranched poly(ester amide)

Dihydroxyalkyl amine

Aliphatic dihydroxy amines, both symmetric and asymmetric β -dihydroxyalkyl amines are used as the trifunctional monomer in the synthesis of HBPEA (Table 1.1).^{31-40,49} The use of secondary mono β -hydroxyalkyl amines results in the formation of linear PEA, in contrast to dihydroxyalkyl amines (DiEA and DiPA) which are used for synthesis of hyperbranched architecture.⁴⁹ The end groups of HBPEA are tuned by using amines like dioctyl amine, 3,3'-iminodipropionitrile, diallyl amine, morpholine, 3,3'-iminobis(N,N-dimethylpropyl amine) (IMPA). They can also act as chain stoppers in the propagation of HBPEA chains.⁴⁹ This is because the esterification of N,N-bis(2-hydroxyethyl)fatty amides with dicarboxylic acid derivative *via* oxazolinium-carboxylic acid ion pair is pH dependent and the secondary amines affect the pH and ultimately lead to incomplete conversion of the amides to the ester-amides.⁴⁹ The combination of DiEA and DiPA are thus used for tailoring of the molecular weight and peripheral end group functionalities in HBPEA framework.³⁶⁻³⁸

Table 1.1 *Dihydroxyalkyl amines and secondary amines used in synthesis and tuning of end functional groups of HBPEA*^{31-40,49}

Name	Structure	Melting point (°C)	Boiling point (°C)
Diethanol amine		28	271
Diisopropanol amine		44.5	249
Dioctyl amine		13-16	297
3,3'-Iminodipropionitrile		-6	205
Diallyl amine		-88	111
Morpholine		-5	129







Vegetable oil

The vegetable oils including drying, nondrying and semidrying oils are used in the synthesis of bio-based PEA. The vegetable oil, a triglyceride generally comprises of 94-96% of fatty acids of its total weight. The different vegetable oils⁵⁰⁻⁵⁷ with their physical properties and major fatty acid(s) content including structure are enlisted in Table 1.2. Among all other non-edible vegetable oils, castor oil is one of the promising feedstocks with desired properties including good shelf life relative to other vegetable oils and its exceptionally high content of ricinoleic acid.⁵⁸ The presence of more than 90-95% of one fatty acid resembles this oil as good as a pure chemical.⁵⁸ The fact that India is the leading producer of castor seed/oil counts in the exploration of appropriate bioresource for the synthesis of PEA.⁵⁹ The vegetable oil derivatives like N,N-bis(2-hydroxyethyl)fatty amides have gained interest as economically attractive starting materials owing to their good functional reactivity and diluents property.⁵⁰⁻⁵⁷ However the use of such fatty amides in the synthesis of HBPEA have not yet been strived for.

Table 1.2 Different vegetable oils and their major fatty acid profiles used in synthesis of HBPEA⁵⁰⁻⁵⁷

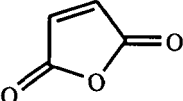
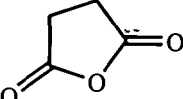
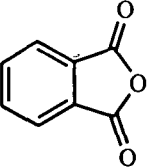
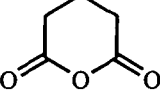
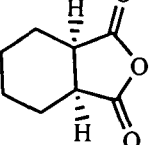
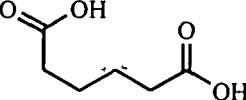
Vegetable oil	Major fatty acids/ structure	Fatty acid content (% of total)	Iodine value
Soyabean	Linoleic	55	125-140
	Oleic	28	
Linseed	Linolenic	40	175-204
	Linoleic	35	
Castor	Ricinoleic	90-92	80-88
Cottonseed	Linoleic	42-52	103-116
	Oleic	18-24	
<i>Mesua</i>	Oleic	55	89-93
<i>ferrea L.</i>	Stearic	14	

<i>Annona squamosa</i>	Oleic		37	83
	Palmitic		25	
<i>Pongamia glabra</i>	Oleic		44-71	86.5
	Linoleic		10-18	

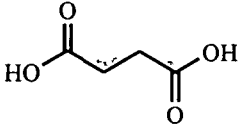
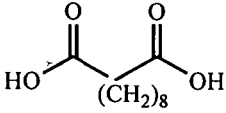
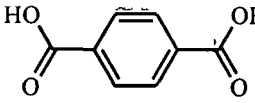
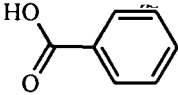
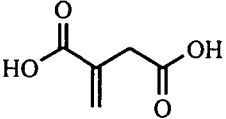
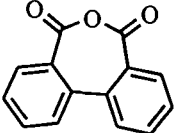
Dibasic acid/anhydride

A number of dibasic acids and anhydrides used as difunctional monomers for the synthesis of HBPEA are listed in Table 1.3.^{32,34-40,49,60-62} The aliphatic diacids are less reactive towards N,N-bis(2-hydroxylalkyl) amides as compared to the aromatic ones.⁴⁹ A combination of the anhydrides can be used to tune the desired properties in the resultant HBPEA.⁴⁹

Table 1.3 *Dibasic acids/anhydrides used in synthesis of HBPEA*^{32,34-40,49,60-62}

Name	Structure	Melting point (°C)	Boiling point (°C)
Maleic anhydride		52.8	202
Succinic anhydride		119–120	261
Phthalic anhydride		131	295
Glutaric anhydride		50-55	150
Cis-hexahydrophthalic anhydride		29-32	296
Adipic acid		152	338

Continued

Succinic acid		184	235
Sebacic acid		131–135	294
<i>p</i> -Benzene dicarboxylic acid		300	402 (sublimes)
Benzoic acid		122	249
Itaconic acid		162-164	381
2,2'-Diphenic anhydride		225-227	424

Catalyst

Basic catalysts such as the metal oxides and alkoxides like PbO, ZnO, CaO, NaOMe and NaOEt, and hydroxides like LiOH, Ca(OH)₂, and KOH aid in the synthesis of HBPEA.⁶² A number of reports exist on the use of NaOMe⁶² and biocatalyst such as immobilized lipases in the transesterification reaction of vegetable oil to alkyl esters,⁶³ which is then subsequently converted to PEA. Bao et al. reported Ti(OBu)₄ as an efficient catalyst among all others like Sn(OBu)₄, Sb₂O₃ and Zn(OBu)₄ for transesterification polymerization by 'thiol-ene' click chemistry approach.⁴²

1.3.1.2. Nanomaterials

The preceding sections were implicative of the fact that nanomaterials are the cornerstones of the emerging nanotechnology that exhibit remarkable physical, chemical and biological properties that are distinctively different than that of the bulk materials. In this vein, three definite classes of the nanomaterials are briefly discussed, underneath.

Zero-dimensional nanomaterials

The zero-dimensional structures are the elementary building blocks in the design of nanomaterials exemplified by nanoparticles including quantum dots. Amongst other noble metal nanoparticles, silver nanoparticles (AgNP) have captivated ample interest in recent years with multitudinous utilities reported across the domains.⁶⁴ They possess distinctive physico-bio-chemical properties *viz.*, optical, catalytic, bactericidal and fungicidal activities which confer them potential in a range of products with high market value.⁶⁵

AgNP are reported to be prepared by both physical and chemical methods. In the top-down physical process, the evaporation/condensation and laser ablation techniques are frequently utilized to prepare the same.⁶⁵ A number of wet chemical bottom-up methods have also been documented for the preparation of these nanoparticles, which includes the use of reductants such as hydrazine, sodium borohydride, N,N-dimethylformamide, citric and ascorbic acid, ammonium formate and elemental hydrogen.⁶⁶ However the surmounting pressure of streamlining research in accordance with the dictates of green technology has instigated the researchers to opt for greener preparative protocols. In this pursuit, Sharma et al.⁶⁵ have coalesced green chemistry approaches in designing five preparative protocols *viz.*, mixed-valence polyoxometallates, polysaccharides, irradiation, Tollens and biological methods. The two prime concerns in the preparation of AgNP were evaluated from the greener perspective namely the choice of environmentally benign reducing and stabilizing agents. The multifunctional roles of polyoxometallates, saccharides and biomolecules including phytochemicals were exploited as reducing agents and nanoscale templates/capping agents for stabilization, consequently imparting surface passivation against agglomeration of the nanoparticles.⁶⁷ The irradiation method aids in fabrication of well-defined AgNP using metal salt solution and surfactant in the absence of any reducing agent. The formation of AgNP proceeds *via* the photolysis of water and radical formation, where the hydrated electrons and H-radicals functions as effective reductants⁶⁷ in the transformation of Ag^+ to Ag^0 .

The differential surface energy of AgNP (of different surface curvatures) and increasing van der Waals forces at microscopic domain forms the stimulus for the thermodynamically-driven process of forming nanoparticle agglomerates (Ostwald ripening).⁶⁸ At this juncture, electrostatic and steric stabilizations are the two pre-requisite stabilization mechanisms.⁶⁸ The surface charges on the nanoparticles in the electrostatic

stabilization emerge due to a number of factors including isomorphic substitution and physical adsorption of ions, dissociation of surface charged species and build-up or depletion of electrons on the surface of AgNP.⁶⁸ The distribution of these co-ions are controlled by electrostatic (or coulombic) force, entropy and Brownian motion. The interaction between two AgNP is the combination of van der Waals attractive and electrostatic repulsive potentials (Derjaguin-Landau-Verwey-Overbeek theory).⁴⁸ This is a kinetic stabilization method apt for dilute systems and for the electrolyte-sensitive or multi-phase systems. Steric exclusion (polymeric stabilization) on the other hand is widely used and enjoys the advantages over the electrostatic repulsion. It is a thermodynamically-driven process wherein the polymeric encapsulation creates a diffusion barrier to the growing nuclei and stabilizes the nanoparticles.⁴⁸ The decrease in the entropy or possible orientations of the polymer chains adsorbed onto AgNP resulting in the volume restriction, and the osmotic effect due to the high concentration of the polymeric chains in between the two nanoparticles forms the basis of the steric stabilization.⁴⁸ The adsorption of polymeric chains would adsorb onto the growth sites and thereby lessen the rate of growth of the nanoparticles. Consequently a complete coverage of polymeric chains would obstruct the diffusion of growing nuclei from the surrounding medium to agglomerate onto the surface of AgNP.^{48,68}

AgNP are endowed with remarkable specific properties including surface plasmon resonance (SPR), catalytic, antimicrobial and so on.^{48,65} The bactericidal effect of AgNP is attributed to change in the cell membrane structure and consequent loss of deoxyribonucleic acid (DNA) replication ability upon interaction with the bacteria.⁶⁴ This is attributed to the strong affinity of AgNP towards sulphur-containing proteins and phosphorus-containing DNA of the bacterial cells or electrostatic attraction of the same with the bacterial cells.⁶⁴ The unique catalytic activity of AgNP is attributed to their morphologies with highly active facets.

One-dimensional nanomaterials

One-dimensional nanostructures form the second class of nanoscale building blocks and possess novel properties owing to their nanoscale size confinement in two dimensions, though the remaining dimension is in microscale. Carbon nanotubes (CNT) and polyaniline (PANI) nanofibers remain, among all others, the focal point of the discussion owing to their myriad utilities across different branches of material and biomedical sciences.

CNT: The outstanding mechanical and unique electrical properties of CNT have spurred up extensive research across the multitudinous domains since the discovery of this novel carbon

allotrope by S. Iijima early 1990s.⁶⁹ CNT are formed by rolling of graphite sheet into a tubular structure having diameters in nanoscale regime, which mainly exist as two types depending on their fabrications. These include CNT of single-walled (SWCNT comprising of hollow cylinder of single graphitic sheet) and multi-walled (MWCNT comprising of concentric SWCNT) architectures.^{69,70} However the ease of mass production, low cost to mass and preserval of intrinsic properties (as only the outer layers are exposed to the modifiers) upon functionalization render the preferential use of MWCNT over SWCNT, although the latter has its own advantages.⁷¹ The breadth of CNT applications is indeed wide ranging from flat panel displays to composites including chemical sensors, conducting and structural materials and so on.^{70,71}

The bonding in CNT comprises of sp^2 hybrid orbital of C-atoms forming hexagons (and occasionally pentagons and heptagons incorporated into the hexagonal framework to form bent and helical defective nanotubes) of honey-comb structure.⁷² CNT are mainly prepared by three techniques namely arc-discharge, laser ablation and chemical vapor deposition.⁷² The arc-grown CNT are produced by evaporation of graphitic electrodes in electric arcs at high temperatures but are highly impure.⁷² The laser ablation technique operates by evaporation of graphite using a high-power laser at high temperature to prepare CNT of high purity but of low yield.⁷² The chemical vapor deposition is a cost-effective and scalable technique for large scale production of CNT employing catalyst-driven thermal decomposition of the hydrocarbons.⁷²

CNT exhibit exceptional material properties including mechanical (high elastic modulus >1 TPa), superior thermal (stable up to 2800 °C under vacuum) and so on.⁷² These outstanding properties of CNT together with their low density make them suitable as reinforcing agents in composites.⁷³ However the realization of the full potential of the outstanding properties of CNT is severely limited owing to chemical inertness of the graphitic network, poor dispersion and lack of interfacial bonding of CNT with the polymer matrix.⁷⁴ To this end, functionalization of CNT is an apt technique to establish a strong chemical affinity of the nanotubes with the surrounding matrix (imparting stability in different solvents) together with the added facet of providing an additional impetus towards widening the horizon of their applications.⁷⁴ Two main approaches are employed for the functionalization of CNT namely covalent (defect and sidewall functionalization) and noncovalent (π -stacking), although reports exist on endohedral functionalization too.⁷⁵ An

overview of the different functionalization methods is summarized in Fig. 1.2.

The nanotube ends are composed of curved fullerene-like hemispheres which are unstable and highly reactive relative to the sidewalls.⁷⁶ The nanotube lattice also contains pentagon-heptagon pairs (known as Stones-Wales defects), sp^3 defects sites and vacancies.⁷⁶ The covalent functionalization may occur on all the above mentioned sites, leading to the disruption of the sp^2 carbon framework and resulting in undesirable alterations of the physical and chemical properties of the nanotubes.⁷⁶⁻⁸² In contrast to the preceding, the noncovalent functionalization is a non-destructive technique targeting modulation of the surface interfacial properties of the nanotubes without disruption of their π -conjugated structural integrity. It exploits supramolecular approach for adsorption of discrete inorganic/organic molecules onto the sidewalls of CNT *via* non-covalent interactions including van der Waals force, charge transfer, π - π stacking and cation- π interactions.⁸³⁻⁸⁶ However, endohedral functionalization strategy involves filling up of the inner empty cavities of CNT to accommodate guest molecules like C_{60} and other small molecules (inorganic species and small proteins) and result in the formation of nanopeapods (host-guest inclusion chemistry).⁸⁶ The encapsulation of the molecules inside the nanotubes is explained by capillary effect wherein van der Waals and hydrophobic forces count for the dynamic interaction between CNT and the engulfed components.⁸⁶ Table 1.4 summarizes the different covalent, noncovalent and endohedral functionalization methodologies of CNT.

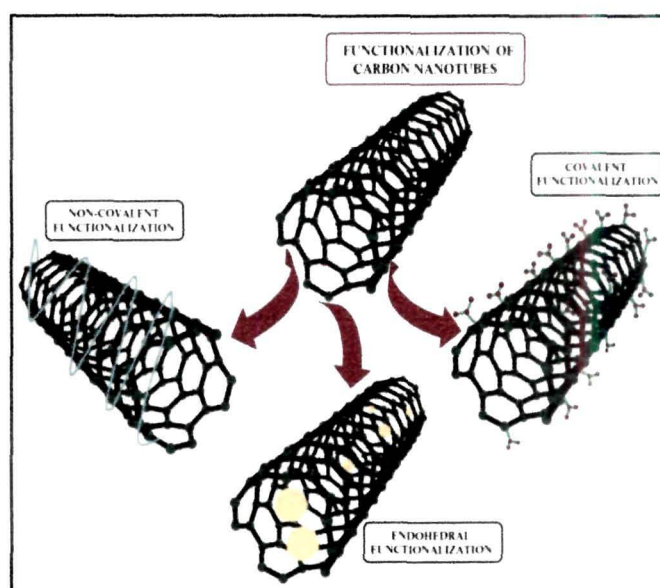


Fig. 1.2 Different strategies for functionalization of CNT

Table 1.4 Typical functionalization methodologies of CNT and their salient features

Type (functionalization)	Methodology
<i>Covalent</i>	
1. Acid functionalization (-COOH)	❖ improves solubility (in polar solvents) precursors for esterification, thiolation creates in defect sites (loss of π -conjugation) ⁷²
2. Diazotization (Aryl)	❖ introduces high degree of functionalization ⁷³
3. Fluorination (-F)	❖ requires high temperature conducive for other reactions ⁷⁴
4. Radical addition (Alkyl)	❖ large scale, reliable and easy strategy ⁷⁵
5. Dissolving metal reduction ($-(CH_2)_5CH_3$, $-(CH_2)_5COOH$ and $-H$)	❖ produces corrugation of both outer and inner surfaces ⁷⁶
6. Azomethine ylides (Prato reaction) nitrene (pyrrolidine)	❖ requires strong thermal activation for generation of ylides ⁷⁷
7. Nitrene (aziridene)	❖ requires excess of nitrene precursor ⁷⁸
8. Bingel reaction/ Dichlorocarbene (Carbene cycloaddition)	❖ insertion of three-membered cyclopropane rings ^{79,80}
<i>Noncovalent</i>	
1. Supramolecular chemistry (Adsorption)	❖ disaggregation of nanotube bundles ⁸³
2. Synthetic and natural polymers (helical wrapping)	❖ a reversible functionalization process ⁸⁴
3. Polynuclear aromatic compounds (π - π stacking)	❖ imparts absorption and emission ⁸⁵
<i>Endohedral</i>	❖ encapsulation of C_{60} , inorganic salts, biomolecules, metal oxides, carborane ⁸⁶

PAni nanofiber: Intrinsically conducting polymers commonly known as ‘synthetic metals’ (possessing highly π -conjugated polymeric backbone) have gained impetus owing to their intriguing redox and electronic properties to find potential applications in diverse domains.⁸⁷⁻

⁹⁰ The one-dimensional PAni nanostructures (nanofiber, nanotube, and nanorod) are

increasingly gaining importance in the polymer nanocomposites because of their notably enhanced dispersibility, processability and significantly improved performance in the material revolution as compared to their bulk analogs (granular and colloidal PANi).⁹⁰ The doping in PANi involves the formation of a stable nitrogen base salt (proceeding *via* chain protonation mechanism), unlike other conducting polymers wherein oxidative *p*-doping occurs at carbonium ion.⁹⁰ PANi exhibits three idealized oxidation states at molecular level: leucoemeraldine (fully reduced), emeraldine (half oxidized) and pernigraniline (fully oxidized).⁹⁰ The electrical conductivity of PANi primarily depends on the degree of oxidation and protonation.⁹⁰

One-dimensional . PANi nanostructures are prepared both chemically and electrochemically by polymerizing aniline with the aid of either 'hard' (zeolite channels and alumina) or 'soft' (surfactants, micelles, oligomer, polymer-assisted and liquid crystals) templates.⁹⁰ A number of other physical methods like electrospinning, sonication, mechanical stretching and microwave irradiation are also employed for the fabrication of PANi nanofiber.⁹⁰ To this end, aqueous/organic interfacial polymerization technique demands a special merit amidst all others because of the advantages *viz.*, template-free preparative route, high-quality nanofiber (with uniform fiber diameter in nanometer regime), scalability, high reproducibility and ease of purification.⁹⁰

Two-dimensional nanomaterials

Layered materials form an integral part of the diverse two-dimensional nanostructures having exotic properties with only one-dimension in the nanoscale regime.⁹¹ Amidst various layered materials, MMT (layered silicates) is the most commonly reported reinforcing material in the polymer matrix because of their ease of availability and intercalation chemistry.⁹¹ The remarkable physico-chemical attributes of MMT including high strength, modulus, thermostability, flame-retardancy and barrier properties forward them as apt reinforcing nanomaterials in the realm of material science.^{92,93}

MMT are the naturally nanosilicates belonging to the 2:1 phyllosilicates family which is commonly used in the preparation of nanocomposites. They are also prepared in laboratory using hydrothermal technology.⁹⁴ They are comprise of units made up of two tetrahedral silica sheets sandwiching an octahedral alumina sheet at the centre (forming a T-O-T structural framework) with approximately 10 Å layer thickness and the lateral dimensions of 300 Å to some microns.⁹⁴ It would be relevant to mention that MMT are nanoclays

possessing substantial isomorphous substitution (Al^{3+} replaced with $\text{Mg}^{2+}/\text{Fe}^{2+}$, Mg^{2+} with Na^+) attribute.⁹⁵ The negative charges generated upon the isomorphous substitution are compensated by alkali/alkaline earth cations.^{93,94} Consequently, MMT are characterized by a surface charge (cation exchange capacity; CEC) which differs from one nanosilicate layer to another and is expressed as mequiv/100 g.⁹¹ It is pertinent to mention that the hydration of the exchangeable cations imparts hydrophilicity to the inorganic MMT, which in turn makes them ineffective for interaction with the organophilic polymer matrices. This intrinsic incompatibility of both can be addressed by modification of MMT by ion-exchange process (pictorially represented in Fig. 1.3a). The intercalation of the alkylammonium or alkylphosphonium cations lowers the surface energy, imparts hydrophobicity and increases the interlayer spacing of MMT, and thereby improving their wettability with the host polymer matrix.⁹⁵ The long chain alkyl amines ($\text{C}_n\text{H}_{2n+1}\text{NH}_2$) intercalated into MMT assumes trans- (Fig. 1.3b) or gauche-conformation (Fig. 1.3c).⁹⁵ The presence of physical impenetrable interface like the nanoplatelets of nanoclay induces both normal and in-plane ordering of the chains.⁹⁵ The interlayer packing density parallels the exchange capacity of the host matrix. The increased trans-conformation (chain ordering) raise the cohesive van der Waals interactions between the chains and lead to an efficient packing, subsequently exhibiting a solid-like character.⁹⁵ On the contrary, the decrease in chain length of the modifier ($n < 12$) and the increase of the active surface area per molecule constrain the modifier chains to progressively adopt a disordered structure and eventually exhibit a liquid-like state.⁹⁵ In this regard, Southern Clay Products (SCP) company commercialized MMT organoclay (modified with specific quaternary ammonium salt) under the trade names of Cloisite 10A, 15A, 20A, 25A 30A, and 93A. These organophilic MMT are imperative for interfacial bonding, efficient load delocalization and strength enhancement of the pristine polymeric matrices.⁹⁵

1.3.2. Methods

The various methods for the synthesis of HBPEA and their nanocomposites are presented underneath.

1.3.2.1. Synthesis of HBPEA

Voluminous synthetic strategies have been documented for the synthesis of HBPEA possessing repertoire of unique structure and properties. The first synthetic approach for HBPEA reported by Kricheldorf and his co-workers in 1995 was based on the bulk polycondensation of 3,5-bis(3-acetoxybenzamido)benzoic acid prepared from acylation

reaction of 3-acetoxybenzoyl chloride and N,N',O-tris (trimethylsilyl)-3,5-diaminobenzoic acid.²⁹ The co-polymerization reaction of same with acetylated tetraphenol 'star centres' (tetrafunctional comonomer) produced star-shaped HBPEA.²⁹ In another report, HBPEA were synthesized from polycondensation of pentafunctional monomer prepared by acylation reaction between silylated 3,5-diaminobenzoic acid with 3,5-bisacetoxybenzoyl chloride.³⁰ These silyl-activated amidation reactions are fast reactions and give quantitative yield.^{29,30} However the repetitive acylation and silylation reactions forms the stumbling block in use of the above synthetic protocols for commercial applications.^{29,30} Thus focus thereafter remained on scrutinizing some cost-effective and industrially convenient strategies.

Following Kricheldorf report,^{29,30} numerous synthetic protocols for HBPEA have been documented till date using the concept of CMM.³² The first attempt in this regard was made by Stanssens and his coworkers to design an appropriate AB₂ type monomer (β -dihydroxyalkyl amides) to yield HBPEA.³¹ These β -dihydroxyalkyl amides possessing high esterification rate with the dibasic acids/anhydrides served as the building blocks in the synthesis of HBPEA.³¹ However the polycondensation reaction between phthalic anhydride (PhAn) and DiEA resulted in partially crosslinked gel product.³² Froehling documented that the pioneering work in the field of industrially viable HBPEA was made by van Benthem of DSM's coatings in 1996.^{32,34} van Benthem found out the root cause of gelation was the

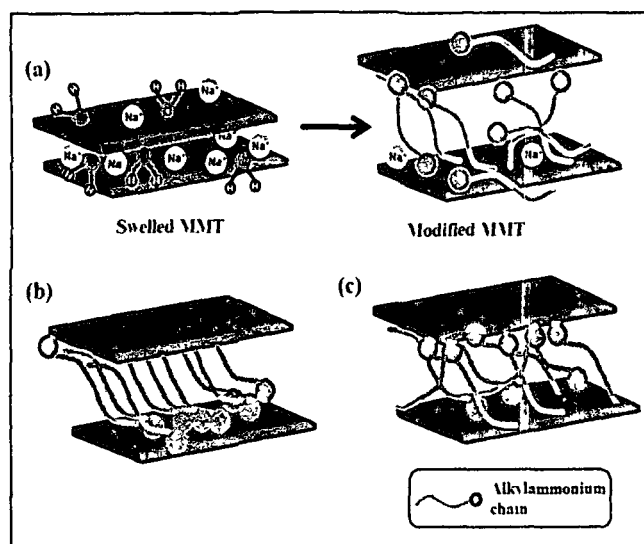


Fig. 1.3 Mechanism of MMT modification (a), *trans* (b) and *gauche* (c) conformations of modifier chains intercalated in MMT

the amine group) of DiEA with the cyclic anhydrides.³² The replacement of DiEA by DiPA helped to avert the above problem owing to the diminished reactivity of its secondary -OH group as compared to the primary one of DiEA.³² The suppression of the side reactions favored the reactivity of the -NH group of the dihydroxy amines with the dibasic acids/anhydrides. The amine reacts preferentially with the cyclic anhydride to form an AB₂ type intermediate (building block), followed by polycondensation.³² The polycondensation reaction involves the formation of an oxazolinium intermediate- the key player in the synthesis of HBPEA.³¹⁻³⁴ Initially the reaction between cyclic anhydride and dihydroxyalkyl amines leads to the formation of N,N-bis(2-hydroxyalkyl) amide (ternary amide containing two hydroxyl and one carboxyl functionalities).³² The -NH group reacts faster than the -OH group, ensuring chemoselectivity of the dihydroxyalkyl amines.^{96,97} The enhanced nucleophilicity of the -OH group due to the formation of intramolecular hydrogen bonding and a partial negative charge on the carbonyl oxygen resulting from the resonance of the amide group of N,N-bis(2-hydroxyalkyl) amide, explains the formation of the oxazolinium ion intermediate.³²⁻³⁴ The carboxylate in the oxazolinium-carboxylate ion pair acts as a nucleophile and aid in the ring opening of the oxazolinium ion and subsequent esterification of the alkyl amides.³²⁻³⁴ However the hydroxyl-amide (N,N-bis(2-hydroxyalkyl) amide) exists in dynamic equilibrium with isomeric ester-amine (2-aminoalkyl ester).³² This internal acyl shift in N,N-bis(2-hydroxyalkyl) amide is slow at room temperature and the population of 2-aminoalkyl ester becomes pronounced at elevated temperatures.³² van Benthem et al. reported that the unwanted reaction of 2-aminoalkyl ester with the oxazolines resulted in uncontrolled molecular weight and finally led to gelation.^{33,34} Authors further reported that the use of DiPA instead of DiEA resulted in steric screening of 2-aminoalkyl ester from attacking the methyl substituted oxazolinium intermediate.³²⁻³⁴ This circumvented the problem of gelation by shifting hydroxyl-amide and ester-amine equilibrium in favor of the former. The detailed reaction mechanism of the formation of HBPEA is shown in Scheme 1.1.

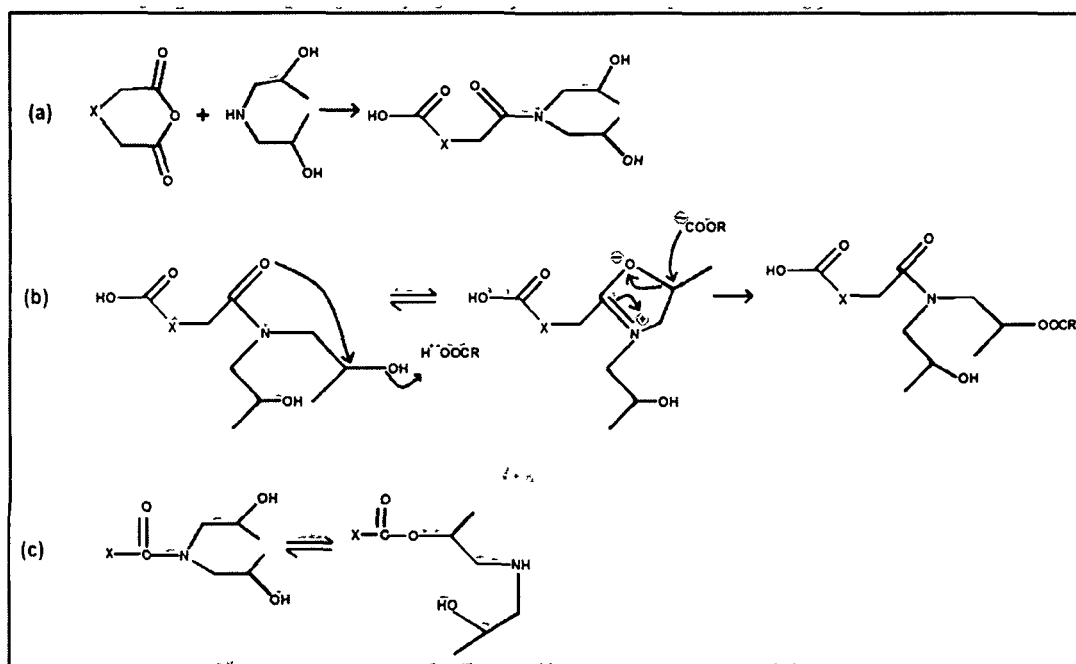
Fang et al. reported the synthesis of HBPEA using molar excess of DiPA (BB'₂ type monomer) as compared to cis-hexahydrophthalic anhydride (HPhAn, an A₂ type monomer).³⁵ The reaction utilizing the above reactants resulted in an AB₂ type monomeric unit, which further underwent polycondensation reaction with the excess BB'₂ in the subsequent step to yield HBPEA. The use of excess BB'₂ eliminated the risk of gelation encountered in the

classical $A_2+BB'_2$ approach.³⁵

The melting polycondensation of aliphatic carboxylic anhydrides and multihydroxyl primary amine (2-amino-2-ethyl-1,3-propanediol (AEPO) and tris(hydroxymethyl) aminomethane (THAM)) has been investigated by Li and his co-workers as a novel approach with the above reaction mechanism, to prepare hydroxyl group terminated HBPEA.³⁶ They reviewed the influence of nature of anhydride and amines in the formation of imides and amides in HBPEA. The use of aromatic anhydrides and amines exclusively forms imides. However if either of two are aromatic, imides are formed in predominance.³⁶ Spurred by the fact that the use of aromatic cyclic anhydrides with contorted structure averts the formation of imides, a thermal polycondensation approach for the preparation of aromatic and semiaromatic HBPEA was explored by the same group using 2,2'-diphenic anhydrides and 1-(4-/3-aminophenyl)-1,1-bis (dihydroxyphenyl) ethane.³⁷ The optimum yield and inherent viscosity of HBPEA was obtained at 200 °C using DMF as the solvent while maintaining 45% solid content. The above two routes to HBPEA extensively reviewed by Li et al.^{36,37} proved to be efficient in synthesizing aliphatic HBPEA with short alkyl backbone because cyclic anhydrides bearing more than six-membered rings are very unstable or even non-existent. However there was an ongoing search for HBPEA possessing long alkyl chains. In this vein, Lin and his coworkers used dicarboxylic acids together with DiEA or DiPA to design an easy and cost-effective $A'A_2+B_2$ approach for the synthesis of aliphatic and semiaromatic HBPEA possessing multihydroxyl end groups.³⁸ It can thus be surmised that dibasic acids and dihydroxyalkyl amines form the suitable monomer pair for the commercial production of HBPEA.

The random polymerization reactions of the monomers result in wide molecular weight distributions of hyperbranched polymer. The difficulty in controlling the molecular weight distributions in random polymerization can be addressed by three strategies, namely addition of multifunctional moiety, controlled monomer feed and differential reactivity of the functional groups in the monomer.³⁹ In this regard, Song et al. illustrated the use of varying weight percentages of ethylene glycol as the multifunctional molecule together with the equimolar amount of DiEA and maleic anhydride (MAN) in the synthesis of HBPEA.³⁹ Following the same strategy, Kou et al. reported the synthesis of pentaerythritol (PETL) multifunctional moiety based HBPEA using an AB_2 type monomer containing two hydroxyl groups and one carboxyl group by core dilution/slow monomer addition strategy.⁴⁰ The

variation in the charging ratio of cis-1,2-cyclohexane-dicarboxylic anhydride to PETL (molar



Scheme 1.1 Reaction mechanism of (a) cyclic anhydride with dihydroxy amine, (b) esterification of *N,N*-bis(2-hydroxyalkyl) amide and, (c) internal acyl shift rearrangement

ratio) by 4:1 and 8:1 have shown that the synthesis of HBPEA with low monomer: multifunctional moiety ratio accord with the ideal case (degree of branching (DB) approaching 1).⁴⁰

During the last decade efforts have been made to synthesize biocompatible HBPEA using non-toxic amino acids and gallic acids.⁴¹ In this vein, approaches like ‘thio-ene’ click chemistry was employed by Bao et al. for the synthesis of α -amino acid based HBPEA.⁴² In this methodology, intermediates were formed *via* thio-Michael addition reaction using vinyl monomer (Michael acceptor) and 1-thiol glycerol (Michael donor).⁴² The self-polycondensation of these intermediates in the presence of catalytic amount of $\text{Ti}(\text{O}i\text{Bu})_4$ resulted in the formation of HBPEA with terminal hydroxyl groups.⁴² In another recent report, Bao et al. extended the above work with acidic and basic amino acids and used 2-mercaptoethanol as the Michael donor.⁴³ The pK_a value of 1-thiol glycerol and 2-mercaptoethanol are high and so weak base Et_3N proved efficient to catalyze the thio-ene reactions and consequently the thiols deprotonated to corresponding thiolate anions. The thiolates are strong nucleophiles that add on to the activated double bond of Michael acceptor to form carbon centered enolate (strong base) which quickly abstracts proton to result in an

Michael addition product (ABB' type intermediate) following regioselective anti-Markownikoff's rule.⁴³ The use of such thio-Michael addition reactions in the synthesis of HBPEA involves advantages like mild reaction conditions, high efficiency and orthogonality of the reactions. But the high cost of the amino acids (starting materials) forwards the synthesized HBPEA to be used for special purpose applications only. The technological progress in the development of HBPEA chemistry is shown in Table 1.5.

Table 1.5 Key milestones in the development of HBPEA chemistry

Year	Ascent in the history of HBPEA
1995	bulk silyl-activated HBPEA by Kricheldorf ^{29,30}
1996	DiPA-PhAn based HBPEA by van Benthem ³²
2004	melting polycondensation of aliphatic/aromatic anhydrides and multihydroxyl primary amine by Li ^{36,37}
2005	gallic and amino acid based HBPEA by Li ⁴¹
2006	DiEA-MAn and ethylene glycol as core reactant based HBPEA by Song ³⁹
2007	slow monomer addition strategy using PETL as core moiety by Kou ⁴⁰
2008	DiPA (molar excess)-HPhAn based HBPEA by Fang ³⁵
2008	dicarboxylic acid-dihydroxy secondary amine based easy and cost-effective A'A ₂ +B ₂ strategy for synthesis of HBPEA by Lin ³⁸
2012	α -amino acid based HBPEA using click chemistry by Bao ⁴²

The technological innovation and the immense commercial prospects of HBPEA can also be envisaged from the patents reports⁹⁸⁻¹²³ (retrieved from the same database SciFinder®) filled across different parts of the globe. Table 1.6 vouch for the testimony of this bottom line.

The present decade has seen an upsurge in the number of reported works on vegetable oil based PEA. The utility of different vegetable oils or their derivatives like N,N-bis(2-hydroxyalkyl)fatty amides are documented for the synthesis of PEA.⁵⁰⁻⁵⁷ These fatty amides act as reactive diluents and maintain the low medium viscosity during the polymerization reaction, and are thus envisaged as potent reactant in the synthesis of bio-based HBPEA without gelation. However the use of the same in the synthesis of its bio-based hyperbranched analog has not been strived for till date and thus are foreseen as one of the imminent research niche.

Table 1.6 List of patents retrieved from SciFinder® for the search queries 'hyperbranched poly(ester amide)' and 'hyperbranched polyesteramide' in the period 2001-2013

Sl No.	Patent No. (year)	Main components	Highlights/role of HBPEA
1	WO 2001077270 (2001) ⁹⁸	Hybrane™ S 1200/ Hybrane™ HA 1300	hydrate inhibitor for inhibiting the plugging of gas conduits
2	WO 2002102928 (2002) ⁹⁹	Hybrane™ SVPC/SPIBC	solubilizing enhancer for asphaltenes in hydrocarbon mixture
3	EP 1306401 (2003) ¹⁰⁰	DiPA-HPhAn- monohydroxyl polyethylene oxide based HBPEA	rheology modifier for petroleum gas oil and antifreeze agent in diesel
4	RD 471078 (2003) ¹⁰¹	HBPEA, BaSO ₄	binder for non-hazzy and glossy coating
5	EP 1424362 (2004) ¹⁰²	DiPA-ScAn/ HPhAn/ PhAn/lauric acid/BA/ stearic acid based HBPEA, modified clay	binder for thermosetting paint formulation
6	WO 2004074389 (2004) ¹⁰³	Hybrane™ P2/P4	anti-curl agent in ink/paint composition
7	CN 101333298 (2008) ¹⁰⁴	polyethylene, HBPEA/rare earth oxide, CaCO ₃	halogen-free flame retardant
8	CN 101381457 (2009) ¹⁰⁵	DiEA-MAn based HBPEA, HB acrylate copolymer	macromolecular component for synthesis of waterborne acrylic resin and acrylic emulsion
9	US 7507474 (2009) ¹⁰⁶	polyamide, HBPEA, glass fibers	non-reactive rheological modifier for fiber-reinforced thermoplastic

10	CN 101397393 (2009) ¹⁰⁷	E 44 epoxy, Hybrane PS 2550	curing agent for epoxy resin
11	CN 101550273 (2009) ¹⁰⁸	poly(3-hydroxybutyrate- 3-hydroxyvalerate), DiPA-PhAn based HBPEA	multipurpose additive to reduce viscosity, increase tensile strength and facilitate spinning of poly(3- hydroxybutyrate-3- hydroxyvalerate)
12	CN 101570625 (2009) ¹⁰⁹	PLA, HBPEA, silica	compatibilizer for PLA/silica nanocomposite
13	WO 2009153334, (2009) ¹¹⁰ WO 2009153333, (2009) ¹¹¹	N,N-bis (dimethylaminopropyl) amine/DiPA- HPhAn/ScAn based HBPEA and anionic surfactant	co-surfactant for shampoo formulation
14	US 20100113668 (2010) ¹¹²	CaF ₂ , semiaromatic polyamide, DiPA/DiEA based HBPEA	viscosity modifier for thermoplastic/conductive filler system
15	EP 2236541 (2010) ¹¹³	unsaturated C ₃₋₅₀ carboxylic acid based HBPEA	radiation curable thermoset
16	KR 2011035526 (2011) ¹¹⁴ KR 2011035527 (2011) ¹¹⁵	HBPEA acrylate oligomer/acid-modified HBPEA acrylate oligomer	photo-polymeric additive for colored photo-resist system
17	US 20110257284 (2011) ¹¹⁶	polyurethane, HBPEA	flame-retardant for polyurethane foams
18	EP 2485716 (2012) ¹¹⁷	Hybrane™ HA 1690/ S 1200	pharmaceutical solubilizer
19	WO	polyethylene glycol/	flocculants for paper

	2013092797 (2013) ¹¹⁸	quaternary ammonium terminated HBPEA with citrate counter ions	production and dishwasher detergents
	WO 013092794 (2013) ¹¹⁹		
20	WO 2013092800 (2013) ¹²⁰	betaine end terminated HBPEA with citrate counter-ions	flocculants for industrial and domestic purposes
21	CN 103184692 (2013) ¹²¹	DiPA-ScA based HBPEA, γ -amino propyl triethoxysilane	textile additive to modify adhesion and render prolong service life
22	CN 101886296 (2013) ¹²²	milk protein fiber, silk, nylon fiber, HBPEA	modifier for milk protein fibers to impart rigidity, stiffness, low textile pilling, good dyeing performance spinning and weaving properties
23	CN 103423593 (2013) ¹²³	DiPA-MAn HBPEA	gas hydrate inhibitor to aid in transportation of natural gas

1.3.2.2. Preparative methods of HBPEA nanocomposites

Motivated by the recent enthusiasm in the domain of nanotechnology, the fabrication of the nanocomposites is one of the rapidly evolving areas of research possessing several edges over the pristine polymers.⁴⁸ The main challenge following the selection of HBPEA matrix and appropriate nanomaterials is the preparative method to yield desired HBPEA nanocomposites. The various strategies to prepare HBPEA nanocomposites are broadly classified into three main categories namely solution, *in-situ* polymerization and melt-mixing which are briefly described below.

Solution technique

This technique is based on the use of an appropriate solvent/solvent mixture which swells and disperses the nanomaterials into the host polymer solution.⁴ The mechanical shearing and ultrasonication aid in the mixing of these two components. The degree of mixing determines the formation of two types of nanocomposites- intercalated and exfoliated,

although the former is only formed in most of the cases.⁴ The interplay of entropic and enthalpic factors dictates the degree of polymer intercalation into the nanomaterials.¹²⁴ The entropic penalty owing to confinement of the polymer chains is compensated by the increased conformational degree of freedom of the modifier anchored onto the nanomaterials as the interlayer spacing increases.¹²⁴ The internal energy determines the thermodynamic feasibility of the intercalation process as the overall change in entropy is negligible.¹²⁴ To this end, Amin et al. documented the preparation of nanocomposites of DiEA/DiPA-PhAn based HBPEA/MMT in water using solution polymerization technique.⁴⁵

However the cost, hazardous impacts and removal of the solvent are the critical issues encountered in this technique (although the problems are averted in case of using water as the solvent).⁴ As the solubilization of the pre-formed polymer and their mixing with the wetted nanomaterials is an energy intensive process, focus remains on the following technique for addressing the same.

In-situ polymerization technique

In this technique, the nanomaterials are swollen/dispersed by a liquid monomer, consequently forming polymer chains in between the intercalated nanomaterials.⁴ In other words, the monomer molecules adsorb onto the surface of the nanomaterials followed by polymerization and thereby resulting in delamination/debundling of the nanomaterial agglomerates.⁴ The low viscosity of the monomers result in their high diffusivity into the nanomaterials, which assist in achieving uniform mixing of the two and preferential formation of well exfoliated nanocomposites.⁴⁸ The low viscosity of the monomers reflects the low energy requirement for the mixing process. This technique is advantageous over the previous one as it eliminates/minimizes the use of solvent and reduces the energy required for the mixing process.⁴ The nanomaterial aids in crosslinking reaction in the case of resins but may also influence the polymerization process.⁴ In this regard, Morales-Gómez et al. reported the thermal polymerization of sodium chloroacetylaminohexanoate monomer in between the platelets of Cloisite 20A/25A to prepare PEA/MMT nanocomposite by *in-situ* polymerization technique at 160 °C.¹²⁴ The temperature dependence of polymerization kinetic study validated the aid of the nanoconfinement in the above polycondensation reaction by lowering the activation energies and pre-exponential frequency factors.

However both the solution and *in-situ* polymerization techniques are convenient for paint and coating industries.⁴

Melt-mixing technique

This technique involves heating of the polymer above its softening temperature and mixing with the appropriate nanomaterials under shearing condition.^{125,126} It is compatible with the prevailing industrial extrusion, kneading and injection moulding processes. This process involves eliminating the use of toxic solvents encountered in the solution technique and results in formation of intercalated or partially exfoliated nanocomposites unlike in *in-situ* polymerization technique.⁴ This process finds utility in mold-making industries.⁴ In this context, Krook et al. prepared nanocomposites of adipic acid-butanediol-aminocaproic acid based PEA/octadecylamine (C₁₈amine) modified MMT by melt-extrusion technique using a Brabender counter-rotating twin-screw extruder.¹²⁷ These nanocomposites exhibited intercalation and partial delamination of MMT platelets in PEA matrix.¹²⁷

However a number of other techniques are documented in literature which includes template synthesis, sol-gel process, plasma induced polymerization, cryogenic ball milling, thermal spraying process and so on.⁴ The cost and the challenge of attaining uniformly dispersed nanomaterials in the polymer matrix impede the practical applicability of these techniques.

1.4. Characterization

Various tools are essential to comprehend the physico-chemical features of polymers and their nanocomposites. However discussions in this section are mainly restricted to HBPEA and its nanocomposites. Different instrumental and analytical techniques are utilized to validate their structural and physical characteristics. A host of techniques including spectroscopic, microscopic, scattering and thermal techniques are employed for the characterization of the same. The structural analysis provides direct evidence of their chemical structure like composition, linkage, degree of branching and nature of functional group, and physical structure including amorphousness or crystallinity, rigidity or flexibility, polarity, isomerism and microstructure.⁴

1.4.1. Analytical techniques

The determinations of acid value, viscosity, molecular mass and so on are important in context of understanding of physical properties of HBPEA based resins.¹²⁸ The lower acid values indicate the presence of meagre amount of free acids in the synthesized resin. The acid value is of importance to HBPEA in regard to their alkali resistance property and reaction

with the basic pigments (in case of paint/coating industry).¹²⁸ It is measured as per the standard ASTM D 974 method. To this end, Fang et al. reported the changes in the acid values from 405 to 209 mgKOH/g and 209 to 2 mgKOH/g for the preparation of monomeric intermediate and polymerization steps respectively for DiPA-HPhAn based HBPEA.³⁵ The decrease in the acid value with the reaction time confirms the reaction between DiPA and HPhAn. The saponification value of the resin gives an inkling of the average molecular weight and chain length depending on the amount of basic solution required to neutralize the carboxylic groups present per unit gram of the resin. It is measured as per the standard ASTM D 1962 method. Ahmad et al. documented the increase in the saponification value from zero in the fatty amides N,N-bis(2-hydroxyethyl) linseed oil to 120-128 mgKOH/g upon polycondensation with the dibasic acids, which supported the formation of sufficient number of ester linkages in PEA.⁵¹ The iodine value of the resin reflects the presence of unsaturation which is important in context to its oxidative stability particularly when used in paint industries. It is measured as per the standard ASTM D 5768 method. In this regard, *Mesua ferrea L.* seed oil based PEA exhibits moderate iodine value of 59-72 gI₂/100g to find use in coating applications.⁵⁵ The specific gravity of the resins is based on Archimedes principle and measured using standard specific gravity bottle. The determination of the same is important in context of determining the strength to weight and cost to weight ratios for its industrial applications. *Mesua ferrea L.* seed oil based PEA possessed low specific gravity of 0.89-0.97, indicating its low weight characteristics.⁵⁵

The determination of solution viscosity is of significance in context of information concerning the frictional property and chain dimensions of HBPEA.¹²⁹ The viscosity of dilute HBPEA solution is measured using capillary viscometer like Ubbelohde viscometer. The inherent viscosity (η_{inh}) of the multihydroxyl primary amine based HBPEA measured at 25 °C was found to vary between 0.08-0.20 dL/g.^{36,37} The low η_{inh} value of the same reflected the presence of less chain entanglements and hydrodynamic radius due to hyperbranched architecture.

Unlike fine chemicals, HBPEA do not have fixed molecular weight due to differential statistical probability of the growth of polymeric chains during polymerization.¹³⁰ Thus HBPEA is characterized by weight average molecular weight (M_w) and polydispersity index (PDI), which are determined by gel permeation chromatography (GPC). It is a rapid, convenient and accurate technique wherein the polymer molecules are separated according to

their hydrodynamic volume and detected from their response towards refractive index or UV absorption. In this regard, Fang et al. reported the M_w of DiPA-HPhAn based HBPEA to be around 12400 g/mol with PDI of 1.22.³⁵ HBPEA possessing broad PDI is relevant for surface coating and adhesive applications as the low molecular weight fractions act as processing aids in processing of higher molecular weight fractions.

1.4.2. Spectroscopic techniques

UV-visible spectroscopy

This tool is one of the most routinely used facile and non-destructive rapid means of analysis to characterize the nanomaterials and nanocomposites. This optical spectroscopy is based on the principle of Beer-Lambert's law.¹³⁰ The small penetration depth of the incident electromagnetic radiation limits their applicability for the bulk materials but is readily useful for the nanomaterials.¹³¹ This tool is thus instrumental in the determination of size and concentration of the nanomaterials with modulations in the spectra being correlated with the stability or aging of the same.¹³¹ However this tool has narrow range of utility in neat polymers like HBPEA (except conjugated polymers) as it cannot provide complete information regarding the chemical structure beyond ascertaining the presence of chromophoric group and conjugation.¹³¹

Fourier transform infrared (FTIR) spectroscopy

This spectroscopy is one of the simple and versatile techniques for the structural elucidation of HBPEA and scrutinizing the nature of functional groups, presence of H-bonding and interactions of the nanomaterials with HBPEA matrix.^{129,130} The reaction of cyclic anhydrides with β -dihydroxyalkyl amines can be investigated by analyzing two absorption bands at around 1736 ($\nu_{C=O}$ in carbonyl group) and 1620 cm^{-1} ($\nu_{C=O}$ in amide group).^{36,37,50-57} The diminution of the characteristic bands of the dibasic acids/anhydrides at 1860, 1791 and 1679 cm^{-1} and the appearance of the carbonyl ester and amide absorption bands indicates the reaction between the secondary amine and the anhydride groups.^{36,37,50-57} Morales-Gómez et al. utilized the sensitivity of FTIR to elucidate the molecular conformation and packing density in crystallization studies of PEA/layered silicate nanocomposites.¹²⁵ The nanoconfinement of PEA chains in the nanosilicate galleries was reported to favor the occurrence of polycondensation reaction.¹²⁵

Nuclear magnetic resonance (NMR) spectroscopy

NMR is an indispensable tool used routinely for detail evaluation of molecular microstructures of HBPEA. ^1H and ^{13}C NMR spectroscopy are widely used for the elucidation of the structural features of the same.^{130,131} The structural similarity of HBPEA with its perfect counterpart (dendrimers) characterized by DB can be determined by comparison of the integral areas of NMR absorption peaks for the dendritic (D), terminal (T) and linear (L) units in HBPEA using Fréchet's equation: $\text{DB} = (\text{D}+\text{T})/(\text{D}+\text{T}+\text{L})$.¹³² Li et al. employed this tool to monitor the reaction mechanism of THAM-HPhAn/GAn based HBPEA.³⁶ This tool is also instrumental in statistical analysis of sequence distributions and study of chain dynamics of polymeric matrix by scrutinizing the magnetic relaxation kinetics of the excited nuclei.¹³³ Xu et al. recently documented the use of spin diffusion averaged paramagnetic enhanced NMR relaxometry for the characterization of interspacing of nanomaterials in the polymer nanocomposites.¹³³

Raman spectroscopy

It is an important tool to investigate the defects, electronic and phonon properties of the nanomaterials and nanocomposites which relies on inelastic scattering of a high-frequency monochromatic light (usually laser light in the visible range).¹³⁰ It is used for fingerprint identification of specific bonds and functional groups in the polymeric backbone like FTIR spectroscopy. The polymeric chain conformation, orientation and anisotropy are evaluated from polarized Raman spectra.^{129,130} Raman lines move to lower wavenumbers with increasing stress for typical bond vibrations, which proves useful in delving into the polymer deformation micromechanics.^{129,130} It is particularly significant for the characterization of nanomaterials such as CNT which are infrared inactive but Raman active.¹³⁴ This tool is sensitive to the shift-induced symmetry, transition energies, electronic density of states and the interaction of the nanotubes with the surrounding matrix in the nanocomposites.¹³⁴

1.4.3. X-ray diffraction

This is another most important and non-destructive technique used to address issues related to the crystal structure (lattice constants and geometry), structural heterogeneity, preferred orientation, strain, spatial dispersion and d -spacing (spacing between the adjacent lattice planes) in molecular architecture of nanomaterials in the nanocomposites.⁴ The small angle and wide angle X-ray diffraction (XRD) are used to obtain microstructural features of nanomaterials or nanocomposites including crystallographic arrangement at very low angles

of less than 2° and wide angle range from 2 - 80° respectively.⁴ XRD of HBPEA exhibits a broad and weak halo, attributed to its amorphous structure. Recently Fotiadou et al.⁴⁷ reported that the incorporation of 5 wt% Hybrane™ S 1200 into MMT shifted the 2θ peak from 8.7 to 6.7° while increasing the amount to 25 wt% resulted in occurrence of second order diffraction peak. This indicated an intercalated structure of HBPEA (mono- and bi-layer) within the nanogalleries, and further increment in the content of the same revealed layer-by-layer intercalation.⁴⁷

1.4.4. Microscopic techniques

Electron microscopy plays an invaluable role in the elucidation of morphology including shape, size, aspect ratio, microstructural entities, lattice defects and strain. However the sample preparation is tedious, labor intensive, cost involved is high and significant numbers of images are required to scrutinize the morphology of the nanocomposites.^{4,48}

Scanning electron microscopy (SEM) and field emission scanning electron microscopy (FESEM)

SEM is one of the most widely used microscopic tools for probing into texture, chemical composition and orientations of the nanomaterials in the nanocomposites.^{4,48} Energy-dispersive X-ray (EDX) microanalysis is complementary to the above tool in determining the chemical composition of the sample.^{4,48} However the build-up of static electricity on the non-conducting samples upon irradiation by electron beam requires a coating by a conducting material.⁴⁸ Amin et al. studied the morphology of DiPA-ScAn based HBPEA/cement admixtures using SEM wherein the polymeric chains were found to be glued between the crystal layers of the cement.¹³⁵ However, FESEM scans the surface of the nanocomposites using a high energy electron beam in a raster scan pattern.¹³⁶ This tool supersedes the former in terms of producing high quality images with negligible electrical charging and thereby eliminating the need of depositing conducting coatings onto the nanocomposites.¹³⁶ However TEM is useful to obtain images of nanomaterials in the nanocomposites with high resolution and magnification as compared to SEM and FESEM.

Transmission electron microscopy (TEM)

This is a vital tool in rendering atomic resolution lattice images and dispersion scenario including size, shape and the distribution of the nanomaterials in the nanocomposites.^{4,48} The imaging of nanomaterials in the host matrix is challenging owing to

small size and their contrast being covered by scattering from the polymer matrix.⁴⁸ High resolution transmission electron microscopy (HRTEM) is instrumental for resolution of the nanomaterials of dimensions less than 1 nm, their interfaces, dislocations and defects.¹³⁷ The selected area electron diffraction (SAED) provides information regarding microdiffraction patterns, symmetry of the lattice, interplanar distances and crystal planes of the nanomaterials.¹³⁷ In this milieu, Bao et al. studied the distribution of gold nanoparticles in alanine based HBPEA matrix using TEM.⁴⁶

1.4.5. Testing and analysis

1.4.5.1. Mechanical and rheological

The mechanical testing embodies a number of standard test methods which are mentioned below.^{129,130} The mechanical properties including tensile strength (TS), modulus, elongation at break (EB) and so on, and lap-shear tensile adhesive strength (either on metal-metal and wood-wood adherents) of HBPEA and its nanocomposites are measured using Universal Testing Machine (UTM) at particular jaw separation speed by the standard ASTM D 882 and ASTM D 4896-01 procedures respectively. Scratch hardness test is carried out by scratch hardness tester in accordance with the standard ASTM G 171 method. Impact strength is carried out by falling ball method using an impact tester (as per ASTM D 1709 method) for thin film applications. The bending test is done by standard ASTM D 522 method using specified mandrel. The rheological study is generally carried out using a rheometer with a parallel plate in both steady shear and oscillatory modes.

1.4.5.2. Thermal

The thermal properties like thermostability, kinetics of degradation and patterns of degradation, and the phase changes including glass transition (T_g), crystallization (T_c) and melting (T_m) temperatures of HBPEA are mainly determined by thermogravimetric analyzer (TGA) and differential scanning calorimetry (DSC) respectively.^{129,130}

Besides TG and DSC, there are many other techniques such as modulated DSC, dynamic mechanical, thermomechanical and dielectric thermal analyses which measures the changes in different material properties (reversible/non-reversible thermal changes, mechanical modulus etc.) with temperature.

1.4.5.3. Chemical resistance

It is one of the durability testing of HBPEA performed in different chemical environments as per the standard ASTM D 543-67 method.

1.4.5.4. Electrical

The covalent bonding in polymers affords them electrical insulation, which is determined by their dielectric strength as per the standard ICE 250 or BS 903 (part C4) method. The high levels of insulating behavior of the polymer led to the build-up of static electric charges which is quantified by their sheet resistance values.⁴ The sheet resistance is measured by the standard four-probe technique with linear probe configuration.

1.4.5.5. Biological

Biodegradation

This testing strives to find the environmental acceptability of the polymeric products after their useful service life in context of 'cradle to cradle' approach.¹³⁸ The standardized tests are divided into three categories namely field, simulation and laboratory tests.¹⁴³ Amongst these, the most reproducible ones are the laboratory tests where defined media are used and inoculated with microbial strains/enzymes or studied using phosphate buffer saline (PBS).¹³⁹ This test is subdivided into the following:

Bacterial degradation: This is evaluated as per the standard ASTM D 4783 wherein the growth profile of the bacterial culture (prepared in mineral salt media in de-mineralized water) is scrutinized by monitoring UV absorption at 600 nm over a period of at least six weeks, complemented by weight loss profile of HBPEA and its nanocomposites.

Enzymatic degradation: This is evaluated by the weight loss profiles of HBPEA and its nanocomposites post immersion in buffer solution (maintaining optimum pH) containing commercial enzymes. Further the degradation in PBS with or without enzymes is also evaluated as per the standard ASTM F 1635-04 method.

Antimicrobial

The antimicrobial activity is determined by different test methods as described below. In these tests, streptomycin sulfate (for antibacterial assay) and nystatin (for antifungal assay) are taken as the positive control while 10% dimethyl sulphoxide as the negative control.

Minimum inhibitory concentration (MIC): The antibacterial activity (against bacteria cultured in respective broth) is determined (post serial dilution of stock solution) as described by micro-well dilution method.¹⁴⁰

Well diffusion method: The log phase culture of the both test bacterial and fungal strains is seeded on the surface of the agar medium with HBPEA and its nanocomposites and the observed zones of inhibition are measured as described by Radhika et al.¹⁴¹ The antialgal assay is performed by seeding the materials onto the solidified algal culture medium as reported by Roy et al.¹⁴²

Colony forming unit (CFU) and total protein concentration: The enumeration of bacterial colonies formed upon interaction of the bacterial inoculum with the tested materials is evaluated by using the standard dynamic shake flask method.¹⁴³ The total bacterial protein adsorbed on the surface of the materials, is estimated according to the method described by Bradford.¹⁴⁴

However the antiviral¹⁴⁵ and antiprotozoan¹⁴⁶ tests are generally avoided as the culturing of viruses and protozoa are invasive and involve complicated procedure owing to their complex life cycles.

Biocompatibility

The surface properties of HBPEA and its nanocomposites play a vital role in dictating their biocompatibility in regard to the cellular adherence and growth onto the same. This property is assessed by the following methods namely cytotoxicity screening and cell adhesion or proliferation. Amidst a number of acceptable cytotoxicity assays, the enzyme based method using 3-(4,5-dimethylthiazol-2-yl)-2,5-diphenyltetrazolium bromide (MTT) solution is most commonly used.¹⁴⁷ The cell adhesion or proliferation is assessed by staining the cells and visualization using light microscope (upon trypan blue staining), SEM and fluorescence microscopy.¹⁴⁸

The aforementioned outline of the fundamental tools and techniques used for the characterization of HBPEA and its nanocomposites is far from being completed. The advances in atomic force and scanning tunneling microscopy, X-ray photoelectron spectroscopy and many other techniques are of considerable importance as well in the characterization of the same.

1.5. Properties

The enhancement in the properties of the nanocomposites relative to the pristine HBPEA is critically discussed to underline their potential utility and the opportunities for advanced applications. The significance of HBPEA nanocomposites relates to value-added

performance in terms of mechanical, barrier, flame-retardancy, thermal, optical, electrical and biodegradation, which are either not significant or completely absent in the neat polymer by the low volume inclusion of suitable nanomaterials.^{4,48} The escalation in the afore-stated properties primarily depends on the nature of nanomaterials and HBPEA, interaction between them and the type of preparative methods, which are described underneath.

Mechanical

The mechanical properties signify the load-bearing characteristics of the nanocomposites, and their strength depends primarily on the structure, configuration and type of arrangement of the nanomaterials in HBPEA matrix.⁴ The enthalpic (interfacial interactions including van der Waals force) and entropic (loss in conformational degrees of freedom of HBPEA chains due to mechanical interlocking within the nanomaterials) interactions between the nanomaterials and HBPEA chains dictate the spatial distribution of the former in the host matrix and tune the macroscopic performance including failure properties of the nanocomposites.⁹⁵ These interfacial interactions dictate the structural organization on the molecular scale and hence the enthalpic interactions play a key role in efficient transfer of the interfacial stress across the HBPEA-nanomaterial interface.⁹⁵ Wen et al. reported the dramatic improvement in the mechanical properties including toughness and stiffness of GAn-AEPO based HBPEA/PLA/silica ternary nanocomposite as compared to the binary nanocomposite of the latter two.⁴⁴ The other mechanical properties like EB, impact resistance and scratch hardness are not explored yet in HBPEA and its nanocomposites.

Thermal

Thermal sensitivity is one of the prime obstacles that constrict the technological applicability of HBPEA.⁴ This problem is addressed by the use of nanocomposites which possesses superior thermal stability as compared to the pristine polymer.⁴ This feature is attributed to the presence of the nanomaterials which act as 'mass transport barrier' and retard the molecular motion of HBPEA chains.⁴⁸ Amin et al. reported that DiPA-MAn/ScAn based HBPEA are thermally more stable as compared to DiEA based one owing to the presence of relatively more carboxyl groups in the latter.⁴⁵ The incorporation of MMT into HBPEA matrix exhibited improvement of thermal stability of the nanocomposites as compared to the pristine polymers.⁴⁵ TGA study was further validated by DSC measurements wherein a profound increase in T_g was observed due to the restricted molecular mobility of MMT nanoplatelets in the nanocomposites.⁴⁵

Electrical

PEA is used as dielectric impregnants for papers and coating of metallic wires to impart electrical insulation together with sufficient dielectric strength to avoid electrical failure and heat generation.¹⁴⁹ The presence of polar groups like hydroxyl groups in the periphery of DiEA/DiPA-dibasic acids/anhydrides based HBPEA accounts for their dielectric behaviors.¹⁵⁰ To this end, Elrehim et al. was the first to report the dielectric properties of HBPEA.¹⁵⁰ Turky et al. further investigated the molecular dynamics and charge transport mechanism associated with the dielectric behavior of the same.¹⁵¹ However the dielectric property results in the build-up of electric charges on the surface of HBPEA owing to a number of factors including friction with other dielectric materials, repeated deformation and contact with ionized gases (in accordance with Coehn's Law).¹⁴⁹ The rate of charge decay, significant for a number of electrical applications depends both on the molecular architecture of HBPEA and environmental factors such as moisture and other impurities.¹⁴⁹ This electrostatic charging can be effectively dissipated by the design of suitable nanocomposites.¹⁵³ In this milieu, an antistatic composition of HBPEA comprising of nanoclay content of 20-40 wt% was patented by Muscat et al.¹⁵²

Barrier

This property reflects the resistance of HBPEA and its nanocomposites to the ingress of small penetrant molecules. The improvement in the barrier properties of the polymer nanocomposites relative to the neat one occurs by a factor approximate to the tortuous path (mean square displacement of penetrant molecules relative to the film thickness) in the nanocomposites.⁴ The formation of complex path within the polymeric matrix upon incorporation of MMT delays the diffusion of the penetrants, to find commendable applicability in food and beverage packaging together with barrier liners in storage tanks in aeronautics.¹⁵³ The modest improvement in the water vapor and oxygen barrier properties of octadecylamine-modified MMT/PEA nanocomposites was reported by Krook et al.¹⁵⁴

Viscoelasticity

The viscoelastic behavior of HBPEA is important in scrutinizing their intrinsic rheological behavior including flow characteristics.¹³⁰ The viscoelastic properties like storage and loss moduli exhibit a phase transition behavior from liquid-like to solid-like upon formation of nanocomposites.¹⁵⁵ The rheological properties influence the stress that is generated during processing and fabrication of HBPEA nanocomposites and aid in analyzing

the dispersion of the nanomaterials in HBPEA matrix, thus offering an insight of their structures and properties.^{4,130,155} Song et al. reported that MAn-DiEA based HBPEA exhibited Newtonian behavior with steady shear viscosities, which validated the formation of hyperbranched polymer with no chain entanglements.³⁹

Biodegradation

Biodegradation is one of the prominent features accountable for the fate of the materials after their useful service lifetime. This is an important aspect contributing towards global sustainability.⁴ It entails fragmentation of the polymeric materials into low molecular-weight/oligomeric fragments (under the influence of microorganisms/enzymes/PBS) followed by mineralization.¹⁵⁶ Galán et al.¹⁵⁷ extensively reviewed the hydrolytic and enzymatic degradation characteristics of SBA-dodecanediol-alanine based PEA. However scrutinizing of the biodegradation of HBPEA nanocomposites- bequeathed with multiple functionalities of hyperbranched architecture together with the catalytic activity of the nanomaterials, which are expected to exhibit superior potency relative to the pristine HBPEA, is yet to be delved into.

Antimicrobial

Antimicrobial nanocomposites are of immense concern in regard to the spread of infections by pathogenic microorganisms particularly the multi-drug resistant ones.¹⁵⁸ They find applications in innumerable domains ranging from medical sciences to textiles including hygiene products and food packaging.¹⁵⁸ The most common microbes responsible for mild infections to severe life-threatening diseases include different bacterial (Gram positive, Gram negative and acid fast positive species), fungal and algal species.¹⁵⁹ In this vein, Zafar et al.¹⁶⁰ documented that vegetable oil based PEA using metals such as cadmium, zinc, manganese, cobalt and copper exhibited potent antibacterial activity. Spur by the above report, Bharathi et al.¹⁶¹ explored the antimicrobial efficacy of cadmium containing bio-based PEA which exhibited pronounced antibacterial activity against *Staphylococcus aureus* (Gram positive) compared to *Salmonella typhi* (Gram negative), and antifungal activity against *Candida albicans*. Although literature exists on antimicrobial potency of PEA but attempts to scrutinize the impact of hyperbranched architecture of HBPEA and the high surface area of the nanomaterials in HBPEA nanocomposites has not yet been strived for.

Biocompatibility

PEAs provide an attractive avenue for biocompatible materials owing to their tunable properties (depending on the ratio of ester to amide linkages) to find wide scale utility in the biomedical domain.¹⁶² The biological response of the nanocomposites reflect their biocompatibility with the cultured cells. To this end, L-alanine based PEA possessing biocompatibility towards L929 fibroblast cell line was reported by Paredes et al.¹⁶³ Thereafter DeFife et al.¹⁶⁴ reported that amino acids (L-Leucine and L-Lysine) based PEA promote *in-vitro* cellular wound healing by constricting the pro-inflammatory response and promoting the growth of endothelial cells for repairing of the tissues. However the prospect of bio-based HBPEA nanocomposites as biocompatible materials is yet to be examined.

1.6. Applications

The previous discussions were reminiscent of the fact that the advent of nanotechnology in the domain of polymer science has unfastened multihued diorama of application oriented utilities. The importance of HBPEA lies in its diverse spectrum of commercial and technological prospects. DSM (stands for former Dutch State Mines) Fine Chemicals, Geleen, Netherlands has portfolio of HBPEA commercialized under the trade name Hybrane[®], more specifically: Hybrane[™] S 1200, Hybrane[™] HA 1300, Hybrane[™] D 2800, Hybrane[™] P/S80 1200, Hybrane[™] DEO750 8500, Hybrane[™] H 1500, Hybrane[™] H/S80 1700, Hybrane[™] HV 2680, Hybrane[™] P 1000, Hybrane[™] PS 1925 and Hybrane[™] PS 2500. The multifarious applications of HBPEA across different realms are presented underneath.

Pharmaceutical

Amidst the above commercially available HBPEA, Hybrane[™] S 1200, Hybrane[™] H 1500 and Hybrane[™] HV 2680 loaded with pharmaceutical acetaminophen find use as efficient drug carriers. Hybrane[™] S 1200 and Hybrane[™] HA 1690 possessing hydroxyl and tertiary amine functional moieties are used as solubility enhancers and drug carriers for poorly water soluble antidiabetic drug like glimepiride.¹⁶⁵

Paper industry

The inclusion of small quantities of water soluble HBPEA in paper coating formulations serves as rheology modifiers in their coating dispersion at very high speeds.¹⁶⁶ Tertiary amine substituted Hybranes quarternized (75%) with dimethyl sulfate is used as a fixing agent to eliminate the colloidal and dissolved substances from the wood fiber

suspension in the paper industries.¹⁶⁶

Azeotrope-breaking additive

Hybrane™ S 1200 is used as an azeotrope-breaking additive for ethanol-water, dioxane-water and so on types of water containing azeotropes.¹⁶⁷ They possess adequate molecular weight and thus leave no undesirable residues in the distillate. The low solution viscosity of the same averts the problems of heat and mass transfer in such process engineering applications.¹⁶⁷

Gas and oilfield operation

DSM commercialized the use of HPhAn-DiPA-IMPA based HBPEA in oil field applications owing to their ability to curb the crystallization of gas hydrates.¹⁶⁸

Cement admixture

DiPA/DiEA-PhAn based HBPEA is reported to be used as a polymeric admixture for cement pastes for dispersion of agglomerated cement particles. HBPEA bridges between the crystal layers of cement, thereby gluing the layers together and resulting in a strengthened microstructure capable of withstanding stresses.¹³⁵ This internal cohesion of HBPEA modified cement led to the formation of cement pastes with smaller amount of microcracks and improved hydration characteristics.¹³⁵ The cement characteristics further improved with the use of water soluble DiPA-ScAn based HBPEA owing to their water solubility at molecular scale, which enhanced their mixing homogeneity with the cement pastes.¹³⁵ In other words, the insertion of HBPEA chains in between the cement particles resulted in an electrostatic repulsion which reduced the attraction between the cement particles, thereby preventing their agglomeration.

Textile industry

Hybrane™ H 1500 also finds use as a dye-binding polymeric additive in polypropylene (PP) fibers in textile industry. PP lack dyeability, albeit is an economically feasible fiber possessing desirable physical and mechanical properties.¹⁶⁹ The incorporation of small amount of HBPEA helped improve dyeability, but did not drastically influence the mechanical properties of PP fibers.¹⁶⁹ The presence of multitude of polar groups in the three dimensional hyperbranched architecture of HBPEA modified PP fibers acted as the ideal receptor sites for the dye molecules.¹⁶⁹ HBPEA was also used as a dye additive or surface modifying agent for compounding fiber grade poly(ethylene terephthalate) (PET).¹⁷⁰ The

dyeability of HBPEA in PET/HBPEA blend is attributed to the reduction in T_g and crystallinity of the blend as compared to pristine PET.¹⁷⁰ This increased the mobility of PET chains and thereby facilitating dye uptake by the same.¹⁷⁰

Toughening agent

HBPEA is used as an epoxy modifier (or thermoset toughener) in coatings for electronic encapsulations, where properties like toughness and low shrinkage are indispensable.¹⁷¹ The shrinkage problem in methyltetrahydrophthalic anhydride cured epoxy leads to reduction in their volume, creating cracks, deformations and decreased adhesion. These results in diminution of the protective capacity of the epoxy coatings.¹⁷¹ The degradability is also an important factor in context of the reworkability or repairing of the electronic devices as these thermosetting materials cannot be recycled. In this milieu, HBPEA proved to be a potent candidate for reducing the viscosity of the reactive mixtures, shrinkage problem and enhancing mechanical properties including flexibility while maintaining their T_g , dielectric properties and thermal degradability.¹⁷¹

Hybrane™ PS 2500 modified PLA exhibits improved inherent brittleness and toughness relative to neat PLA together with high biocompatibility and good biodegradability. They find wide uses across the domains including biomedical sciences.¹⁷² The abundance of hydroxyl end of HBPEA induces interfacial interactions and adhesion with PLA, particularly by H-bonding and helps in the improvement of the toughness and mechanical properties as compared to pristine PLA.¹⁷² The use of HBPEA served as a multifunctional material ranging from process aid to heterogeneous nucleating agent including T_g depressant for improving the crystallization of PLA.¹⁷² Hybrane™ H 1500 is a novel toughening agent for acrylic/melamine resins which finds utility in automotive clearcoats.¹⁷³ AEPO/THAM-HPhAn/GAn based HBPEA is also reported to be used for toughening of poly(propylene carbonate) *via* H-bonding interactions.¹⁷⁴

Crosslinking agent

DiPA-ScA based HBPEA is employed as a crosslinker for polyurethanes which are widely used in different realms including coatings, foaming materials, adhesives and so on.¹⁷⁵ Pedrón et al.¹⁷⁶ explored the use of Hybrane™ S1200 as a crosslinker for the fabrication of hydrogels of tunable properties.

Miscellaneous utilities

The bromine terminated HBPEA find uses as a polymeric surfactant, hydrophobic drug carrier, detergent, dispersion stabilizer and lubricant.¹⁷⁷ HBPEA possessing abundant functional groups is used as a macroinitiator for the preparation of amphiphilic biodegradable star-poly(ϵ -caprolactone)s.¹⁷⁸ These amphiphilic core-shell star polymers are attractive candidates as nanocarriers for controlled drug delivery and dye-phase transfer applications.¹⁷⁸ Dimethyl sulfate quaternized HBPEA has myriad of applications ranging from papermaking to paints including waste water treatment and cosmetics.¹⁷⁹ The long alkyl chain terminated HBPEA can be tailored to find use as dielectric materials.¹⁵⁰

Viscosity modifier

HBPEA with terminal hydroxyl groups is used as a viscosity modifier for engineering thermoplastics comprising of semiaromatic polyamide and calcium fluoride (as the thermally conducting filler) for uses in automotive, electrical and industrial sectors.¹⁸⁰

Desalination of water

HBPEA-trimesoyl chloride based reverse osmosis membranes possess chlorine-, alkaline- and acid-resistance abilities to find applications in desalination of water.¹⁸¹

Although there exists a number of reports on the wide utility of HBPEA, but reports on the use of HBPEA nanocomposites are scanty. The most significant work on the potential applicability of HBPEA nanocomposites was reported by Bao et al. as multifunctional materials.⁴⁶

Smart material

The pH-sensitive stimulus response of poly[2-(dimethylamino)ethyl methacrylate] arms in alanine based HBPEA forward the nanocomposites of HBPEA/gold nanoparticles as controlled drug delivery agents.⁴⁶ The star-shaped HBPEA serves the twin role as a size-tunable nanoreactor and a pH-sensitive matrix for the nanocomposites.⁴⁶ The dendritic interiors of these nanocomposites have scaffolding properties to envelope small organic guest molecules in their nanocavities.⁴⁶ The organic molecules then accommodate themselves near the surface of gold nanoparticles and this nano-confinement of the organic molecules in the nanocomposites forwards them in various catalytic applications including *in-situ* catalysis for the reduction of *p*-nitrophenol.⁴⁶ Fig. 1.4 vouch for testimony of the wide application spectrum of HBPEA.

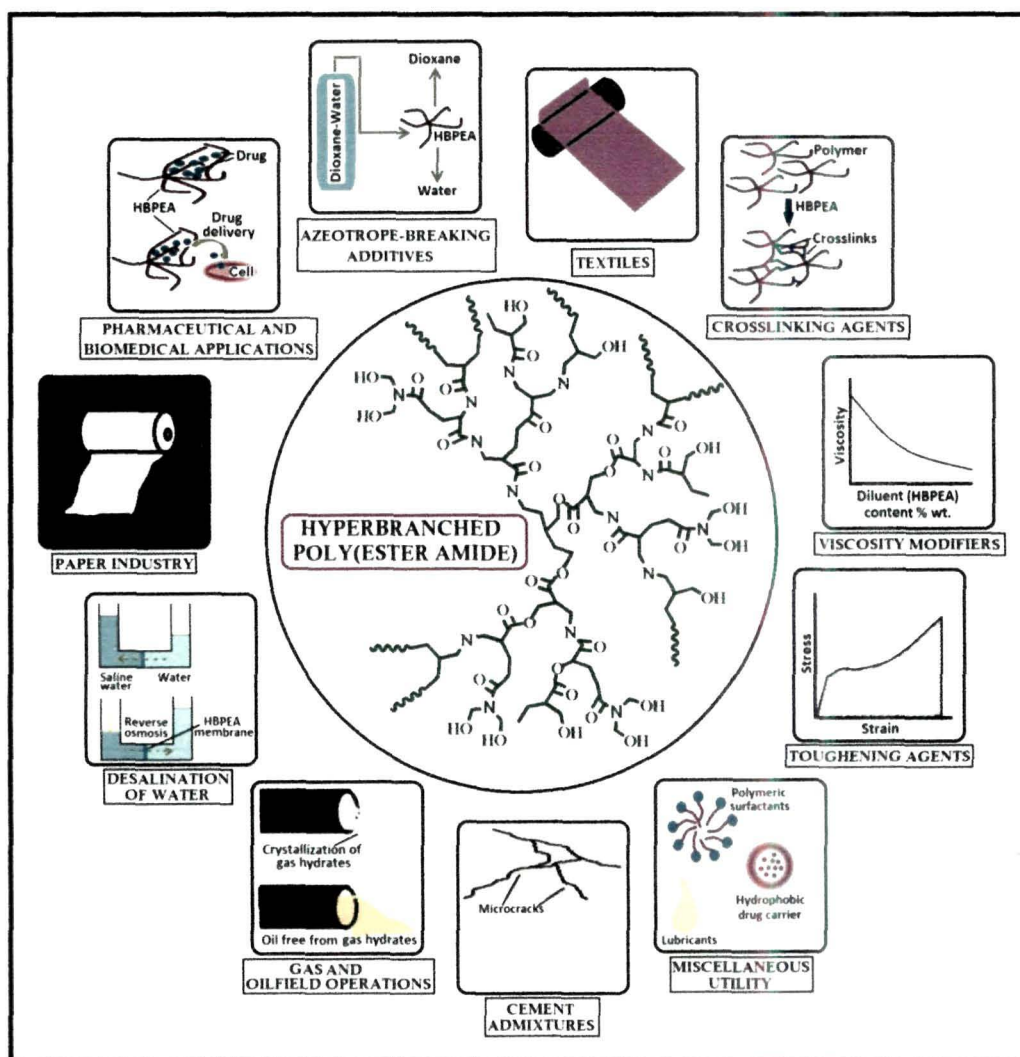


Fig. 1.4 Schematic representation of HBPEA (at the centre) and its diverse spectrum of applications (peripheral images)

1.7. Scopes of investigation

The perusal of discussion encountered in the preceding sections validated the immense potentials and ever-widening avenues of HBPEA together with encompassing the prospects remained in this endeavor. Albeit past estimates of using vegetable oils as raw materials for the synthesis of PEA have proven to be optimistic in hindsight, but the exploration of the same for the synthesis of HBPEA has not yet been strived for. The burgeoning fields of HBPEA nanocomposites are yet to reach a pinnacle in regard to its prospective applications. The need of high performance materials for advanced applications has prompted the exploration of HBPEA nanocomposites to address cocktail of problems ranging from sustainable resources to environmental footprints. In this vision, the bio-based HBPEA

nanocomposites which are envisaged as one of the key players to drive in the revolutionary advances in the arena of material science have sparked up with the following queries.

- (1) Whether castor oil or its immediate derivative can be used as one of the starting materials for the synthesis of bio-based HBPEA?
- (2) How much superiority can be achieved from bio-based HBPEA compared to its linear analog?
- (3) Whether functionalized nanomaterials can be used for performance improvement of the bio-based HBPEA?
- (4) What would be the apt functionalization of these nanomaterials and whether any greener tool can address the same?
- (5) What would be the probable bio-physico-chemical interactions at bio-nano interface of the bio-based HBPEA matrix and nanomaterials for the biological application of these nanocomposites?
- (6) Whether such nanocomposites could find application as antistatic materials?

1.8. Objectives of the present work

Spurred by the aforementioned scopes, the main objective of the proposed research work is to fabricate bio-based HBPEA nanocomposites for multimodal applications. This main objective is associated with the following sub-objectives:

- (1) To synthesize HBPEA using castor oil, DiEA and dibasic acids/anhydrides.
- (2) To characterize the synthesized HBPEA using various spectroscopic and analytical techniques.
- (3) To prepare different nanocomposites by incorporating various nanomaterials such as PANi nanofiber, MWCNT, MMT and silver nanoparticles decorated MWCNT into HBPEA matrix.
- (4) To characterize and evaluate different physical, rheological, mechanical, antistatic and antimicrobial properties of the prepared nanocomposites.
- (5) To optimize the performance characteristics of the nanocomposites by monitoring the dose level of nanomaterials to obtain the best material for various possible applications.

1.9. Plans of the present work

In order to implement and execute the proposed objectives, the research work is planned in the following ways:

- (1) A thorough state-of-art literature survey in the field of HBPEA, vegetable oil based PEA and their nanocomposites will be conducted.
- (2) Bio-based HBPEA will be synthesized by using double-monomer methodology.
- (3) The synthesized HBPEA will be characterized by different analytical and spectroscopic techniques including determination of acid value, saponification value, FTIR, NMR, TGA etc.
- (4) The physical, mechanical and chemical properties of the synthesized resin will be evaluated by the standard methods.
- (5) The thermal and the rheological behaviors of the synthesized resin will be studied by using TGA/DSC and rheometer respectively.
- (6) Greener tools of microwave and sonication will be exploited for the functionalization of the nanomaterials.
- (7) HBPEA nanocomposites will be prepared by both *ex-situ* and *in-situ* polymerization techniques.
- (8) The surface morphology of the prepared nanocomposites will be studied by using SEM and TEM.
- (9) The mechanical properties of the nanocomposites will be evaluated by the standard methods.
- (10) The biodegradability, biocompatibility and bio-physico-chemical properties of the nanocomposite will be tested.
- (11) Optimization of the performance characteristics of the nanocomposites will be done by monitoring the dose level of nanomaterial to obtain the best material for a possible application.

The proposed research work may involve collaboration and receipt of cooperation (for both sophisticated instruments and interdisciplinary works) from the other Departments of Tezpur University like Physics and Molecular Biology and Biotechnology (MBBT), NEHU Shillong and others depending on the requirement.

References

1. Voit, B.I., & Lederer, A. *Chem. Rev.* **109**, 5924--5973, 2009.
2. Gao, C., Frey, H. & Yan, D. Conclusions and perspective: Toward hyperbranched/dendritic states, in *Hyperbranched Polymers: Synthesis, Properties, and Applications*, D. Yan et. al, eds., John Wiley & Sons, Inc., Hoboken, 2011, 441—452.
3. Gao, C., & Yan, D. *Prog. Polym. Sci.* **29** (3), 183--275, 2004.
4. Karak, N. *Fundamentals of Polymers: Raw Materials to Finish Products*, PHI Learning Private Ltd., New Delhi, 2009.
5. Yates, C.R., & Hayes, W. *Eur. Polym. J.* **40** (7), 1257--1281, 2004.
6. Jikei, M., & Kakimoto, M. *Prog. Polym. Sci.* **26** (8), 1233--1285, 2001.
7. Voit, B. *J. Polym. Sci., Part A: Polym. Chem.* **38** (14), 2505--2525, 2000.
8. Kim, Y.H., & Webster, O.W. *Polym. Prepr. (Am. Chem. Soc., Div. Polym. Chem.)* **29** (2), 310--331, 1988.
9. Scholl, M., et al. *Prog. Polym. Sci.* **34** (1), 24--61, 2009.
10. Bolton, D.H., & Wooley, K.L. *Macromolecules* **30** (7), 1890--1896, 1997.
11. Ambade, A.V., & Kumar, A. *J. Polym. Sci., Part A: Polym. Chem.* **42** (20), 5134--5145, 2004.
12. Gao, C., et al. *Polymer* **42** (18), 7603--7610, 2001.
13. Abdelrehim, M., et al. *J. Polym. Sci., Part A: Polym. Chem.* **42** (12), 3062--3081, 2004.
14. Schömer, M., et al. *J. Polym. Sci., Part A: Polym. Chem.* **51** (5), 995--1019, 2013.
15. Hawker, C.J., et al. *J. Am. Chem. Soc.* **113** (12), 4583--4588, 1991.
16. Hult, A., et al. *Macromol. Symp.* **98** (1), 1159--1161, 1995.
17. Dutta, N., et al. *Prog. Org. Coat.* **49** (2), 146--152, 2004.
18. Tian, H., et al. *Prog. Polym. Sci.* **37** (2), 237--280, 2012.
19. Christ, R.E. *Manufacture of polyestēramides*, UK Patent No. 561108-A, May 5, 1944.
20. Gunatillake, P., et al. *Biotechnol. Annu. Rev.* **12**, 301--347, 2006.
21. Fonseca, A.C., et al. *Prog. Polym. Sci.* **39** (7), 1291--1311, 2014.
22. Lligadas, G., et al. *Mater. Today* **16** (9), 337--343, 2013.
23. Xia, Y., & Larock, R.C. *Green Chem.* **12** (11), 1893--1909, 2010.
24. Malmström, E., & Hult, A. *J. Macromol. Sci. Polymer Rev.* **37** (3), 555--579, 1997.
25. Young, R.J., & Lovell, P.A. *Introduction to Polymers*, 3rd ed., CRC Press, London, 2011.

26. Balzani, V. *Small* **1** (3), 278--283, 2005.
27. Roco, M.C. *J. Nanopart. Res.* **5** (3-4) 181--189, 2003.
28. Vollath, D. *Nanomaterials: An Introduction to Synthesis, Properties and Applications*, Wiley VCH, Germany, 2008.
29. Kricheldorf, H.R., & Löhden, G. *Macromol. Chem. Phys.* **196** (6), 1839--1854, 1995.
30. Kricheldorf, H.R., et al. *Macromol. Chem. Phys.* **198** (9), 2651--2666, 1997.
31. Stanssens, D., et al. *Prog. Org. Coat.* **22** (1-4), 379--391, 1993.
32. Froehling, P. *J. Polym. Sci., Part A: Polym. Chem.* **42** (13), 3110--3115, 2004.
33. van Benthem, R.A.T.M. *Prog. Org. Coat.* **40** (1-4), 203--214, 2000.
34. van Benthem, R.A.T.M., et al. *Macromolecules* **34** (11), 3559--3566, 2001.
35. Fang, K., et al. *Polym. Bull.* **60** (4), 533--543, 2008.
36. Li, X., et al. *Macromolecules* **37** (20), 7584--7594, 2004.
37. Li, X., et al. *Macromolecules* **38** (20), 8235--8243, 2005.
38. Lin, Y., et al. *J. Polym. Sci., Part A: Polym. Chem.* **46** (15), 5077--5092, 2008.
39. Song, W., et al. *e-Polymers* **6** (1), 677--689 2006.
40. Kou, Y., et al. *React. Funct. Polym.* **67** (10), 955--965, 2007.
41. Li, X., et al. *Biomacromolecules* **6** (6), 3181--3188, 2005.
42. Bao, Y.M., et al. *J. Polym. Sci., Part A: Polym. Chem.* **48** (23), 5364--5374, 2010.
43. Bao, Y., et al. *Polymer* **53** (1), 145--152, 2012.
44. Wen, X., et al. *Macromol. Mater. Eng.* **295** (5), 415--419, 2010.
45. Amin, A., & Samy, M. *International Journal of Polymer Science* **2013**, 8, 2013.
46. Bao, Y., et al. *Polymer* **54** (2), 652--660, 2013.
47. Fotiadou, S., et al. *Macromolecules* **46** (7), 2842--2855, 2013.
48. Koo, J.H. *Polymer Nanocomposites: Processing, Characterization, and Applications*, McGraw-Hill, New York, 2006.
49. Muscat, D., & van Benthem, R.A.T.M. *Top. Curr. Chem.* **212**, 41--80, 2001.
50. Shende, P., et al. *Pigm. Resin Technol.* **32** (1), 4--9, 2003.
51. Ahmad, S., et al. *J. Appl. Polym. Sci.* **104** (2), 1143--1148, 2007.
52. Shende, P.G., et al. *Pigm. Resin Technol.* **31** (5), 310--314, 2002.
53. Meshram, P.D., et al. *Prog. Org. Coat.* **76** (9), 1144--1150, 2013.
54. Bharathi, N.P., et al. *J. Inorg. Organomet. P* **20** (4), 839--846, 2010.
55. Mahapatra, S.S., & Karak, N. *Prog. Org. Coat.* **51** (2), 103--108, 2004.

56. Ahmad, S., et al. *J. Macromol. Sci. A* **43** (9), 1409--1419, 2006.
57. Ahmad, S., et al. *Prog. Org. Coat.* **47** (2), 95--102, 2003.
58. Ogunniyi, D.S. *Bioresour. Technol.* **97** (9), 1086--1091, 2006.
59. Kumar, A., & Sharma, S. *Renew. Sust. Energ. Rev.* **15** (4), 1791--1800, 2011.
60. Koster, S., et al. *J. Am. Soc. Mass Spectrom.* **14** (4), 332--341, 2003.
61. Kelland, M.A. *J. Appl. Polym. Sci.* **121** (4), 2282--2290, 2011.
62. Karak, N. *Vegetable Oil-Based Polymers: Properties, Processing and Applications*, Woodhead Publishing Limited, Cambridge, 2012.
63. Ganesan, D., et al. *Rev. Environ. Sci. Biotechnol.* **8** (4), 367--394, 2009.
64. Tran, Q.H., et al. *Adv. Nat. Sci: Nanosci. Nanotechnol.* **4** (3), 033001, 2013.
65. Sharma, V.K., et al. *Adv. Colloid Interfac.* **145** (1-2), 83--96, 2009.
66. Eutis, S., et al. *Photochem. Photobiol. Sci.* **4** (1), 154--159, 2005.
67. Li, X., et al. *Langmuir* **28** (2), 1095--1104, 2012.
68. El Badawy, A.M., et al. *Sci. Total Environ.* **429**, 325--331, 2012.
69. Iijima, S. *Nature* **354**, 56--58, 1991.
70. Jorio, A., Dresselhaus, G. & Dresselhaus, M.S. (eds.). *Carbon Nanotubes, Advanced Topics in the Synthesis, Structure, Properties and Applications*, Springer, Berlin, 2008.
71. Baughman, R.H., et al. *Science* **297**, 787--792, 2002.
72. Ma, P.C., et al. *Compos. Part A-Appl. S* **41** (10), 1345--1367, 2010.
73. Balasubramanian, K., & Burghard, M. *Small* **1** (2), 180--192, 2005.
74. Hirsch, A. *Angew. Chem. Int. Ed.* **41** (11), 1853--1859, 2002.
75. Peng, H., et al. *J. Am. Chem. Soc.* **125** (49), 15174--15182, 2003.
76. Bahr, J.L., et al. *J. Am. Chem. Soc.* **123** (27), 6536--6542, 2001.
77. Mickelson, E.T., et al. *Chem. Phys. Lett.* **296** (1-2), 188--194, 1998.
78. Ying, Y, et al. *Org. Lett.* **5** (9), 1471--1473, 2003.
79. Coleman, K.S., et al. *J. Am. Chem. Soc.* **125** (29), 8722--8723, 2003.
80. Georgakilas, V., et al. *J. Am. Chem. Soc.* **124** (5), 760--761, 2002.
81. Holzinger, M., et al. *J. Am. Chem. Soc.* **125** (28), 8566--8580, 2003.
82. Kamaras, K., et al. *Science* **301** (5639), 1501, 2003.
83. Crescenzo, A.D., et al. *Eur. J. Org. Chem.* **2011** (28), 5641--5648, 2011.
84. O'Connell, M.J., et al. *Chem. Phys. Lett.* **342** (3-4), 265--271, 2001.
85. Gotovac, S., et al. *Nano Lett.* **7** (3), 583--587, 2007.

86. Tasis, D., et al. *Chem Rev.* **106** (3), 1105--1136, 2006.
87. Kang, E.T., et al. *Prog. Polym. Sci.* **23** (2), 277--324, 1998.
88. MacDiarmid, A.G., et al. *Synth. Met.* **18** (1-3), 393--398, 1987.
89. Huang, J., et al. *J. Am. Chem. Soc.* **125** (2), 314--315, 2003.
90. Stejskal, J., et al. *Prog. Polym. Sci.* **35** (12), 1420--1481, 2010.
91. Ray, S.S., & Okamoto, M. *Prog. Polym. Sci.* **28** (11), 1539--1641, 2003.
92. Flessner, U., et al. *J. Mol. Catal.* **168** (1-2), 247--256, 2001.
93. Zhang, D., et al. *Appl. Clay Sci.* **50** (1), 1--11, 2010.
94. Alexandre, M., & Dubois, P. *Mater. Sci. Eng., R* **28** (1-2), 1--63, 2000.
95. Lagaly, G., Ogawa, M. & Dékány, I. Clay mineral Organic interactions, in *Handbook of Clay Science*, F. Bergaya et. al, eds., Elsevier Ltd., Amsterdam, 2006, 309—377.
96. Wicks, Z.W.(Jr.), & Chen, G.F. *J. Org. Chem.* **44** (8), 1244--1247, 1979.
97. Immediata, T., & Day, A.R. *J. Org. Chem.* **5** (5), 512--527, 1940.
98. Klomp, U.C. *Method for inhibiting the plugging of conduits by gas hydrates*, **WO Patent No. 2001077270**, October 18, 2001.
99. Cornelisse, P.M.W. *Method for solubilising asphaltenes in a hydrocarbon mixture*, **WO Patent No. 2002102928**, May 22, 2003.
100. Muscat, D. and Stanssens, D.A.W. *Oil soluble hyperbranched polyesteramides and method for making the same*, **EP Patent No. 1306401**, May 2, 2003.
101. DSM Coating Resins *Diminished cloudiness in dark coloured powder coating formulations*, **RD Patent No. 471078**, July 10, 2003.
102. Muscat, D., Stanssens, D.A.W., Heise, A., and Dorschu, M. *Process for preparing hyperbranched polyesteramide compositions containing modified clays*, **EP Patent No. 1424362**, June 2, 2004.
103. Edmunds, J.M. *Ink or paint compositions comprising a hyperbranched anionic polyesteramide*, **WO Patent No. 2004074389**, September 2, 2004.
104. Chen, Q., Chen, R., Xiao, L., Liu, X., Xu, J., Huang, B. and Qian, Q. *Producing halogen-free flame retardant plastic masterbatch and special resin from hyperbranched polyesteramide and mixed rare earth oxide*, **CN Patent No. 101333298**, December 31, 2008.

105. Liu, B., Chen, H., Luo, R. and Xu, Q. *Preparation method of aqueous hyperbranched intermediate and water soluble hyperbranched propenoic acid resin*, **CN Patent No. 101381457**, March 11, 2009.
106. Varlet, J., Clement, F., Touraud, F., Rochat, S. and Scherbakoff, N. *Thermoplastic polymer composition comprising a hyperbranched polymer and articles made using said composition*, **US Patent No. 7507474**, March 24, 2009.
107. Zhang, Y., Hu, H., Chen, Y., Liu, S., Zhang, W. and Yan, B. *Toughened and reinforced epoxy resin/hyperbranched polyesteramide composite material*, **CN Patent No. 101397393**, April 1, 2009.
108. Chen, Y., Wu, W., Chen, L., Yu, H., Shi, S. and Liu, J. *Hyperbranched polyamide-polyester-modified poly(3-hydroxybutyrate-3-hydroxyvalerate) and its spinning method*, **CN Patent No. 101550273**, October 7, 2009.
109. Wen, X., Lin, Y., Li, Y. and Dong, L. *Method for manufacturing poly(lactic acid)/hyperbranched polyesteramide/nanoscale silica ternary composite*, **CN Patent No. 101570625**, November 4, 2009.
110. Derks, F.J.M., Foster, S., Lochhead, R., Maini, A. and Weber, D. *Shampoo containing a hyperbranched polyester-amide*, **WO Patent No. 2009153334**, December 23, 2009.
111. Foster, S., Lochhead, R., Maini, A., Weber, D. and Derks, F.J.M. *Shampoo containing a hyperbranched polyester-amide*, **WO Patent No. 2009153333**, December 23, 2009.
112. Saga, Y. and Zhang, W.W. *Thermoplastic composition including thermally conductive filler and hyperbranched polyesteramide and molded articles*, **US Patent No. 20100113668**, May 6, 2010.
113. Vermeulen, J.A.A., Witters, S., Benthem, V.R.A.T.M., Bueckmann, A.J.P. and Martin, E. *Polyesteramide macromolecule and radiation-curable composition with polyesteramide macromolecule*, **EP Patent No. 2236541**, October 6, 2010.
114. Lee, S.N., Jeon, J.M. and Sang, T. *Colored photoresist compositions with good patternability for color filters*, **KR Patent No. 2011035526**, April 6, 2011.
115. Lee, S.N., On, J.H. and Kim, S.H. *Colored photoresist compositions with good patternability for color filters*, **KR Patent No. 2011035527**, April 6, 2011.

116. Bruchmann, B., Schonfelder, D., Ferbitz, J., Eisenhardt, A. and Peretolchin, M. *Process for producing flame-retardant PU foams*, **US Patent No. 20110257284**, October 20, 2011.
117. Reven, S. and Zagar, E. *Pharmaceutical composition comprising poorly soluble active ingredient and hyperbranched polymer*, **EP Patent No. 2485716**, August 15, 2012.
118. Arts, H.J., Derks, F.J.M. and Witters, S. *Hyperbranched polymers*, **WO Patent No. 2013092797**, June 27, 2013.
119. Arts, H.J. and Derks, F.J.M. *Hyperbranched polymers*, **WO Patent No. 2013092794**, June 27, 2013.
120. Arts, H.J., Derks, F.J.M., Hyett, W. and Witters, S. *Hyperbranched polymers*, **WO Patent No. 2013092800**, June 27, 2013.
121. Shou, C., Bo, Q., Lei, Y., Wen, D., You, G., Liu, J. and Zhao, M. *Application of hyperbranched polymer in belt core interface agent of flame-retardant conveying belt*, **CN Patent No. 103184692**, July 3, 2013.
122. Gu, Y., Pan, M., Zhou, L., Lin, H. and Zhang, W. *Hyperbranched milk protein fiber, tencel and polyamide fiber blended yarn and preparation method thereof*, **CN Patent No. 101886296**, January 23, 2013.
123. Liu, C., Dai, X., Guo, H., Chang, W., Zhang, Z., Li, G., Hao, J., Liu, G. and Yin, K. *One kind of hyperbranched kinetic hydrate inhibitor and its preparation method*, **CN Patent No. 103423593**, December 4, 2013.
124. Morales-Gámez, M., et al. *Express Polym. Lett.* **5** (8), 717--731, 2011.
125. McNally, T., et al. *Polymer* **44** (9), 2761--2772, 2003.
126. Vaia, R.A., et al. *Chem. Mater.* **8** (11), 2628--2635, 1996.
127. Krook, M., et al. *Polym. Eng. Sci.* **42** (6), 1238--1246, 2002.
128. Gast, L.E., et al. *J. Am. Oil Chem. Soc.* **45** (7), 534--536, 1968.
129. Young, R.J. & Lovell, P.A. *Introduction to Polymers*, 3rd ed., CRC Press, New York, 2011.
130. Maiti, S. *Polymer materials: Science. Technology. Developments*, Anisandhan Prakashan, Midnapore, 2009.
131. Jean-Mary, F. *Spectroscopic and Microscopic Studies of Aggregated Molecules Coated Onto Nanomaterials*, ProQuest, New York, 2006.

132. Höltér, D., et al. *Acta Polym* **48** (1-2), 30--35, 1997.
133. Xu, B., et al. *Nanoscale* **6** (3), 1318--1322, 2014.
134. Zhao, Q., & Wagner, H.D. *Philos. Trans. R. Soc. London, Ser. A* **362** (1824), 2407--2424, 2004.
135. Amin, A., et al. *J. Appl. Polym. Sci.* **121** (1), 309--320, 2011.
136. Liu, J. *Mater. Charact.* **44** (4-5), 353--363, 2000.
137. Wal, R.L.V., et al. *J. Nanopart. Res.* **6** (6), 555--568, 2004.
138. Braungart, M., et al. *J. Clean. Prod.* **15** (13-14), 1337--1348, 2007.
139. Muller, R. Biodegradability of Polymers: Regulations and methods for testing, in *Biopolymers Online*, G.D. Glick ed., Wiley, Weinheim, 2005.
140. Wiegand, I., et al. *Nat. Protoc.* **3**, 163--175, 2008.
141. Radhika, P., et al. *Res. J. Biotech.* **3** (3) 62--63, 2008.
142. Roy, B., et al. *Int. J. Mater. Res.* **105** (3), 296--307, 2014.
143. Fernandes, S.C.M., et al. *ACS Appl. Mat. Inter.* **5** (8), 3290--3297, 2013.
144. Bradford, M.M., et al. *Anal. Biochem.* **72** (1-2), 248--254, 1976.
145. Wood, D.J., & Hull, B. *J. Med. Virol.* **58** (2), 188--192, 1999.
146. Visvesvara, G.S., & Garcia, L.S. *Clin. Microbiol. Rev.* **15** (3), 327--328, 2002.
147. Niu, Q., et al. *J Immunol Methods* **251** (1-2), 11--19, 2001.
148. Owen, G.R. *Eur. Cells Mater.* **9**, 85--96, 2005.
149. El-Henawii, S.A. *J. Mater. Sci. Technol.* **11** (2), 119--121, 1995.
150. Elrehim, M.A., et al. *Macromol. Symp.* **254** (1), 1--8, 2007.
151. Turky, G., et al. *J. Polym Sci, Part B: Polym. Phys.* **48** (14), 1651--1657, 2010.
152. Muscat, D., Stanssens, D.A.W., Heise, A., & Marko, D. *Process for preparing a composition*, **EP Patent No. 1424362A1** June 2, 2004.
153. Fredrickson, G.H., & Bicefano, J. *J. Chem. Phys.* **110** (4), 2181-2188, 1999.
154. Krook, M., et al. *Polym. Eng. Sci.* **42** (6), 1238--1246, 2002.
155. Miri, T. Viscosity and Oscillatory Rheology, in *Practical Food Rheology: An Interpretive Approach*, I.T. Norton et al., Wiley-Blackwell, Chichester, 2011, 7--26.
156. Scott, G. Part III Properties and mechanisms of degradation, in *Biodegradable polymers for industrial applications*, R. Smith et al, CRC Press, Boca Raton, 2005, 357--395.
157. Galán, A.R., et al. *J. Appl Polym Sci.* **74** (9), 2312--2320, 1999.

158. Huh, A.J., & Kwon, Y.J. *J. Control. Release* **156** (2), 128--145, 2011.
159. Beltz, L.A. *Emerging Infectious Diseases, A guide to Diseases, Causative Agents, and Surveillance*, Jossey-Bass, San Francisco, 2011.
160. Zafar, F., et al. *J. Inorg. Organomet. Polym.* **21** (3), 646--654, 2011.
161. Bharathi, N.P., et al. *J. Inorg. Organomet. Polym.* **20** (4), 839--846, 2010.
162. Imai, Y., et al. *J. Biomed. Mater. Res.* **17** (6), 905--912, 1983.
163. Paredes, N., et al. *J. Appl. Polym. Sci.* **69** (8), 1537--1549, 1998.
164. DeFife, K.M., et al. *J. Biomater. Sci., Polym. Ed.* **20** (11), 1495--1511, 2009.
165. Pahovnik, D., et al. *J. Pharm. Sci.* **100** (11), 4700--4709, 2011.
166. Wågberg, L., et al. *Ind. Eng. Chem. Res.* **46** (7), 2212--2219, 2007.
167. Seiler, M., et al. *J. Chem. Eng. Data* **48** (4), 933--937, 2003.
168. Villano, L.D., & Kelland, M.A. *Chem. Eng. Sci.* **64** (13), 3197--3200, 2009.
169. Sari, M.G., et al. *Polym. Int.* **63** (2), 195--205, 2014.
170. Khatibzadeh, M., et al. *Color. Technol.* **126** (5), 269--274, 2010.
171. Morell, M., et al. *Eur. Polym. J.* **46** (7), 1498--1509, 2010.
172. Nyambo, C., et al. *J. Mater. Sci.* **47** (13), 5158--5168, 2012.
173. Yari, H., et al. *J. Appl. Polym. Sci.* **129** (4), 1929--1939, 2013.
174. Chen, L., et al. *Polym. Int.* **60** (12), 1697--1706, 2011.
175. Lin, D., et al. *J. Appl. Polym. Sci.* **121** (2), 957--963, 2011.
176. Pedrón, S., et al. *Acta Biomater.* **6** (11), 4189--4198, 2010.
177. Amin, A., et al. *Polym. Plast. Technol. Eng.* **47** (12), 1250--1255, 2008.
178. Lin, Y., et al. *Biomacromolecules* **9** (10), 2629--2636, 2008.
179. Ondaral, S., et al. *J. Colloid Interf. Sci.* **301** (1), 32--39, 2006.
180. Kobayashi, T., & Fredrickson, B. *Combined with calcium fluoride, fibrous filler, liquid crystalline polymer and polymeric toughening agent; molded or extruded heat resistant plastic automotive motor and lamp housings*, **US20050176835 A1**, Aug 11, 2005.
181. Qin, J., et al. *ACS Appl. Mat. Inter.* **5** (14), 6649--6656, 2013.

Chapter 2

Castor oil based hyperbranched poly(ester amide) resin

Highlights

The twin crises of depletion of the fossil fuels and environmental degradation have necessitated the search for oleaginous plants as techno-economically competitive alternatives. Amongst all others, the non-edible vegetable oils like castor oil hold great potential as a building block in the realm of polymeric materials. In this milieu, the synthesis of hyperbranched poly(ester amide) (HBPEA) resin *via* an $A_2+B_2+A'A_2$ approach using diethanol fatty amide of castor oil as an A_2 monomer, dibasic acids as a B_2 monomer and varying weight percentages of diethanol amine as an $A'A_2$ monomer is documented in the present chapter. This is an attempt to coalesce the innate advantages of using bioresource and hyperbranched architecture bequeathed with multiple numbers of functionality for new perspectives in the domain of advanced surface coating materials. The present study is focused on probing into the varied performance of the same and establishing its supremacy over the linear analog. The superior performance and thermal stability of epoxy-poly(amido amine) cured HBPEA thermosets complemented by microbial and lipolytic degradation forward the same as biodegradable thin film materials.

Parts of this chapter are published in

1. *Prog. Org. Coat.* **75** (4), 569--578, 2012.
2. *Prog. Org. Coat.* **76** (4), 689--697, 2013.

2.1. Introduction

Hyperbranched poly(ester amide) (HBPEA) are embryonic group of polymeric materials¹⁻³ wherein the regular enchainment of ester and amide linkages in a single polymeric backbone endows green credentials to this class of polymers especially when they are obtained from renewable resources. The advent of greener approaches towards technological advancements of HBPEA continues to be a burgeoning prospective owing to their reduced dependence on dwindling petrochemicals and exploration of renewable raw materials.⁴⁻⁶ The use of renewable feedstocks meets the 7th postulate out of the twelve green chemistry principles, which contributes towards sustainability.⁷ Amidst all renewable materials including lignins, carbohydrates and plant proteins, vegetable oils hold platform as potent raw materials for the synthesis of polymers owing to their ease of availability, diversity in structural attributes and inherent biodegradability.⁸ The use of non-edible vegetable oils demands a special merit over edible ones, amongst which castor oil is increasingly becoming a promising bioresource and viable substitute for petroleum-based resources.⁹ It is one of the few naturally occurring triglycerides that comprises of more than nine-tenth ricinoleic acid (a single hydroxyl containing fatty acid) which make them comparable with that of pure chemicals.⁹ The presence of hydroxyl group, miscibility with alcohols and high viscosity bequeath them with unusual versatility to be explored in the realm of advanced polymeric materials.¹⁰

In context to the above, dehydrated castor oil was used as one of the starting materials for the synthesis of bio-based poly(ester amide) (PEA).¹¹ The properties like film forming ability, mechanical and so on of the synthesized PEA limit their practical utility for structural applications. To this end, blending this dehydrated castor oil based PEA with poly(methacrylic acid)¹² and poly(vinyl alcohol)¹³ separately, proved to be a simple and viable technique. Even though the film forming property of the dehydrated castor oil based PEA improved upon such blending with the above conventional polymers,^{12,13} but the level of improvement of properties like moisture absorption and toughness of the former were found to be marginal. Furthermore, the blending process needs an extra operation apart from the synthesis of the individual polymers, and the thermodynamic instability of these partially miscible or immiscible PEA blends further limits their applicability. In addition the authors employed solution blending where large amount of high boiling and deleterious solvent like dimethyl sulfoxide (DMSO) was used.^{12,13}

The foregoing discussion in Chapter 1 was reminiscent of the fact that HBPEA has attested a special niche compared to their linear analogs in terms of low viscosity, high

reactivity and so on. It is relevant to mention that the synthesis of bio-based HBPEA has not been explored so far. Eventually the design of castor oil based HBPEA is envisaged to overcome the afore-stated problems and bring in unique features of hyperbranched architecture. Further curing plays a paramount role in imparting requisite material properties even to the low molecular weight resinous HBPEA, which can wheel a number of application oriented utilities. Amongst the reported approaches as discussed in section 1.2. of Chapter 1 for the synthesis of HBPEA, couple-monomer methodology (CMM) is instigating enormous interests. The scarce availability and gelation problem confronted in the use of the AB_x monomer or even the A_2+B_3 approach provide the *raison d'être* for the efforts in the search of unequal reactivity or multifunctional character of the monomers in CMM.¹⁴

Thus spur by the above discussions, the synthesis of castor oil based HBPEA using an $A_2+B_2+A'A_2$ approach was delved into in this present work. The physico-mechanical properties including percent gel fraction, scratch hardness, tensile strength (TS) and so on of the synthesized HBPEA were investigated. The curing study, rheological behavior and biodegradation were also scrutinized, together with the exploration of its prospective advanced coating applications. Further the superiority of the hyperbranched architecture was proved by comparing the properties with that of its linear analog.

2.2. Experimental

2.2.1. Materials

2.2.1.1. Chemicals

Castor oil

It was purchased from Merck, India. It is viscous (950-1100 mPa s), non-edible and pale yellow colored non-drying oil (possessing iodine value ~82-90). The presence of hydroxyl group (with hydroxyl value ≥ 160) in the glyceride chain of the oil imparts extra stability and good shelf life by preventing the formation of hydroperoxides (inhibiting rancidity unless subjected to extreme heat). The derivative of castor oil (methyl ester) was used as one of the starting chemicals for the synthesis of bio-based HBPEA.

Diethanolamine (DiEA)

It was purchased from Merck, India with chemical purity of 95-99%, density of 1.097 g/mL at 25 °C and molecular weight of 105.14 g/mol. It was kept under vacuum at 75-85 °C for overnight and then stored with 4A type molecular sieves (purchased from Merck, India

with an equilibrium water adsorption capacity at 30 °C, 75% relative air humidity of $\geq 20\%$ and bulk density of 650-700 g/c.c). It was used as an A'A₂ monomer in the transamidation and polycondensation reaction for the synthesis of HBPEA.

Dibasic acids/anhydrides

Maleic anhydride (MA_n) with density of 1.32 g/cm³ at 55 °C and molecular weight of 98.06 g/mol was used after drying in a desiccator for 2 days. It was used as an unsaturated dibasic anhydride (to impart rigidity) for the synthesis of HBPEA. Phthalic anhydride (PhAn) with density of 1.527 g/cm³ at 20 °C and molecular weight of 148.11 g/mol was used as one of the saturated dibasic anhydride to impart flexibility to the backbone of HBPEA. Isophthalic acid (IPhA) with density of 1.54 g/cm³ at 20 °C and molecular weight of 166.13 g/mol was used to improve hydrolytic stability, heat deflection point, toughness and chemical resistance relative to the other phthalic diacid isomers. These two saturated dibasic acid/anhydrides were used after drying *in vacuo* at 50 °C for overnight. All the dibasic acids were purchased from Merck, India.

Catalyst

Sodium (Na) metal with atomic mass of 22.90 g/mol was obtained from Merck, India (purity 98.8%). Elemental Na is kept in paraffin oil as it is highly flammable in air/water, and used after cutting into small pieces as it tarnishes forming a white coating layer of sodium hydroxide and sodium carbonate. Magnesium (Mg) turnings were purchased from SRL, India (purity 99.8%) with atomic weight of 24.31 g/mol. It was purified by thorough treatment with 5-10% aqueous HCl (36.46 g/mol, 11.6 N purchased from Merck, India,) followed by washing with distilled water and acetone and finally dried under vacuum at 45 °C for 30-45 min, and used immediately. Both Na and Mg turnings were used in the preparation of sodium methoxide.

Solvent

N,N-Dimethylacetamide (DMAc) has molecular mass of 87.12 g/mol, density of 0.94 g/cm³ at 20 °C, boiling and melting points of 165-166 and -20 °C respectively. It was used as a solvent after drying over CaO (Merck, India) for an overnight followed by distillation under reduced pressure. The solvents like dimethylformamide (DMF) and DMSO were also distilled in the similar manner. Methanol possesses a molecular mass of 32.04 g/mol, density of 0.79 g/cm³, boiling and melting points of 64.70 and -97.60 °C respectively. Tetrahydrofuran (THF) has molecular mass of 72.11 g/mol, density of 0.89 g/cm³ at 20 °C, boiling and melting points of 65-66 and -108.5 °C respectively. Both methanol and THF were

and used for the biodegradation study. The chemicals like $(\text{NH}_4)_2\text{SO}_4$, Na_2HPO_4 , KH_2PO_4 , $\text{MgSO}_4 \cdot 7\text{H}_2\text{O}$, $\text{CaCl}_2 \cdot 2\text{H}_2\text{O}$, $\text{MnSO}_4 \cdot 5\text{H}_2\text{O}$, $\text{ZnSO}_4 \cdot 7\text{H}_2\text{O}$, H_3BO_3 , $\text{CuSO}_4 \cdot 7\text{H}_2\text{O}$, $\text{FeSO}_4 \cdot 7\text{H}_2\text{O}$ and MoO_3 used in the preparation of nutrient broth for the culturing of bacteria were purchased from Merck, India. The borate buffer of pH 8 (as the lipase is active in pH range of 6.5-9) was prepared using disodium hydrogen phosphate (Na_2HPO_4) and sodium dihydrogen phosphate (NaH_2PO_4) (purchased from Sigma-Aldrich, India). The gluteraldehyde solution and ethanol were used as fixing and dehydrating agents for microscopic observation of microbe adhered/degraded samples. The reagents used for the preparation of nutrient broth medium for bacterial culture and gluteraldehyde solution were of reagent grade and purchased from HiMedia, India. Ethanol was procured from Merck, India.

2.2.2. Methods

2.2.2.1. Preparation of 'super dry' methanol and sodium methoxide

At first 'super dry' methanol was obtained by the standard method, which was further used for the preparation of NaOCH_3 .¹⁵ Briefly, the distilled methanol was refluxed with iodine-activated Mg turnings and the distillate obtained on subsequent distillation was known as 'super dry' methanol, which was kept with 4A type molecular sieves prior to use.¹⁵ NaOCH_3 was then prepared by adding Na metal to the stirred solution of 'super dry' methanol followed by refluxing and vacuum distillation, and finally dried to the powdered form and kept in a desiccator before use.¹⁶

2.2.2.2. Preparation of methyl ester of castor oil

Castor oil (1 mmol) was refluxed with molar excess (10 mmol) of 'super dry' methanol in the presence of NaOCH_3 (1 wt% with respect to oil) as the catalyst for 4-5 h under the blanket of nitrogen. The excess methanol was distilled off and extracted (from glycerol) with petroleum ether. It was then washed with NaCl solution and dried over anhydrous Na_2SO_4 followed by distilling off the petroleum ether.¹⁷ The yield of methyl ester of castor oil (MECO) obtained was found to be about 95%.

2.2.2.3. Preparation of diethanol fatty amide of castor oil

A nitrogen-flushed two-necked reactor vessel equipped with a mechanical stirrer was charged with MECO and DiEA by maintaining the mol ratio of 1:1.2 in presence of 0.5 wt% NaOCH_3 (with respect to MECO) as the catalyst. The reaction mixture was heated to 110-115 °C for 4 h with constant stirring. The crude product was washed with water to remove excess

distilled and kept with 4A type molecular sieves prior to use. Petroleum ether with a density of 0.67 g/cm^3 at $20 \text{ }^\circ\text{C}$ and boiling point of $60\text{-}80 \text{ }^\circ\text{C}$ was used as received for extraction of methyl ester of the oil. All the solvents were purchased from Merck, India with a chemical purity of $\geq 98.0\%$.

Miscellaneous chemicals

Sodium chloride (NaCl) has a density of 2.16 g/cm^3 , molar mass of 58.44 g/mol , boiling and melting points of 1413 and $801 \text{ }^\circ\text{C}$ respectively. The saturated aqueous solution of the same was used for washing of methyl ester of the oil. Anhydrous sodium sulfate (Na_2SO_4) with molecular mass of 142.04 g/mol and density of 2.66 g/cm^3 was used as desiccant in the drying of methyl ester of the oil. Both the salts were obtained from Merck, India with a chemical purity of 99.5% .

Curing agent

Epoxy based curing system: The commercial diglycidyl ether of bisphenol A based epoxy resin (Araldite GY250) with an epoxy equivalent of 190 g/equiv , viscosity of $450\text{-}650 \text{ mPa}\cdot\text{s}$ at $25 \text{ }^\circ\text{C}$ and density of 1.15 g/cm^3 at $25 \text{ }^\circ\text{C}$ was purchased from Ciba Geigy, India. Poly(amido amine) (HY840) with an amine value of $5\text{-}7 \text{ equiv/kg}$, viscosity of $10000\text{-}25000 \text{ mPa}\cdot\text{s}$ at $25 \text{ }^\circ\text{C}$ and density of 0.98 g/cm^3 at $25 \text{ }^\circ\text{C}$ was purchased from Ciba Geigy, India. Cycloaliphatic amine (amine value $260\pm 30 \text{ mgKOH/g}$ and viscosity of $38\text{-}60 \text{ cPs}$ at $25 \text{ }^\circ\text{C}$) was procured from Asian Paints (I) Ltd., India. A combination of epoxy with poly(amido amine) or cycloaliphatic amine was used as a curing system for the resins. These components were used as received without any purification.

Conventional curing system: Methyl-ethyl ketone peroxide and cobalt octoate were obtained from the local market India. Methyl-ethyl ketone peroxide is a clear liquid with density of 1.053 g/mL and cobalt octoate is 2% solution of cobalt octoate in cyclohexanone. Styrene was obtained from Merck, India with $\geq 99\%$ purity and density of 0.91 g/mL , and containing tertiary butyl catechol as the inhibitor. The inhibitor was removed by washing with 4% sodium hydroxide (Merck, India) solution followed by distilled water and then drying over a calcium hydride (Merck, India). This curing system is generally used for free-radical crosslinking of unsaturated resin.

2.2.1.2. Microbial strains and enzyme

The bacterial strains viz., *Pseudomonas aeruginosa* (MTCC 7814) and *Bacillus subtilis* (MTCC 441), and lipase with an enzyme activity of $40\text{-}70 \text{ U (unit)/mL}$ protein, were obtained from the Department of Molecular Biology and Biotechnology, Tezpur University

DiEA. Quantitative yield of diethanol fatty amide of castor oil (DEFA) obtained by this technique.

2.2.2.4. Synthesis of linear and hyperbranched resins

HBPEA was synthesized *via* an $A_2+B_2+A'A_2$ approach using DEFA as the A_2 monomer, dibasic acids/anhydrides like MAn, PhAn and IPhA (30:35:35 mol ratio) as the B_2 monomer with varying weight percentages of DiEA (5, 10 and 15 wt% with respect to DEFA) as the $A'A_2$ monomer in the presence of 0.8 wt% NaOCH₃ (with respect to DiEA) as the catalyst. The reaction mixture was initially heated at 150 °C for 30 min, then at 185 °C for another 1.5 h and finally at 200-220 °C for 10 min with continuous mechanical stirring under the nitrogen atmosphere, until a viscous mass was obtained. The product obtained was dried under vacuum at 50 °C for 24 h and then kept in an air tight container. The resins synthesized using 5, 10 and 15 wt% DiEA were coded as HBPEA5, HBPEA10 and HBPEA15. The linear analog of this hyperbranched polymer was synthesized by the afore-stated procedure and under the same conditions described above without using any $A'A_2$ monomer and coded as PEA.

2.2.2.5. Curing of resins

The synthesized PEA resin was cured by using three curing systems comprising of epoxy based curing systems with poly(amido amine) and cycloaliphatic amine, separately and methyl-ethyl ketone peroxide, cobalt octoate and styrene curing system. In the first system, the resin was mechanically mixed with epoxy resin (at 60:40 weight ratio) followed by mixing with poly(amido amine) (50 wt% with respect to epoxy resin) and the cured system was coded as PEA1. In the second system, the resin was cured with the same epoxy resin (at 60:40 weight ratio) and cycloaliphatic amine (25 wt% with respect to epoxy resin as higher weight percent resulted in brittle material) by the similar process as above and coded as PEA2. The resin was homogeneously mixed with styrene (30 phr, as the reactive diluents), methyl-ethyl ketone peroxide (4 phr, as the initiator) and cobalt octoate (2 phr, as the activator) in the third curing system and the tried to cure system was coded as PEA3. The resin mixtures were cast on mild steel plates (of dimension 150 mm×50 mm×1.60 mm) and glass plates (dimension 75 mm× 25 mm×1.75 mm) under ambient conditions, degassed under vacuum and then baked in furnace at a definite temperature for specified period of time to obtain the desired thermosets. The curing system which provided the best results in terms of performance characteristics was used for the crosslinking of hyperbranched polymers.

2.2.3. Instrumentation

The different physical properties including acid value, saponification value, iodine value, specific gravity and inherent viscosity of the oil, intermediate products and resins were determined by the standard ASTM methods as discussed in section 1.4.1. of Chapter 1. The specific gravity and solution viscosity (0.1 g/dL in THF) of the oil, reaction intermediates and the resins were measured at (30 ± 0.1) °C using pycnometer and Ubbelohde viscometer respectively. The weight-average molecular weight (M_w) and polydispersity index (PDI) of the resins were obtained by gel permeation chromatography, GPC (Waters 515 HPLC Pump, Waters 2489 RI detector) with polystyrene as the standard and THF as the eluent at 25 °C. FTIR spectra were recorded by Impact-410, Nicolet, USA after grinding the sample with KBr (Sigma Aldrich, India) pellet which melts upon exerting pressure and thereby seals the sample into a matrix. ^1H and ^{13}C NMR spectra were recorded by 400 MHz FTNMR (JEOL, Japan) spectrometer using CDCl_3 (Merck, India) as the solvent and tetramethylsilane (purchased from Merck, India) as the internal standard with total scans of 32 and 2000 respectively, after purification (by re-precipitation technique using THF as good solvent and water as the bad solvent) of the resinous products. The rheological behavior of the resins was studied using a rheometer, CVO100 (Malvern, UK) with a 20 mm diameter parallel plate under controlled rate and steady strain of 20 Pa at room temperature. The solubility of the same in different solvents ranging from highly polar to non-polar hydrocarbon solvents was determined at room temperature using 0.01 g/mL of sample.

Thermogravimetric analysis was carried out in Shimadzu TGA-50 thermal analyzer, USA by heating ~5 mg of the vacuum dried thermosets from 25 to 700 °C using under 30 mL/min nitrogen flow rate. The mechanical properties such as TS and elongation at break (EB) of the thermosets were measured using a universal testing machine (UTM) of model Zwick Z010, Germany with a load cell of 5 kN and at 40 mm/min jaw separation speed as per the ASTM methods mentioned in section 1.4.5.1. of Chapter 1. The gloss characteristic of the thermosets was measured by a mini glossmeter (Sheen instrument Ltd, U.K) at an angle of incidence of 60°. The scratch hardness test of the thermosets was performed by a scratch hardness tester (Sheen instrument Ltd, UK, Model no. 705) moving at the speed of 6 mm/s. Impact resistance was determined by an impact tester (S.C. Dey Co., India) as per the standard falling weight (ball) method wherein a weight of 850 g was allowed to fall on the film coated on a mild steel plate from minimum to maximum falling heights of 100 cm. The maximum height up to which the film was not damaged was noted as the impact resistance. The

chemical resistance test was performed in according to the ASTM method mentioned in section 1.4.5.3. of Chapter 1.

The surface morphology of the thermosets was observed by scanning electron microscope (SEM) (model JSM-6390LV, JEOL, Japan) after platinum coating on their surfaces. The microbes adhered onto the biodegraded films were chemically fixed using 2.5-3% (w/v) of gluteraldehyde followed by dehydration in gradient of different ethanol-water concentrations (20-100% (v/v) ethanol) and air drying for probing into the morphological texture of the same using SEM. The total organic carbon content (TOC) of aqueous solution post enzymatic degradation was determined using a Shimatzu liquid TOC-2 instrument.

2.2.4. Biodegradation study

Bacterial degradation

A nutrient broth was prepared by dissolving 2.0 g $(\text{NH}_4)_2\text{SO}_4$, 2.0 g Na_2HPO_4 , 4.75 g KH_2PO_4 , 1.2 g $\text{MgSO}_4 \cdot 7\text{H}_2\text{O}$, 0.5 mg $\text{CaCl}_2 \cdot 2\text{H}_2\text{O}$, 100 mg $\text{MnSO}_4 \cdot 5\text{H}_2\text{O}$, 70 mg $\text{ZnSO}_4 \cdot 7\text{H}_2\text{O}$, 10 mg H_3BO_3 , 100 mg $\text{CuSO}_4 \cdot 7\text{H}_2\text{O}$, 1 mg $\text{FeSO}_4 \cdot 7\text{H}_2\text{O}$ and 10 mg MoO_3 in 1.0 L of millipore water. The nutrient media was sterilized and cooled down to room temperature before culturing the bacterial strains (for 2 days at 37 °C) in the same. UV sterilized cured films (≈ 250 mg) were incubated in a conical flask containing the culture media inoculated with 100 μL of microbes ($1 \times 10^8 \text{ mL}^{-1}$ as calculated from McFarland turbidity method)¹⁸. The culture media containing no polymer film was taken as the negative control for the study. The bacterial growth was scrutinized spectrophotometrically at 600 nm against the blank culture media at the regular interval of one week and calculated from the absorbance data using McFarland turbidity as the standard.¹⁸ The weight loss profile of the same (averaged over three specimens) was also evaluated to delve into the bio-erosion of the films. The bacterial adhesion on to the films was studied from SEM micrographs.

Enzymatic technique

The weighed amount of the films was immersed in borate buffer solution (having pH 8) containing lipase at 37 °C. The weight loss profile of the films was determined post immersion (after 7, 14, 21 and 28 days) in the buffer solution. The film without the enzyme was taken as the negative control. The TOC of aqueous solution produced upon enzymatic degradation was determined using the following equation (2.1):

$$\text{TOC}_{\text{reported}} = \text{TOC}_{\text{hydrolytic degradation with enzyme}} - \text{TOC}_{\text{hydrolytic degradation without enzyme}} \quad \text{-----} \quad (2.1)$$

The surface plots of SEM micrographs of enzyme degraded thermosets were generated using Fiji software.¹⁹ The luminance of an image was interpreted as height for the

plots. The image was scaled internally to a square image using nearest neighbor sampling and the bounding box of the selection was used for the surface plot.

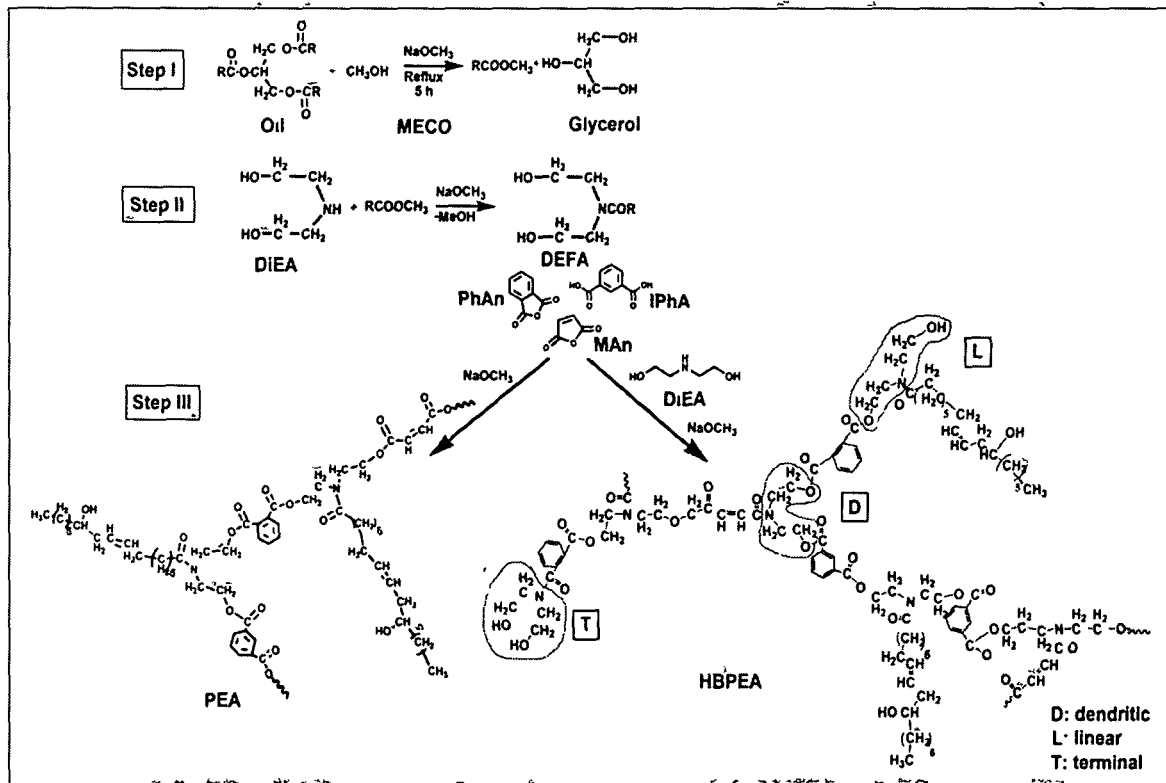
2.3. Results and discussion

2.3.1. Synthesis of resins

The quantitative yield of the intermediates like MECO and DEFA obtained in the present study is attributed to the use of appropriate reaction conditions and compositions of the reactants including catalyst. The 1:1.2 mol ratio of MECO to DiEA together with the removal of methanol formed during the course of the reaction helped to drive the transamidation reaction to completion and result in quantitative yield of DEFA (which is in contrast to all other preceding reports).^{4-6,20-25} The mol ratio of saturated:unsaturated diacids maintained at 30:70 helped to achieve optimum performance. The stability at resinification temperature and protection from UV radiation forms the rationale behind the use of PhAn.²⁶ The aromatic diacid, IPHA is resistant to hydrolysis (relative to PhAn) at pH 4-8 which is important in context of its use in outdoor coating formulations (exterior durability).²⁶ A combination of the two saturated dibasic acids was used for attaining the optimum performance of the resins.

The use of DiEA played a profound role in the generation of branching unit in the hyperbranched architecture of the resin. The polycondensation reaction of B₂ (dibasic acids/anhydrides) with A₂ (DEFA) and A'A₂ (DiEA at three different weight percentages *viz.*, 5, 10 and 15 respectively) monomers resulted in the formation of hyperbranched polymers (Scheme 2.1) with about 80% yield in all the cases. The A and A' functionalities reacted differentially with B₂. B-BA'-A₂ intermediate is formed *in-situ* during the reaction (of B₂ with A'A₂) and thereby the tendency for gelation was circumvented. However the absence DiEA (branch generating unit) in PEA rules out any probability of gelation. As discussed in section 1.2. of Chapter 1, the occurrence of gelation between dihydroxyalkyl amine and dibasic acids/anhydrides is due to the spontaneous chain reaction in the bulk polymerization process.²⁷ In this milieu, DEFA acts as a reactive diluent and maintains the low medium viscosity during polymerization reaction and thus makes it a solution rather than bulk polycondensation in the early reaction stage when the amount of different reactants is high. Moreover DEFA does not exhibit any kind of equilibrium between its isomeric states (hydroxyl-amide/ester-amine)²⁷ (as shown in Scheme 1.1 of Chapter 1) owing to steric factor of long fatty acid chains of the vegetable oils. Accordingly the attack of 2-aminoalkyl ester

with oxazolinium species gets suppressed even at high temperature due to dilution and hence gelation is averted. In a nutshell, DEFA serves as the difunctional monomer in the synthesis of HBPEA and thus imparts the advantages of the solution polymerization and thereby tailoring –OH/alkyl chain ratio at the periphery of the polymeric architecture together with the added facet of adequate bio-content without encountering any probability of side reactions.



Scheme 2.1 Synthesis of resins

2.3.2. Physical properties of resins

The physical properties of resins like color, acid value, saponification value, specific gravity and inherent viscosity are given in Table 2.1. The low acid values of the resins affirmed that the reaction between diols and dibasic acids has almost reached completion. M_w (2793 and 2263 g/mol for PEA and HBPEA10 respectively) and saponification value (145 and 128 mgKOH/g for PEA and HBPEA10 respectively) of the resins indicate the presence of 7.23 and 5.17 equivalent ester groups/molecule of PEA and HBPEA respectively (Table 2.1). The formation of sufficient amount of ester linkages in the molecular chain of the resins was also further corroborated with FTIR study (as discussed below in section 2.3.3.). It was evident from Table 2.1 that M_w and number equivalent ester groups/molecule of HBPEA and its linear analog were almost comparable. However the controlled polymerization reaction

and molecular growth of HBPEA resulted in narrower distribution (or PDI) than that of PEA (Table 2.1).²⁸ The relatively low value of inherent viscosity of HBPEA in comparison to its linear analog is attributed to the formation of highly branched structure of the former with low hydrodynamic volume.²⁸

From the solubility study, it was observed that HBPEA was completely soluble in most of the polar solvents like DMAc, DMF, DMSO and THF, partially soluble in methanol but insoluble in petroleum ether, diethyl ether, formic acid and 4% (w/v) aqueous sodium hydroxide solution; whereas the linear polymer remained completely insoluble in methanol and only partially soluble in THF. Moreover, owing to the presence of the low secondary forces, HBPEA are found to exhibit higher solubility (1.2 g/mL) in a THF as compared to its linear analog (0.5 g/mL), which further supported the formation of hyperbranched structure of the synthesized resin.¹⁴

Table 2.1 Physical characterization of castor oil, MECO, DEFA and resins

Property	Oil	MECO	DEFA	PEA	HBPEA5	HBPEA10	HBPEA15
Color	Light yellow	Yellowish white	Yellowish brown	Light brown	Light brown	Light brown	Light brown
Acid value*	0.32	2.5	2.5	2.55	2.51	2.5	2.52
Saponification value*	180	175	-	145	128	128	130
Specific gravity	0.95	0.90	0.96	0.98	0.99	0.98	0.98
Viscosity**	0.06	0.05	0.07	0.09	0.06	0.04	0.04
M _w (g/mol)	-	-	-	2793	-	2263	-
PDI	-	-	-	1.93	-	1.39	-

* (mg KOH/g)

** η_{inherent} in 0.2% THF at 25 °C

2.3.3. FTIR study

FTIR spectra of castor oil, MECO, DEFA, PEA resin, PEA1 and PEA2 (before curing) are shown in Fig. 2.1. The sharp absorption band of MECO at around 1736 cm⁻¹ (Fig. 2.1b) confirmed the formation of the ester linkages.^{20,21} The various literature reports on FTIR spectrum of DEFA showed the presence of carbonyl amide band together with a carbonyl ester band at around 1736 cm⁻¹.^{4-6,20-25} The disappearance of the band for carbonyl

ester and the appearance of a carbonyl amide band at around 1620 cm^{-1} affirmed the formation of DEFA (Fig. 2.1c). Further, the appearance of both the carbonyl ester and amide FTIR bands (Fig. 2.1d) confirmed the formation of the ester and amide linkages in the resins. PEA1 and PEA2 before curing (Fig. 2.1e and f) showed blue shifting together with decrement in the intensity of $-\text{OH}$ band upon curing, indicating the occurrence of H-bonding of PEA with epoxy-poly(amido amine) and epoxy-cycloaliphatic amine curing systems separately.

However the shifting of carbonyl ester band from 1735 cm^{-1} in MECO to $1725\text{--}1727\text{ cm}^{-1}$ in hyperbranched resins (Fig. 2.2a-c) is attributed to the introduction of double bond (from dibasic acids/anhydrides) adjacent to the carbonyl group, which lead to delocalization of π -electrons and consequently lowering their force constants and absorption frequencies. On the other hand the conjugation of the amide moiety with the aromatic rings led to an increment in the absorption frequency of the amide linkage from 1620 cm^{-1} in DEFA to $1631\text{--}1638\text{ cm}^{-1}$ in hyperbranched resins. This increment is ascribed to the introduction of sp^2 -hybridized carbon atoms in the molecular chain which increased the bond order and consequently the bond strength. In addition to the above bands, the $-\text{OH}$ absorption band appeared at 3420 cm^{-1} , C-O (ester) at 1177 cm^{-1} , C-N at 1070 cm^{-1} , $-\text{CH}_2$ asymmetrical and symmetrical stretching at 2926 cm^{-1} and 2857 cm^{-1} respectively, which confirmed the presence of important linkages in the structure of the resins.

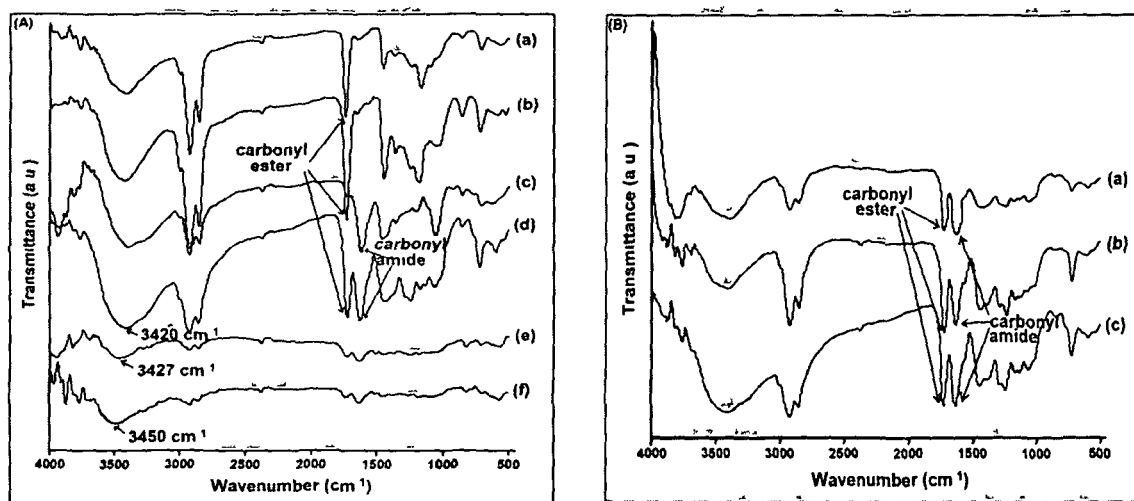


Fig. 2.1 FTIR spectra of (A) castor oil (a), MECO (b), DEFA (c), PEA resin (d), PEA1 (before curing) (e) and PEA2 (before curing) (f), and (B) HBPEA5 (a), HBPEA10 (b) and HBPEA15 (c) resins

2.3.4. NMR study

^1H NMR of MECO, DEFA and PEA, and HBPEA5, HBPEA10 and HBPEA15 resins are shown in Fig. 2.2 and Fig. 2.3 respectively. The peaks (expressed in ppm) of the fatty acid part of the oil due to the terminal $-\text{CH}_3$ at 0.89, internal $-\text{CH}_2$ at 1.22–1.31, β - CH_2 protons to $-\text{OH}$ at 1.44–1.45 and β' - CH_2 protons to $-\text{OH}$ on double bond side at 2.2, and protons of MAn, PhAn and IPhA at 2.63, 7.6–8.0 and 7.5–8.3 respectively were observed in the spectra.^{23,29} On one hand the $-\text{CH}$ proton attached to the $-\text{OH}$ group of ricinoleic acid and $-\text{CH}_2$ protons attached to the $-\text{OH}$ of the fatty amide group were found at 3.5 ppm and 3.9 ppm respectively (Fig. 2.2). On the other hand, upon substitution of $-\text{OH}$ peaks by ester moieties, the peak values shifted to 3.7 ppm and 4.4 ppm (when both $-\text{OH}$ groups of DEFA are replaced by ester moieties)³⁰ respectively (Fig. 2.3). However when either of the two $-\text{OH}$ groups of DEFA is attached to ester moiety, the peak shifted to 4.3 ppm.

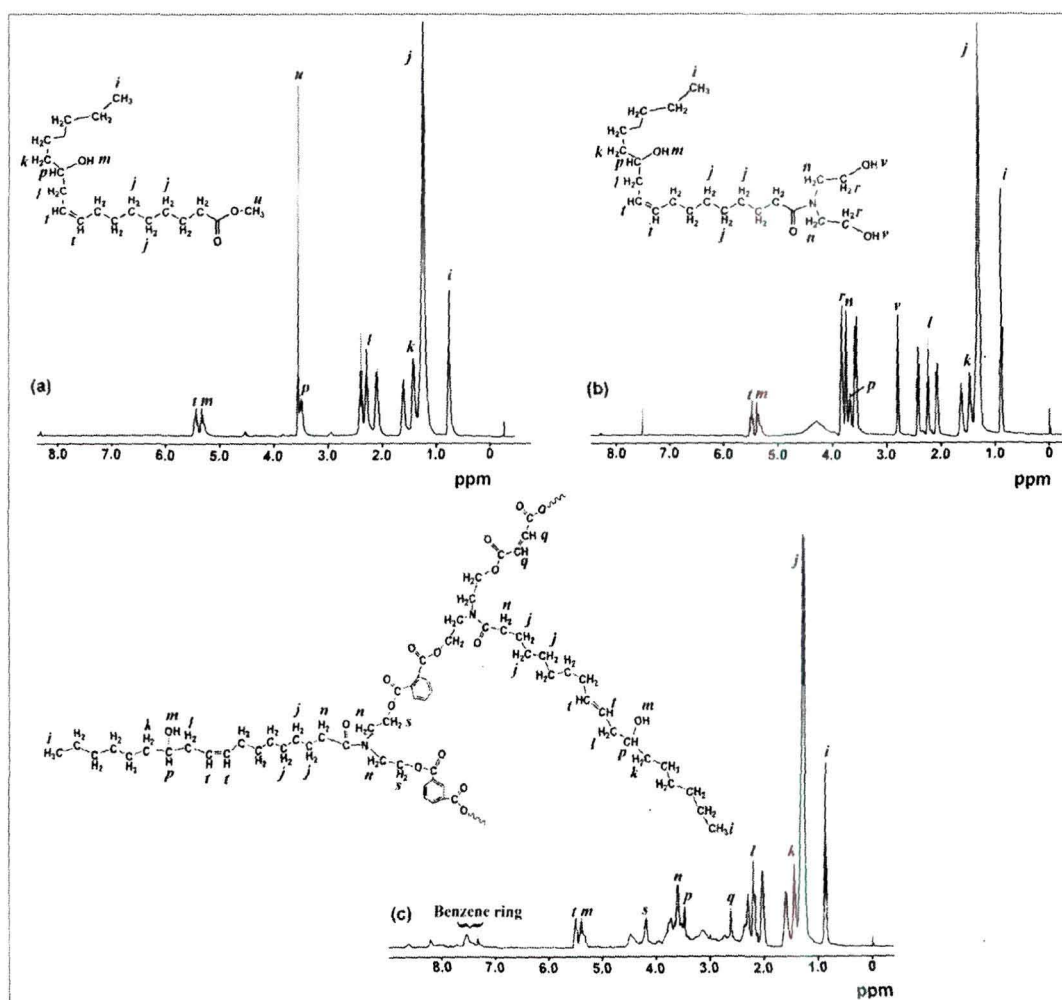


Fig. 2.2 ^1H NMR spectra of MECO (a), DEFA (b) and PEA resin (c)

The integration ratio of substituted to the sum of substituted and unsubstituted in case of PEA (Fig. 2.2) indicated the extent of $-OH$ substitution in the resin. The observed integration ratio was 1.91, which indicated that out of three $-OH$ groups 1.91 $-OH$ groups were only substituted. This integration ratio reflected that the molecular architecture of the synthesized resin was linear since the integration value of more than two only results in the formation of branched structure.

The degree of branching (DB) was determined by comparing of the integration of 1H NMR peaks for the dendritic (D), terminal (T) and linear (L) units in hyperbranched resins using Frechet's equation. $DB=(D+T)/(D+T+L)$.³¹ The relative amounts of the aforementioned D at ($\delta = 4.4$ ppm), T at ($\delta = 3.9$ ppm) and L at ($\delta = 4.3$ ppm) units were obtained from the integration ratio of 1H NMR spectrum (Fig. 2.3). The DB was found to be 0.67, 0.72 and 0.75 for HBPEA5, HBPEA10 and HBPEA15 resins respectively.

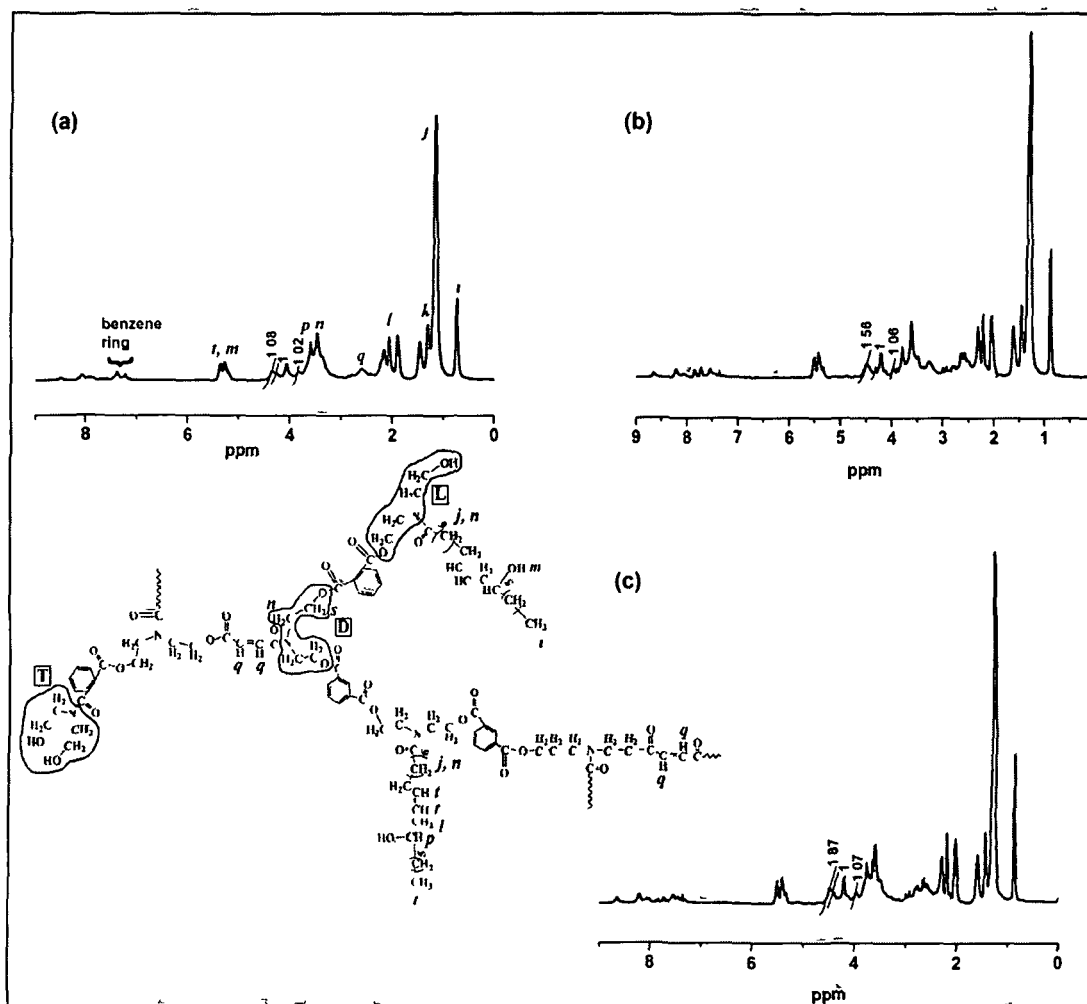


Fig. 2.3 1H NMR spectra of HBPEA5 (a), HBPEA10 (b) and HBPEA15 (c) resins

^{13}C NMR of MECO, DEFA and PEA, and HBPEA5, HBPEA10 and HBPEA15 resins are shown in Fig. 2.4 and Fig. 2.5 respectively. The chemical shift values observed at δ value 14 ppm and 22.6-31.8 ppm are due to the $-\text{CH}_3$ group and $-\text{CH}_2$ of fatty acid chain respectively.³² The peaks (in ppm) observed at 33.8-34.7, 125.4, 132.8, 173-174.5 and 175 are due to the to $-\text{CH}_2$ attached to amide carbonyl, aromatic carbons, ring carbon attached to $-\text{COOCH}_2$ group of resin, $-\text{C}=\text{O}$ of ester and amide groups respectively.³²

2.3.5. Rheological study

The shear viscosities of castor oil, PEA and its intermediates determined under controlled rate and steady strain of 20 Pa at room temperature showed Newtonian-type behavior (Fig. 2.6). MECO exhibited lower dynamic viscosity compared to the oil. This is due to the lower molecular mass and inter-/intra- molecular attraction of MECO than the oil. However, PEA resin exhibited the highest viscosity amongst the studied systems. The viscosity of a material is related to the dynamic extension, segment density and intermolecular chain entanglement within the volume of the same.³³ The high viscosity of PEA resin is attributed to the entanglements among molecular chains, and the presence of intermolecular interactions among different functionalities like amide and hydroxyl groups.³² HBPEA5 and HBPEA10 resins, however, exhibited Newtonian-like while HBPEA15 resin showed rheopectic behavior under similar isothermal conditions (Fig. 2.6). The increment of the A'A₂ monomer content led to the buildup of secondary interactions like H-bonding, polar-polar interactions and so on between the polar functionalities like ester, amide and hydroxyl groups, which consequently enhanced the viscosity. However the rheopectic behavior of HBPEA15 resin is attributed to the alignment of molecular chains with increasing shear in the direction perpendicular to the applied force, owing to the presence of such interactions. The effect of shear rate on shear viscosity of the resin together with the intermediates and oil are shown in Fig. 2.7 (A). The decrease of viscosity of PEA resin with shear rate (2-100 s⁻¹) indicated shear thinning behavior; while all other intermediates showed Newtonian-like behavior i.e. their shear viscosity is independent of shear rate. The rheological behavior of hyperbranched resins studied in steady shear mode was found to be dependent on the loading of A'A₂ monomer (Fig. 2.7 (A)). HBPEA5 and HBPEA10 resins showed a shear thinning behavior, attributed to the micro-structural deformation particularly the molecular alignments and disentanglements of the long polymer chains with the increasing shear rate. The main mechanism of stress relaxation (and shear thinning) is the rate at which the chain detachment occurred from the elastically active network, activated by the elastic force in the chain, which

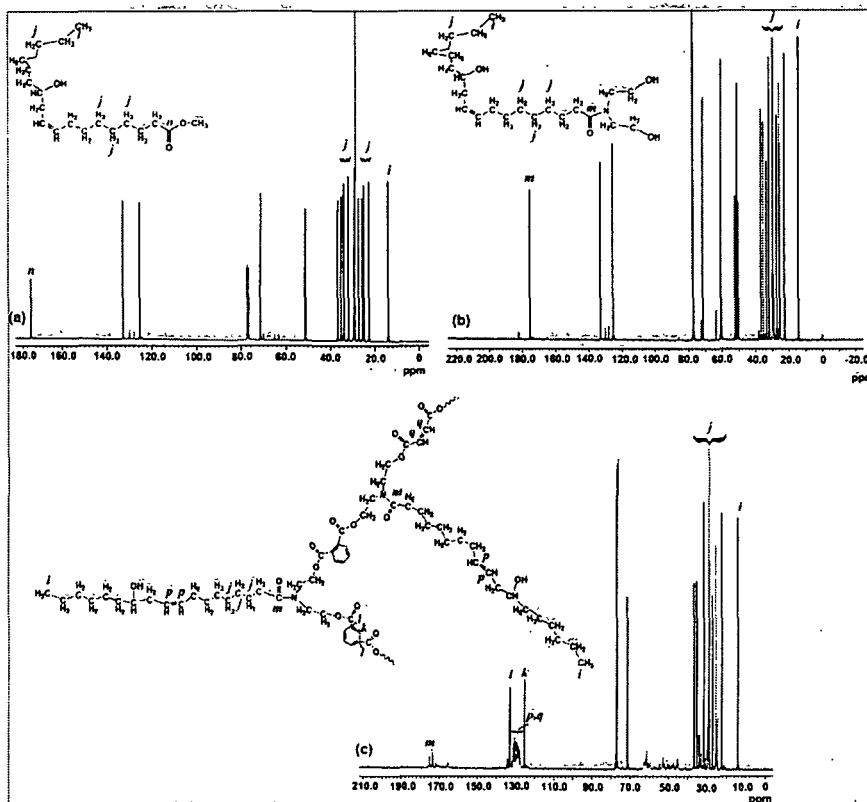


Fig. 2.4 ^{13}C NMR spectra of MECO (a), DEFA (b) and PEA resin (c)

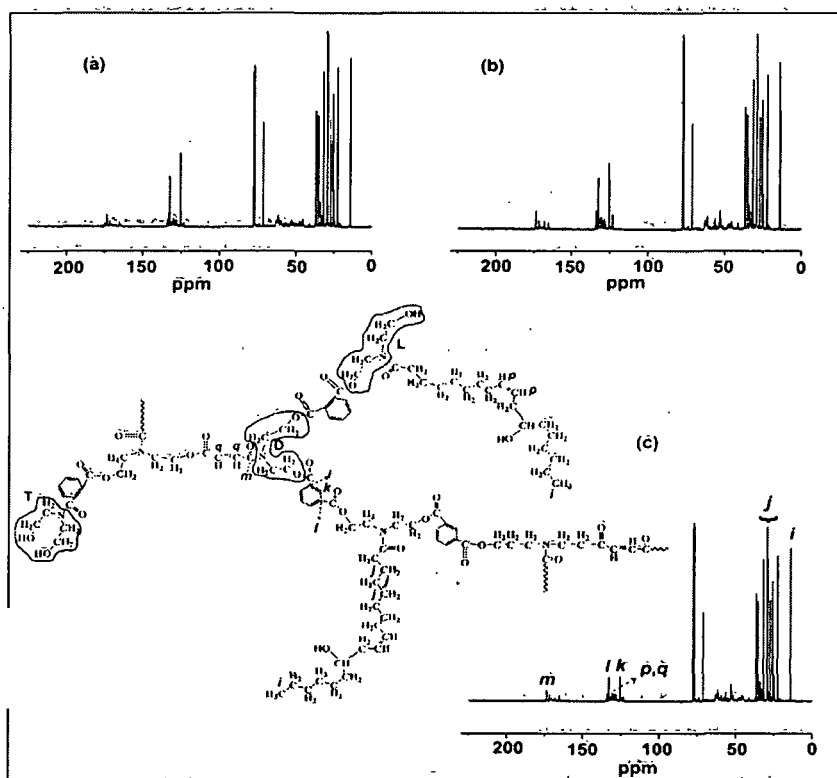


Fig. 2.5 ^{13}C NMR spectra of HBPEA5 (a), HBPEA10 (b) and HBPEA15 (c) resins

consequently resulted in the drop in viscosity.³¹ The shear thinning nature of the resin implied that the flowability of the resin increased with increment in the rate of shear. This behavior of the resins can be related to the fact that the polymer chains became progressively aligned with increase in shear rate in the direction of applied force.³⁴ This shear thinning behavior also signified good processibility of the resins. In other words, instead of the relatively random intermingled state which exists when the resin is at rest, the major axes are brought into line with the direction of flow. The shear viscosity continues to decrease with the increase of apparent shear rate until no further alignment along the streamlines is possible and subsequently the flow curve became linear. However, HBPEA15 resin showed a steep increase in viscosity at lower shear rate, attained a maximum and finally exhibited shear thinning at higher rates. This behavior is attributed to the presence of multitude of surface functionalities which tried to align in perpendicular to the direction of shear stress, attain a threshold shear rate and then align parallel along the direction of shear stress.³⁵

The temperature sensitivity of the shear viscosity of the resins (having a profound effect on the processing conditions) is shown in Fig. 2.7 (B). The shear viscosities of the resins decreased with the increase of temperature in the range of 25-100 °C, indicating that the increase of temperature improved their flow behavior.³⁴ The decrease of resin viscosity with temperature (Fig. 2.7 (B)) is attributed to the increase of molecular mobility with temperature, which in turn decreased the inter-/intra- molecular interactions within the polymer chains (supported by Eyring's theory).³⁶ This observation may be attributed to the increase in the molecular motion or kinetic energy of the polymeric chains which is directly related to the decrease of viscosity.³⁶ It was also found that the temperature sensitivity of shear viscosity was higher in lower shear rate region, which dropped at higher shear rates.³⁶ This phenomenon is in agreement with the fact that elevating shear rate is accompanied by a rapid decrease of the entanglement of macromolecules and hence their viscosities.

2.3.6. Curing study

The curing study of PEA using three different curing systems revealed that the resin was not cured by the conventional methyl-ethyl ketone peroxide-cobalt octoate-styrene curing system, though it was found to be cured by epoxy-poly(amido amine) as well as cycloaliphatic amine systems. PEA films cast on the steel and glass plates were cured at temperatures between 150-200 °C for varied time periods and subsequently their swelling values were monitored to obtain optimum curing temperature and time (Table 2.2). The optimum temperature of baking of PEA was found to be 185 °C for the specified time as

given in Table 2.2. There is a prospect of the occurrence of crosslinking reaction between the hydroxyl groups of the fatty acid part of the resin along with the amino group of the hardener, with the epoxide groups of the epoxy resin in the presence of the amine hardener, which also acts as an active base and thus aids in the curing process. FTIR study of PEA1 and PEA2 (Fig. 2.1(A) e and f) showed the presence of H-bonding between epoxy cured PEA resin with poly(amido amine) and cycloaliphatic amine, separately. Figs. 2.1A (e) and 2.1A (f) showed blue shifting together with the decrement in intensity of H-bonding of –OH band in PEA. The H-bonding so formed due to the associated blue shifting is known as the “weak H-bonding”.³³ In the above cured systems, the epoxy cured PEA acts as a donor (X-H) and both cycloaliphatic amine and poly(amido amine) as acceptors (Y). The above blue shifting is attributed to the increased percentage of ‘s’ character in the X-H moiety when Y approached

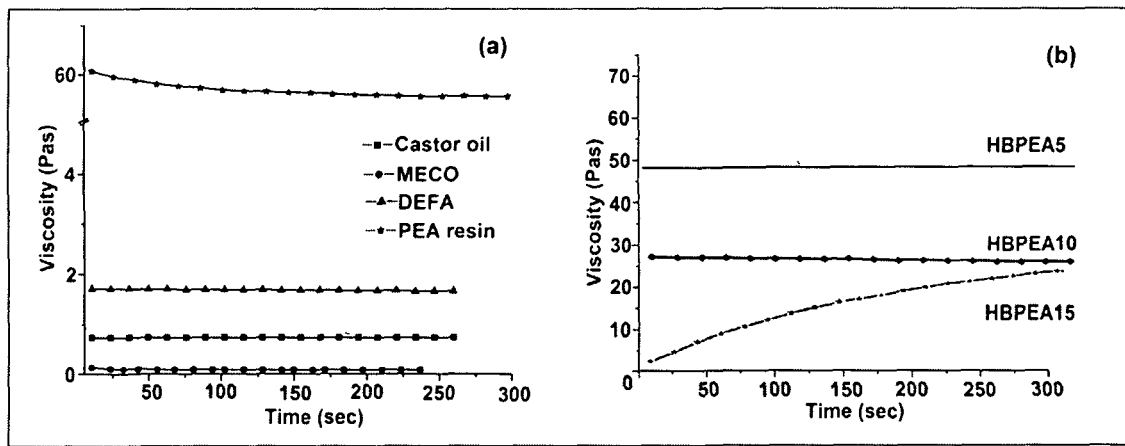


Fig. 2.6 Variation of viscosity as a function of time

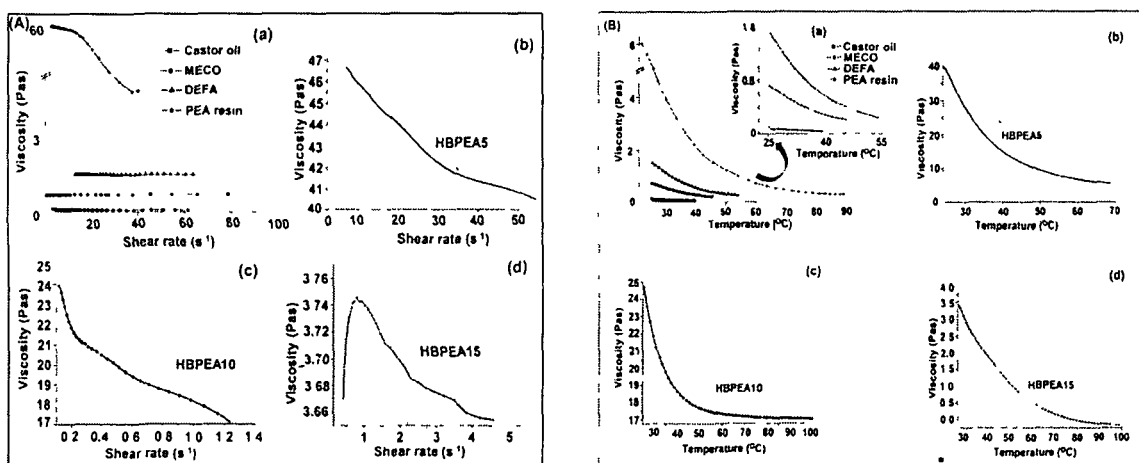
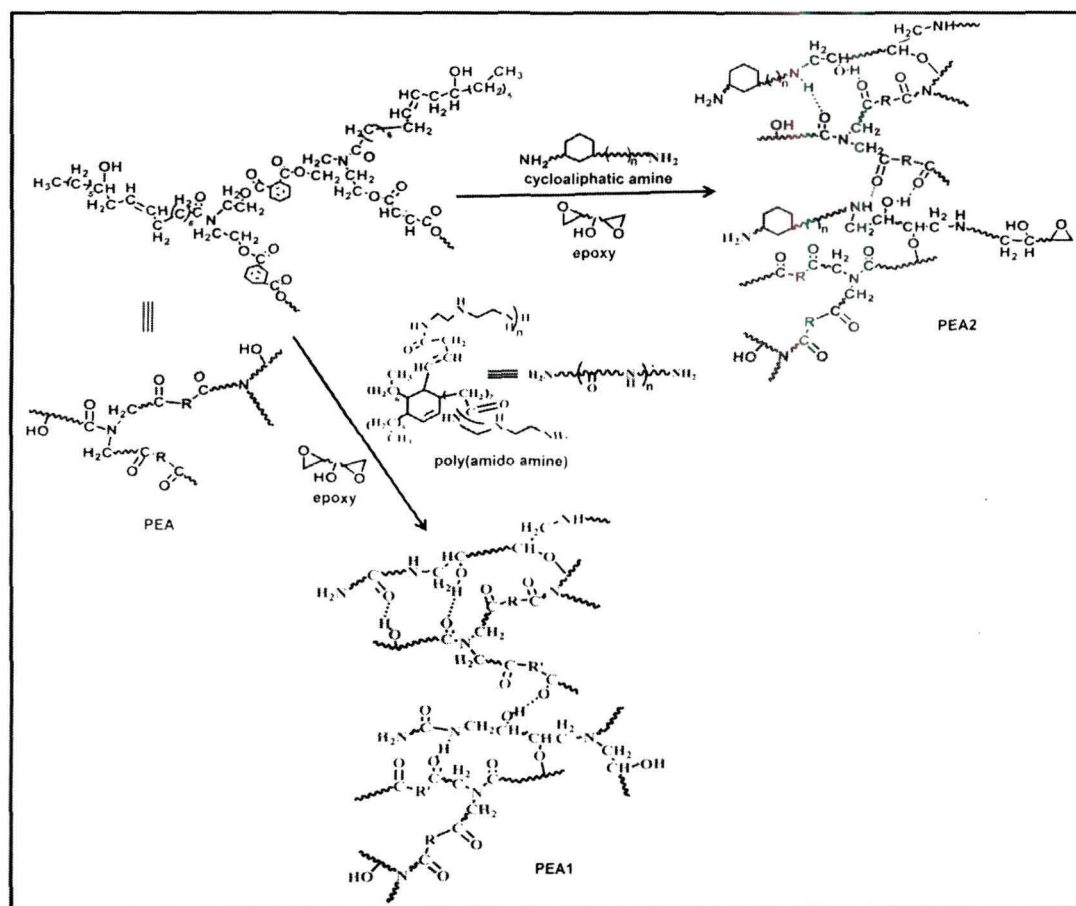


Fig. 2.7 Variation of viscosity with (A) shear rate; and (B) temperature

towards 'H' atom.³⁷ The X-H bond contraction is ascribed to a weak hyperconjugation to σ^* orbital of the donor moiety. There appeared a loss of electron density between H and Y and this depletion is due to the tendency to attract electrons by X in presence of Y, which in turn increased the attraction between X and H causing X-H bond to contract.³⁷ Since cycloaliphatic amine is more basic (strong H-bonding acceptor) compared to the poly(amido amine), the former tends to attract the electron density of X-H bond towards itself more than the latter. Consequently the X-H bond contraction was less in the former compared to the latter. Thus the blue-shifting was more in PEA1 than PEA2. All such possible interactions of PEA with the epoxy, cycloaliphatic amine and poly(amido amine) are shown in Scheme 2.2. The resinous hyperbranched resins were converted to solid thermoset by the process of crosslinking through different types of possible chemical reactions with hydroxyl and epoxide groups of epoxy resin and amino groups of poly(amido amine) hardener with hydroxyl and ester group of the resin. The presence of large number of surface groups of hyperbranched resin compared to its linear analog contributes toward faster hard drying of



Scheme 2.2 Possible crosslinking mechanism for formation of PEA1 and PEA2

the former thermosets than the latter (Table 2.2). It is pertinent to mention that poly(amido amine) was used as the crosslinker with epoxy to cure the resins because it resulted in better performance compared to the other system (as discussed below). The hard dry time, however, decreased with increase of DB (Table 2.2) owing to the increase of surface functionalities.

2.3.7. Physico-mechanical performance study

The performance in terms of gloss, impact resistance, scratch hardness, TS and EB of the thermosets are tabulated in Table 2.2. The gloss values of the cured PEA thermosets reflected good compatibility of the same with the curing systems. However lower gloss value of PEA2 compared to PEA1 may be attributed to the lower dimensional stability of epoxy-cycloaliphatic amine cured thermoset compared to epoxy-poly(amido amine) cured one. Further the cycloaliphatic amine has low molecular weight and it is hygroscopic in nature and thus has a tendency to react with atmospheric carbon dioxide and moisture to form an ammonium carbamate thereby causing blushing or blooming problems, which may also contribute to the low gloss value of PEA2. The high impact resistance of both PEA1 and PEA2 reflected optimum crosslinking (as evident from the percent gel fraction) together with adequate flexibility due to the presence of long hydrocarbon chain of the oil. Better scratch hardness of PEA1 over PEA2 may be due to enhanced combined effect of strength and flexibility of the former than the latter. The long aliphatic chain of poly(amido amine) imparted flexibility to the resin together with strength. TS of PEA1 was found to be higher compared to PEA2, which may be attributed to the optimum crosslinking (as evident from Table 2.2) in the former than in the latter. However, higher EB of the former than the latter may be due to better plasticizing effect of the poly(amido amine), used in PEA1 than cycloaliphatic amine used in PEA2. The changes in mass of the cured films upon immersion in various chemical environments for 30 days are given in Table 2.3. PEA1 exhibited slightly better resistance against different chemical media compared to PEA2 which is due to the optimum curing of PEA1.

It can be inferred from the above discussions that the epoxy-poly(amido amine) cured PEA thermoset showed superior performance together with good chemical resistance compared to cycloaliphatic amine cured one. Thus the curing study gave impetus for the use of epoxy-poly(amido amine) system to crosslink hyperbranched resins. The coating properties (mechanical and optical) of hyperbranched thermosets effectively changed with varying amounts of A'A₂ monomer (Table 2.2). The increase of gloss with A'A₂ moiety in the hyperbranched thermosets indicated their good dimensional stability together with smooth

surface texture. The enhanced synergism of strength and flexibility of the polymeric chains accounted for the increment of scratch hardness of hyperbranched thermosets with A'A₂ monomer content. The change in the impact resistance of the thermosets was difficult to chart out owing to the instrumental limit. The increase of TS and decrease of EB of the thermosets with A'A₂ monomer content was attributed to the increase of crosslinking density in the polymeric structure with DB, as supported by percent gel fraction measurement (Table 2.2). The good chemical resistance (Table 2.3) particularly the alkali resistance of hyperbranched thermosets is ascribed to the presence of amide moiety and adequate amount of crosslinking (Table 2.2).

Table 2.2 *Physico-mechanical performance of thermosets*

Physico-mechanical property	PEA1	PEA2	HBPEA5	HBPEA10	HBPEA15
Curing time (h)	3±0.02	2.5±0.02	2.25±0.01	2.08±0.02	2±0.02
Gel fraction (%)	78.6±0.9	86.1±0.7	74.4±0.7	77.7±0.5	79.82±0.7
Scratch hardness (kg)	8±0.2	6±0.2	8±0.3	8.5±0.2	9±0.2
Impact resistance (cm)*	100	100	100	100	100
Gloss at 60°	90±0.5	82±0.4	85±0.4	90±0.5	93±0.4
TS(MPa)	8.7±0.3	7.3±0.1	7.0±0.3	7.3±0.5	8.7±0.2
EB (%)	114±0.6	98±0.7	94.71±0.8	88.1±0.8	74.57±0.7

*Maximum limit of the instrument is 100 cm

Table 2.3. *Weight changes of thermosets in different chemical media*

Medium	Weight change (g)				
	PEA1	PEA2	HBPEA5	HBPEA10	HBPEA15
Water	1.7×10 ⁻²	3.9×10 ⁻²	1.2×10 ⁻²	2.5×10 ⁻²	2×10 ⁻²
	±0.06	±0.09	±0.06	±0.05	±0.06
5% aq. HCl	2.5×10 ⁻²	4.1×10 ⁻²	2.7×10 ⁻²	3.1×10 ⁻²	2.5×10 ⁻²
	±0.05	±0.08	±0.06	±0.05	±0.05
10% aq. NaCl	5.0×10 ⁻³	1×10 ⁻²	3×10 ⁻³	1×10 ⁻²	1.5×10 ⁻²
	±0.06	±0.08	±0.07	±0.06	±0.06
3% aq. NaOH	1×10 ⁻²	3×10 ⁻²	0.9×10 ⁻²	1.2×10 ⁻²	1×10 ⁻²
	±0.04	±0.07	±0.05	±0.04	±0.04

2.3.8. Thermal study¹

The hyperbranched thermosets exhibited a two-step degradation pattern (Fig. 2.8) with the initial degradation ascribed to the presence of aliphatic segments and thermally labile ester moiety while the final degradation associated with degradation of the thermally stable aromatic moiety and amide linkages in the polymeric backbone.³⁸ The onset decomposition temperature (T_{first}) and initiation of end set/second decomposition temperature (T_{second}) for the thermosets are tabulated in Table 2.4. The increase of surface functionalities with A₂ monomer content ensured increase in reaction probability with the curing system, thereby increasing the rigidity in the structure and hence their thermal stability. It is also worthy to mention that higher thermostability of the hyperbranched thermosets than its linear analog functionalities in the former compared to the latter. However, higher thermal stability of may be attributed to the inter- and intra-molecular forces between the multitude of PEA1 thermoset as compared to PEA2 one is attributed to the adequate crosslinking.

2.3.9. Biodegradation study

Bacterial degradation

The microbial degradation of PEA1 thermoset was probed into using two different varieties of bacteria depending on Gram staining namely *P. aeruginosa* (Gram negative) and *B. subtilis* (Gram positive). It is evident from Fig. 2.9 (a) that the films were degraded to a significant extent post 6 weeks of inoculation. This is indicative of the fact that the bacteria used PEA1 (carbon source) as its growth medium where they can thrive. The differences in the biodegradation, as evident from their weight loss profiles using different bacterial strains showed microbial specificity for the polymer substrate (higher degradation rate of *P. aeruginosa* compared to *B. subtilis*). The difference in their cell wall structures (an active barrier) is supposed to dictate the accessibility of the polymeric substrate. The former possesses higher biosurfactant activity and high cell surface hydrophobicity than the latter and thus are envisaged to colonize the surface of PEA1 and aid in biodegradation process.³⁹

Prompted by the fact that *P. aeruginosa* resulted better biodegradation compared to *B. subtilis*, so the former bacterial strain was used for the degradation of the hyperbranched thermosets. Biodegradation assessed by time-course dependent growth of *P. aeruginosa* (weight loss profiles) augmented in parallel lines with the increase in A₂ monomer content. It is evident from Fig. 2.9 (b) that the bacterial growth (lag phase) took about one week for acclimatization followed by a faster growth from the second week onwards. SEM micrographs (Fig. 2.9 (c-f)) are illustrative of bacterial adherence (and proliferation) on the

surface of hyperbranched thermosets. The increasing trend of biodegradation with A'A₂ monomer content may also be attributed to the increment in the polar functional moieties which aid in fragmentation by oxidation or hydrolysis.

Enzymatic degradation

The extracellular enzymes play key role in the assimilation of fragmented (oxidized and hydrolyzed) products of the thermosets. In this context, dictated by the premonition that lipase biodegrades polymer *via* its oxidative action onto the ester moieties present in the polymeric backbone, the degradation behavior of the thermosets was delved into by the same. The weight loss profiles and TOC measurements of the thermosets attested the increased lipase-induced hydrolysis of hyperbranched thermosets with A'A₂ monomer content (Fig. 2.10 (a-b)). The presence of large free volume in the hyperbranched architecture facilitates greater molecular mobility of lipase targeting the ester moiety of organophilic substrates.⁴⁰ Lipase acts as an ideal catalyst for the fragmentation of thermosets into low molecular weight oligomeric products. SEM micrographs (Fig. 2.10 (c-e)) of lipase inoculated films showed the formation of pores (possibly acting as the focal points of enzymatic invasion) of about ~0.4 μm. The surface plots exhibited wider spectrum of pixel distribution and greater luminance for lipase degraded hyperbranched thermosets, indicating the inhomogeneity of the surface profile of the films post incubation with the biocatalyst.

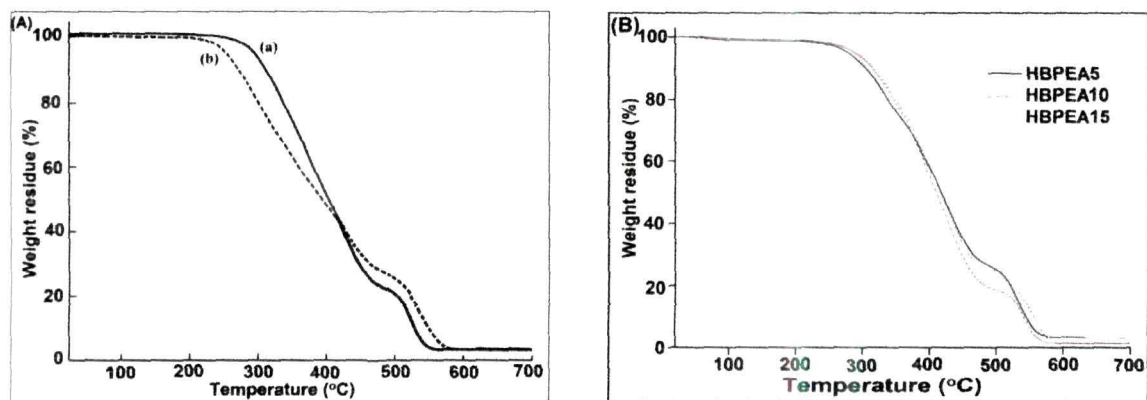


Fig. 2.8 TG thermograms of (A): PEA1 (a), and PEA2 (b); and (B) HBPEA5, HBPEA10 and HBPEA15 thermosets

Table 2.4 Degradation temperatures of thermosets

Degradation temperature	PEA1	PEA2	HBPEA5	HBPEA10	HBPEA15
T _{first} (°C)	250	220	269	277	280
T _{second} (°C)	502	503	508	521	524

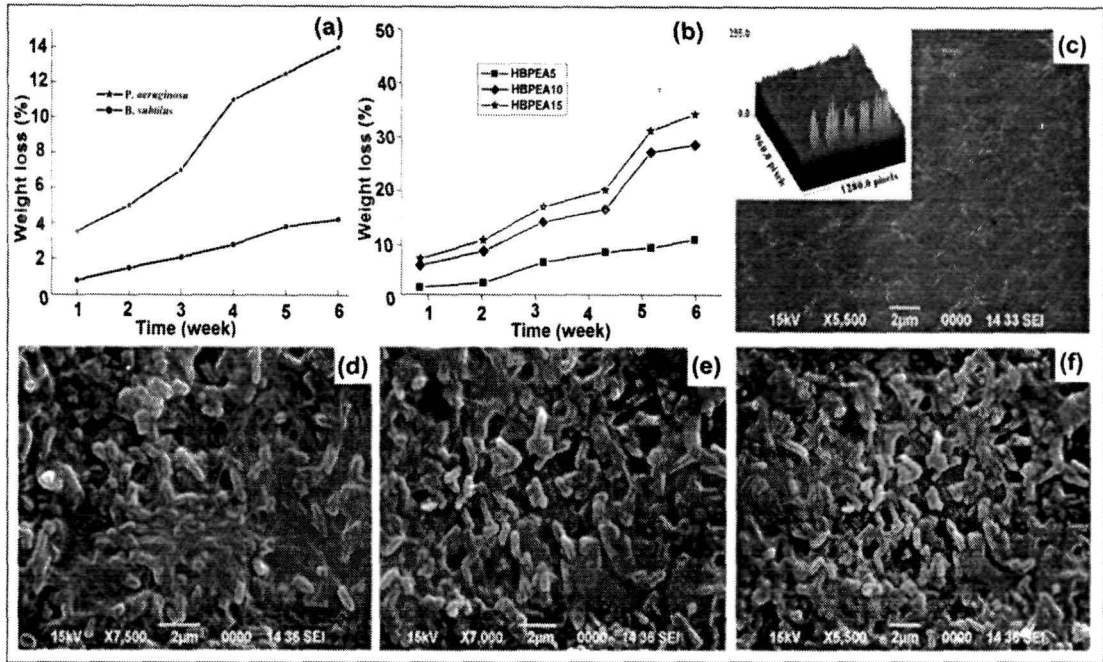


Fig. 2.9 Weight loss profile of PEA (a) and hyperbranched (b) thermosets, SEM micrographs of: HBPEA5 (c), *P. aeruginosa* degraded HBPEA5 (d), HBPEA10 (e) and HBPEA15 (f) thermosets

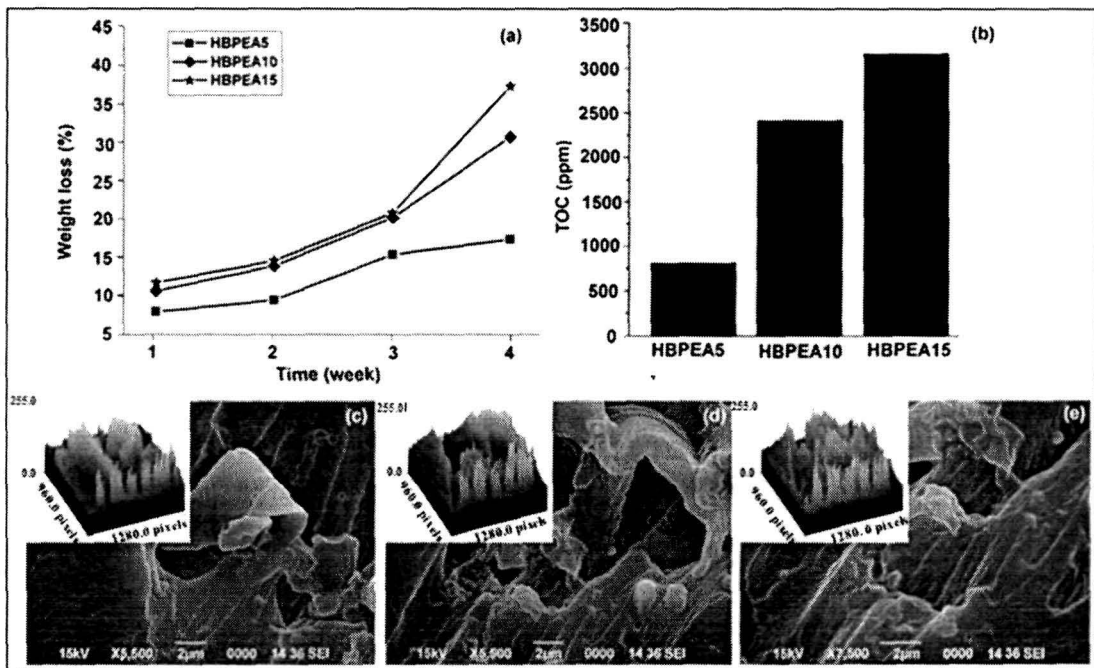


Fig. 2.10 Weight loss profile (a) and TOC measurements (b) of thermosets post enzyme inoculation, SEM micrographs of enzymatically degraded thermosets (with surface plots as the inserts) of HBPEA5 (c), HBPEA10 (d) and HBPEA15 (e)

The plausible layer by layer delamination (or peeling off) of the films post four weeks of enzymatic degradation is envisaged for the high surface roughness (indicated by the non-homogeneity of the surface profile). This indicates that lipase impregnates into the polymeric matrix and thereby assists in the biodegradation process.

2.4. Conclusion

The present chapter describes the use of castor oil in the synthesis of linear and hyperbranched PEA resins. The physico-chemical properties of the synthesized resins were characterized by various analytical and instrumental techniques. FTIR and NMR spectral analyses confirmed the chemical structures of the resins. The rheological study demonstrated differential flow behavior of hyperbranched resins with respect to A'A₂ monomer content. The curing study of PEA showed that the nature of curing system has a profound effect on the properties of the thermoset. The epoxy-poly(amido amine) cured PEA thermoset exhibited better performance compared to the epoxy-cycloaliphatic amine cured one. Thermal stability of the hyperbranched thermosets increased with the increase of A'A₂ monomer content. The study also attested the superiority of bio-based hyperbranched thermosets with varying amounts of multifunctional monomer over the linear analog of the same oil. The desirable scratch hardness, gloss, impact strength and mechanical properties foster them as polymeric thin film materials. The afore-mentioned properties together with the added facet of biodegradability endowed hyperbranched resins with 'green credits' in the arena of advanced surface coating technology. The best performance of HBPEA10 amongst other hyperbranched thermosets has confirmed the potentiality of the same as the matrix for further studies in the preparation of different nanocomposites. For the sake of simplicity, HBPEA10 is denoted as HBPEA in the subsequent chapters.

References

1. Lin, Y., et al. *J. Polym. Sci., Part A: Polym. Chem.* **46** (15), 5077--5092, 2008.
2. Bao, Y., et al., *Polymer* **54** (2), 652--660, 2013.
3. Fotiadou, S., et al. *Macromolecules* **46** (7), 2842--2855, 2013.
4. Shende, P.G., et al. *Pigm. Resin Technol.* **31** (5), 310--314, 2002.
5. Ahmad, S., et al. *J. Macromol. Sci. A* **43** (9), 1409--1419, 2006.
6. Mahapatra, S.S., & Karak, N. *Prog. Org. Coat.* **51** (2), 103--108, 2004.
7. Anastas, P., & Eghbali, N. *Chem. Soc. Rev.* **39**, 301--312, 2010.
8. Raquez, J.M., et al. *Prog. Polym. Sci.* **35** (4), 487--509, 2010.
9. Ogunniyi, D.S. *Bioresour. Technol.* **97** (9), 1086--1091, 2006.
10. Cvengroš, J., et al. *Eur. J. Lipid Sci. Tech.* **108** (8), 629--635, 2006.
11. Shende, P.G., et al. *Pigm. Resin Technol.* **31** (5), 310--314, 2002.
12. Ashraf, S.M., et al. *J. Appl. Polym. Sci.* **103** (2), 1367--1374, 2007.
13. Sharma, H.O., et al. *Int. J. Polym. Mater.* **56** (4), 437--451, 2007.
14. Gao, C., & Yan, D. *Prog. Polym. Sci.* **29** (3), 183--275, 2004.
15. Furniss, B.S., Hannaford, A.J., Smith, P.W.G. & Tatchell, A.R. *Vogel's Textbook of Practical Organic Chemistry*, 5th ed., Pearson, Harlow, 1989.
16. Mabry, T.J., Markham, K.R. & Thomas, M.B. *The Systematic Identification of Flavonoids*, Springer, Berlin, 1970.
17. Meneghetti, S.M.P., et al. *Energ. Fuel* **20** (5), 2262--2265, 2006.
18. Andrews, J.M. *J. Antimicrob. Chemoth.* **56** (1), 60--76, 2005.
19. Schindelin, J., et al. *Nat. Methods* **9** (7), 676--682, 2012.
20. Shende, P., et al. *Pigm. Resin Technol.* **32** (1), 4--9, 2003.
21. Ahmad, S., et al. *J. Appl. Polym. Sci.* **104** (2), 1143--1148, 2007.
22. Meshram, P.D., et al. *Prog. Org. Coat.* **76** (9), 1144--1150, 2013.
23. Bharathi, N.P., et al. *J. Inorg. Organomet. P* **20** (4), 839--846, 2010.
24. Ahmad, S., et al. *J. Macromol. Sci. A* **43** (9), 1409--1419, 2006.
25. Ahmad, S., et al. *Prog. Org. Coat.* **47** (2), 95--102, 2003.
26. Karak, N. *Vegetable Oil-Based Polymers: Properties, Processing and Applications*, Woodhead Publishing Limited, Cambridge, 2012.
27. Froehling, P. *J. Polym. Sci., Part A: Polym. Chem.* **42** (13), 3110--3115, 2004.
28. Karak, N. & Maiti, S. *Dendrimers and Hyperbranched Polymers: Synthesis to Applications*, MD Publications Pvt Ltd, New Delhi, 2008.

29. Zafar, F., et al. *React. Funct. Polym.* **67** (10), 928--935, 2007.
30. Alam, M., et al. *Journal of Chemistry*, **2013**, 962316, 2013.
31. Höfner, D., et al. *Acta Polym.* **48** (1-2), 30--35, 1997.
32. Zafar, F., et al. *J. Inorg. Organomet. P* **21** (3), 646--654, 2011.
33. Asif, A., et al. *Colloid Polym. Sci.* **283** (2), 200--208, 2004.
34. Z. Tadmor & C.G. Gogos (ed.). *Principles of Polymer Processing*, 2nd ed., John Wiley & Sons, New York, 2006.
35. Kumar, A., Gupta, R.K. & Yan, D. (ed.). *Fundamentals of Polymer Engineering*, CRC Press, New York, 2003.
36. Dazhu, C., et al. *Compos. Sci. Technol.* **65** (10), 1593--1600, 2005.
37. Joseph, J., & Jemmis, E.D. *J. Am. Chem. Soc.* **129** (15) 4620--4632, 2007.
38. Ruijter, C.D., et al. *J. Polym. Sci. Pol. Chem.* **46** (19), 6565--6574, 2008.
39. Priya, T., & Usharani, G. *Botany Research International* **2** (4), 284--287, 2009.
40. Zhu, X., Zhou, Y. & Yan, D. *Hyperbranched Polymers: Synthesis, Properties, and Applications*, 1st ed., John Wiley & Sons, Hoboken, 2010.

Chapter 3

Hyperbranched poly(ester amide)/polyaniline nanofiber nanocomposites

Highlights

Spotlighting nanotechnology for revolutionizing the arena of bio-based hyperbranched poly(ester amide) (HBPEA) in pursuit of advanced engineering applications is the need of hour. In the broad milieu of application-oriented electrically conducting nanostructured polymers, polyaniline (PAni) nanofiber has captured a unique niche owing to its controllable conductivity by exploiting doping/de-doping chemistry. PAni nanofiber is thus envisaged to control the build-up of static electric charges, which has been creating electrostatic ignition hazards to both industries and mankind over the years. In this scenario and in continuation of our earlier study, fabrication of bio-based HBPEA/PAni nanofiber nanocomposites proved to be an appealing avenue to impart improvement in the performance of HBPEA, particularly their electrical properties together with addressing the sustainability and industrial requisites. The nanocomposites at different loading of nanofiber were prepared by an *ex-situ* polymerization technique. The efficacy of the green chemistry tool of sonication was exploited in modulating the interfacial interactions of benzenoid-quinoid moieties of PAni with HBPEA, which resulted in improved mechanical and antistatic properties together with thermostability as compared to the pristine polymer. The afore-stated findings carve out the potentiality of the prepared nanocomposites as antistatic materials.

Parts of this chapter are published in

1. *J. Appl. Polym. Sci.* **126** (3), 830--836, 2012.
2. *Ind. Eng. Chem. Res.* **52** (16), 5700--5707, 2013.

3.1. Introduction

As noted in earlier chapters, the design of castor oil based HBPEA brings in twin assets of economic and environmental credentials. However the optimal performance of these HBPEA limits their utility in structural and special purpose applications. In this vein, the advent of nanotechnology has great implications in meeting the demands for high performance materials and consequently remodeling the arena of polymeric materials.¹ The synergistic features of HBPEA along with unique and fascinating properties of the nanomaterials forge the design of *avant-garde genre* of materials.

The insulating nature of HBPEA² impedes the dissipation of build-up of the static electric charges on its surface which may otherwise lead to attraction of dusts and electrostatic hazards like electric shocks. The interest in antistatic materials combined with desirable properties like acceptable rheological behavior, adequate mechanical strength and high thermal stability may be an apt choice for utility across the domains. In this regard, it becomes a herculean task to select appropriate nanomaterials which can afford pronounced augmentation in the desired electrical property or reduce the sheet resistivity of HBPEA to the range of 10^5 - 10^6 Ω/sq .³ The conventional antistatic additives such as carbon black,⁴ 1-*n*-tetradecyl-3-methylimidazolium bromide⁵ carbon fibers⁶ and metal particles⁷ suffer from limitations like high cost, blushing and blooming problems together with moisture-dependency, which in turn reduce their antistatic action during active service lifetime.⁸ Researches in the field of conducting polymers led to the discovery of polyaniline (PANI) which forms one of the potent antistatic materials. PANI demands a special merit amidst the genre of π -conjugated polymers owing to its good environmental stability and versatile doping/de-doping properties.^{9,10} Further the reduction in the size of the conductive materials from macro to nano results in the abatement of the percolation threshold in terms of amount together with enhancement of other desired properties of the pristine polymer.¹¹ The inclusion of conducting nanomaterials in an insulating matrix imparts a precipitous drop in the electrical resistivity depending on aspect ratio and distribution of the same. Moreover among the various aspects of nanotechnology, nanofiber technology, wherein fibrous materials are fabricated at nano scale regime is an emerging field of research interest. Amongst the reported approaches including 'nanofiber seeding' method,¹² 'high-gravity oxidative polymerization',¹³ and, the use of 'structure directing agents' like surfactants,¹⁴ polyelectrolytes¹⁵ and so on, interfacial polymerization developed by Huang et al.¹⁶ is instigating colossal interests owing to its facile and template-free approach. Thus PANI

nanofiber hold potent as a conducting nanomaterial to impart improvement in the dissipation of the electrostatic charges build-up on the surface of the pristine polymeric matrix. To this end, Oviedo et al.³ showed that the incorporation of 30 wt% PANi-organoclay nanohybrid into ethylene propylene diene monomer rubber resulted in the achievement of the electrical resistivity of $10^5 \Omega/\text{cm}$ in the nanocomposites. The antistatic property of HBPEA was also explored using 20-40 wt% nanoclay by Muscat and his coworkers.¹⁷ As discussed earlier (section 2.4. of Chapter 2), HBPEA containing 10 wt% DiEA (which was coded earlier as HBPEA for simplicity from this chapter onwards) exhibited significant performance amongst all others was thus, used as the matrix in the preparation of the nanocomposites.

In the light of the afore-stated discussions and research findings in the literature, the role of organic solvents of varied solubility parameters in the preparation of PANi nanofiber by interfacial polymerization has been delved into to unveil the effect of solvent interaction on the structure and properties of the same. PANi nanofiber was thereafter incorporated at different loadings of 5, 7.5, 10 and 12.5 wt% into HBPEA matrix to fabricate castor oil based HBPEA/PANi nanofiber nanocomposites. Thus the prime objective remained in scrutinizing the rheological behaviors, mechanical and thermal properties and sheet resistances of the prepared nanocomposites for prospective use as antistatic materials.

3.2. Experimental

3.2.1. Materials

The materials used for the synthesis of HBPEA were of same specification, and purified and dried by the same methods as illustrated in section 2.2.1.1. of Chapter 2. In brief, castor oil, DiEA, MAn, PhAn and IPhA were used as the starting materials together with NaOCH_3 as the catalyst. Further epoxy-poly(amido amine) was used as the curing system.

Aniline purchased from Sigma Aldrich, India was purified by vacuum distillation in the presence of zinc dust having atomic weight 65.37 g/mol (purchased from S.D. Fine-Chem Ltd, India) and kept in an air-tight container away from light under low temperature prior to use. The solvents like butanol (boiling point, 118 °C, density 0.81 g/cm³), benzene (boiling point 80 °C, density 0.88 g/cm³), carbon tetrachloride (boiling point 78 °C, density 1.594 g/cm³), dichloromethane (boiling point 40 °C, density 1.32 g/cm³) and tetrahydrofuran (THF, boiling point 65 °C, density 0.89 g/cm³) were distilled before use. Ammonium peroxydisulfate (APS) and hydrochloric acid (HCl) (36.46 g/mol, 11.6 N) were used as

purchased (Merck, India).

3.2.2. Methods

3.2.2.1. Preparation of PANi nanofiber

HCl doped PANi nanofiber was prepared following the interfacial polymerization technique¹⁶ using organic solvents of varied solubility parameters *viz.*, dichloromethane, 1-butanol, benzene and carbon tetrachloride and coded as P1, P2, P3 and P4 respectively. In brief, PANi nanofiber was prepared in an organic/aqueous biphasic system with APS dissolved in 1 mol aqueous HCl solution and aniline in the organic solvent (maintaining the mol ratio of aniline:APS at 4:1 and under static condition).¹⁶ The nanofiber was washed with water followed by methanol for several times until the filtrate became colorless. The product obtained was dispersed in THF (1 g/mL) prior to its incorporation into the polymer matrix.

3.2.2.2. Preparation of nanocomposites

The castor oil was transesterified with methanol to produce MECO, which was then reacted with DiEA in the presence of NaOCH₃ to obtain DEFA. The details of the synthetic protocol of HBPEA using A₂+B₂+A'A₂ approach have been described in section 2.2.2. of Chapter 2. Briefly, DEFA served as the A₂ monomer, MAn, PhAn and IPhA served as the B₂ monomer and DiEA the A'A₂ monomer (10 wt% with respect to DEFA) for the preparation of HBPEA. The condensation reaction of A₂ and A'A₂ with B₂ monomer in the presence of 0.8 wt% NaOCH₃ was carried out at 150 °C for 30 min followed by heating at 185 °C for another 1.5 h and finally at 200-220 °C for 10 min with continuous mechanical stirring under the nitrogen atmosphere. The dispersed PANi nanofiber in THF (coded as P4) was then added (in varying weight percentages of 5, 7.5, 10 and 12.5 wt%, separately) to the preformed HBPEA at 60-65 °C with constant stirring for 30 min followed by sonication for 15 min. The weight ratio of PANi nanofiber to HBPEA to THF was maintained at 5-12.5:100:4. HBPEA/PAni nanofiber nanocomposites with varying weight percentages of 5, 7.5, 10 and 12.5 wt% of nanofiber were coded as HBPEAP5, HBPEAP7.5, HBPEAP10 and HBPEAP12.5 respectively. HBPEA and the prepared nanocomposites were cured by using bisphenol-A based epoxy resin (60:40 weight ratio of resin is to epoxy) and 50 wt% poly(amido amine) (with respect to epoxy resin) at 150 °C.

3.2.3. Instrumentation

The mixing of PANi nanofiber in HBPEA was aided with a standard sonotrode (tip-diameter 3 mm, acoustic power density 460 W/cm²) in a high intensity ultrasonic processor

(UP200S, Hielscher, Germany). The ultrasonication was carried out at 60% amplitude and 0.5 cycles in a thermostatic bath for maintaining the temperature of the reaction vessel at 4 °C. The wide-angle X-ray diffractograms of the nanocomposite films and powdered PANi nanofiber were measured at scanning rate of 0.05 min⁻¹ over a wide scanning angle of 2θ=10-60° using CuKα radiation by a Rigaku X-ray diffractometer (Miniflex, UK). The morphology of PANi nanofiber and their dispersion scenario in the nanocomposites were studied using a JEOL, JEM 100 CX- transmission electron microscope (TEM) at an operating voltage of 100KV, after casting on carbon-coated copper grids. The sheet resistance of the nanocomposite thin films and PANi nanofiber pellet were measured by the standard four-probe technique with linear probe configuration (M/S Osaw Industrial Products, India) and the reported results were averaged over a set of three independent measurements.

FTIR and TG analyses together with the study of rheological behavior were carried out using same instruments and techniques as described in section 2.2.3. of Chapter 2. The performance characteristics of the nanocomposites in terms of curing time, percent gel fraction, scratch hardness, impact resistance, gloss, TS and EB were evaluated according to the standard methods as mentioned in section 2.2.3. of Chapter 2. The chemical resistance test was also performed in the same way as described in section 1.4.5.3. of Chapter 1.

3.3. Results and discussion

3.3.1. Preparation of PANi nanofiber

The polymerization of aniline in different organic solvents by interfacial polymerization¹⁶ was monitored in terms of ‘induction time’ (the period from the addition of the two aqueous/organic biphasic systems to the beginning of the formation of PANi nanofibers at the interface of the two solvent systems). It is evident from Table 3.1 that the induction time is a function of the intermolecular interaction between the organic solvent and aniline (which in turn is dictated by the differences in their solubility parameters). Stronger interaction of aniline with the organic solvent (close solubility parameters) retards their interaction with APS in the aqueous phase containing HCl and hence results in longer “induction time”. In other words, smaller difference in the solubility parameter indicates similar internal energies and results greater interaction between aniline and organic phase, which consequently retards their interaction with the components of the aqueous phase. However although the difference in the solubility parameter are same in cases of 1-butanol and benzene, but the induction period of the former is more compared to the latter owing to

the polar-polar and H-bonding interactions of the former with aniline monomer. This interaction between aniline and the organic solvents has a profound influence on the degree of conjugation of PANi nanofibers (discussed in section 3.3.6.). Greater the interaction, lesser was the degree of conjugation. This forms the rationale behind the use of P4 in the preparation of HBPEA/PAni nanofiber nanocomposites.

Table 3.1 *Physical properties of organic solvents and induction time for the formation of PANi nanofiber*

Solvent	Solubility parameter (δ_s) (cal/cm^3) ^{1/2}	$\delta_a^* - \delta_s$ (cal/cm^3) ^{1/2}	Dielectric constant	Dipole moment	Induction period
dichloromethane	9.7	0.6	9.1	1.6	90
butanol	11.4	1.1	17.8	1.66	75
benzene	9.2	1.1	2.3	0	60
carbon tetrachloride	8.6	1.7	2.2	0	30

δ_a^* (solubility parameter of aniline) = 10.3 (cal/cm^3)^{1/2}

3.3.2. Preparation of nanocomposites

HBPEA containing 10 wt% DiEA as the trifunctional moiety was prepared by $A_2+B_2+A'A_2$ approach, as described in section 2.2.2. of Chapter 2.

The preparative protocol of the nanocomposites by an *ex-situ* polymerization technique is presented in Scheme 3.1. The nanoscale dispersion of PANi nanofiber in HBPEA matrix led to the effective interfacial interactions between the two, which subsequently confined the nanofibers in-between the polymer chains. These interfacial interactions (evident from FTIR study, discussed below in section 3.3.3.) of the nanofiber with HBPEA matrix helped in the improvement of the mechanical, thermal and antistatic properties as compared to that of the pristine polymer.

3.3.3. FTIR study

FTIR spectra of PANi nanofiber, HBPEA and its nanocomposites are shown in Fig. 3.1. FTIR absorption band at around 3435, 1300 and 1150 cm^{-1} were assigned to N–H, C–N and C=N stretching vibrations of PANi nanofiber respectively (Fig. 3.1 (A)). The strong band at 1150 cm^{-1} was ascribed to be a measure of the degree of delocalization of electrons, a characteristic band of conducting PANi nanofiber.¹⁸ FTIR spectral signatures of PANi were

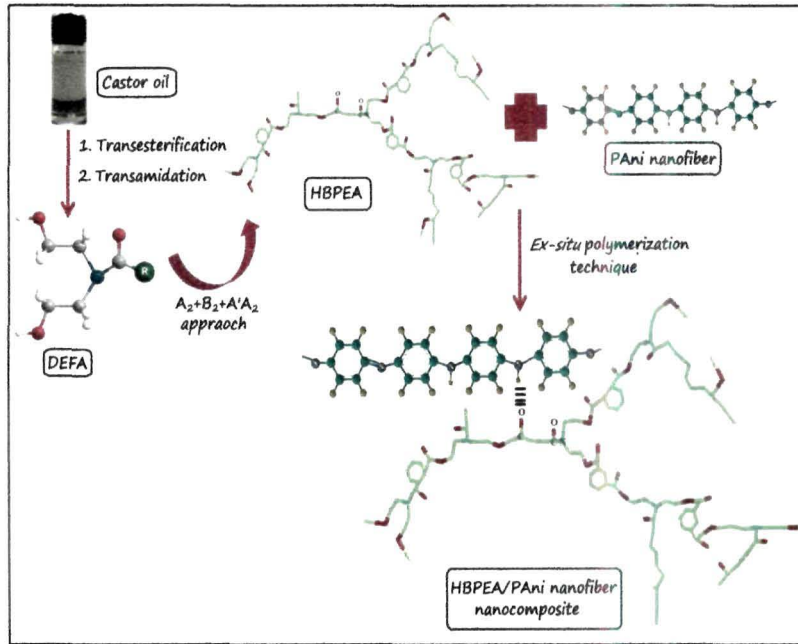
observed at 1490 and 1576 cm^{-1} corresponding to the benzenoid and quinoid rings,¹⁹ respectively (Fig. 3.1 (A)). These bands of PANi nanofiber shifted to lower wavenumbers of 1460 and 1556 cm^{-1} in the nanocomposites (Fig. 3.1 (B)), which is due to the π - π interactions of the same with the aromatic moieties of HBPEA. It was also observed that the absorbance band of carbonyl ester moiety shifted from 1730 cm^{-1} in the pristine polymer to \sim 1725 cm^{-1} in the nanocomposites, which is attributed to the interaction between the carbonyl and the nitrogenous groups of PANi. The shift in the amide band from 1632 cm^{-1} in the pristine polymer to 1637 cm^{-1} is attributed to the restriction of the vibrational motion of the carbonyl amide bond of HBPEA due to H-bonding with $-\text{NH}$ group of PANi nanofiber.

3.3.4. Rheological behavior

The dynamic modulus of HBPEA and its nanocomposites reflects their elastic and viscous character, which are characterized by the storage modulus (G') and loss modulus (G'') respectively. The viscoelastic properties of the same were explored by the frequency sweep experiment. The time sweeps of G' and G'' for HBPEA and its nanocomposites showed a Newtonian-type behavior over a period of time from 25-100 s up to the stress value of 20 Pa. This justifies the conduction of the oscillatory experiments under the oscillatory stress of 20 Pa (Fig. 3.2).

The variation of G' and G'' of HBPEA and its nanocomposites (Fig. 3.3) as a function of frequency from 1-10 s^{-1} at 25 °C under a constant stress of 20 Pa revealed that both G' and G'' values increased with the increase of frequency and loading of PANi nanofiber. It is pertinent to mention that G' was higher in magnitude as compared to G'' over the whole frequency region owing to the strong dependence of G' on interfacial energy of the nanofibers with the matrix as compared to G'' . This consequently enhanced the elastic behavior of the nanocomposites with increasing nanofiber content. The transition from viscous liquid-like behavior ($G'' > G'$) of HBPEA dominated by a polymer–polymer entangled structure, to solid-like elastic behavior ($G'' < G'$) in case of the nanocomposites dictated by the amalgamation of polymer–polymer, nanofiber–nanofiber and polymer–nanofiber interactions, indicated the formation of a continuous nanofibrous network within HBPEA.²⁰ The interactions between the nanofiber became prominent with its loading, which eventually led to the formation of continuous interconnected structures within HBPEA matrix. The abrupt increment in G' and G'' values with frequency became pronounced when PANi nanofiber content increased from 7.5 to 10 wt%. This is attributed to the percolation threshold that is, the formation of continuous PANi nanofibrous network within HBPEA as evident from TEM micrographs

(discussed in section 3.3.5). However G' and G'' values decreased beyond 10 wt% loading of PANi nanofiber. This is attributed to the poor dispersion of the nanofibers along with the formation of discrete nanofiber rich domains (agglomeration) in HBPEAP12.5 (as evident from TEM study discussed below in section 3.3.5.). Fig. 3.4 showed the variation of G' and G'' for the dynamic temperature sweep experiment under isochronal condition of 1 Hz from



Scheme 3.1 Preparative protocol for HBPEA/PAni nanofiber nanocomposite

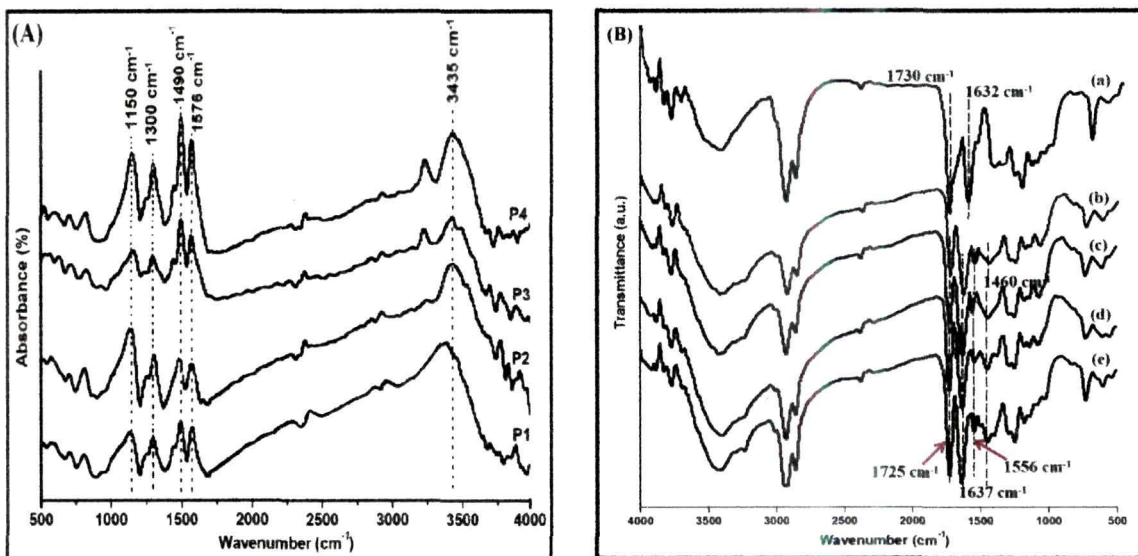


Fig. 3.1 FTIR spectra of (A): PANi nanofiber; and (B): HBPEA (a), HBPEAP5 (b), HBPEAP7.5 (c), HBPEAP10 (d) and HBPEAP12.5 (e)

25-75 °C. at controlled oscillatory stress of 20 Pa. The decrease in the values of G' and G'' with temperature is attributed to the increase of kinetic energy and free volume of the polymer chains with temperature which in turn decreases the entanglement density and inter- and intra- molecular interactions within the polymer chains. The alignment of PANi nanofiber along with the thermo-labile polymer chains along the direction of shear stress with temperature also aided to the decrease in the values of G' and G'' .²¹ The highest G' and G'' values of HBPEAP10 is attributed to the significant interactions of HBPEA with dispersed PANi chains (as evident from FTIR study in section 3.3.3.). However, owing to the occurrence of agglomeration in HBPEAP12.5 (as evident from TEM study in section 3.3.5.), the afore-stated interactions were not pronounced.

3.3.5. TEM study

HBPEA thermoset exhibited smooth surface morphology, as evident from Fig. 3.5a. The prepared PANi exhibited a nanofibrillar morphology with average diameter and length of around 25-30 and 300 nm respectively (Fig. 3.5b). An increment in the nanofiber connectivity within the polymer matrix was observed with the increase of PANi nanofiber content in the nanocomposites (Fig. 3.5c-f). The continuous formation of nanofibrous network was more prominent in case of HBPEAP10 (Fig. 3.5e)) and HBPEAP12.5 (Fig. 3.5f), while the latter showed the occurrence of agglomeration of the nanofiber in the polymer matrix.

3.3.6. XRD study

PAni nanofiber (Fig. 3.6 (A)) displayed broad X-ray diffractogram pattern at around 2θ values of 19.2° and 26° , typical of HCl doped PANi.²² The peaks at 19.2° and 26° due to (100) and (110) diffractions are assigned to the regular spacing between phenyl rings of adjacent chains of PANi in a parallel and perpendicular orientations, respectively.²² The more intense reflection peak at about 26° was deconvoluted computationally (Fig. 3.6 (B)) to calculate the d -spacing, domain length and strain produced in PANi chains. It was observed that with increasing interaction between the organic solvent and aniline, the d -spacing between the polymer planes increased. The increase in the d -spacing from 3.45 Å, in the case of P4, to 3.53 Å in P1 indicated an increase in the angle at which the chains tilted with respect to the basal plane of PANi nanofiber.²² The increase in the tilt angle of $C_{ring}-N-C_{ring}$ indicated reduction in π -stacking among PANi chains. Moreover the contributions of domain length and strain towards the line broadening of X-ray diffractions were calculated and

summarized in Table 3.2. The domain length or the range of order in PANi nanofiber was found to decrease with the increase in the interaction between the organic solvent with aniline. Table 3.2 shows that the strain corresponding to (110) diffraction increased from P4 to P1. This is interpreted as an increase in the concentration of defects within the polymeric backbone of PANi nanofiber. Thus the broadening of (110) reflection is attributed to the

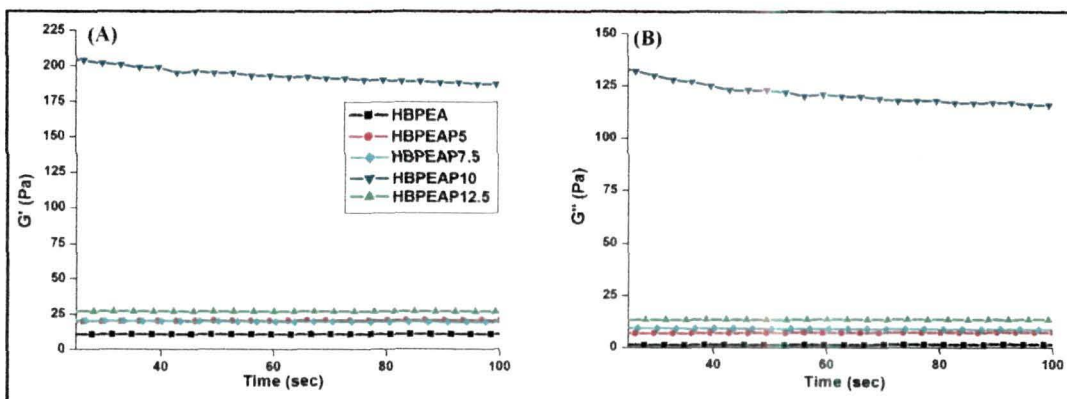


Fig. 3.2 Variations of (A) G' ; and (B) G'' with time

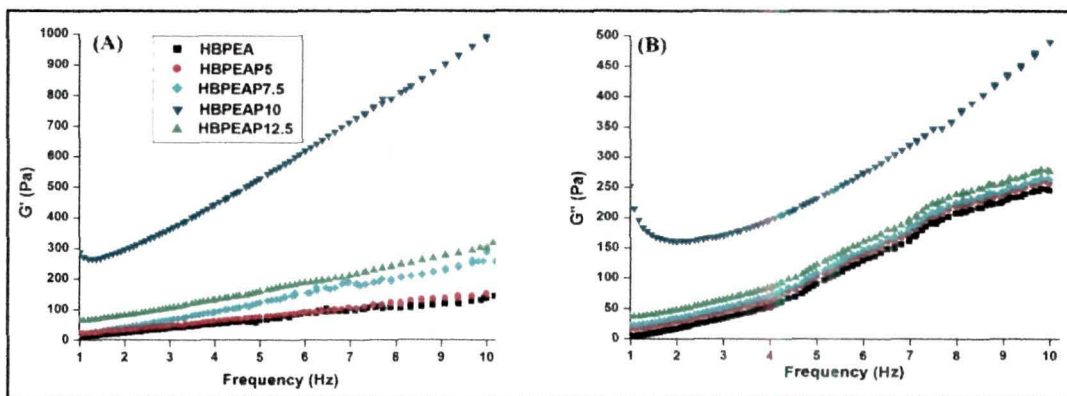


Fig. 3.3 Variations of (A) G' ; and (B) G'' with frequency

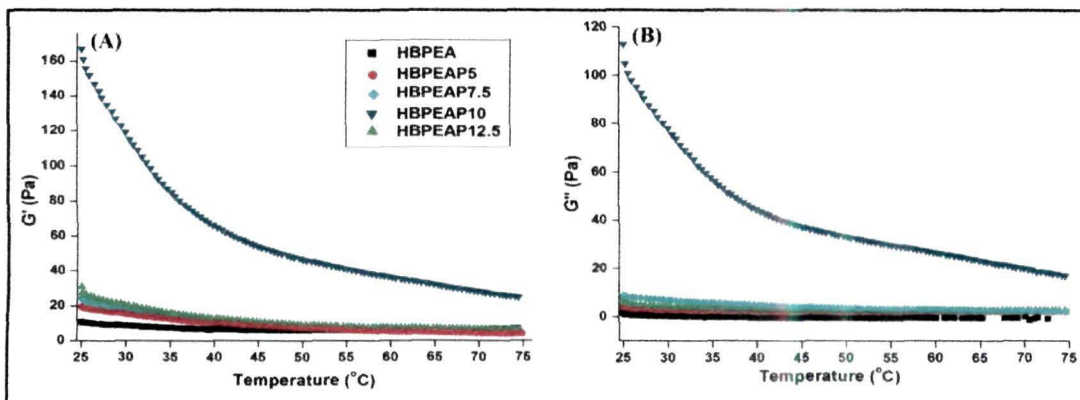


Fig. 3.4 Variations of (A) G' ; and (B) G'' with temperature

decrease in the domain length along with the increasing strain in the nanofiber. Lesser the organic solvent-aniline interaction, greater is the π -stacking of PANi chains and the degree of conjugation. This validates the use of P4 in achieving pronounced antistatic property of the nanocomposites (discussed in section 3.3.9.).

XRD patterns of HBPEA, HBPEAP5, HBPEA7.5, HBPEA10 and HBPEA12.5 thermosets are shown in Fig. 3.7. HBPEA exhibited a broad XRD peak, which is attributed to its amorphous structure. Upon formation of nanocomposites using PANi nanofiber, an intense broad diffraction peak appeared at around 19-20°. This diffraction peak of the nanocomposites is attributed to the presence or intercalation of PANi nanofiber in between the HBPEA chains.

An increase in the degree of crystallinity with increasing content PANi nanofiber was evident from Table 3.3. Origin 6.1 software was used to calculate the area under the broad diffraction peak at 2θ value around 19-20° of the nanocomposites by Gaussian fitting. The total area under the diffractogram was calculated by integrating the area from 10 to 60° (of 2θ values). The degree of crystallinity (k) or range of order in the nanocomposites was thus calculated²³ using the following equation 3.1.

$$k = (\text{area under diffraction peak} / \text{total area under the diffractogram}) \times 100 (\%) \text{ ----- (3.1)}$$

Greater the value of k , greater is the presence of nanofibrous network within the matrix, and consequently lesser is the electrical resistance of the nanocomposites. In other words, PANi nanofiber incorporated into HBPEA acts as a coherent electrical carrier in between HBPEA chains, which is also evident from the sheet resistance study discussed later in section 3.3.9.

3.3.7. Physico-mechanical performance study

The performance characteristics of the epoxy-poly(amido amine) cured HBPEA/PAni nanofiber thermosetting nanocomposites effectively changed with the incorporation of varying amounts of PANi nanofiber (Table 3.3). The curing time of epoxy-poly(amido amine) cured HBPEA and its nanocomposites decreased with the increase of the nanofiber content. This is attributed to the presence of N-atom of PANi which acts as a base and aids in the crosslinking reaction between HBPEA, epoxy and poly(amido amine). The increase in gloss with the increase of PANi nanofiber content in the nanocomposites indicated that the cured thermosets possessed good dimensional stability together with the smooth surface texture. The increment of scratch hardness of the thermosetting nanocomposites with nanofiber content is attributed to the enhanced synergism of strength and, flexibility of the polymeric

chains. The high impact resistance of the thermosets reflected optimum crosslinking together with flexibility of the long hydrocarbon chains in the backbone of HBPEA (as evident from the %gel fraction in Table 3.3).

The inclusion of the nanofiber into HBPEA resulted in the improvement the mechanical properties due to nano-reinforcing effect. The mechanical property of a nanomaterial-reinforced polymer depends on several parameters such as distribution and orientation, aspect ratio, domain size, shape and degree of compatibility of the nanomaterials with the polymer matrix.²⁴ The efficiency of transferring of stress between PAni nanofiber

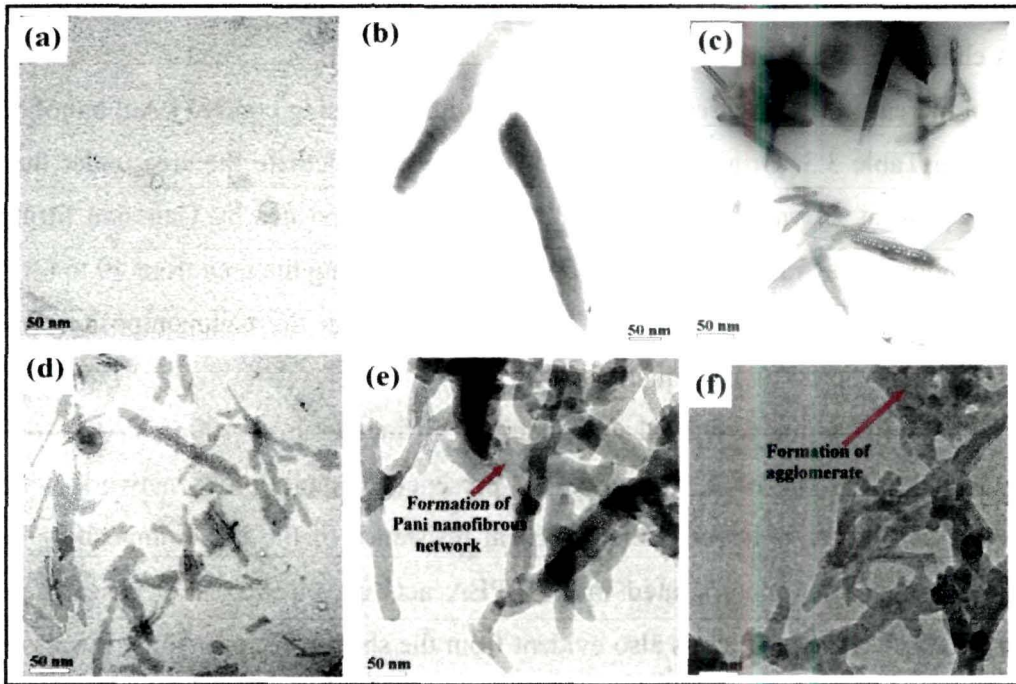


Fig. 3.5 TEM micrographs of HBPEA (a), PAni nanofiber (b), HBPEA/P5 (c), HBPEA/P7.5 (d), HBPEA/P10 (e) and HBPEA/P12.5 (f)

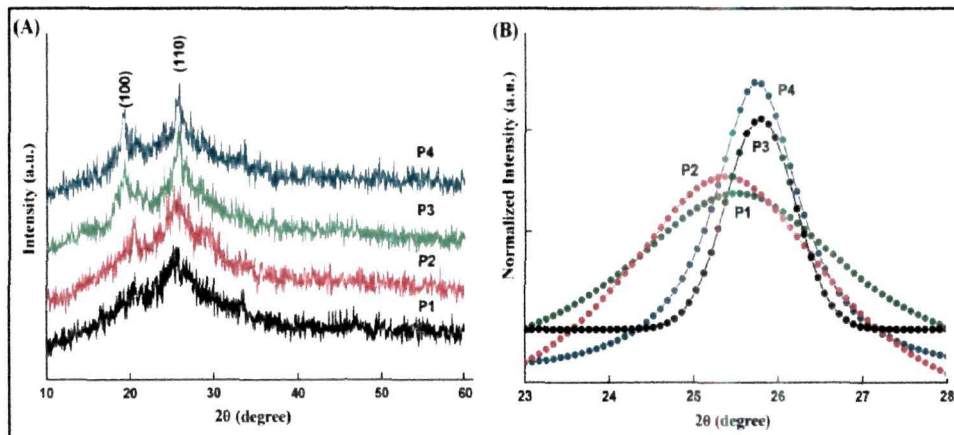


Fig. 3.6 (A) XRD patterns; and (B) deconvolution of (110) diffraction peak of PAni nanofiber

and HBPEA matrix is the key factor in improving the mechanical properties of the nanocomposites. TS of HBPEA was 7.3 MPa while it increased from 7.89 to 10.5 MPa with the increase of PANi nanofiber content from 5 wt% to 10 wt%. However the increment in TS even at 12.5 wt% was not so significant, which is due to the agglomeration of the nanofiber in HBPEA matrix (as evident from TEM study in section 3.3.5.). The improvement in the mechanical properties of the nanocomposites as compared to HBPEA is attributed to the interfacial bonding between the resin and PANi nanofiber. The decrease of EB of the thermosets with the nanofiber content is due to the decrease in molecular mobility of the polymer chains (Table 3.3). The good chemical resistance of the nanocomposite thermosets (Table 3.4), particularly the alkali resistance is attributed to the presence of amide moiety and PANi nanofiber which aid in adequate amount of crosslinking in the thermosets.

Table 3.2 Domain length, *d*-spacing and strain of PANi nanofiber

Sample	<i>d</i> -spacing (Å)	Domain length (Å)	Strain (%)
P1	3.53	19.01	2.3
P2	3.49	21.70	1.6
P3	3.48	22.77	0.68
P4	3.45	81.08	0.26

3.3.8. Thermal study

It is evident from Fig. 3.8 (A) that incorporation of PANi nanofiber into HBPEA matrix resulted in the dose-dependent increment in the thermostability of the nanocomposites. PANi nanofiber loses the adsorbed moisture at around 100 °C and the degradation of PANi chains occurred above 390 °C.²⁵ The thermosets of HBPEA and HBPEA/PANi nanofiber nanocomposites exhibited a two step degradation pattern with the increment in the thermal stability on inclusion of PANi nanofiber. While HBPEA thermoset was stable up to 277 °C (as discussed in section 2.3.8. of Chapter 2), the thermal stability increased to 307 °C in HBPEA/PANi12.5 thermoset. PANi nanofiber acts as a physical crosslinker in improving the interfacial interactions of the nanofibers with the polymer matrix, and consequently obstructing the movement of the polymer chains and resulting in enhancement of the thermal stability of the nanocomposites.

3.3.9. Antistatic property

The variations of sheet resistance of HBPEA and its nanocomposite films with PANi nanofiber content are shown in Fig. 3.8 (B). The incorporation of PANi nanofiber of varying

weight percentages from 5 to 12.5 (wt%) lead to the formation of electrically conductive networks and subsequent decrease in the electrical resistivity (as evident from the magnitude of sheet resistances of the nanocomposites). PANi nanofiber has sheet resistance of the order of 10^4 , while the inclusion of 5 and 7.5 wt% PANi nanofiber in HBPEA matrix caused a

Table 3.3 *Physico-mechanical performance of thermosetting HBPEA/PAni nanofiber nanocomposites*

Physico-mechanical property	HBPEA	HBPEAP5	HBPEAP7.5	HBPEAP10	HBPEAP12.5
curing time (h)	10±0.02	3.5±0.02	3.2±0.01	2.85±0.01	2.6±0.02
gel fraction (%)	77±0.5	79±0.7	79.8±0.7	81±0.5	81.2±0.6
scratch hardness (kg)	8.5±0.2	9±0.3	9.5±0.2	10	10
impact resistance (cm)*	100	100	100	100	100
gloss at 60°	90±0.5	93±0.6	93.5±0.5	95±0.4	95.2±0.4
TS (MPa)	7.3±0.5	7.89±0.5	8.4±0.5	10.5±0.4	12.25±0.5
EB (%)	88.1±0.8	84.7±0.9	79.5±0.8	74.2±0.8	70.3±0.9
crystallinity (%)	-	16.34	19.47	25.65	26.74

*Maximum limit of the instrument is 100 cm

Table 3.4 *Weight changes of thermosetting HBPEA/PAni nanofiber nanocomposites in different chemical media*

Type of medium	Weight change (g)				
	HBPEA	HBPEAP5	HBPEAP7.5	HBPEAP10	HBPEAP12.5
Water	2.3×10^{-2}	2.1×10^{-2}	2.1×10^{-2}	1.5×10^{-3}	1.4×10^{-2}
	±0.09	±0.07	±0.07	±0.08	±0.06
5% aq. HCl	3.2×10^{-2}	2.6×10^{-2}	2.4×10^{-3}	2.3×10^{-3}	2.3×10^{-3}
	±0.05	±0.05	±0.04	±0.02	±0.04
10% aq. NaCl	1.3×10^{-2}	1.0×10^{-2}	1.1×10^{-2}	1.1×10^{-2}	1.2×10^{-2}
	±0.08	±0.06	±0.06	±0.05	±0.06
3% aq. NaOH	1.2×10^{-2}	1.2×10^{-2}	1.1×10^{-3}	0.7×10^{-3}	0.7×10^{-3}
	±0.07	±0.05	±0.04	±0.04	±0.03

change of approximately one order of magnitude (10^6) as compared to HBPEA thermoset ($2.94 \times 10^7 \Omega/\text{sq}$). Although this decrease in the electrical resistivity of the nanocomposites is not large, but at 10 wt% loading of PANi nanofiber, a noticeable decrement in the resistivity of approximately two orders of magnitude ($7.37 \times 10^5 \Omega/\text{sq}$) relative to the pristine polymer occurred, indicating the formation of a percolation threshold. Further increase in the concentration of PANi nanofiber (12.5 wt%) into HBPEA did not significantly augment the decrease in the sheet resistance ($9.21 \times 10^5 \Omega/\text{sq}$) of the nanocomposite. Thus the electrical percolation threshold at 10 wt% indicated the formation of conductive nanofibrous networks in the polymer matrix.⁶ The interaction between HBPEA and PANi nanofiber also has profound influence in effecting the percolation threshold of the nanocomposites.

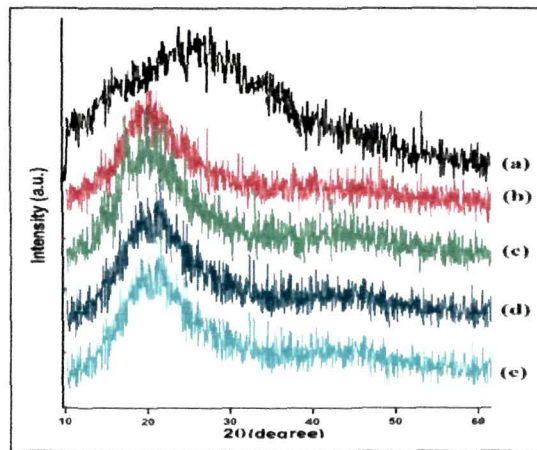


Fig. 3.7 XRD patterns of HBPEA (a), HBPEAP5 (b), HBPEAP7.5 (c), HBPEAP10 (d) and HBPEAP12.5 (e)

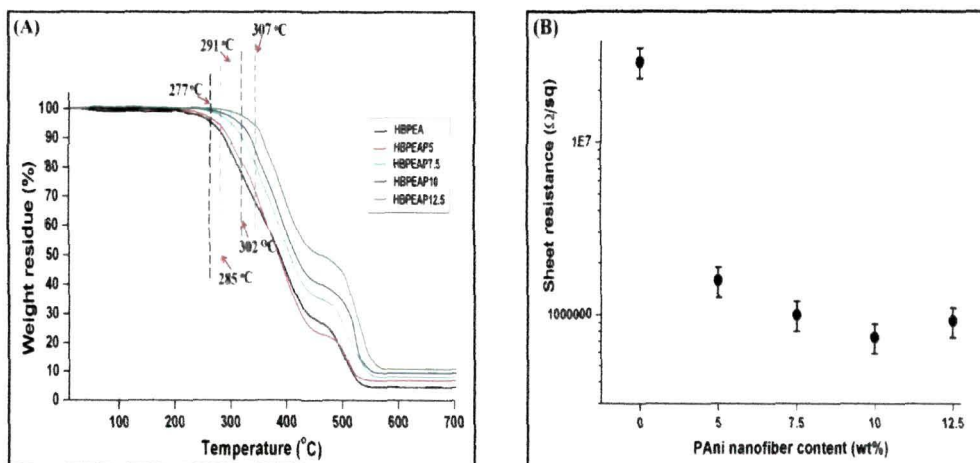


Fig. 3.8 (A) TG thermograms; and (B) variation of sheet resistance of HBPEA and HBPEA/PANI nanofiber nanocomposites

Mamunya et al.²⁶ reported that higher the interaction of the polymer with the nanomaterial, higher will be the wettability and dispersion of the nanomaterial. Consequently higher percolation threshold resulted due to lowering in the clustering of the nanomaterial, which is required for conductivity.²⁶

3.4. Conclusion

The present chapter focused the role of secondary interactions like dipole-induced-dipole, polar-polar and H-bonding in dictating the changes in the internal morphology and conformation of PANi nanofiber with the change in the organic solvents in the interfacial polymerization technique. Further PANi nanofiber complemented by the templating facet of the hyperbranched framework has significant impact on the mechanical, thermal and antistatic properties of HBPEA/PAni nanofiber nanocomposites. The alteration in the absorption frequencies (FTIR study) of the nanofibers upon interaction with HBPEA matrix marshaled in support of the enhanced physico-mechanical properties of the nanocomposites as compared to the pristine polymer. The formation of nanofibrous network with the increase of nanofiber content in the HBPEA and the occurrence of agglomeration above 10 wt% loading of the nanofiber was justified by TEM study. Dynamic rheological behavior study showed the transition from viscous liquid like behavior of the pristine resin to solid-like elastic behavior upon the formation of the nanocomposites. XRD study threw light on the ordering of PANi nanofiber together with the preferential orientation and crystallinity in the nanocomposites. The increase in connectivity between the conducting nanofibers in HBPEA matrix resulted in the decrease in the sheet resistance values. The noticeable rheological behavior, adequate mechanical strength, high thermal stability and desirable sheet resistance values forward the epoxy cured thermosetting nanocomposites as potential bio-based antistatic materials.

References

1. Balzani, V. *Small* **1** (3), 278--283, 2005.
2. Sattler, F.A., and Trunzo, F.F. *Polyesteramide wire enamels and conductors insulated therewith*, US Patent No. 3361593 A, January 2, 1968.
3. Soto-Oviedo, M.A., et al. *Synth. Met.* **156** (18-20), 1249--1255, 2006.
4. Narkis, M., et al. *J. Appl. Polym. Sci.* **25** (7), 1515--1518, 1980.
5. Ding, Y., et al. *Eur. Polym. J.* **44** (4), 1247--1251, 2008.
6. Dudler, V., et al. *Polym. Degrad. Stab.* **68** (3), 373--379, 2000.
7. Jeong, M.Y., et al. *T. Nonferr. Metal Soc.* **19** (1), s119--s123, 2009.
8. Zheng, A., et al. *Appl. Surface Sci.* **258** (22), 8861--8866, 2012.
9. Tsai, T.C., et al. *Ind. Eng. Chem. Res.* **33** (11), 2600--2606, 1994.
10. Zhang, R., et al. *Ind. Eng. Chem. Res.* **49** (20), 9998--10004, 2010.
11. Li, D., et al. *Acc. Chem. Res.* **42** (1), 135--145, 2009.
12. Zhang, X., et al. *J. Am. Chem. Soc.* **126** (14), 4502--4503, 2004.
13. Lu, X.W., et al. *Ind. Eng. Chem. Res.* **50** (9), 5589--5595, 2011.
14. Saravanan, C., et al. *Mater. Lett.* **62** (6-7), 882--885, 2008.
15. Song, G., et al. *J. Mater. Sci.* **44** (3), 715--720, 2009.
16. Huang, J., & Kaner, R.B. *J. Am. Chem. Soc.* **126** (3), 851--855, 2004.
17. Muscat, D., Stanssens, D.A.W., Heise, A., & Marko, D. *Process for preparing a composition*, EP Patent No. 1424362A1, June 02, 2004.
18. Li, X.G., et al. *Chem. Eur. J.* **14** (33), 10309--10317, 2008.
19. Jayakannan, M., et al. *J. Polym. Sci. Polym. Phys.* **43** (11), 1321--1331, 2005.
20. Gelves, G.A., et al. *Nanotechnology* **19** (21), 215712, 2008.
21. Dazhu, C., et al. *Compos. Sci. Technol.* **65** (10), 1593--1600, 2005.
22. Banerjee, S., et al. *Nanotechnology* **21** (4), 045101, 2010.
23. Hussain, A.M.P., et al. *Nucl. Instrum. Meth. B* **240** (4), 871--880, 2005.
24. Michler, G.H. & Calleja, F.J.B. *Mechanical Properties of Polymers Based on Nanostructure and Morphology*, 1st ed., Taylor & Francis Group, Germany, 2005.
25. Kulkarni, M., et al. *Chemistry & Chemical Technology* **5** (1), 55--58, 2011.
26. Mamunya, E.P., et al. *Compos. Interfaces* **4** (4), 169--176, 1997.

Chapter 4

Hyperbranched poly(ester amide)/polyaniline nanofiber modified montmorillonite nanocomposites

Highlights

The worldwide drive to miniaturize and the initiative to stride out towards greener technology continue to embrace diverse domains across the globe including biomedical sciences. Montmorillonite (MMT) has most arguably enjoyed the economical competitiveness to a wider context within the two-dimensional nanomaterials. To this end, fabrication of HBPEA/PAni nanofiber modified MMT nanocomposites possessing potent antimicrobial efficacy is a contribution towards the advancement of nano-biotechnology concerning environmental and health issues. The prepared nanocomposites exhibited potent efficacy against Gram positive bacteria like *Bacillus subtilis* and *Staphylococcus aureus* as compared to Gram negative ones like *Pseudomonas aeruginosa* and *Escherichia coli*. The nanocomposites showed significant antifungal activity against *Aspergillus niger*, *Fusarium oxysporium* and *Coleotricum capcii* and antialgal activity against an algal consortium comprising of *Chlorella*, *Hormidium* and *Cladophorella* species. The formation of thermosetting nanocomposites resulted in the acceptable improvement of desired physico-chemical and mechanical properties including thermostability. The pronounced antimicrobial activity of the nanocomposites against a spectrum of bacterial and fungal strains as well as a consortium of algal species along with their desired performance vouched them as potent antimicrobial materials in the realm of health and biomedical industry.

-
1. *RSC Adv.* **3** (14), 4574--4581, 2013.
 2. *Mat. Sci. Eng. C- Mater.* **35**, 61--69, 2014.

4.1. Introduction

“Nano-biotechnology is a growing field, but will it emulate the biotech boom?” argued by V. Gewin in an archive hosted by Nature’s group,¹ has been a daunting roster of challenges in various industrial and biomedical domains. Mankind has been constantly interacting with the world of microorganisms- one of the most deadly ‘enemies’ confronted by the human. The adherence of the microorganisms to the surfaces poses infection and device failure problems in the biomedical equipments, and many other domains such as healthcare products, food packaging, textile industry and so on.^{2,3} The unison of coating technology and potent antimicrobial nanomaterials therefore offers cutting-edge solutions for the afore-stated problems in the realm of health and biomedical industry, food processing industry and so on.³

As discussed in Chapter 2, HBPEA is one of the most versatile biodegradable thin film coating materials. The confluence of HBPEA and nanotechnology are thus foreseen to be instrumental in designing an efficient antimicrobial coating material. The ‘osmotic effect’ (which states that antimicrobial efficacy) of metal ions like mercury, silver, copper, iron, lead, zinc, bismuth, gold, aluminium and so on is known for centuries and it is based on the interaction of the released metal ions with specific microbial species.⁴ The epidemic of microbial resistance in the microorganisms has seriously complicated the existence of the conventional antimicrobial materials and necessitated to explore new and effective materials.⁵ Amidst all others, montmorillonite (MMT) is the preferred choice for nanomaterial that fits the current quest for cost-effective, easily available, sustainable and eco-friendly materials.^{6,7} However the full potential of this ubiquitous nanomaterial for such high-tech applications can be realized upon incorporation of the same into HBPEA matrix, which intend to synergistically bring out the advantages of both the components. Further the hydrophilic nature of MMT hinders the dispersion of discrete monolayers of MMT tactoids in HBPEA matrix.⁸ This intrinsic incompatibility of the hydrophilic layered silicates with the hydrophobic HBPEA can be addressed by the substitution of the inorganic cations in the galleries of MMT by long hydrophobic chain containing organo-modifier.^{8,9} The nature of organo-modifier in MMT plays a key role in imparting antimicrobial potency to MMT.⁸ Prompted by the above fact, the modification of MMT using potent antimicrobial and organic nanomaterial has sparked the concept of the design of organically modified MMT based antimicrobial materials. In this regard, PANi nanofiber is chosen for its twofold advantage *viz.*, inherent antimicrobial activity¹⁰ and modifying agent for hydrophilic MMT.^{11,12} Binitha et al.¹³ prepared PANi nanofiber within the chromium polyoxocation pillared MMT (19 wt%)

at 0 °C. However, the simultaneous preparation of PANi nanofiber and modification of MMT without pillaring of MMT using any guest molecules other than aniline has not yet been attempted. Further as noted in Chapter 3, PANi nanofiber exhibited pronounced interactions with HBPEA matrix and thus the fabrication of HBPEA/PANi nanofiber modified MMT nanocomposites is envisaged to confer better performance as compared to HBPEA. Zafar et al. examined the antibacterial potency of vegetable oil based PEA-metal nanocomposites upon inclusion of different *d*-block elements.¹⁴ In another report, Bharathi et al. explored the antifungal and antibacterial activity of cadmium containing vegetable oil based PEA.¹⁵ Literature reports on the antimicrobial efficacy of its hyperbranched analogs or its nanocomposites are rare to find, although they have strong potential in this regard.

Against the perspective outlined above, an attempt was made to prepare PANi nanofiber by an *in-situ* intercalative polymerization of aniline hydrochloride within the nanolayers of MMT and in turn afford modification of the latter. PANi nanofiber modified MMT (nanohybrid) was incorporated at varied weight percentages of 1, 2.5 and 5 wt% into HBPEA matrix by an *ex-situ* technique. FTIR tool was used to confirm the formation of the nanohybrid and delve into the structural changes of HBPEA upon interaction with the same. TEM and XRD analyses were used to investigate the morphology (intercalated/exfoliated structure) of both the nanohybrid and the nanocomposites. The mechanical properties and thermal stability of the nanocomposites were also scrutinized along with the investigation of the antimicrobial efficacy of the prepared nanocomposites against a spectrum of bacterial and fungal strains as well as an algal consortium in order to find out their suitability as antimicrobial coating materials.

4.2. Experimental

4.2.1. Materials

4.2.1.1. Chemicals

The materials used for the preparation of HBPEA such as castor oil, DiEA, MAn, PhAn, IPHA, epoxy resin and poly(amido amine), and the solvents were of same specification as described in section 2.2.1.1. of Chapter 2.

The materials used for the preparation of PANi nanofiber such as aniline, APS and HCl were of same specification as discussed in section 3.2.1. of Chapter 3. Aniline was purified by the same method as illustrated in section 3.2.1. of Chapter 3 and kept with 4A molecular sieves at low temperature prior to use. Hydrophilic MMT (Nanomer[®] PGV,

Sigma-Aldrich, India) with cation exchange capacity (CEC) of 89 mequiv/100 g was used as received.

4.2.1.2. Microbial strains

The bacterial strains viz., *Pseudomonas aeruginosa* (MTCC 7814), *Bacillus subtilis* (ATCC 11774), *Escherichia coli* (MTCC 40) and *Staphylococcus aureus* (ATCC 11632), and algal consortium comprising of *Chlorella sp.*, *Hormidium sp.* and *Cladophorella sp.* used in the present investigation were collected from the Department of Molecular Biology and Biotechnology, Tezpur University. The fungal strains such as *Aspergillus niger*, *Fusarium oxysporium* (MTCC 284) and *Coleotricum capcii* were brought from the Department of Mycology, Assam Agricultural University, India. The reagents like streptomycin sulphate, DMSO, nystatin and salts like KH_2PO_4 , KCl, $\text{MgSO}_4 \cdot 7\text{H}_2\text{O}$, $\text{Ca}(\text{NO}_3)_2$, $\text{FeSO}_4 \cdot 7\text{H}_2\text{O}$ and KOH used in the preparation of Knop's medium were of reagent grade and purchased from HiMedia, India. The media such as Mueller Hinton agar and Sabouraud dextrose agar used for the microbial cultures were also purchased from HiMedia, India.

4.2.2. Methods

4.2.2.1. Preparation of PANi nanofiber modified MMT

Aniline (1.78 g, double the amount of CEC of MMT) was pretreated with 1 M aqueous HCl (for 1 h at room temperature) to form water soluble anilinium hydrochloride ion. The same was added drop wise to the water dispersed MMT over a period of 30 min and stirred continuously at 70 °C for 5 h. An aqueous solution of APS (maintaining aniline:APS molar ratio = 4:1)¹⁶ was added drop wise to the water dispersed aniline hydrochloride absorbed MMT and stirred continuously for 5 h at room temperature. It was then filtered and washed with water followed by methanol. The nanohybrid was dispersed in THF (1 g/mL) prior to inclusion into the polymeric matrix.

4.2.2.2. Ex-situ preparation of nanocomposites

HBPEA was prepared by the same $A_2+B_2+A'A_2$ approach as described in section 2.2.2. of Chapter 2. The nanohybrid dispersed in THF was added (in varying weight percentages of 1, 2.5 and 5 wt% separately) to the above resin when the resinification temperature was brought down to 60-65 °C with continuous stirring for 30 min. The dispersion of the nanohybrid in HBPEA matrix was aided using sonication for a time period of 15 min. The weight ratio of nanohybrid to HBPEA to THF was maintained at 1-5:100:4. The nanocomposites of HBPEA/nanohybrid with varying weight percentages of 1, 2.5 and 5

wt% were coded as HBPEAC1, HBPEAC2.5 and HBPEAC5 respectively. The nanocomposites obtained were cured according to the procedure discussed in section 3.2.2.2. of Chapter 3.

4.2.3. Instrumentation

FTIR and TG analyses, and X-ray diffractograms were carried out using the same instruments as described in section 3.2.3. of Chapter 3. The dispersion of the nanohybrid in HBPEA using ultrasonication was carried out under same conditions and using same probe sonicator as mentioned in section 3.2.3. of Chapter 3. The surface morphology of the nanohybrid was studied using a JEOL JSM-6700F (Japan) field-emission scanning electron microscope (FESEM) equipped with energy dispersive X-ray (EDX) tool (for elemental analysis). High resolution TEM (HRTEM) micrographs of the nanocomposites were obtained using the using a JEOL JEM-2100 microscope at an operating voltage of 200 kV. The evaluation of curing time, percent gel fraction, scratch hardness, impact resistance, gloss, TS and EB were performed according to the standard methods and instruments as mentioned in section 2.2.3. of Chapter 2.

4.2.4. Antimicrobial activity

4.2.4.1. Antibacterial and antifungal activities

The antibacterial and antifungal efficacies of HBPEA and its nanocomposites were determined using well diffusion method as described by Radhika et al.¹⁷ An amount of 200 μL of the log phase culture (approximately 10^8 cells as per McFarland standard)¹⁸ of the test bacterial strains (as mentioned above in section 4.2.1.2.) were seeded on the surface of the Mueller Hinton agar medium. The prepared nanocomposites were dissolved in DMSO (0.1 g/mL), filter-sterilized through a 0.22- μm membrane filter and then introduced into one of the wells (of diameter 6 mm) in the above prepared agar plate. The test was performed using streptomycin sulphate (1 mg/mL) as the positive control while 10% DMSO (v/v) as the negative control. The culture plates were incubated at (37 ± 2) °C for 24 h and the observed zones of inhibition were measured using a transparent metric ruler.

Similarly, 200 μL of overnight grown culture ($0.5\text{-}2.5\times 10^6$ spores /mL as per McFarland standard)¹⁸ of the test fungal strains (mentioned earlier in section 4.2.1.2.) were seeded on the surface of Sabouraud dextrose agar medium.¹⁷ The experiments were performed using nystatin (1mg/mL) as the positive control, while the negative control used was same as earlier. The zone of inhibition was determined by measuring the diameter of

inhibition zone post incubation for 48 h at (25±2) °C. The reported results were averaged over a set of three independent experiments and the mean of inhibition diameter was determined.

4.2.4.2. Antialgal activity

Preparation of Knop's medium

The Knop's medium used for the culturing of algae was prepared by the method reported by Reski and Abel.¹⁹ Briefly, 10 mL of each of the stock solution comprising of KH_2PO_4 (25 g/L), KCl (25 g/L), $\text{MgSO}_4 \cdot 7\text{H}_2\text{O}$ (25 g/L), $\text{Ca}(\text{NO}_3)_2$ (100 g/L) was added to 12.5 mg of $\text{FeSO}_4 \cdot 7\text{H}_2\text{O}$ (maintaining the pH at 5.8 using KOH or HCl) to prepare the nutrient solution. The solid Knop's medium was formed upon adding 2% (w/v) agar and 0.5% (w/v) dextrose to the above prepared nutrient solution. The medium was sterilized by autoclaving prior to use.

Algal culturing

Antialgal assay of the prepared samples was investigated against an algal consortium (as mentioned in section 4.2.1.2.) using solid Knop's medium (as prepared above). An aliquot of 200 μL of fresh algal suspension was spread over the solidified Knop's medium using a sterilized glass spreader. The prepared film samples (2×1 cm^2) were then laid on the above solidified culture medium and then incubated at (25±2) °C for a photoperiod of 15 h maintaining the humidity level of (83±2)% for 5 weeks. The growth of the algal bloom onto the surface of the films was scrutinized post 5 weeks of incubation.

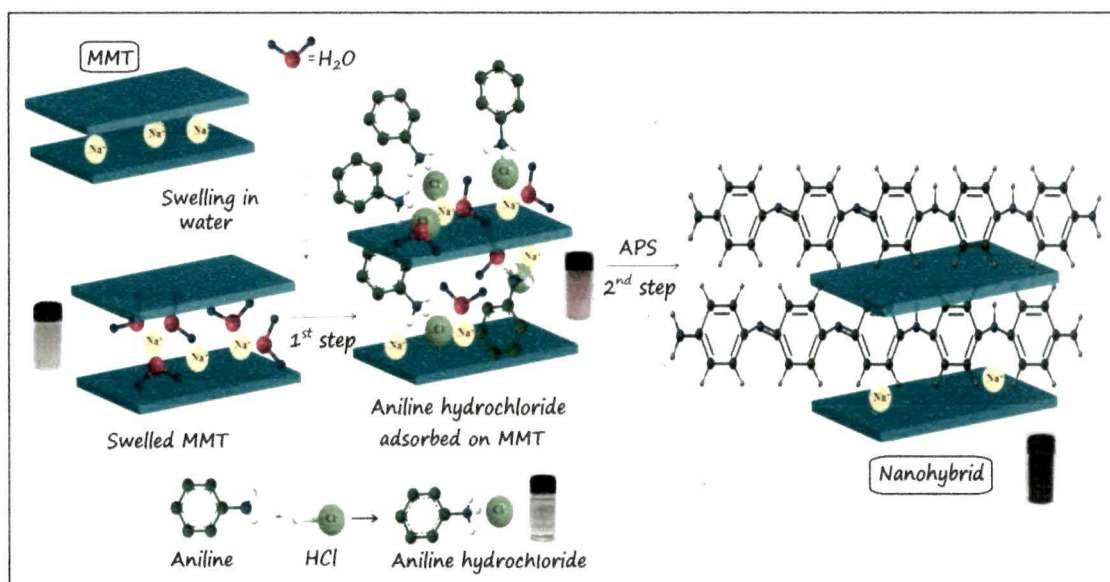
4.3. Result and discussions

4.3.1. Preparation of nanohybrid

PAni nanofiber was formed within MMT by stepwise expansion of the interlayer spacing of the nanosilicates by the 'propping-open' procedure as shown in Scheme 4.1. In this first step, the aniline hydrochloride adhered onto MMT *via* cation- π charge transfer interactions²⁰ between the former (π donors) and MMT (formation of pink coloration). In the second step, these expanded MMT layers were used as confined nano-reactors for the oxidative polymerization of aniline hydrochloride using APS. These expanded nanolayers of the silicate galleries favored the formation of PAni nanofiber, as evident from FESEM micrographs (discussed below in section 4.3.4.). The adsorption of organo-modifier PAni nanofibrous chains onto MMT rendered structural modification of the nanosilicate surface (evident from the dispersion stability of the nanohybrid in different organic solvents as shown in Fig. 4.1), and provided a hydrophobic locale for intercalation of HBPEA precursors.

4.3.2. Preparation of nanocomposites

The preparative protocol for the nanocomposites of HBPEA/nanohybrid obtained by an *ex-situ* polymerization technique is shown in Scheme 4.2. The charging of the nanohybrid galleries with HBPEA primarily depended on the density of the organic modifier chains in MMT.²¹ A low density domain of PANi chains (as evident from TG study, discussed later in section 4.3.7.) within the nanosilicates provided more intergallery space to accommodate HBPEA. The strong elastic force within the nanohybrid galleries effectively exerted strain on the nanoplatelets and compelled them to open up.²² The high diffusibility of the low molecular weight hyperbranched resin (as discussed in section 2.3.2. of Chapter 2) was also instrumental in the increment of elastic forces within the nanohybrid. Park and Jana²³ reported that the exfoliation process starts at the edge of the nanosilicate layers and continues



Scheme 4.1 Preparative protocol for nanohybrid

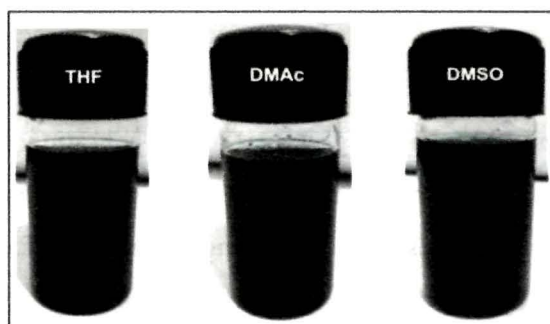


Fig. 4.1 Dispersion stability of nanohybrid in different organic solvents

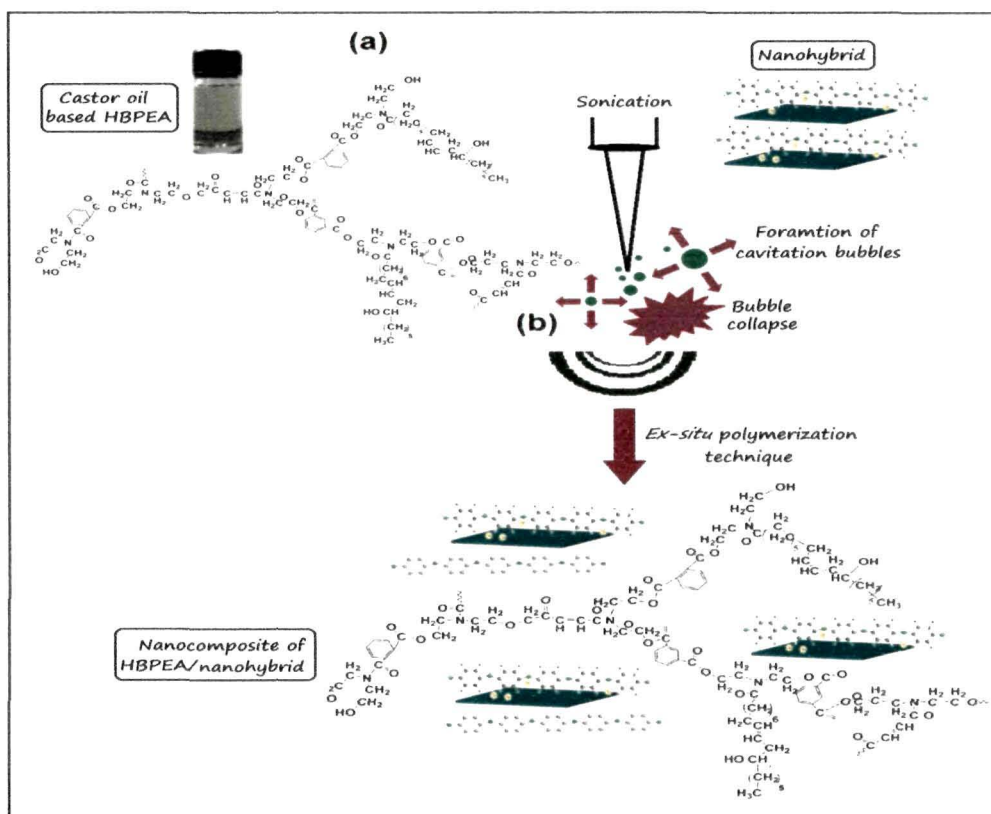
towards the centre of the tactoid until the nanoplatelets are separated out. The continuous mechanical stirring aided in the dispersion of the nanohybrid layers in the polymer matrix.²⁴ The nanohybrid galleries continued to expand with sonication resulting in the formation of the partially exfoliated nanocomposites.²⁵ The formation and sudden collapse of small cavitation bubbles as a function of rarefaction and compression cycles of sonication resulted in the formation of microjets.²⁶ These release of large amount of energy²⁶ formed the rationale behind the partial exfoliation of the nanohybrid platelets, as evident from HRTEM study (discussed below in section 4.3.4.). The interfacial interactions between the nanosilicate layers of the nanohybrid and the polar moieties of HBPEA matrix helped to enlarge the *d*-spacing and break the basal plane stacking of the nanoplatelets to induce exfoliated structure. This was further confirmed from XRD study (discussed in section 4.3.5.).

4.3.3. FTIR study

FTIR spectra of MMT, nanohybrid, HBPEA and the nanocomposites of HBPEA/nanohybrid are shown in Fig. 4.2 ((A) and (B)). The in-plane Si–O–Si characteristic stretching vibrational and bending vibrations corresponding to Si–O–Al and H–O–H of the adsorbed water in MMT were observed at 1031, 529 and 1637 cm^{-1} respectively (Fig. 4.2 (A)).²⁷ The asymmetric and symmetric stretching of freely bonded water molecule on MMT surface appeared at 3603 and 3506 cm^{-1} respectively.²⁸ The appearance of additional bands of the nanohybrid at around 1315, 3433 and, 1483 and 1627 cm^{-1} ascribed to the stretching vibrations of C–N, N–H and C=C aromatic rings respectively of PANi chain confirmed the structural modifications in MMT (Fig. 4.2 (A)).²⁹ The disappearance of the band at around 3500–3600 cm^{-1} in the nanohybrid indicated the absence of bonded water molecule and increase in the hydrophobicity, which inturn helped in good dispersion stability of the same in different organic solvents (Fig. 4.1).

As discussed in section 2.3.3. of Chapter 2, the characteristic bands of HBPEA corresponding to $\text{C}=\text{O}$ appeared at 1730 cm^{-1} , amide group at 1632 cm^{-1} and hydrogen bonded OH stretching at 3420 cm^{-1} (Fig. 4.2 (B)). The vibrational bands of the nanohybrid were found to be retained upon the formation of the nanocomposites, although with slight shifting in the wavenumber values. The stretching frequency of carbonyl ester and amide shifted to 1725 and 1635 cm^{-1} upon formation of the nanocomposites. This shifting of FTIR bands in the nanocomposites as compared to the pristine polymer was attributed to the interaction of the nanohybrid with HBPEA chains. The red shifting of the carbonyl ester band in the nanocomposites was attributed to the interaction of the same with the nitrogenous

groups of PANi chains in the nanohybrid. The slight blue shifting of the carbonyl amide band was ascribed to the hydrogen bonding with the –NH group of the nanohybrid (which removes electron density from highly stabilized amide group and strengthens the amide bond). The H-bonding was further confirmed from the broadening of –OH band in FTIR spectra of the nanocomposites as compared to the pristine polymer.



Scheme 4.2 Preparative protocol for nanocomposite of HBPEA/nanohybrid

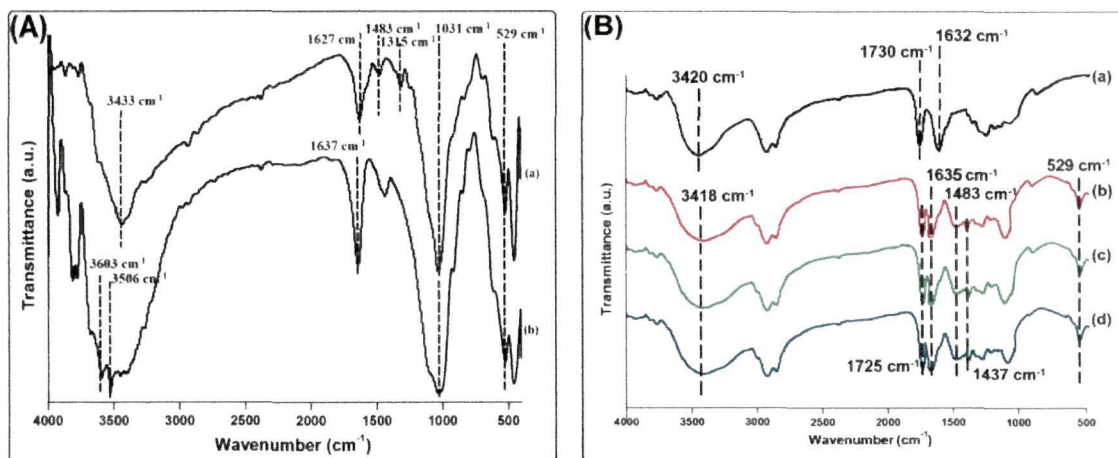


Fig. 4.2 FTIR spectra of (A): nanohybrid (a) and MMT (b); and (B): HBPEA (a), HBPEAC1 (b), HBPEAC2.5 (c) and HBPEAC5 (d)

4.3.4. Morphological study

FESEM was used to examine the stepwise formation scenario of PANi nanofibrous chains adsorbed onto the nanosilicate layers of MMT. It was evident from Fig. 4.3a that MMT consisted of stratified nanoplatelets with a layer thickness of around 1 nm. The formation of nucleation sites of PANi (upon addition of APS solution to aniline hydrochloride-MMT dispersion) was observed from Fig. 4.3b. The formation of nanofibrous structure of PANi within the confined geometry of MMT progressed with increasing time of polymerization. The average diameter of PANi nanofiber adsorbed onto different MMT layers was observed to be around 10-30 nm. Further the formation of PANi nanofiber was confirmed from EDX analysis. The inset in Fig. 4.3d showed that the presence of nitrogen and chlorine elements in the nanohybrid, which in turn confirmed the presence of PANi.

The distribution of the partially exfoliated nanoplatelets of the nanohybrid in the HBPEA matrix was evidenced from Fig. 4.4. HRTEM micrographs of the nanocomposites with a scale bar of 200 nm exhibited a uniform distribution of the nanoplatelets within HBPEA matrix. The micrographs at higher magnification scale bar of 50 nm revealed the formation of partially exfoliated structure of the nanocomposites, although a few agglomerated stacks of the nanohybrid were observed along with the exfoliated layers at higher loading of 5 wt%. It was thus inferred from Fig. 4.4b that the partial exfoliation of the nanocomposites has taken place by the delamination of the nanoplatelets. This exfoliation did not occur by the removal of the nanoplatelets sheet by sheet but *via* exfoliation process starting from the edge of the nanolayers and fanning away in outward direction.³⁰

4.3.5. XRD study

XRD diffractograms of MMT and the nanohybrid are shown in Fig. 4.5 (A). The shift of (001) basal diffraction peak from 6.9° in MMT to 5.8° in the nanohybrid indicated an increase in the interlayer spacing of the nanosilicates (change of *d*-spacing from 12.83 Å to 15.41 Å).¹⁵ Further the occurrence of two broad peaks at around 19-20° and 25-26° of the nanohybrid was ascribed to the characteristic parallel and perpendicular periodicity of PANi nanofiber chains.³¹

As mentioned in section 3.3.6. of Chapter 3, HBPEA exhibited a broad XRD peak attributed to its amorphous structure. The absence of (001) basal plane of the nanohybrid upon formation of the nanocomposites provided an inkling for the formation of the partially exfoliated structure of the nanohybrid tactoids with irregular repeating distance between the individual nanoplatelets in the nanocomposites (Fig. 4.5 (B)). This observation was further

supported by the works of Lan et al.²¹ They reported the formation of the exfoliated nanocomposites upon modification of MMT using primary and secondary onium ions, while the tactoid structure (prototype of the intercalated ones) was retained on using tertiary and quaternary onium ions. In lines with the above finding, modification of MMT using

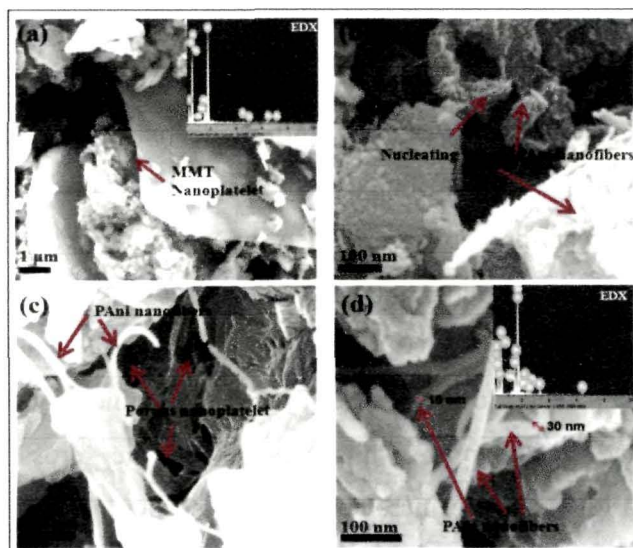


Fig. 4.3 FESEM micrographs of MMT with inset of EDX (a) and nanohybrid at time: 10 min (b), 2 h (c) and 5 h with inset of EDX (d)

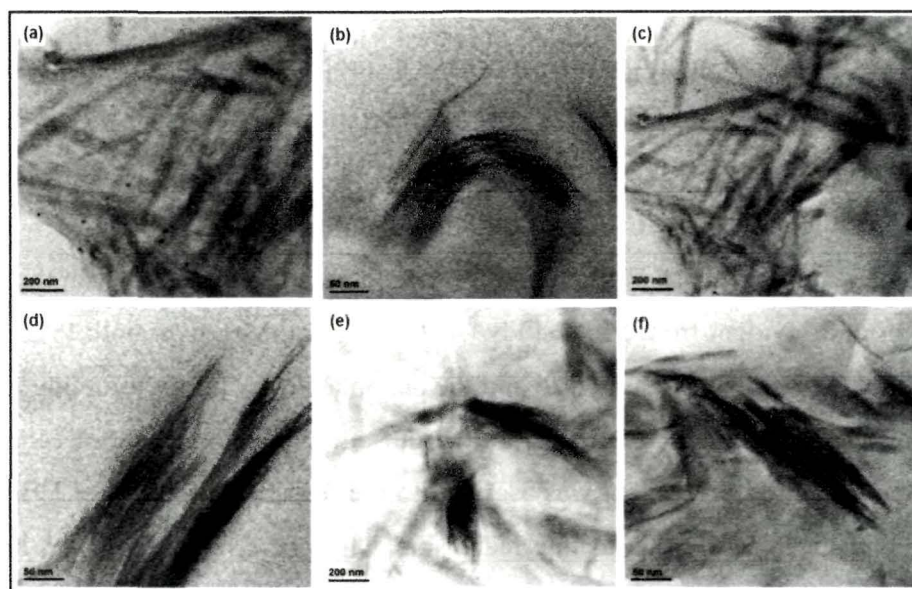


Fig. 4.4 HRTEM micrographs of HBPEAC1 (a) and (b), HBPEAC2.5 (c) and (d), and HBPEAC5 (e) and (f), at magnification scale bar of 200 nm and 50 nm respectively

secondary anilinium ions of PANi exhibited partially exfoliated structure upon formation of the nanocomposites with HBPEA matrix. The appearance of the diffraction peak at around

19-20° reflected the interaction of HBPEA with (100) plane of PANi chains of the nanohybrid (which coincides with our earlier report as mentioned in section 3.3.6. of Chapter 3).

4.3.6. Physico-mechanical performance study

The performance of the epoxy-poly(amido amine) cured thermosetting nanocomposites effectively changed with the incorporation of varying amounts of the nanohybrid (Table 4.1). It was found that the curing time of the epoxy-poly(amido amine) cured HBPEA nanocomposites baked at 150 °C decreased drastically with the increase of nanohybrid content. This was attributed to the presence of PANi chains which catalyzed the intra-gallery curing reaction between HBPEA, epoxy and poly(amido amine) (Fig. 4.6). The increment in the gloss with the increase of nanohybrid content in the nanocomposites indicated that the thermosets possessed good dimensional stability and smooth surface texture. This was attributed to the basic nature of the amine groups (of PANi) present in the partially exfoliated nanohybrid which aided in the crosslinking reaction of the nanocomposites (Fig. 4.6). The increment of scratch hardness of the nanocomposites with nanohybrid content was due to the enhanced strength and flexibility imparted by the nanohybrid and HBPEA chains respectively. The high impact resistance of the thermosets showed optimum crosslinking and flexibility of the long hydrocarbon chains of HBPEA.

The nanoscale dispersion and interfacial interaction (Fig. 4.6) of the partially exfoliated nanohybrid and HBPEA optimized the mechanical properties of the nanocomposites.³² As discussed in section 2.3.7. of Chapter 2 HBPEA thermoset possesses TS of 7.3 MPa, which increased from 8.9 to 14.3 MPa with the increment in the nanohybrid content from 1 to 5 wt% in the nanocomposites. The two-fold improvement in TS with 5 wt% nanohybrid containing nanocomposite was attributed to the interfacial interaction between the matrix and the nanohybrid, as evident from FTIR study (section 4.3.3.). Moreover both PANi nanofibers absorbed onto the exfoliated nanohybrid and the nanoplatelets afford reinforcing effect to the nanocomposites. The decrease of EB of the thermosetting nanocomposites (Table 4.1) with the increase of nanohybrid content was ascribed to the restricted mobility of HBPEA chains at the nanoplatelet interface due to interfacial interaction of HBPEA with the high surface area of the nanohybrid (Fig. 4.6). However the decrease in EB of the nanocomposites was not much pronounced owing to the plasticization effect of the long hydrocarbon chains of poly(amido amine) as well as the polymeric organo-modifier chains of PANi nanofiber.

4.3.7. Thermal study

The thermal stabilities of MMT, nanohybrid and thermosets of HBPEA and its nanocomposites as examined by TGA are shown in Fig. 4.7. MMT exhibited thermal stability up to 700 °C with 9–11 wt% loss at around 105 °C attributed to the adsorbed moisture. PANi nanofiber loses adsorbed moisture at around 100 °C, while its degradation starts only above 400 °C.³³ The nanohybrid exhibited 28-30 wt% loss at around 450 °C due to the degradation of PANi nanofiber.

The thermosets of HBPEA and its nanocomposites exhibited a two-step degradation pattern with dose-dependent increase of thermal stability. As mentioned in section 2.3.8. of Chapter 2, HBPEA exhibited thermal stability upto 277 °C (onset degradation temperature of first degradation step), which increased to 318 °C upon incorporation of 5 wt% nanohybrid into the polymeric matrix. The increment in the thermal stability of the nanocomposites as compared to that of HBPEA was attributed to the dense and stable dispersion of the partially exfoliated nanosilicate layers, which aided in the increase of the intra-gallery crosslinking reactions. The nanoplatelets of the nanohybrid also played an important role by acting as a heat barrier along with the PANi chains. These factors consequently enhanced the overall thermal stability of the nanocomposites together with assisting in the formation of char upon thermal decomposition.

Table 4.1 *Physico-mechanical performance of thermosetting nanocomposites of HBPEA/nanohybrid*

Physico-mechanical property	HBPEA	HBPEAC1	HBPEAC2.5	HBPEAC5
Curing time (h)	10±0.02	2.5±0.03	2.2±0.03	2.0±0.02
Gel fraction (%)	77±0.5	78±0.5	79.2±0.2	80±0.3
Scratch hardness (kg)	8.5±0.2	9±0.2	9.5±0.2	10
Impact resistance (cm)	100	100	100	100
Gloss at 60°	90±0.5	91±0.6	92.5±0.6	95±0.4
TS (MPa)	7.3±0.5	8.9±0.3	11.4±0.6	14.3±0.5
EB (%)	88.1±0.8	85.1±0.5	84.5±0.5	82.6±0.4

*Maximum limit of the instrument is 100 cm

4.3.8. Antimicrobial activity

The mean zones of inhibition observed in the antibacterial and antifungal tests of HBPEA and its nanocomposites are tabulated in Table 4.2.

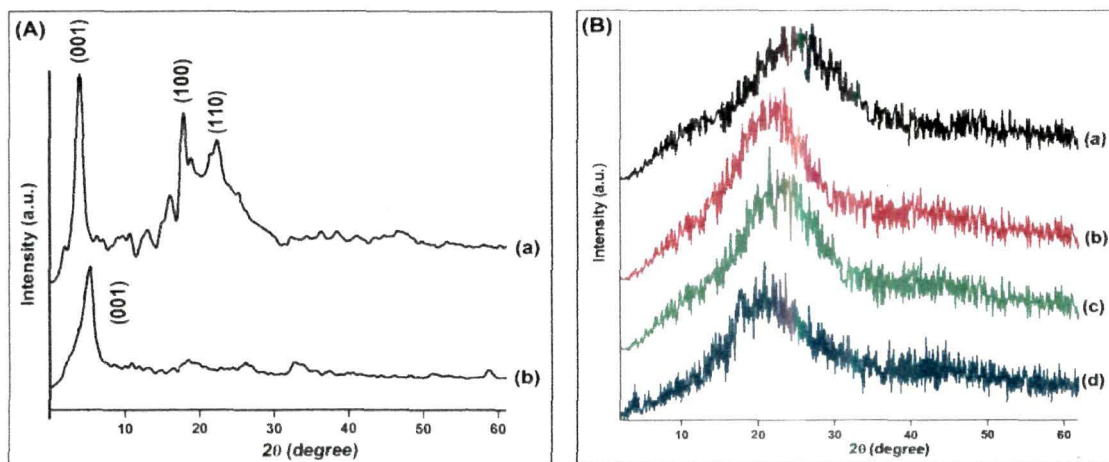


Fig. 4.5 XRD patterns of (A): nanohybrid (a) and MMT (b); and (B): HBPEA (a), HBPEAC1 (b), HBPEAC2.5 (c) and HBPEAC5 (d)

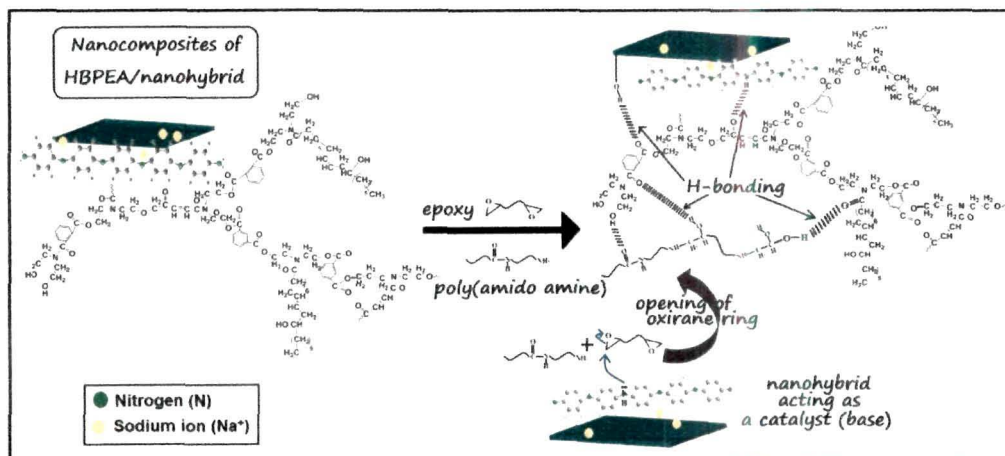


Fig. 4.6 Possible interactions during curing of nanocomposite of HBPEA/nanohybrid

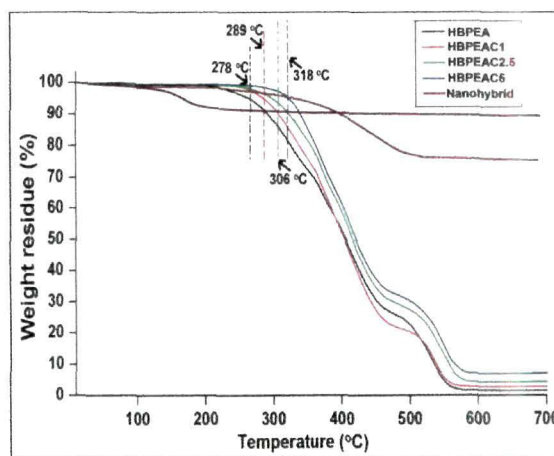


Fig. 4.7 TG thermograms of MMT, nanohybrid and thermosetting nanocomposites of HBPEA/nanohybrid

Fig. 4.8 depicts representative culture plates showing antibacterial activity of HBPEA and its nanocomposites. HBPEA exhibited comparatively less antibacterial activity against the tested bacterial strains than the nanocomposites. The zone of inhibition of the antibacterial tests of the nanocomposites increased with the increase of nanohybrid content in HBPEA matrix. The observed zone of inhibition ranges 10-15 mm. The nanocomposites exhibited pronounced antibacterial efficacy against *B. subtilis* and *S. aureus* as compared to *P. aeruginosa* and *E. coli*. This selective efficacy of the nanocomposites against Gram positive bacteria as compared to the Gram negative ones was attributed to the differential interaction of the same with the molecular moieties present on the surface of the two different bacterial groups. The basic architectural differences between the cell wall structures of those two classes of bacterial groups play a key role in the determination of their antibacterial activities.³⁴ The inhibition of the bacterial growth by the nanocomposites was attributed to the presence of the emeraldine form of PANi nanofiber of the nanohybrid in the partially exfoliated nanocomposites. The pronounced antibacterial activity of the emeraldine form of PANi was attributed due to its structural similarity with that of the active antibacterial compound tetracyclines, which inhibit the protein synthesis in the bacterial cells through bacteriostatic mode of action.³⁵

The representative culture plates showing antifungal activity of HBPEA and its nanocomposites are shown in Fig. 4.9. The results showed that the materials exhibited potent biocidal activity against the tested fungal strains. The well diffusion method of the tested samples showed clear inhibition zone of 10-14 mm (Table 4.2). The antifungal activity of HBPEA is attributed to the binding affinity of the same with ergosterol, an essential component of the cell membrane for the normal growth and viability of fungal cells.³⁶ The hyperbranched architecture of the nanocomposites bequeathed with multiple functionalities and large number of internal cavities provided greater accessibility and interaction of the polymer chains with the microbial cells. The interaction of the long fatty acid chains of pristine polymer and nanocomposites with the cellular ergosterol composition of fungi may also be a probable cause of the inhibitory action. The improved antifungal activity of the nanocomposites may also be attributed to the presence of benzyl amine structure in PANi backbone of the nanohybrid, which interferes with the production of ergosterol.³⁷

The anti-algal assay examined the ability of the pristine and nanocomposite samples to inhibit the growth of an algal consortium constituting of *Chlorella*, *Hormidium* and *Cladophorella* sp. (summarized in Table 4.2). The light source used for the above test emitted

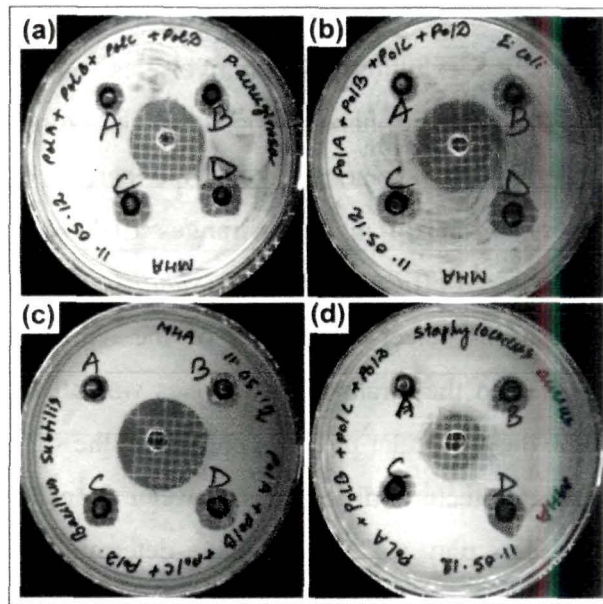


Fig. 4.8 Representative culture plates showing antibacterial activity of (A) HBPEA; (B) HBPEAC1; (C) HBPEAC2.5; and (D) HBPEAC5 against *P. aeruginosa* (a), *E. coli* (b), *B. subtilis* (c) and *S. aureus* (d)

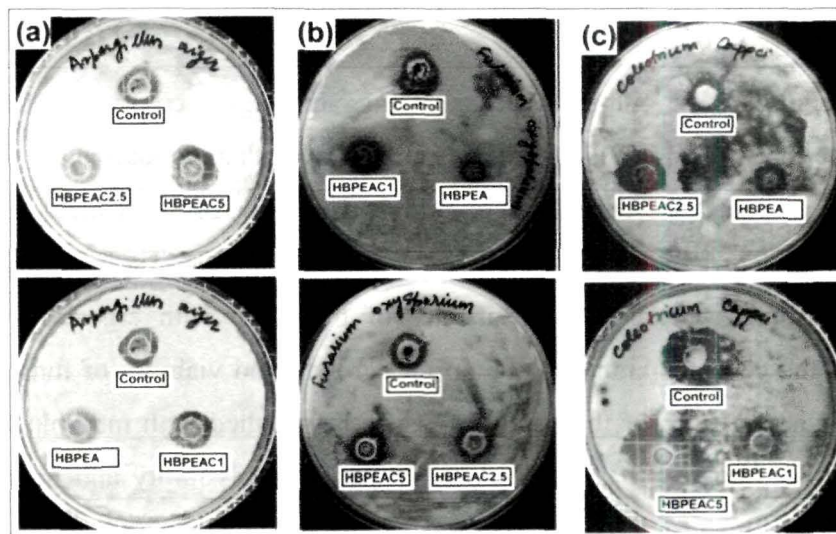


Fig. 4.9 Representative culture plates showing antifungal activity of HBPEA and nanocomposites of HBPEA/nanohybrid against *A. niger* (a), *F. oxysporium* (b) and *C. capcii* (c)

trace amounts of UV light particularly UVA (315–400 nm) and UVC (100–280 nm). The probable mode of antifungal activity of the nanocomposites was attributed due to UVA absorption by PANi nanofiber (at around 340 nm)³⁸ of the exfoliated nanohybrid platelets and

funneling it to the algal cells, which in turn hampered their photosynthetic process, thereby posing a risk to their growth and replication.

Table 4.2 Antimicrobial activity of HBPEA and nanocomposites of HBPEA/nanohybrid

Test organism	Zone of Inhibition (mm)				
	Control ^{a,b}	HBPEA	HBPEAC1	HBPEAC2.5	HBPEAC5
<i>P. aeruginosa</i> ^a	18±0.3	9±0.5	11±0.5	12±0.4	13±0.5
<i>E. coli</i> ^a	24±0.2	9±0.4	10±0.3	11±0.5	12±0.4
<i>B. subtilis</i> ^a	18±0.5	10±0.4	12±0.5	14±0.6	15±0.5
<i>S. aureus</i> ^a	18±0.4	11±0.5	12±0.6	13±0.3	15±0.4
<i>A. niger</i> ^b	16±0.5	10±0.5	12±0.4	12±0.6	15±0.2
<i>F. oxysporium</i> ^b	14±0.2	9±0.6	10±0.4	11±0.3	12±0.4
<i>C. capcii</i> ^b	16±0.3	9±0.4	12±0.4	14±0.5	15±0.6
Algal consortium ^c	√	×	√	√	√

^a streptomycin sulphate; ^b nystatin; ^c √: positive antialgal activity, ×: negative antialgal activity

However, the establishment of the molecular level interaction mechanism for the antimicrobial activity of the nanocomposites needs further delving employing multi-disciplinary integrated approach.

4.4. Conclusion

The present chapter provided avenue in addressing the emerging problems of microbial infection and contamination using nano-biotechnology. The low density of PANi nanofiber in the nanohybrid afforded nanocomposites of HBPEA/nanohybrid with partial layer exfoliated structure. FTIR study vouched for the interaction of the nanohybrid with HBPEA matrix, while the formation of partially exfoliated structure of the nanocomposites was validated by HRTEM micrographs. The antimicrobial activity of the nanocomposites against broad spectrum microbes including bacteria and fungi as well as algal consortium, enhances with the increase of nanohybrid content. The nanocomposites possessed potent antimicrobial properties with added facet of desirable physico-mechanical properties and thermal stability to carve out the applicability of the same as bio-based multifunctional antimicrobial materials in the biomedical domain.

References

1. Gewin, V. *Nature* **444** (7118), 514--515, 2006.
2. Bugatti, V., et al. *Appl. Clay Sci.* **52** (1-2) 34--40, 2011.
3. Sambhy, V., et al. *J. Am. Chem. Soc.* **128** (30), 9798--9808, 2006.
4. Galiano, K., et al. *Neurol. Res.* **30** (3), 285--287, 2008.
5. Huh, A.J., & Kwon, Y.J. *J. Control. Release* **156** (2) 128--145, 2011.
6. Reynolds, R.C. *Clay Clay Miner.* **18** (1), 25--36, 1970.
7. Nagendrappa, G. *Resonance* **7** (1), 64--77, 2002.
8. Zhou, L., et al. **332** (1), 16--21, 2009.
9. Park, S., et al. *J. Colloid Interf. Sci.* **251** (1), 160--165, 2002.
10. Girdavic-Nikolaidis, M.R., et al. *Acta Biomater.* **7** (12), 4204--4209, 2011.
11. Jia, W., et al. *Synthetic Met.* **128** (1), 115--120, 2002.
12. Song, D.H., et al. *J. Phys. Chem. Solids* **69** (5-6), 1383--1385, 2008.
13. Binitha, N.N., & Sugunan, S. *J. Appl. Polym. Sci.* **107** (5), 3367--3372, 2008.
14. Zafar, F., et al. *J. Inorg. Organomet. Polym.* **21** (3), 646--654, 2011.
15. Bharathi, N.P., et al. *J. Inorg. Organomet. Polym.* **20** (4), 839--846, 2010.
16. Huang, J., & Kaner, R.B. *J. Am. Chem. Soc.* **126** (3), 851--855, 2004.
17. Radhika, P., et al. *Res. J. Biotech.* **3** (3) 62--63, 2008.
18. Andrews, J.M. *J. Antimicrob. Chemoth.* **56** (1), 60--76, 2005.
19. Reski, R., & Abel, W.O. *Planta* **165** (3), 354--358, 1985.
20. Zhu, D., et al. *J. Environ. Qual.* **33** (4), 1322--1330, 2004.
21. Lan, T., et al. *Chem. Mater.* **7** (11), 2144--2150, 1995.
22. Gintert, M.J., Jana, S.C., & Miller, S.G. Evaluation of nanoclay exfoliation strategies for thermoset polyimide nanocomposite systems, in: Proceedings of Antec. Britain (2007), NASA Glenn Research Center, Cleveland, 1399-1403.
23. Park, J., & Jana, S. *Macromolecules* **36** (8), 2758--2768, 2003.
24. Martin, Z., et al. *J. Phys. Chem. B* **113** (32), 11160--11165, 2009.
25. Haq, M, et al. *Compos. Part A- Appl. S.* **40** (4), 394--403, 2009.
26. Konwarh, R., et al. *Ultrason. Sonochem.* **19** (2), 292--299, 2012.
27. Bao, Y., et al. *Carbohydr. Polym.* **84** (1), 76--82, 2011.
28. Gungor, N., & Karaoglan, S. *Mater. Lett.* **48** (3-4), 168--175, 2001.
29. Arasi, Y.A., et al. *Spectrochim. Acta A* **74** (5), 1229--1234, 2009.
30. Xu, W., et al. *J. Appl. Polym. Sci.* **88** (14) 3225--3231, 2002.

31. Banerjee, S., et al. *Nanotechnology* **21** (4), 045101, 2010.
32. Ollier, R., et al. *Compos. Part A- Appl. S.* **48**, 137--143, 2013.
33. Kulkarni, M., et al. *Chemistry & Chemical Technology* **5** (1), 55--58, 2011.
34. Konwarh, R., et al. *Appl. Microbiol. Biotechnol.* **87** (6), 1983--1992, 2010.
35. Sun, C., et al. *J. Med. Chem.* **54** (11), 3704--3731, 2011.
36. Iwatani, W., et al. *Antimicrob. Agents Ch.* **37** (4), 785--788, 1993.
37. Mironava, T., et al. *Photochem. Photobiol.* **88** (6), 1497--1506, 2012.
38. Stejskal, J., & Kratochvil, P. *Synthetic Met.* **61** (3), 225--231, 1993.

Chapter 5

Hyperbranched poly(ester amide)/ functionalized multi-walled carbon nanotube nanocomposites

Highlights

Emerging technological advancements in the domain of multi-walled carbon nanotubes (MWCNT) call for the exploration of functionalization strategies to endow the nanotubes into new ventures with multifunctional applications. In context of exploiting greener tools, the power of the microwave irradiation and ultrasonication are being tamed for the functionalization of the nanotubes. In this vein, the first part of the chapter (subchapter 5A) deals with the use of microwave irradiation in the functionalization of the nanotubes through a single pot covalent-noncovalent approach. The *ex-situ* prepared HBPEA/functionalized nanotubes nanocomposites were found to be biocompatible for *in vitro* adhesion and proliferation of peripheral blood mononuclear cells. On the other hand, the second part of the chapter (subchapter 5B) builds on the concept of exploiting the noncovalent functionalization of the nanotubes using DEFA and green tool of ultrasonication in lieu of microwave irradiation. The use of DEFA functionalized nanotubes as a reactive component in the *in-situ* polycondensation reaction to form HBPEA nanocomposites was explored in the subchapter 5B. The facile and promising functionalization of the nanotubes presented in this chapter paves way for the fabrication of HBPEA/functionalized nanotube nanocomposites with multifunctional properties to be explored in bio-medical to textile industries.

Parts of this chapter are published in

1. *Carbon* **55**, 34--43, 2013.
2. *Biomaterials Science* **2** (2), 192--202, 2014.
3. *J. Phys. Chem. C* **117** (47), 25097--25107, 2013.

5A. Covalent-noncovalent functionalized multi-walled carbon nanotube/hyperbranched poly(ester amide) nanocomposites

5A.1. Introduction

The inherent extraordinary physico-chemical, electrical, thermal and mechanical properties have bequeathed multi-walled carbon nanotubes (MWCNT) a unique niche in the realm of material science.¹ However the potential applications of MWCNT are restrained by challenges such as chemical inertness of the graphitic network, cohesion of the aggregated nanotubes, poor interfacial bonding and so on.² The reasons for functionalization of MWCNT are efficient dispersion of the individual nanotubes and establishment of a strong chemical affinity or adherence of the nanotubes (covalent or noncovalent) with the surrounding matrix.³ The different functionalization approaches, as discussed in Table 1.4 of Chapter 1 are instrumental in introducing functional moieties onto the nanotube surface, which eventually led to efficient wettability of nanotubes with polymer matrices.⁴⁻⁶ Amongst all covalent functionalization methods, the epoxy-functionalization of the nanotubes is relevant in context to curing of HBPEA resins for using it as advanced nanocomposite materials.

As noted in section 3.1. of Chapter 3, PANi nanofiber, a prototype of conducting polymer that has emerged as a promising one-dimensional material in the family of π -conjugated polymers. This is attributed to its unique properties including good environmental stability and simple doping/de-doping chemistry.⁷ Moreover amidst the genre of nanomaterials, PANi nanofiber⁸ and MWCNT⁹ demand a special mention owing to their potent antibacterial activity in the realm of biomedical sciences. Thus elucidation of the unique properties of these nanostructured materials- MWCNT and PANi nanofiber are consistently vouching for their inclusion in the fabrication of advanced materials.

Streamlining research in various scientific domains in conformity with the objectives of green chemistry has laid impetus for the use of greener tools like microwave heating for the functionalization of the nanotubes.¹⁰ The response of MWCNT and PANi to the multifaceted aspects of this green technology has been explored in recent years.^{10,11} In this regard, microwave-assisted functionalization of the nanotubes using both covalent and noncovalent approaches in a single pot reaction seems to be promising. Further the potential toxicity of these nanomaterials calls for an urgent need for the development of biocompatible materials. To this end, the unison of nanotechnology and polymer science sounds imperative in amalgamating the biocompatibility together with antibacterial efficacy to address the

aforementioned problems. The inclusion of small wt% of functionalized MWCNT into a biocompatible polymeric matrix holds potential in reducing the cytotoxicity of the nanotubes. The biodegradability of the polymeric materials is another aspect of paramount importance to leave room for tissue regeneration.¹² In addition to the above, no post-healing treatment is required for the biodegradable dressing material. In this milieu, HBPEA is a promising matrix because of the global scientific community thrust to opt for renewable bioresources endowing green credentials and other favorable attributes as discussed in section 2.1. of Chapter 2.

Thus the judicious inclusion of the antibacterial functionalized MWCNT into HBPEA matrix constitutes an interesting strategy for the fabrication of novel antibacterial, biocompatible and biodegradable material. A perusal of literature has shown that the preparation of bio-based HBPEA/MWCNT nanocomposites with the above attributes has never been attempted, which encouraged us to initiate the present study. The response of these nanocomposites towards a number of bacteria including drug resistant bacterial species was investigated. Further the potential of the same to support attachment and proliferation of PBMC, and biodegradability in simulated body fluid was also delved into.

5A.2. Experimental

5A.2.1. Materials

5A.2.1.1. Chemicals

The materials such as castor oil, DiEA, MAN, PhAn, IPhA, epoxy resin and poly(amido amine) used for the preparation of HBPEA were of same specification as described in section 2.2.1.1. of Chapter 2.

Aniline was purchased from Merck, India and purified by same method as reported in section 3.2.1. of Chapter 3. The solvents such as THF, DMF, CCL₄ and DMSO were distilled before use as mentioned in section 2.2.1.1 and 3.2.1 of Chapter 2 and Chapter 3 respectively. MWCNT with purity ~95 wt% and diameter of about 10-15 nm was purchased from Hanwha Nanotech Corp., Korea. Glycidyl methacrylate (GMA) and 2,2'-azobis-(isobutyronitrile) (AIBN) were obtained from Merck, India and used as received. The materials used for preparing PANi nanofiber such as aniline, APS and HCl were of same specification as discussed in section 3.2.1. of Chapter 3.

5A.2.1.2 Microbial strains and peripheral blood mononuclear cells

The bacterial strains viz, *Bacillus subtilis* MTCC441, *Staphylococcus aureus* (MTCC373), *Escherichia coli* (DH5 α) and *Klebsiella pneumoniae* (MTCC618), *Mycobacterium smegmatis* (mc² 155, ampicillin resistant) and *Mycobacterium smegmatis* (ATCC14468) used in the present investigation were obtained from the Department of Molecular Biology and Biotechnology, Tezpur University.

Peripheral blood mononuclear cells (PBMC) were separated from the goat blood, which was collected in a heparinized tube from the local slaughter house. RPMI (Roswell Park Memorial Institute)-1640 medium, fetal calf serum and antibiotic Penicillin-Streptomycin-Neomycin solution used for culturing of PBMC were purchased from HiMedia, India. Other chemicals including streptomycin sulfate (the positive control for antibacterial activity), Mueller Hinton Broth, 3-(4,5-dimethylthiazol-2-yl)-2,5-diphenyltetrazolium bromide (MTT), NaCl, histopaque, DMEM (Dulbecco's modified eagle medium), fetal calf serum, sodium azide (NaN₃), bovine serum albumin (BSA), phosphate buffer saline (PBS), sodium citrate, 2,4,6-tripyridyl-s-triazine (TPTZ), acetate buffer, ferric chloride hexahydrate (FeCl₃ 6H₂O), glutaraldehyde and lipase with enzymatic activity of ~16 U/mg were purchased from HiMedia, India and used as received. Bradford reagent used in the protein estimation of the bacterial cells was purchased from Sigma-Aldrich, India. Ethanol was procured from Merck, India.

5A.2.2. Methods

5A.2.2.1. Functionalization of MWCNT

PAni nanofiber doped with 1 mol HCl was prepared following the interfacial polymerization technique⁷ (and coded as P4) as discussed in section 3.2.2.1. of Chapter 3.

MWCNT (0.001 g) was first grinded with a small amount of benzene and then transferred to a round bottom flask containing GMA (2.14 g), AIBN (1.5 wt% with respect to GMA) and PAni nanofiber (5.6 wt% with respect to GMA) in THF. The mixture was stirred using a magnetic needle in a microwave oven at 60-80°C for 10 min under reflux condition. The free radical polymerization of GMA in the presence of AIBN initiator resulted in the formation of poly(glycidyl methacrylate) (PGMA). A control reaction of GMA and AIBN with the nanotubes was also carried under the same reaction conditions. Benzene (5 mL) was added to the above mixture to dissolve the unreacted GMA. The functionalized nanotubes so formed was washed with ethyl acetate followed by acetone and finally some amount of it was dried at 48 °C under vacuum for 24 h for structural elucidation. The rest of the functionalized nanotubes was kept dispersed in THF (1 g/mL) prior to inclusion in HBPEA matrix.

MWCNT, PGMA functionalized MWCNT and PANi nanofiber wrapped PGMA functionalized MWCNT were designated as M1, M2 and M3 respectively.

5A.2.2.2. *Ex-situ* preparation of nanocomposites

HBPEA was prepared by the same technique as mentioned in section 2.2.2. of Chapter 2. THF dispersed M3 was added (1, 2.5 and 5 wt%, separately) to the preformed HBPEA at 60-65 °C with vigorous stirring for 30 min, followed by sonication for 15 min. The covalent-noncovalent functionalized MWCNT/HBPEA nanocomposites with varying weight percentages of 1, 2.5 and 5 wt% of the functionalized nanotubes were coded as HPMWNT1, HPMWNT2.5 and HPMWNT5 respectively. The casted films were placed in a microwave chamber and exposed to the intermittent irradiation of 2 min in a pulse mode (with six cycles of irradiation for 10 s with a gap of 10 s) succeeded by post-curing (by the same method as described in section 3.2.2.2 of Chapter 3). The porous nanocomposite films were fabricated using particulate leaching technique wherein an aqueous NaCl solution (maintaining salt particulate:HBPEA = 10:1) was added into the mixture of epoxy and poly(amido amine) as an porogen additive. The cured films were immersed in excess amount of hot water wherein the salt particulates leached out to yield the porous films. The pore size of the prepared film was calculated from SEM micrograph. The percentage of porosity of the polymer was determined by subtracting the volume of the polymer obtained from its dimensions from the neat volume of the porous scaffold (calculated from its mass and density).

5A.2.3. *Instrumentation*

The functionalization of MWCNT was carried out in Catalyst Scientific Microwave System, India at 30% power of 210 W. FTIR, SEM and TG study were performed by the same instruments as mentioned in section 2.2.3. of Chapter 2. The ultrasonication assisted dispersion of the functionalized nanotubes in HBPEA matrix together with XRD and HRTEM analyses were carried out using the same instruments as described in section 4.2.3. of Chapter 4. The determination of curing time, percent gel fraction, scratch hardness, impact resistance, gloss and mechanical properties including TS and EB were performed as per the standard methods, mentioned in section 2.2.3 of Chapter 2. Raman spectra of the functionalized nanotubes were acquired using a SPEX 1403 double monochromator coupled to a SPEX 1442 Raman microscope, with an argon ion laser, of 0.5 mW power and at 514.5 nm excitation for the exposure time of 10 s.

The absorbance of the cultured cells in MTT assay was recorded spectrophotometrically using a UV-1700 PharmaSpec spectrophotometer from Shimadzu, Japan. The visual distinction between unstained and blue-stained cells was done using hemocytometer under Leica compound microscope at 20X magnification.

5A.2.4. Antibacterial activity

The bacterial strains were cultured in Mueller Hinton Broth media at 37° C for 18 h and harvested in the mid-exponential growth phase. The bacteria were then suspended in an isotonic solution (0.85% NaCl) to adjust the McFarland standard¹³ of the cells to a turbidity of 0.5, corresponding to approximately 1×10^8 colony forming unit (CFU)/mL. The following antibacterial assays were performed using streptomycin sulphate as the positive control and the results were averaged over a set of three independent experiments.

CFU count

The individual bacterial colonies growing onto the nanocomposite films were assessed with the test bacterial strains by the standard dynamic shake flask method.¹⁴ The films together with the bacterial inoculum in phosphate buffer and nutrient broth were incubated at 37 °C under vigorous shaking condition to determine the CFU. The flask containing only broth media served as the reference for the bacterial growth.

Total protein content

The protein content of the live bacteria growing onto the nanocomposite films was determined by the method described by Bradford.¹⁵ According to this method, 200 μL of (1 g/mL) BSA was mixed with Bradford reagent (1.25 mL) and a standard curve was plotted for the absorbance at 595 nm versus protein concentration (mg/mL) with correlation coefficient ($R^2 = 0.9997$). The absorbance of the bacterial protein adhered onto film was also measured at the same wavelength and the total protein content was estimated using the following linear fit equation 5A.1.

$$Y = 0.2658X \quad \text{-----(5A.1)}$$

where Y is the absorbance and X is the protein concentration.

5A.2.5. In vitro biocompatibility assay

5A.2.5.1. Isolation and culturing of peripheral blood mononuclear cells

PBMC were separated from the goat blood by sedimentation technique (density gradient centrifugation) using histopaque.¹⁶ Briefly, the differential migration of the blood cells during centrifugation (layered with a Pastuer pipette on 3:2 ratio histopaque) resulted in

its separation into different layers. PBMC fraction appeared at the interface between the unbound histopaque and uppermost platelet layer, which was collected post centrifugation (2-3 times) at $400\times g$ for 15 min and suspended in serum free DMEM. The cells were cultured in RPMI-1640 media containing 10% fetal calf serum and Penicillin-Streptomycin-Neomycin solution as an antibiotic for 2 h, followed by incubation in a humidified atmosphere (containing 95% O_2 with 5% CO_2) at 37 °C. This protocol supports the isolation of approximately 90% of the nonspecific esterase positive cells which are rich in macrophages.¹⁶

5A.2.5.2. MTT assay

PBMC seeded onto 96 well microplates (maintaining density of 1×10^4 cells/well) at 37 °C under 5% CO_2 humidified atmosphere were allowed to grow for 2 h. The nanocomposite films (having diameter ~ 4 mm) were added into each microplate followed by incubation under the same conditions for 18 h. MTT was added to each wells at different time intervals (0, 1, 12, 24 and 48 h) followed by 4 h of incubation under the similar conditions as above. DMSO was added to the wells for dissolution of formazon crystals (so formed) and the absorbance of the same was recorded spectrophotometrically at 550 nm.¹⁷ The well with untreated cells was taken as the control and the tests were performed in triplicates.

5A.2.5.3. *In vitro* cell response

The interaction of PBMC (adhesion and proliferation) with the nanocomposite films was evaluated using SEM study. A number of 1×10^4 cells were seeded onto the films for 48 h and PBMC adhered onto the same were fixed before imaging under SEM by the same method as described in section 2.2.3 of Chapter 2.

5A.2.6. *Reactive oxygen species study*

The toxic effect of the nanocomposites was evaluated by the ferric reducing ability of plasma (FRAP) assay. In brief, 300 μL of FRAP reagent (acetate buffer + TPTZ + $FeCl_3 \cdot 6H_2O$) was added to 10 μL of nanocomposite, followed by dilution with 30 μL of water. The change in the absorbance in presence of the nanocomposites was measured at 593 nm using ascorbic acid as the positive control. This quantified the amount of quenched reactive oxygen species (ROS).¹⁸

5A.2.7. *Biodegradation study*

The nanocomposite films were cut into small discs weighing about 10 mg each and incubated in the lipase containing 100 mM PBS medium (maintaining pH at 7.4 and weight

ratio of film to medium at 1:3) under a static condition at 37 °C.¹² The tested films were periodically taken out from the medium post incubation of 7, 14, 21 and 28 days and rinsed with water. This helped in removal of the adhered salts on the film surface and dried under vacuum for 72 h at 40 °C. The percentage of degradation was calculated from the residual mass post degradation with time period. The alterations in the ratio of intensity of the ester and amide groups ($I_{\text{ester}}/I_{\text{amide}}$) of the nanocomposite films (assessed by fitting with a Lorentzian profile in FTIR spectra) were also scrutinized (before and after degradation).

5A.3. Results and discussion

5A.3.1. Functionalization of MWCNT

In the presence of microwave irradiation, MWCNT with a reactive surface provided the loci for the free radical polymerization of GMA. The active PGMA polymeric radicals generated in THF (post dissociation of the initiator molecules) terminated onto the nanotube surface. This functionalization protocol required 10 min as compared to 24 h reported under reflux condition.¹⁹ The functionalized nanotubes had least tendency to aggregate owing to the shielding of the nanotube surface from van der Waals' attraction. However M3 had better dispersion stability of 180 days compared to M2 in different organic solvents due to the strengthened interfacial bonding of MWCNT with both PANi nanofiber and PGMA (Fig. 5A.1(A)).

Plausible mechanism for functionalization of MWCNT

The role of energetic microwave irradiation is of paramount importance in the functionalization of MWCNT. The microwave assisted heating primarily depended on two factors, viz, dipolar polarization and heat conduction (Joule heating). The dipolar polarization seemed to have little contribution to the microwave absorption by the nanotubes because of the lack of electric dipole in the same. However the presence of electrically conductive impurities, such as, metals or graphitic structure of carbon particles in the nanotubes supported the mechanism based on conduction heating. In other words, Joule's heating induced by the random electronic motion of above mentioned particles (due to the electric field) caused localized superheating.²⁰ HCl doped PANi nanofiber possessed a permanent electric dipole and hence its dipolar polarization caused localized superheating. These microwave absorbing materials viz, MWCNT and PANi nanofiber dominated the microwave spectrum and resulted in localized superheating and formation of hot spots. On one hand the loci of M2 are the nanotubes, while on the other hand the loci of M3 comprised

of both the nanotubes and the PANi nanofiber. The functionalization process in M3 occurred sequentially with covalent attachment of PGMA followed by noncovalent wrapping of PANi nanofiber because of the differential reactivity GMA and PANi nanofiber. The localized thermal energy generated by the microwave active nanomaterials was transferred to the reaction mixture, which aided in the thermolysis of AIBN molecules to yield two (2-cyanoprop-2-yl) radicals. These initiator radicals quickly reacted with GMA because of its higher reactivity over PANi nanofiber (poor reactivity of (2-cyanoprop-2-yl) radicals with secondary amine and imine functional groups of PANi nanofiber). This initiated the polymerization reaction to produce PGMA-centered macroradicals capable of terminating onto the nanotube surface. The functionalization process in M2 was analogous to 'fishing process' wherein the nanotubes acted as the 'fishhook', and the 'polymer radicals' (PGMA centered radicals) were the 'fishes'.²¹ These 'polymer radicals' were enthalpically favored to terminate the polymerization reaction by absorbing onto the nanotube surface²² due to the active nature of π -bonds in the sp^2 -hybridized graphitic framework within the nanotube lattices. MWCNT are a good electron acceptor of free polymer radicals due to their high electron affinity (2.65 eV)²² and hence formed bond with PGMA by accepting the active radicals of the same. This was further vouched by the documented density functional theory studies wherein the radical coupling onto the nanotube surface was favourable. The nanotube-bound radicals formed in this process were delocalized over several carbon atoms and stabilized by ~ 168 kJ/mol²³ PANi nanofiber wrapped onto PGMA-MWCNT scaffold and continued wrapping of PANi nanofiber disengaged the nanotubes to smaller bundles owing to π - π stacking interactions (as evident from HRTEM study in section 5A.3.1.4.). This resulted in stable dispersion of the functionalized nanotubes in different organic solvents (Fig. 5A.1 (A)). In a nutshell, functionalization the strategy involved covalent interactions of PGMA chains through the free radical reaction with the double bonds of the nanotubes, followed by noncovalent wrapping of PANi nanofiber onto the functionalized nanotubes. Scheme 5A.1 highlights the microwave assisted covalent-noncovalent functionalization of MWCNT.

5A.3.1.1. FTIR study

FTIR spectra of M1, M2, M3 and P4 are shown in Fig. 5A.1 (B). Although no prominent FTIR bands were seen in the absorption spectrum of pristine nanotubes, several vibration bands in the spectra of functionalized ones were observed. The bands corresponding to the presence of the ester and epoxide moieties were noticed at 1730 and 915 cm^{-1} respectively in the spectrum of M2. The characteristic FTIR bands at 1490 and 1576 cm^{-1}

were assigned to the benzenoid and quinoid rings of PANi nanofiber, respectively as mentioned in section 3.3.3. of Chapter 3.²⁵ FTIR spectrum of M3 was found to exhibit essentially the same absorption bands as PANi nanofiber, but with decreased intensity. This can be attributed to PANi chains being constrained by wrapping onto PGMA-MWCNT, thereby attenuating their vibrational modes. The benzenoid and quinoid units were analyzed by fitting with a Lorentzian profile. The band positions, full width at half maximum (FWHM) and benzenoid to quinoid band intensity ratio (I_B/I_Q) were determined from the deconvolution of the corresponding band profiles and tabulated in Table 5A.1. M3 exhibited an increased I_B/I_Q compared to P4 (Table 5A.1) owing to the interaction of the quinoid rings in PANi nanofiber with the nanotubes.²⁶ The decrease in the wavenumber of the carbonyl absorption from 1730 in M2 to 1717 cm^{-1} in M3 is attributed to the interaction of $-\text{NH}$ bond of PANi nanofiber with $-\text{C}=\text{O}$ bond of M2. These observations justified that both PANi nanofiber and PGMA were appended onto the nanotube surface.

5A.3.1.2. XRD study

XRD of M1 (Fig. 5A.1 (C)) showed diffraction peak at around 26.2° attributed to (002) plane of nanotube related graphitic structure.²⁷ This reflection peak shifted to 2θ value of 25.7° upon functionalization using PGMA owing to the increase in d -spacing (from 3.41 to 3.51 Å). The appearance of additional peak of M2 at 2θ value of 18.7° was indicative of the presence of pendent moiety anchored on to the nanotube surface. As mentioned in section 3.3.6. of Chapter 3, XRD peaks of P4 centered at around 19° and 25.3° reflected (100) and (110) planes of the orthorhombic unit cell of nanofiber. These two planes are assigned to the parallel and perpendicular periodicity of PANi nanofiber respectively.²⁸ The wrapping of P4 onto PGMA-MWCNT template showed a shift in 2θ value to around 20.3° and 25.1° respectively which was ascribed to π - π interaction of the same with the nanotubes.

5A.3.1.3. Raman study

The three principal Raman bands of M1 at around 1318 cm^{-1} associated with the disorder-induced D-band, 1572 cm^{-1} attributed to the high frequency E_{2g} first-order phonon mode of the tangential G-band and an additional overtone 2D band at 2642 cm^{-1} were observed (Fig. 5A.1 (D)).²⁹ Table 5A.2 shows the values of the band position, FWHM and intensity ratio corresponding to D- and G- bands of M1 and M2 fitted using a Lorentzian function. M2 showed all the characteristic peaks of the nanotubes, but with an increment in the intensity ratio of D-band (I_D) and G-band (I_G), I_D/I_G (Table 5A.2). This is attributed to the covalent interaction between PGMA radicals and nanotube surface. Raman bands of P4

appeared at 1318 cm^{-1} corresponding to the characteristic semiquinone radical cation. The band at 1388 cm^{-1} was attributed to the stretching modes of delocalized polaronic charge carrier, which was indicative of the doped state of PANi nanofiber. The bands at 1494 cm^{-1} and 1603 cm^{-1} corresponded to the C=N stretching mode of quinoid rings and C-C deformation of benzenoid rings respectively.³⁰ M3 showed all the characteristic bands of PANi nanofiber, with an increase in the intensity of the bands at around 1387 and 1495 cm^{-1} as compared to P4. This validated the presence of strong interaction of the quinoid rings with the nanotubes. However the prominent Raman bands of the nanotubes in M3 were not observed owing to complete coverage of the same by PANi nanofiber, which was further supported by HRTEM micrographs (discussed below in section 5A.3.1.4.).

Table 5A.1 Benzenoid and quinoid bands and their intensity ratios for P4 and M3

Sample	Position	FWHM	Intensity	I_B/I_Q
P4	1466.9	91.741	7.3684	0.65
	1579.4	56.636	11.2733	
M3	1470.1	109.31	9.4397	1.63
	1579.6	41.545	5.7959	

5A.3.1.4. HRTEM study

Fig. 5A.2a showed that eleven walls were stacked in M1 with an average internal and external diameter of about 5.6 and 15.2 nm, respectively and an inter-tube distance of 0.37 nm. PANi exhibited nanofibrillar morphology with an average diameter of 30 nm (Fig. 5A.2b). HRTEM imaging was found to be consistent with functionalization of nanotubes, as indicated by an apparent increase in the outer diameter of the same (Fig. 5A.2c). The nanotube surface was observed to be unevenly coated with PGMA layers exhibiting a different surface texture than the pristine ones (Fig. 5A.2c). The average thickness of the outer layer of M2 was found to increase as compared to M1 by ~10 nm, indicating a successful functionalization onto the nanotube surface. M3 exhibited a helical conformation (appearing to mimic the tendrils of a pea plant) (Fig. 5A.2d) owing to π - π stacking and electrostatic interactions of PANi nanofiber with the nanotubes. This explains the formation of stable nanotube dispersion in different organic solvents.

5A.3.2. Preparation of nanocomposites

The epoxy group and benzenoid-quinoid moieties generated by microwave assisted functionalization of the nanotubes inferred interfacial adhesion and wettability of the same

with HBPEA matrix. The preparative layout of the covalent-noncovalent functionalized MWCNT/HBPEA nanocomposite is shown in Scheme 5A.2.

Possible mechanism of the formation of nanocomposites

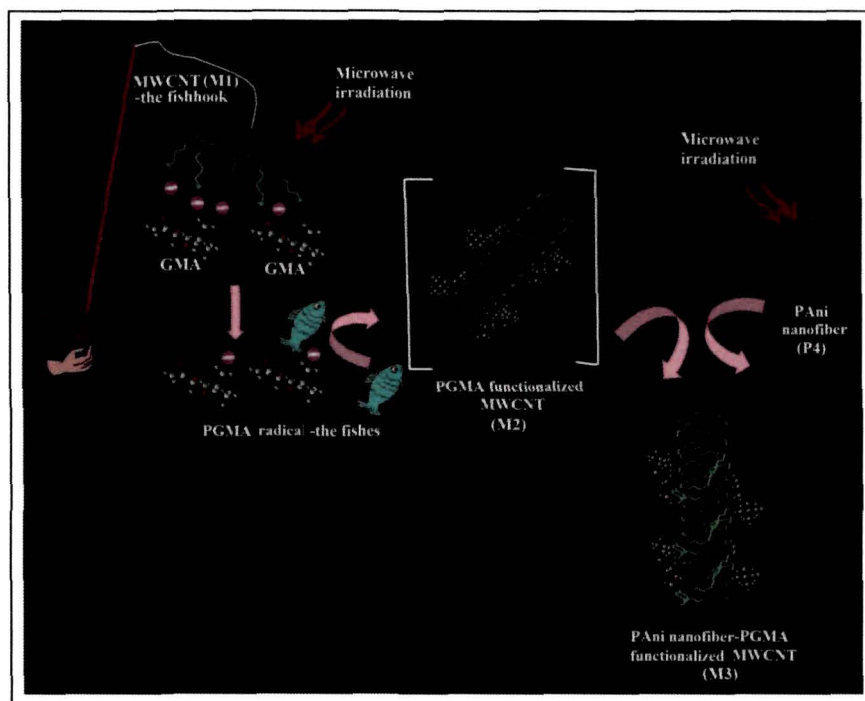
The ultrasonic wave as well as microwave irradiation played vital roles in the in exfoliation and dispersion of M3 and subsequent formation of the nanocomposites with a preferred directionality, as evident from HRTEM study (discussed in section 5A.3.2.2.). The effects of ultrasound are associated with the rapid collapse of cavitation bubbles at microsecond time scale, creating microscopic domains of high temperature and pressure.³¹ This opened up the noncovalently wrapped PANi nanofiber from the nanotube surface. Dictated by the active microwave absorption by MWCNT and PANi nanofiber,^{10,11} the prepared nanocomposites were exposed to microwave radiation to assist in the dispersion of M3 in HBPEA matrix. The strong microwave absorption is ascribed to the presence of free π electrons moving out of the graphitic framework of the nanotubes with simultaneous volume expansion of the nanotubes. The microwave absorption by the nanotubes at relatively low temperature caused thermal expansion of the nanotube layers and thereby facilitating the formation of interfacial interaction between the functionalized nanotubes and polymer matrix.³² The microwave irradiation induced localized heating of M3 at the nanotube-HBPEA interface, created static temperature gradients such that the nanotubes aligned themselves in a preferred direction within the matrix.³² This is further supported by HRTEM study (discussed in section 5A.3.2.2.).

5A.3.2.1. FTIR study

FTIR spectra of HBPEA and its nanocomposites are shown in Fig. 5A.3 (A). The characteristic FTIR bands of HBPEA corresponding to -C=O of carbonyl ester and amide appeared at same wavenumbers as reported in section 3.3.3. of Chapter 3. FTIR bands of M3 centered at 1490 and 1576 cm^{-1} were found to shift to 1462 and 1557 cm^{-1} respectively in the nanocomposites. This is attributed due to π - π interaction of delocalized π -bonds on M3 (due to sp^2 hybridization) with the aromatic rings in the backbone of HBPEA. Further the shift in absorbance band of carbonyl ester and amide were in lines parallel with the findings in section 3.3.3. of Chapter 3 owing to the presence of dispersed PANi nanofiber in these nanocomposites along with the nanotubes.

5A.3.2.2. HRTEM study

The stable and uniform dispersion of M3 in HPMWNT5, as evident from HRTEM study is instrumental in comprehending the enhancement of structural and thermal properties.



Scheme 5A.1 Schematic representation for functionalization of MWCNT

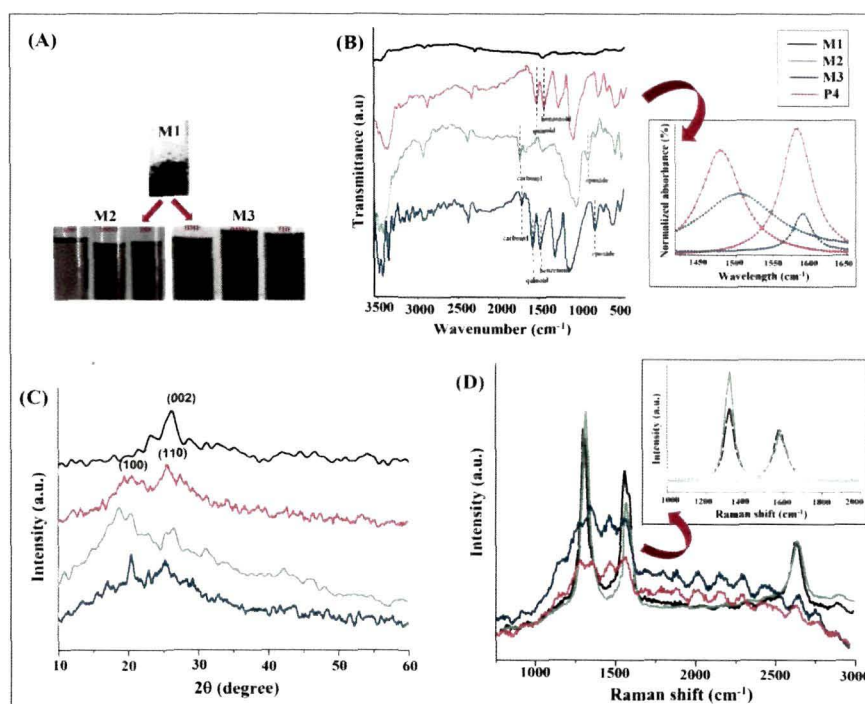


Fig. 5A.1 (A) Dispersion stability of M2 and M3; FTIR spectra with the inset of deconvoluted peaks for benzenoid and quinoid rings; (C) XRD patterns; and (D) Raman spectra with the inset of deconvoluted peaks for D- and G-bands of M1 and M2

Table 5A.2 Position, FWHM and intensity ratios of D- and G- bands for M1 and M2

Sample	Position	FWHM	I _D /I _G
M1	1319.9	56.345	0.8
	1579.4	70.834	
M2	1321.1	53.142	1.52
	1581.0	63.663	

of the nanocomposites. The appearance of furrowed-like architecture (evident from Fig. 5A.3 (B)) validated the fact that the microwave irradiation suffices for the formation of nanotube arrays in the nanocomposites.

5A.3.2.3. XRD study

XRD patterns of the thermosets of HBPEA and its nanocomposites using functionalized nanotubes are shown in Fig. 5A.3 (C). The appearance of diffraction peaks at around 19-20° and 25-26° in the nanocomposite indicated the occurrence of strong interfacial interaction between M3 and HBPEA.

The single-line method using a Voigt function is employed to analyze the presence of long range order in the prepared nanocomposites. The employment of a Voigt function was according to the method reported by Kieser et al.³³ The more intense 2θ peak at 20.3° has been deconvoluted computationally to calculate the domain length present in the nanocomposites. This gave an indication about the range of order present in the nanocomposites. According to this method, X-ray profile can be fitted to a Voigt function which is a convolution of a Gaussian and a Lorentz function. The domain length was calculated using the equation 5A.2.

$$\text{domain length} = \lambda/\beta\cos\Theta \quad \text{-----(5A.2)}$$

where β is Cauchy component of integral breadth.

It is evident from the Table 5A.3 that the domain length increased from 9.7 to 16.2 Å with increasing M3 content in the nanocomposites.

5A.3.2.4. Performance study

The performance of epoxy-poly(amido amine) cured thermosetting nanocomposites effectively changed with the varying wt% of M3. Table 5A.3 lists the properties like curing time, gel fraction, scratch hardness, impact resistance, gloss, TS and EB of the nanocomposites. It is evident from Table 5A.3 that the curing time of functionalized

nanotubes/HBPEA nanocomposites baked at 150 °C decreased significantly with the increase of M3 content. This was attributed to the presence of N-atom of benzenoid ring and O-atom of oxirane ring (of M3) which aided in the crosslinking reaction of HBPEA, and consequently in imparting strong interfacial adhesion between the nanotubes and polymer matrix. Further the preferred orientation of M3 in HBPEA matrix, as evident from HRTEM study also helped in decreasing the curing time. The increment in the gloss and scratch hardness with M3 content in the nanocomposites was attributed to the good compatibility of the nanotubes with HBPEA which amalgamated the strength of the nano-reinforcing functionalized nanotubes and flexibility of the polymer chains in the nanocomposites. The high impact resistance of the thermosets resulted due to optimum crosslinking and flexibility. HBPEA thermoset possessed TS of 7.3 MPa which increased from 9.5 to 16.2 MPa with increase in M3 content from 1 to 5 wt% in the nanocomposites. The increment in TS of HBPEA nanocomposites to ~170%, as compared to the pristine one further supported the presence of strong interfacial interaction between M3 and HBPEA. This led to the formation of dense crosslinked structure. The restricted mobility of the long fatty acid chains due to the incorporation of M3 justified the decrease (20.2%) in EB of the nanocomposites.

Table 5A.3 Performance and domain length of thermosetting covalent-noncovalent functionalized MWCNT/HBPEA nanocomposites

Physico-mechanical property	HBPEA	HBPEAM1	HBPEAM2.5	HBPEAM5
curing time (h)	10±0.02	1.5±0.02	1.2±0.01	1±0.02
gel fraction (%)	77.7±0.5	78.4±0.6	79.7±0.5	80.2±0.4
scratch hardness (kg)	8.5±0.2	9.5±0.3	10	>10
impact resistance (cm) ^a	100	100	100	100
TS (MPa)	7.3±0.5	9.5±0.4	12.7±0.6	16.7±0.5
EB (%)	88.1±0.8	83.3±0.5	77.5±0.7	70.3±0.4
domain length (Å)	–	9.7	12.4	16.2

^aMaximum limit of the instrument is 100 cm.

5A.3.2.5. Thermal study

The thermosets of HBPEA and its nanocomposites exhibited a two-step degradation pattern, similar to HBPEA (as mentioned in section 2.3.8. of Chapter 2) with dose-dependent increment of thermal stability Fig. 5A.3 (D). The initial degradation temperature increases from 278 °C in HBPEA to 325 °C in HPMWNT5. This is attributed to the nano-mechanical

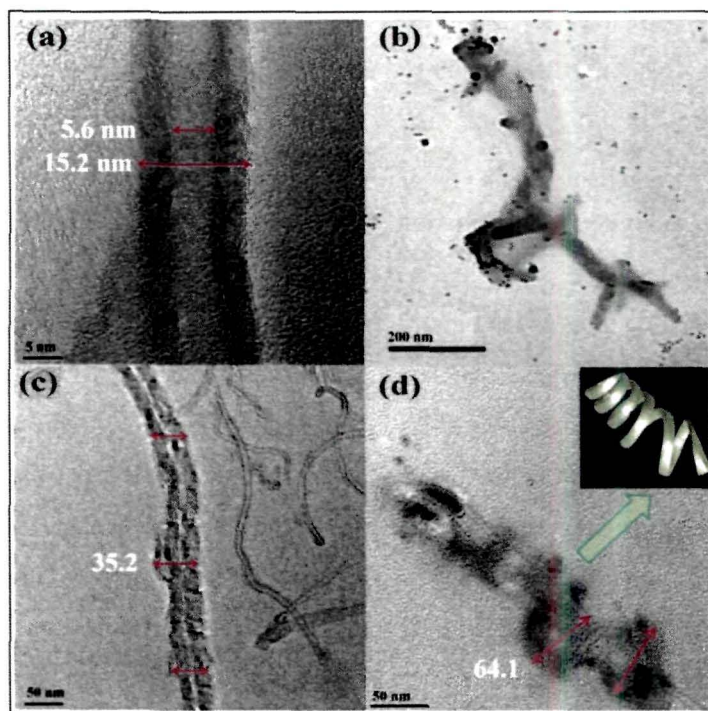
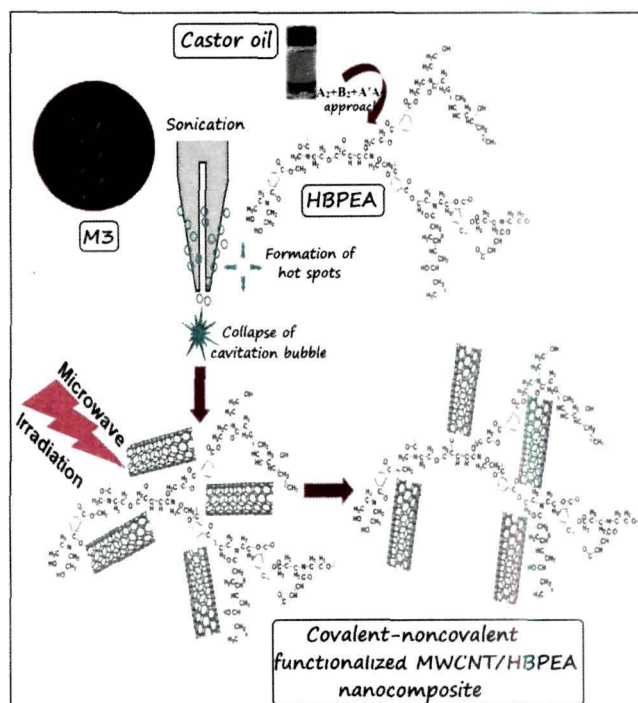


Fig. 5A.2 HRTEM micrographs of M1 (a), P4 (b), M2 (c), and M3 with the inset of tendrillar morphology (d)



Scheme 5A.2 Preparative protocol for covalent-noncovalent functionalized MWCNT/HBPEA nanocomposite

interlocking of the functionalized nanotubes within HBPEA matrix as a result of interfacial interactions between the two (as evident from FTIR study discussed in section 5A.3.2.1.). An increment of the weight residue of the nanocomposites (~2-3% as compared to HBPEA) observed at 800 °C reflected the presence of thermostable nanotubes.

5A.3.2.6. Antibacterial activity

Enumeration of CFU count

The bacterial growth was assessed by inoculating the nanocomposite films with the test strains wherein a substantial reduction in the attachment of the Gram positive and acid fast bacterial species onto the films was observed (Fig. 5A.4 (A)). The attachment of the bacterial strains was markedly less on the nanocomposite films than HBPEA film, reflecting the superiority of the antibacterial efficacy of the nanocomposites as compared to HBPEA. It was evident from Fig. 5A.4 (A) nanocomposite films possessed pronounced antibacterial activity against Gram positive bacteria (*B. subtilis* and *S. aureus*) as compared to Gram-negative ones (*E. coli* and *K. pneumonia*). The selective efficacy towards the bacterial strains is ascribed due to the differential interaction of the nanocomposites with the cell wall architecture of the two different bacterial strains.³⁴ The nanocomposite films supported relatively low viability of the acid fast bacterial strains including *M. smegmatis* mc² 155 (conventionally available antibiotic ampicillin resistant) and *M. smegmatis* ATCC14468, as compared to HBPEA films.

Protein content

In the context to bacterial adhesion onto the film surface, it is apt to mention that proteins are one of the main components of the extracellular matter during their growth.¹⁵ The reduction in the protein adsorbed on the nanocomposite films was found to be in lines parallel to CFU count (Fig. 5A.4 (B)). The bacterial colonization onto the nanocomposite films decreased with increase of M3 content, with the lowest in the case of HPMWNT5. This observation was attributed due to the presence of potent antibacterial nanomaterials viz., nanotubes and PAni nanofibers (as discussed in section 5A.1. and section 4.3.8. of Chapter 4) possessing large active surface area for the strong bacterial adsorption in the nanocomposites. This finding is further supported by the work of Liu et al.³⁵ The protein content of *B. subtilis* decreased by 80.6% as compared to *K. pneumoniae* upon culturing on HPMWNT5. The decrease of protein content resulted from the presence of M3 which retarded the bacterial cell growth, resulting in decreased proliferation rates instead of cell death. Evidently, the selective antibacterial potency and bacterial death rate enumerated by CFU count were in parallel lines

with that of the protein content results.

5A.3.2.7. *In vitro* biocompatibility study

MTT assay

The biocompatibility of the nanocomposite films was determined by spectroscopic measurement of the solubilized formazan crystals (an indirect measurement of the activity of the mitochondrial dehydrogenase) in colorimetric MTT assay (Fig. 5A.5 (A)).¹⁷ The time- and dose-dependent increment in viability of PBMC with M3 content was observed upon culturing onto the nanocomposite films. This incremental attributes of supporting PBMC testified that M3 is the key player in modulating their adhesion and proliferation on the *nanocomposite films*. *The similar cell viability upon culturing on HPMWNT5 post 48 h of incubation*, as that of the control indicated no cytotoxic effect of the nanocomposite films on the cultured cells. Shvedova et al. documented “Janus-like” properties of the nanotubes, wherein the pristine nanotubes are cytotoxic while the functionalized ones are not owing to the lowering of their surface activity.³⁶ In analogy to the above report, the attachment of PGMA and PANi nanofiber onto the surface of the nanotubes along with their dispersion in the polymeric matrix altered their cytotoxicity, and accordingly regulated the cellular interactions and biocompatibility of the nanocomposite films with PBMC.

PBMC adhesion and proliferation studies

SEM micrographs were found to be consistent with the proliferation of PBMC with M3 content in the nanocomposite films, as indicated by an apparent increase in the magnitude of the adhered cells (Fig. 5A.5 (B)-(F)). The macro- and micro-pores with diameter ranging from 0.7 to 10 μm and 39.90% porosity (Fig. 5A.5 (B)) were effective as anchoring sites for the attachment and proliferation of PBMC. The interconnected three dimensional porous structure appeared to mimic the elements of extra-cellular matrix of the cells, which subsequently improved cell attachment and growth. The optimum crosslinking density of the films resulting in low shrinkage aided in cell adhesion and imparted good biocompatibility, which corroborated well with the reports of Fernandes et al.³⁷ An interconnected structure of PBMC (appearing to imitate mesocarp of a watermelon pepo) was observed upon culturing onto HPMWNT2.5 porous film (Fig. 5A.5 (E)). However PBMC cultured onto porous HBPEAM5 film exhibited a mat-like conformation (mimicing a pseudo-graphene like sheet) with complete masking of the pores of the film by the continuous mesh of PBMC (Fig. 5A.5 (F)). The porosity of the films was instrumental in gas exchange and harboring PBMC

growth *via* passage of cell signals.³⁸ In addition to the above, the hyperbranched architecture and presence of multitude of surface functionalities also accounted for the indispensable biocompatible perspectives of HBPEA nanocomposites. To this end, Rajaraman et al.³⁹ reported that proliferation of PBMC depended on the active surface area, number density of the adhesion sites and other substrate receptors. The decreased activation of mitochondria mediated apoptotic pathway of the cells by carbonyl groups present in HBPEA and its nanocomposites too played an influential role in imparting biocompatibility.⁴⁰ Thus PBMC proliferation study using SEM correlated well with the findings of MTT assay.

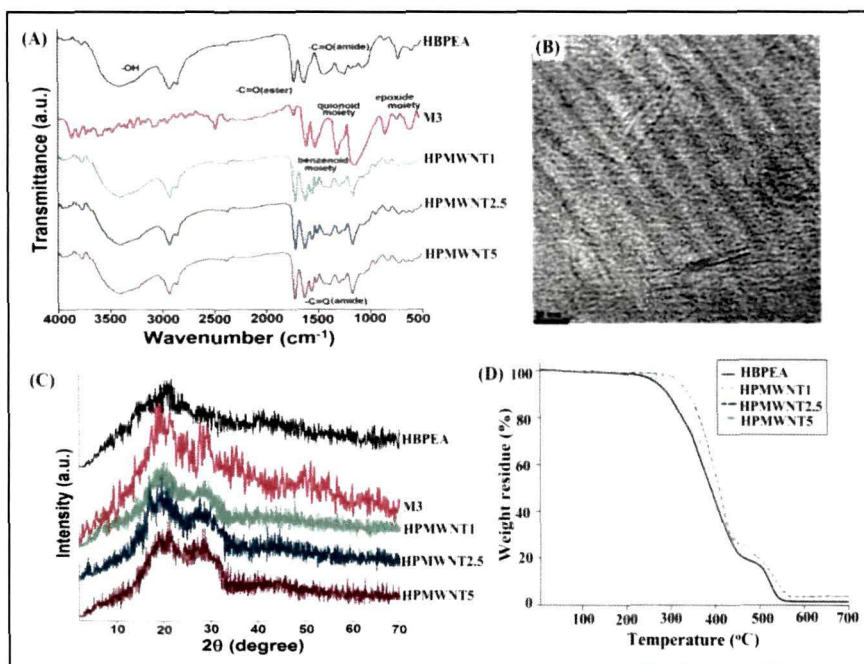


Fig. 5A.3 (A) FTIR spectra; (B) HRTEM micrograph of HPMWNT1; (C) XRD diffractograms; and (D) TG thermograms of HBPEA and covalent-noncovalent functionalized MWCNT/HBPEA nanocomposites

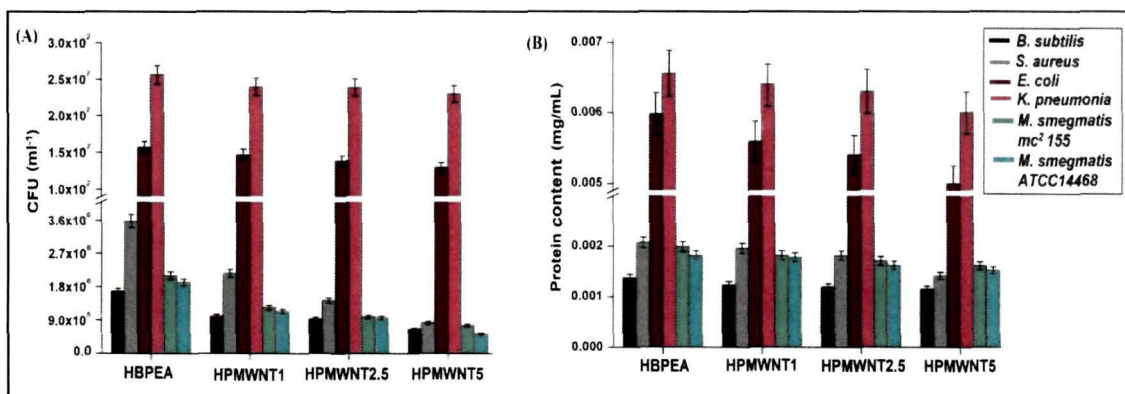


Fig. 5A.4 (A) CFU count; and (B) protein content

5A.3.2.8. ROS study

FRAP assay is imperative from the perspective of toxicity concerns of the production of ROS is one of the health hazards concerned with the exposure to the nanotubes.⁴¹ FRAP assay relies on the reduction of Fe³⁺ (ferric)-TPTZ complex to an intense blue colored Fe²⁺ (ferrous) form.¹⁸ The reducing ability of the nanocomposites (proportional to the amount of Fe²⁺ formed) was quantified spectrophotometrically at 593 nm (Fig. 5A.6 (A)). Ascorbic acid and the nanocomposites exhibited an absorbance of 0.68 and ~0.5 respectively, post 10 min interaction with Fe³⁺-TPTZ. While M1 showed no absorbance at 593 nm owing to its pronounced oxidative nature, M3 exhibited a low absorbance value of 0.09. The functionalization of the nanotubes thus played a prime role in quenching of ROS relative to the pristine nanotubes, and consequently in imparting low toxicity to the nanocomposites.

5A.3.2.9. Biodegradation study

In vitro biodegradation of HBPEA and functionalized nanotubes/HBPEA nanocomposite films occurred as an extracellular process in PBS catalyzed by lipase *via* enzymatic oxidative mechanism. The scission kinetics of ester bond was evident from the decrement of $I_{\text{ester}}/I_{\text{amide}}$ of the biodegraded films (Fig. 5A.6 (B) and (C), and Table 5A.4). The mass loss profile of the biodegraded films characterized by surface erosion mechanism showed considerable decrement of 17.09, 25.04, 31.16 and 38.19% in the mass of HPMWNT1, HPMWNT2.5 and HPMWNT5 films respectively (Fig. 5A.6 (D)).

Lipase which is interfacially activated at the water-polymer interface, assists in the enzymatic hydrolysis of the ester moieties present in the polymeric backbone.⁴² The enzyme contains buried catalytic sites and their activation occurs as a result of a conformational change induced upon binding to the polymeric substrate. In aqueous media, the helical lid covers the active site of the enzyme and blocks its access to the substrate. The same rolls back and the active site becomes accessible upon contact with the hydrophobic polymeric substrate and consequently the enzyme attains its active conformation.⁴² Lipase catalyzed ester bond hydrolysis and subsequent surface erosion at the interface of water-substrate takes place post imbibition of water into substrate *via* its polar functional groups. The increase of polar moiety with M3 content in the nanocomposites increased the wettability of the films by sorption and penetration of water into the same which promoted the accessibility of the polymer chains towards lipase, and thus justified the dose-dependent increment in its degradability. However the release of the nanotubes in the human body upon degradation of the nanocomposites in due course of time yields concern in context to their cytotoxicity. In

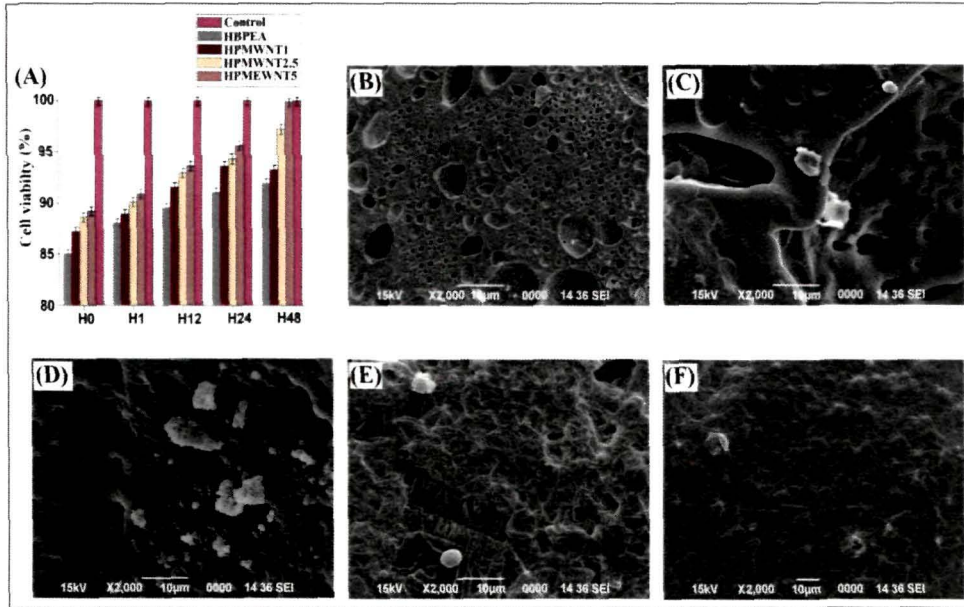


Fig. 5A.5 (A) MTT assay; (B) SEM micrograph of porous film; SEM micrographs of PBMC adhesion and proliferation upon seeding onto: (C) HBPEA; (D) HPMWNT1; (E) HPMWNT2.5; and (F) HPMWNT5

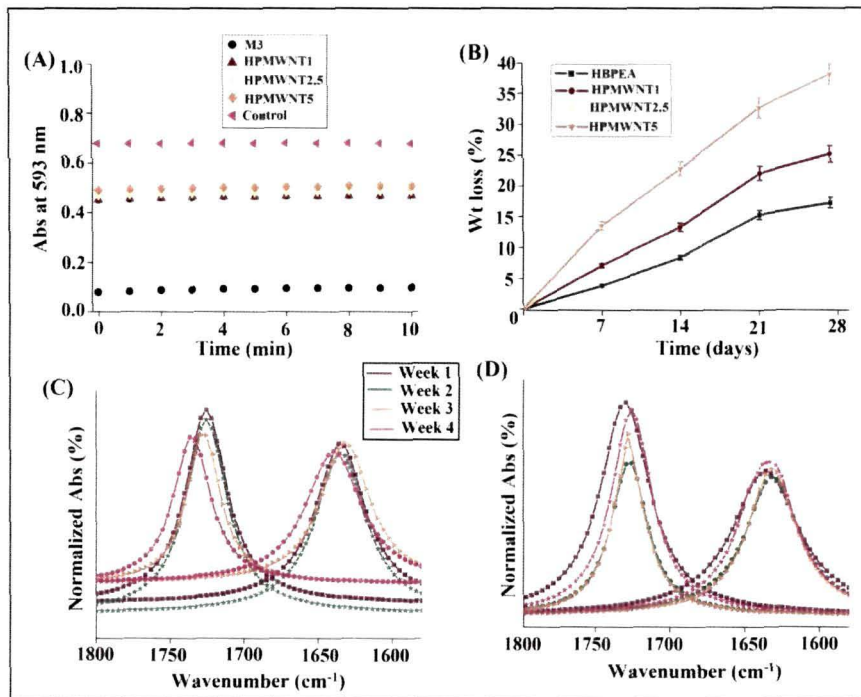


Fig. 5A.6 (A) ROS kinetics; (B) weight loss profile; (C) and (D) deconvoluted I_{ester}/I_{amide} of HBPEA and HPMWNT5

Table 5A.4. Ratio of intensity of ester and amide bands of HBPEA and HPMWNT5

Sample	$I_{\text{ester}}/I_{\text{imide}}$			
	1 st week	2 nd week	3 rd week	4 th week
HBPEA	1.12	1.05	0.92	0.89
HPMWNT5	1.11	0.89	0.75	0.61

this vein, the findings of Kagan et al.⁴³ proved effective in addressing the same. The radical intermediates generated inside the human bio-fluids such as myeloperoxidase and hypochlorite catalytically biodegrades the nanotubes releasing carbon dioxide without generating any inflammatory response.

5A.4. Conclusion

The subchapter 5A documented the microwave induced fast and facile approach for the covalent-noncovalent functionalization of the nanotubes and, the preparation of multifaceted functionalized nanotubes/HBPEA nanocomposites by the *ex-situ* technique. Various spectroscopic and microscopic tools validated the covalent functionalization of the nanotubes using PGMA and noncovalent wrapping onto the same by PAni nanofiber and the formation of the nanocomposites. The pronounced and selective antibacterial efficacies of the nanocomposites towards Gram positive and acid fast bacterial strains, biocompatibility with PBMC and biodegradation augmented in parallel lines with the increase in the functionalized nanotube content in the nanocomposites. The formation of thermosetting nanocomposites resulted acceptable improvement of desired properties including mechanical property instrumental for providing mechanical integrity to the cultured cells. The above findings open up promising avenue of these microporous and multifunctional nanocomposites to be exploited as antibacterial dressing materials for infected burn wounds. The adherence and proliferation of PBMC which stimulates the release of interleukin 2 (IL2) (whose production is inhibited by the lipid protein layer produced in the skin post burning accident), an essential component for the growth of IL2-dependent lymphocytes in the periphery of the infected burn wound region, forms the rationale behind the practical utility of the same as the aforementioned dressing material. Further decrease in the bacterial colonization onto the wound surface is favorable for reduction in the infection rate post burn accidents. However, the safe utility of these nanocomposites in bio-medical domain demands for the *in vivo* assessments.

5B. Noncovalent functionalized multi-walled carbon nanotube/hyperbranched poly(ester amide) nanocomposites

5B.1. Introduction

Despite our earlier effort on realizing the extraordinary potential of MWCNT through a single pot covalent-noncovalent combined approach, an apt functionalization strategy proceeding without distortion of the high aspect ratio and π -conjugated structure of the nanotubes using greener technology remains on the horizon. Further even though significant performance of the HBPEA nanocomposites prepared by using microwave-assisted functionalized nanotubes was tantalizing, but attainment of remarkable properties of the nanotubes including high electrical conductivity and thermostability was difficult owing to its low content in the nanocomposites. As remarked in section 5A.1. of subchapter 5A, a large amount of functionalizing agent such as GMA was utilized, which drastically reduced the amount of the nanotubes in the nanocomposites. This hindered in the utilization of the complete potential of the nanotubes in the nanocomposites. Thus the modulation of the interfacial surface properties of the nanotubes necessitated the search for a novel recipe for noncovalent functionalization of the same, which relies on supramolecular interactions including π - π stacking, van der Waals and charge transfer.^{44,45} Moreover the global impetus on opting for greener functionalization protocols for the nanotubes has instigated the search for an appropriate bioresource for the noncovalent functionalization of the same. In this vein, DEFA, which appears to mimic an amphiphilic surfactant seemed to be a promising bio-based resource for tuning the surface properties of the nanotubes. At this juncture it is pertinent to mention that DEFA can serve the twin role as a modifying agent and a precursor for the preparation of HBPEA. However the noncovalent functionalization of the nanotubes and *in-situ* preparation of bio-based HBPEA/MWCNT nanocomposites simultaneously in a single pot reaction has never been attempted. Our current target also engulfs to scrutinize the properties of the nanocomposite and probe into its potential applications.

In context to the above, the exploitation of specific properties of the nanotubes including inhibition of microbial adhesion, high thermostability and unique electrical conductivity in the nanocomposites proved instrumental in tailoring the antibacterial, thermal and antistatic properties. These engineered materials have high demand in commercial and industrial applications as high-value added products like flooring materials, sizing agent, textile materials, computer housing materials, and exterior automotive parts and so on.

Thus motivated by the *avant-garde* prospects of such multifunctional materials, the present work focused on the noncovalent functionalization of nanotubes using DEFA and using the same as the precursor for the polycondensation reaction to yield HBPEA/MWCNT nanocomposites. A comprehensive study of thermal degradation kinetics of the nanocomposites and probing into their antibacterial and antistatic properties were also performed.

5B.2. Experimental

5B.2.1. Materials

5B.2.1.1. Chemicals

The materials required for the preparation of HBPEA thermosets and solvents such as THF and DMSO (distilled before use) are the same specification as mentioned in section 2.2.1.1. of Chapter 2.

MWCNT purchased was of same specification as discussed in section 5A.2.1.1. of subchapter 5.

5B.2.1.2. Microbial strains

The bacterial strains *viz.*, *B. subtilis* (MTCC441), *S. aureus* (MTCC373), *Escherichia coli* (DH5 α) and *P. aeruginosa* (MTCC 7814) used in the antibacterial study were obtained from the Department of Molecular Biology and Biotechnology, Tezpur University. The reagents including Mueller Hinton Broth, streptomycin sulfate, BSA and Bradford reagent were of same specification as mentioned in section 5A.2.1.2. of subchapter 5.

5B.2.2. Methods

5B.2.2.1. Noncovalent functionalization of MWCNT

DEFA was prepared by transamidation reaction as described in section 2.2.2.3. of Chapter 2. MWCNT (in varying wt% of 0.25, 0.5 and 1) was mixed with DEFA (0.01 M) and subjected to sonication for an interval of 15 min.

5B.2.2.2. *In-situ* preparation of nanocomposites

The nanocomposites were prepared by *in-situ* polymerization technique using nanoconjugate (A₂, in varying wt% of 0.25, 0.5 and 1) and dibasic acids (B₂) as bifunctional monomers and DiEA as the trifunctional monomer (A'A₂). The appropriate composition of the reactants and the reaction conditions were as described in section 2.2.2.4. of Chapter 2. The nanocomposites prepared using varying wt% of 0.25, 0.5 and 1 nanoconjugate were

coded as HPFCNT0.25, HPFCNT0.5 and HPFCNT1 respectively. The prepared nanocomposites were cured by the same method as described in section 3.2.2.2. of Chapter 3.

5B.2.3. Instrumentation

FTIR analysis and X-ray diffractograms were obtained using the same instruments as described in section 3.2.3. of Chapter 3. The nanoconjugate was prepared using same probe sonicator and under same conditions as mentioned in section 3.2.3. of Chapter 3. HRTEM micrographs of the nanoconjugates and nanocomposites were obtained using the same instrument as discussed in section 4.2.3. of Chapter 4. The directional coherency coefficient of the dispersed nanotubes in the nanocomposites was evaluated using Fiji software. The plug-in used in the software evaluates the local orientation and isotropic properties like coherency and energy of every pixel of HRTEM micrograph based on structure tensors. The measurements including curing time, percent gel fraction, scratch hardness, impact resistance, gloss, TS and EB were performed according to the standard methods as mentioned in section 2.2.3. of Chapter 2. The sheet resistance of the nanocomposite films was measured by the same technique as discussed in section 3.2.3. of Chapter 3. Dynamic thermogravimetric degradation analyses were performed at four linear heating rates (denoted as β) of 5, 7.5, 10 and 12.5 °C/min using Perkin-Elmer TGA-4000 thermobalance from 25-700 °C at the nitrogen flow rate of 30 mL/min.

5B.2.4. Thermal degradation kinetics study

The thermal degradation kinetics and mechanism of degradations were evaluated from the TG curves using Ozawa-Wall-Flynn non-isothermal integral isoconversion method.^{46,47} This is an isoconversional method based on the fact that the reaction mechanism is independent of heating rate for a given degree of conversion (denoted as α), in a non-isothermal experiment. In other words, the iso-conversional plots evaluate activation energy (denoted as E_a) regardless of the reaction mechanism. In thermogravimetric analysis, the rate of degradation (dx/dt , where 'x' is the mass of degraded product at time 't') is correlated with the function $x [f(x)]$ using the following Arrhenius equation 5B.1.

$$\frac{dx}{dt} = A \exp\left(\frac{E_a}{RT}\right) f(x) \quad \text{-----(5B.1)}$$

where 'A' is the frequency factor, 'R' is the gas constant and 'T' is the absolute temperature.

Since heating rate, $\beta = \frac{dT}{dt}$, the equation (5B.1) can be rewritten as

$$\int_{x_2}^{x_1} \left(\frac{dx}{f(x)}\right) = \int_{t_2}^{t_1} A \exp\left(\frac{-E_a}{RT}\right) dt = \frac{A}{\beta} \int_{T_2}^{T_1} \exp\left(\frac{-E_a}{RT}\right) dT \quad \text{-----(5B.2)}$$

$$\int_{x_2}^{x_1} F(x) = \frac{A}{\beta} \int_{T_2}^{T_1} \exp\left(\frac{E_a}{RT}\right) dT \quad \text{----- (5B.3)}$$

$$\text{when } \int_{x_2}^{x_1} F(x) = \int_{x_2}^{x_1} \left(\frac{dx}{f(x)}\right)$$

Then equation (5B.3) becomes

$$F(x_1) - F(x_0) = \frac{AE_a}{\beta R} \{P(E_a/RT_1) - P(E_a/RT_0)\} \quad \text{----- (5B.4)}$$

$$\text{where } y = E_a/RT, p(y) = \frac{e^{-y}}{y} - \int_y^\infty \frac{e^{-y}}{y} dy \quad \text{----- (5B.5)}$$

As $T_1 > T_0$, the term in equation (5B.4) can be neglected.

$$\text{Thus } F(x_1) - F(x_0) = \frac{AE_a}{\beta R} \{P(E_a/RT_1)\} \quad \text{----- (5B.6)}$$

x_1 is determined by putting $x_0 = 0$

$$AE_a/\beta R \{P(E_a/RT_1)\} = \text{constant} \quad \text{----- (5B.7)}$$

T_1 at x_1 varies with the change of β and so the right hand side of the equation (5B.6) is constant. Using the above approximations, the following equation (5B.8) is obtained.

$$\log \beta = -0.4567 E_a/R \times 1/T_1 + \text{constant} \quad \text{----- (5B.8)}$$

This equation was used to determine the E_a for the degradation process.

5B.2.5. Antibacterial activity

The culturing of bacterial strains and determination of the antibacterial activity of the nanocomposites by enumeration of CFU count¹⁴ and total protein content.¹⁵ They were performed by the same methods as mentioned in section 5A.2.4. of subchapter 5A.

5B.3. Results and discussion

5B.3.1. Preparation of nanoconjugate

The interactions between the nanotubes and DEFA in the nanoconjugate depend on the surface properties, particularly surface energy of both the components.^{48,49} As the nanotubes have much higher surface energy as compared to DEFA molecules, the latter exhibited a tendency to spontaneously aggregate on the surface of the nanotubes, thereby minimizing the total energy of the nanoconjugate system and hence imparting stable dispersion without coalescing.⁴⁹ Thus a scenario aroused wherein the hydrophobic portion of DEFA got anchored to the surface of the nanotubes through secondary interactions, while the hydrophilic -OH groups of DEFA (extending outwards from the nanotubes) induced electrostatic repulsions between DEFA adsorbed nanotubes, thereby preventing

reagglomeration of the nanotubes.

Plausible mechanism for the formation of nanoconjugate

DEFA mimics the amphiphilic properties of a non-ionic surfactant and thus tends to adsorb onto MWCNT and self-assemble into supramolecular architecture. The concomitant use of sonochemistry and surfactant led to the exfoliation of the nanotube aggregates.⁴⁸ The sonication provided a high local shear to MWCNT agglomerates generating dangling bonds at high energy adsorption sites of the nanotubes.⁴⁹ The propagation of ultrasound energy through a series of compression and rarefaction⁴⁹ produced shock waves in medium that facilitated the unzipping⁴⁸ of individual nanotubes from the aggregates, followed by the impregnation of DEFA molecules in the space between the two curved surfaces of the nanotubes. Consequently DEFA got hooked onto these interstitial and groove regions of the nanotubes.⁴⁸ In other words, the formation and sudden collapse of small cavitation bubbles and formation of microjets of energy caused brownian motion of the nanotubes.⁴⁹ These consequently created adsorption sites onto the surface of the nanotubes, thereby facilitating the adsorption of DEFA molecules. The preparation of the nanoconjugate is presented in Scheme 5B.1 (A).

5B.3.2. Preparation of nanocomposites

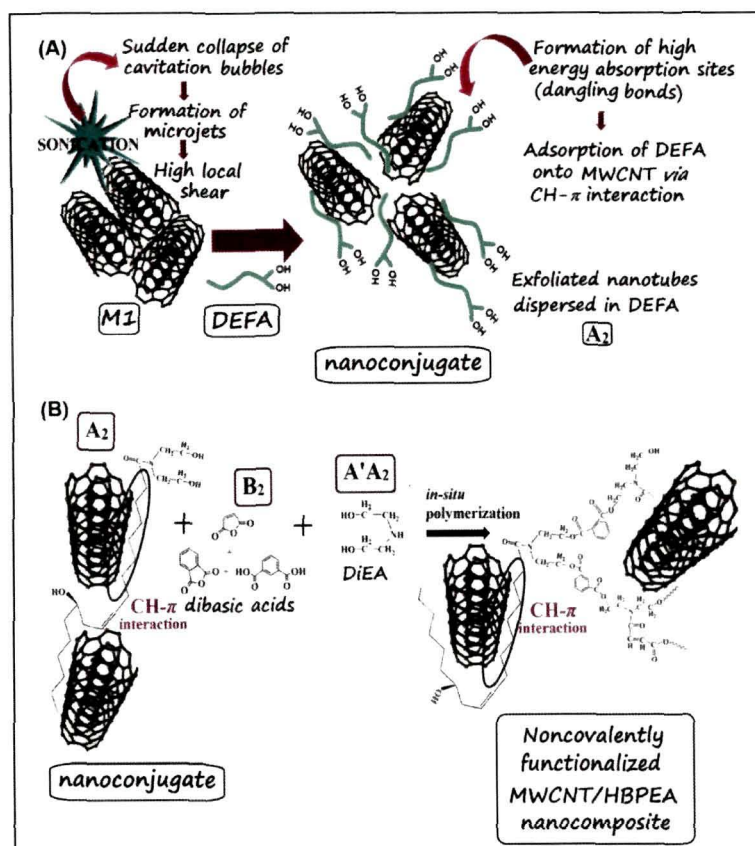
The prepared nanoconjugate was used as one of the reactive components for the *in-situ* preparation of the noncovalent functionalized MWCNT/HBPEA nanocomposites (Scheme 5B.1 (B)). The interaction between the delocalized π -bonds of the nanotubes became strong upon π -stacking with the aromatic rings of the dibasic acid/anhydrides (supported by FTIR study discussed in section 5B.3.3.). The wetting of the nanotubes by the adsorbed HBPEA chains triggered two types of interactions namely, entropic repulsive interactions and enthalpic attractive interactions.⁵⁰ The entropic repulsive interactions are associated with the abatement in the conformational degrees of freedom of HBPEA, which is attributed to the excluded volume interactions between the nanotubes and the polymer chains.⁵⁰ However the presence of enthalpic attractive interactions attributed to the CH- π interactions,⁵¹ competed and superseded over the entropic repulsive effect and led to the adsorption of HBPEA chains. This consequently led to the formation of dense polymer layers onto the surface of the nanotubes similar to that of the 'polymer brush'.⁵⁰ Thus the adsorption of HBPEA onto the surface of the nanotubes is driven by the minimization of the free energy of the polymer-nanotube system by maximizing the energetically favorable secondary interactions between the same. Further Star and Stoddart⁵² studied the molecular modeling of

hyperbranched polymers and reported that their free volume provided an adequate fit of the nanotubes dispersed in the matrix.

5B.3.3. FTIR study

FTIR spectra of M1, DEFA, nanoconjugate, HBPEA and HPFCNT1 are shown in Fig. 5B.1 (A). The carbonyl amide absorption band and $-\text{CH}=\text{CH}-$ bending vibration of DEFA appeared at around 1620 and 772 cm^{-1} respectively, while no prominent absorption band appeared for M1. FTIR spectrum of the nanoconjugate exhibited the same absorptive bands of DEFA with slight shifting of carbonyl amide stretching and C-H bending vibrations (both $-\text{CH}=\text{CH}-$ and $-\text{CH}_2$ (CH_b)) of the fatty acid chain. The shifting of the above-mentioned carbonyl amide band and $-\text{CH}=\text{CH}-$ bending vibration of DEFA to 1626 and 716 cm^{-1} respectively in the nanoconjugate are attributed to the interactions of the carbonyl amide and, π -bond of $-\text{CH}=\text{CH}-$ with the π -aromatic framework of the nanotubes. The presence of the nanotubes broadened and shifted the CH_b vibration band (1441-1454 cm^{-1}) in the nanoconjugate (Fig. 5B.1 (B)), which is attributed to the $\text{CH}-\pi$ interactions.⁵¹ The appearance of several functional groups in FTIR spectrum of the nanoconjugate thus supported the functionalization strategy. The bands of HBPEA corresponding to $-\text{C}=\text{O}$ appeared at 1730 cm^{-1} , amide group at 1632 cm^{-1} and hydrogen bonded $-\text{OH}$ stretching at 3422 cm^{-1} . Further the broadening of CH_b of HPFCNT1, positioned at 1457 cm^{-1} and splitting of the same into doublets (Fig. 5B.1 (C), analyzed by deconvolution) upon interaction of HBPEA chains with the nanoconjugate confirmed the presence of $\text{CH}-\pi$ interaction between the same.⁵¹ $\text{CH}-\pi$ interaction is basically a 'soft acid-soft base' interaction, which increases owing to the increase in the chain length and cooperative multiple interactions in HPFCNT1.⁵¹

Further, one obvious question which arises is whether the $-\text{OH}$ groups of the nanoconjugate are free and reactive for polycondensation reaction or not. To answer this question, a reaction was carried out between the nanoconjugate and the dibasic acid/anhydride in the absence of DiEA under the same conditions as described in section 2.2.2.4. of Chapter 2. FTIR spectrum (Fig. 5B.1 (D)) of the above resulted polymer showed the formation of ester linkages upon interaction of $-\text{OH}$ groups of nanoconjugate with dibasic acid/anhydride (Fig. 5B.2). This confirmed the hydrophobic interaction between the nanotubes and DEFA, with freely exposed $-\text{OH}$ groups in the nanoconjugate. Thus the presumption of the presence of free and reactive $-\text{OH}$ groups on the surface of the nanoconjugate was reasonably validated from the above finding.



Scheme 5B.1 (A) Schematic representation for coupled action of sonication and DEFA in noncovalent functionalization of MWCNT; and (B) proposed mechanism for formation of noncovalently functionalized MWCNT/HBPEA nanocomposite

5B.3.4. XRD study

Fig. 5B.2 shows XRD patterns of HBPEA and its nanocomposites. M1 exhibits (002) plane owing to its π -aromatic framework at around 26.2° ,²⁷ while HBPEA exhibits a broad amorphous peak at around 20 - 21° . The appearance of a sharp diffraction peak at around 25 - 26° in the nanocomposites is attributed to the presence of nanotubes in HBPEA matrix. However the minimal intensity of the above peak in the nanocomposites is due to low content of the nanotubes.

5B.3.5. HRTEM study

Fig. 5B.3 showed HRTEM micrographs of M1, nanoconjugate, HPFCNT0.25 and HPFCNT0.5. It is evident from the micrographs that the organization of DEFA onto the surface of the nanotubes indicated random adsorption with no preferential arrangements of the DEFA molecules, which is also supported by the report of Vaisman et al.⁵³ The surface

roughness and thickness (by 30 nm) of the nanotubes increased upon functionalization using DEFA as compared to the smooth and fine sidewalls of the pristine ones (Fig. 5B.3 (A)) owing to the adherence of DEFA chains on the external surface of the nanotubes (Fig. 5B.3 (B)). The coiled geometry of a few nanotubes envisaged from HRTEM micrograph of the nanoconjugate (Fig. 5B.3 (C)) is attributed to the formation of dangling bonds (incorporation of strained pentagons and heptagons in the hexagonal framework of the nanotubes)⁵⁴ during sonication. Fig. 5B.3 (B) also showed the intercalation of the low-molecular weight DEFA (381 g/mol) into the internal diameter of the nanotubes.⁵⁵ However upon polycondensation reaction of the nanoconjugate with the dibasic acids, efficient filling up of the internal cavity⁵⁵ of the nanotubes was evident from Fig. 5B.3 (D). The increase of thickness of the nanotubes in the nanocomposite (Fig. 5B.3 (D)) is attributed to the formation of ‘polymer brush’ (increment in the thickness of the nanotubes by 5 nm in the nanocomposites as compared to the nanoconjugate). In other words, HBPEA chains attached onto the surface of the nanotubes, tethered their ends and resulted in the formation of dense layers (‘polymer brush’).⁵³ An increment in connectivity of the nanotubes in HBPEA matrix was observed with the increase of content of the nanoconjugate in the nanocomposites (Fig. 5B.3 (E) and (F)).

Further the formation of continuous network of the nanotubes together with Y-shaped junctions in case of HPFCNT1 was confirmed by HRTEM micrograph (Fig. 5B.4 (A)). The directional analysis of HPFCNT1 showed that the dispersed nanotubes were oriented isotropically with a mean coherency coefficient of 0.229 (Fig. 5B.4 (B)-(D)). Coherency coefficient value is bounded between 0 and 1. The values close to 1 represents the orientation of the nanotubes in the direction of an ellipse long axis, indicating a highly oriented structure.⁵⁶ On the other hand, the values close to 0 represents a circle, indicating no preferential orientation.⁵⁶ It is evident from the selected area electron diffraction (SAED) patterns (Fig. 5B.4 (E)) that the periodic structure of the nanotubes exhibited consecutive and continuous prominent rings. However the diffused ring pattern (Fig. 5B.4 (F)) of HPFCNT1 is attributed to the absence of long range order or masking of the nanotubes by the tethered polymer chains.

5B.3.6. Physico-mechanical performance study

The performance of the epoxy-poly(amido amine) cured thermosetting noncovalently functionalized MWCNT/HBPEA nanocomposites effectively changed upon incorporation of varying wt% of the nanoconjugate (Table 5B.1). The decrease of curing time of the

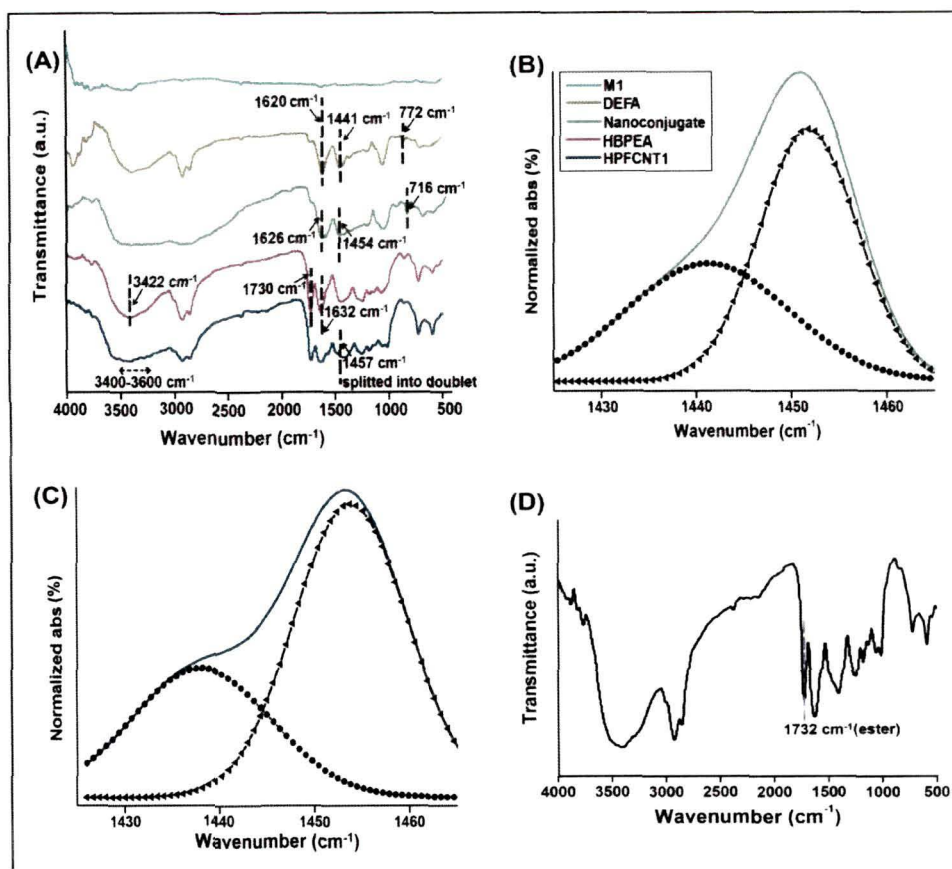


Fig. 5B.1 (A) FTIR spectra; (B) deconvoluted FTIR peak of CH_b of nanoconjugate; (C) deconvoluted FTIR peak of CH_b of HPFCNT1; and (D) FTIR spectra of polymer showing the formation of ester linkage

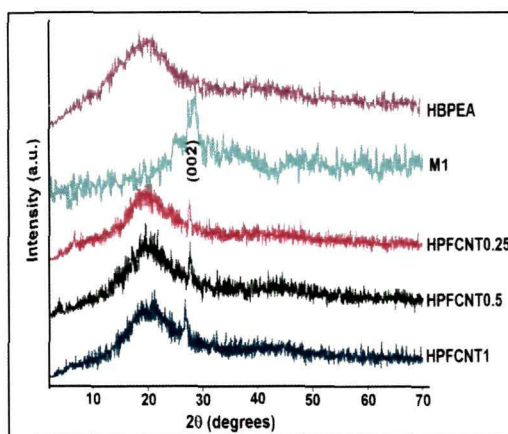


Fig. 5B.2 XRD patterns of HBPEA and noncovalent functionalized MWCNT/HBPEA nanocomposites

nanocomposites baked at 150 °C is attributed to the presence of high thermally conducting nanotubes (3000 W/mK)^{57,58} within HBPEA matrix, which supported the effective heat transfer and thereby creating a uniform temperature throughout the matrix. The increment in the gloss was attributed to the homogeneous dispersion and strong interaction of the nanotubes with HBPEA matrix. The increase of scratch hardness of the nanocomposites with nanoconjugate content is due to the high strength of the nanotubes coupled with the flexibility of the long chain fatty acid chains of HBPEA. The high impact resistance of the thermosets reflected the presence of optimum percentage of gel fraction imparting rigidity and flexibility of the nanocomposites.

The increment in TS of the nanocomposite (7.3 MPa in HBPEA thermoset to 12.3 MPa in HPFCNT1) is attributed to the strong interfacial interaction between the nanoconjugate and the HBPEA matrix (as evident from the above studies). These interactions greatly enhanced the dispersion of the nanotubes and the interfacial adhesion of the both, thereby strengthening the mechanical performance of the resultant nanocomposites.⁵⁸ The high aspect ratio of the homogeneously dispersed nanotubes also aided in affording reinforcing effect to the nanocomposites. The reduction in EB of the thermosetting nanocomposites with the increasing nanoconjugate content is ascribed to the restricted molecular mobility of the HBPEA chains at the interfacial region between the nanotubes and the long polymer chains (Table 5B.1). However the decrease in EB was not much pronounced because of the plasticization effect of the fatty acid chains attached onto and intercalated within the nanotubes.

5B.3.7. Antibacterial activity

It was evident from Fig. 5B.5 (A) that the death rate of the bacteria obtained from CFU count was higher for the nanocomposites as compared to HBPEA. The incorporation of 1 wt% nanoconjugate in HBPEA matrix increased the death rate of *S. aureus* by 137.5% and *B. subtilis* by 107.6% as compared to that of HBPEA. The architectural difference in the cell wall structures of the two different bacterial forms the rationale behind the selective efficacy of the nanocomposites.

The reduction in the amount of protein adsorbed on the nanocomposite films correlated well with the bacterial death rate (Fig. 5B.5 (B)). The enumeration of the viable cells and their protein content films indicated the anti-adhesion property of the nanocomposites. HPFCNT1 exhibited more than ten-fold higher anti-adhesion activity than HBPEA films owing to the presence of the nanotubes. This is attributed due to the presence

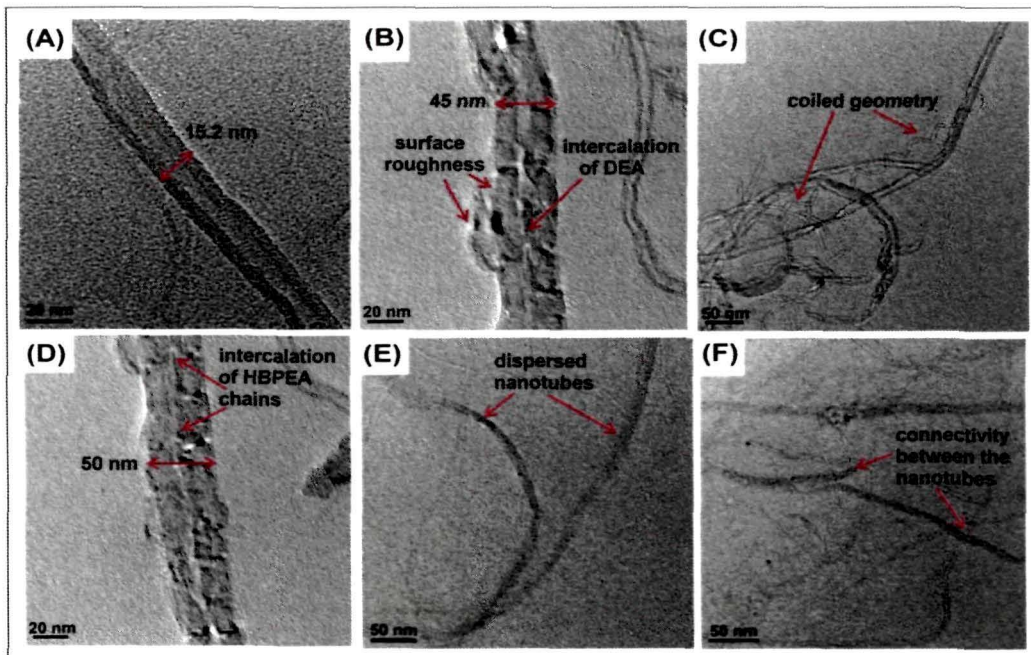


Fig. 5B.3 HRTEM micrographs of: (A) M1; (B) nanoconjugate; (C) coiled geometry of the nanoconjugate; and (D) surface roughness of nanoconjugate; (E) HPFCNT0.25; and (F) HPFCNT0.5

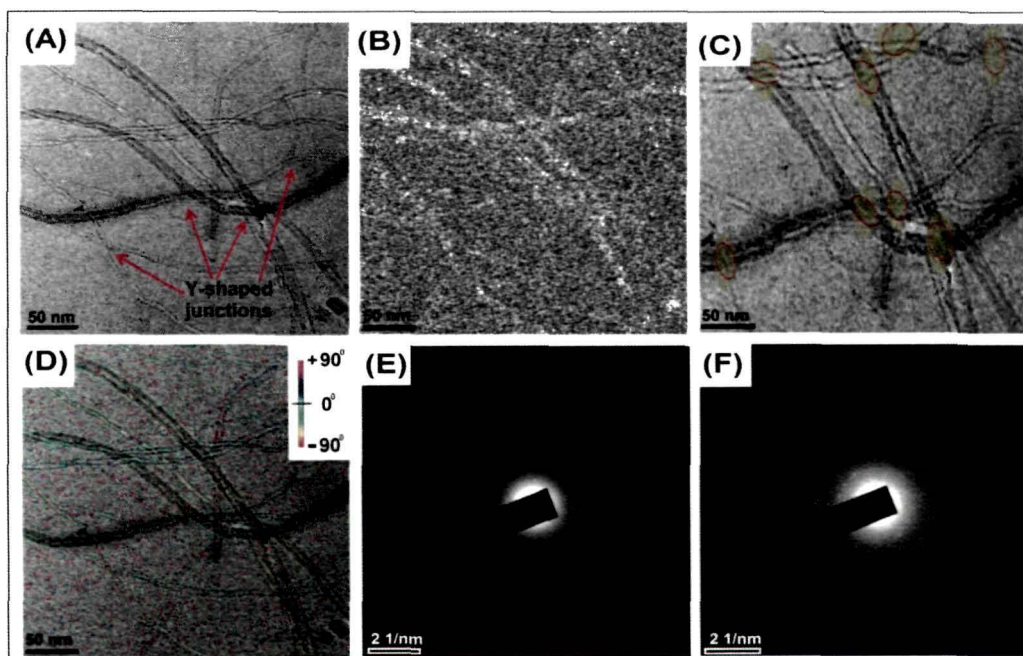


Fig. 5B.4 HRTEM micrographs of HPFCNT1; (B) coherency map; (C) HRTEM micrograph (for calculation of coherency coefficient); (D) HSB-color coded map; and SAED pattern of: (E) M1; and (F) HPFCNT1

Table 5B.1 *Physico-mechanical performance of thermosetting noncovalent functionalized MWCNT/HBPEA nanocomposites*

Physico-mechanical property	HBPEA	HPFCNT0.25	HPFCNT0.5	HPFCNT1
Curing time (h)	10±0.02	3.2±0.03	2.9±0.03	2.5±0.02
Gel fraction (%)	77±0.5	77.9±0.5	79.3±0.2	80.5±0.3
Scratch hardness (kg)	8.5±0.2	9±0.2	10	>10
Impact resistance (cm)	100	100	100	100
Gloss at 60°	90±0.5	91.5±0.6	91.7±0.6	92.2±0.4
TS (MPa)	7.3±0.5	8.7±0.3	10.4±0.6	12.3±0.5
EB (%)	88.1±0.8	86.1±0.5	85.3±0.5	82.7±0.4

of the nanotubes which act as 'nano darts' in degrading the bacterial cell integrity by physical puncture mechanism.³⁵

5B.3.8. Thermal degradation kinetics study

The degradation kinetics study provided a convenient platform for quantifying the performance of the nanocomposites in terms of their thermal stability. The kinetic parameters like activation energy, E_a was calculated from the slope of the linear plot of $\ln \beta$ versus $1000/T$ employing the following equation 5B.8.

The thermal degradation patterns of the HBPEA and its nanocomposite assessed by thermogravimetric analyses (Fig. 5B.6) are a two-step degradation process, with first and second degradation steps attributed to the degradation of the ester and amide linkages respectively (as discussed in section 2.3.8. of Chapter 2). It was evident from Fig. 5B.7 and Fig. 5B.8 that the linear straight line fittings are approximately parallel at different ' β ' against reciprocal of temperature ($1000/T$) for different extents of ' α ' for both first and second steps of degradation kinetics. E_a corresponding to the different α values under nitrogen atmosphere were determined from the slope of the plots of β versus $1000/T$.⁴⁶ The values of correlation factors ranges between 0.990 and 0.998, which justified the linear association between β and T , resulting statistically significant values of E_a . Fig. 5B.9 (A) shows the plot of E_a calculated by Ozawa–Flynn–Wall method, against percent conversion, α .⁴⁶ It is evident from Fig. 5B.9 (A) that E_a of the first and second steps of the degradation remained fairly constant throughout most of the degradation process ($0.2 < \alpha \leq 0.8\%$). However the slight variation of E_a may be attributed to the presence of different chemical environments associated with the ester and amide linkages, requiring different energies for their degradations. As the aliphatic

neighbouring moiety to both ester and amide $-C=O$ bonds are comparatively more thermolabile than the aromatic ones, accordingly the thermostability follows the following order.

aliphatic-CO-aliphatic < aliphatic-CO-aromatic < aromatic-CO-aromatic

Further the nature of aliphatic and aromatic moieties like the presence of double bond, heteroatom in the aromatic ring and so on has profound influence on the kinetics of degradation reaction. The byproduct formed in the degradation of first step of different ester linkages may either stabilize or destabilize the non-degraded part, thereby causing a change in E_a for the degradation. The same is true for the second degradation step of different amide linkages in the polymer matrix. The presence of thermally stable nanotubes in between HBPEA chains significantly increased E_a , indicating their superior thermal stability over HBPEA. It was evident from Fig. 5B.9 (A) that the increment of E_a was relatively more in the second step as compared to the first step of the degradation of the nanocomposites. It can thus be inferred that the nanotubes interacted more with the amide group as compared to the ester groups in the nanocomposites. The degradation reaction initially started at the weak linkages like ester and then moved on to the amide linkages. Thus the overall rate of degradation is controlled by the unzipping of the polymer chain in case of HBPEA. The incorporation of the nanotubes resulted in the suppression of unzipping process of the polymer chains. The physicochemical bonding of the nanotubes with HBPEA chains and heat dissipation along the polymer matrix without getting accumulated dictated the degradation pattern of the nanocomposites. In other words, the nanotubes acted as the 'mass transport barrier' due to their network structures in the polymer matrix. This rationale is further supported by the experimental fact that both initial decomposition temperatures and E_a increased with the content of the nanoconjugate in the nanocomposites. Thus TG study provided insight into the structural relationship between HBPEA and the nanotubes, and characteristic thermal degradation parameters.

5B.3.9. Antistatic property

Fig. 5B.9 (B) shows the variation of surface sheet resistance of the pristine and the nanocomposites with the content of the nanotubes. The surface sheet resistance of HBPEA thermoset is of the order of 10^7 , which decreased by approximately three order of magnitude with the increase of the content of nanotubes from 0.25 to 1 wt%. The inclusion of varying wt% of nanotubes led to the formation of electrically conductive three dimensional network structures (evident from HRTEM study discussed in section 5B.3.5.), which are imperative

for creating the charge dissipation pathways within HBPEA matrix at minimal loading of the nanotubes. Thus the high aspect-ratio nanotubes formed a conductive pathway for the dissipation of static electric charges. The rationale behind the electrical conduction of the nanotubes is that the movement of free electron per carbon atom (similar to free electrons in the metals) present in a planar graphene sheet, throughout the matrix. The rolling-up of the graphene sheets into nanotubes resulted in the electronic structure similar to that in metals with low band gap.⁵⁹ The decrease in the surface sheet resistance (from 10^7 to $10^4 \Omega/\text{sq}$) with minimal loading of 1 wt% nanotubes is attributed to the formation of increased number of charge transmission paths in HBPEA matrix. Our results supersede the findings of Li et al.⁶⁰ wherein sufficient antistatic property was reported upon incorporation of 15 wt% of nanotubes into a polymer matrix.

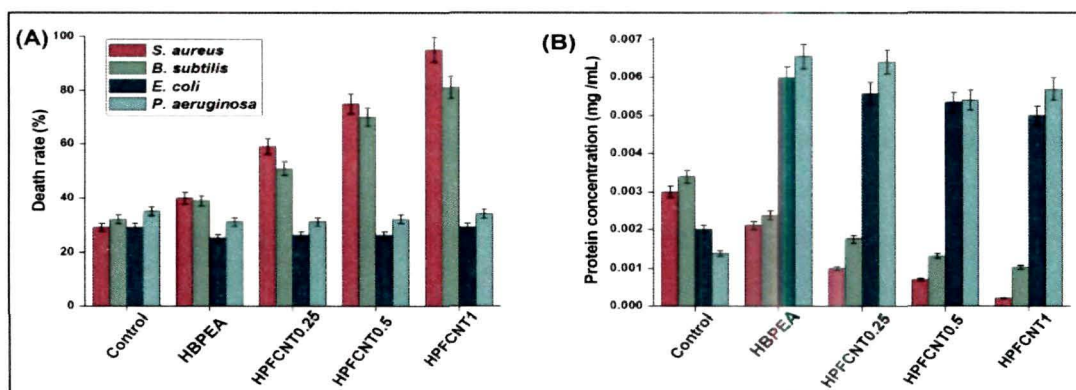


Fig. 5B.5 Antibacterial activity in terms of (A) CFU count; and (B) protein content

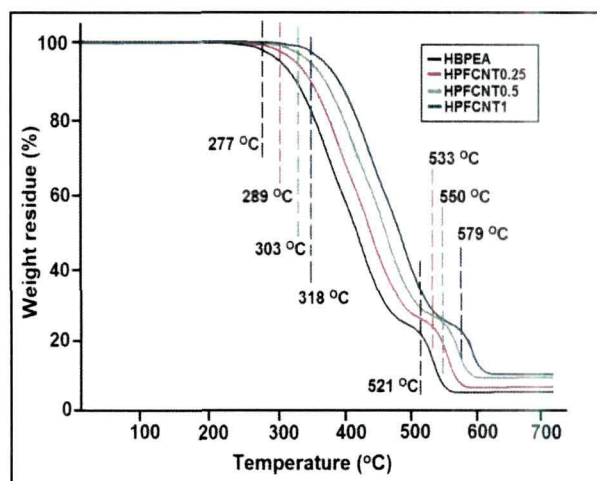


Fig. 5B.6 TG thermograms of HBPEA and noncovalent functionalized MWCNT/HBPEA nanocomposites

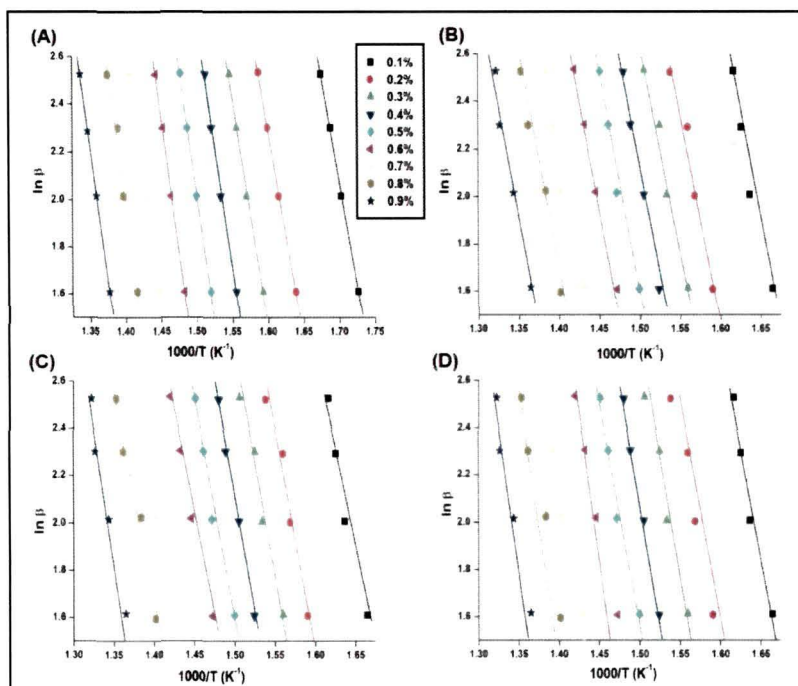


Fig. 5B.7 Plots of $\ln \beta$ versus $1000/T$ for first step of degradation at different ' α ' of: (A) HBPEA; (B) HPFCNT0.25; (C) HPFCNT0.5; and (D) HPFCNT1

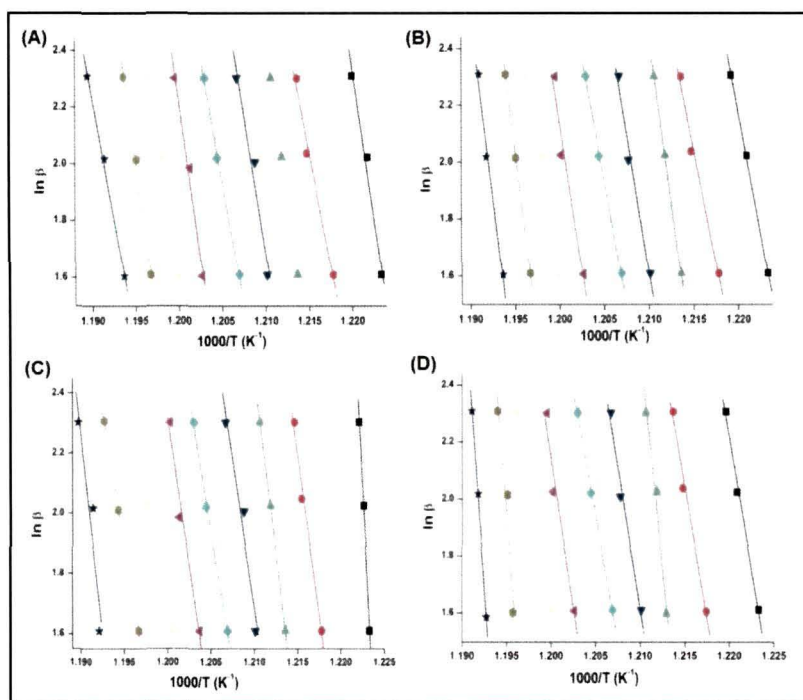


Fig. 5B.8 Plots of $\ln \beta$ versus $1000/T$ for second step of degradation at different ' α ' of: (A) HBPEA; (B) HPFCNT0.25; (C) HPFCNT0.5; and (D) HPFCNT1

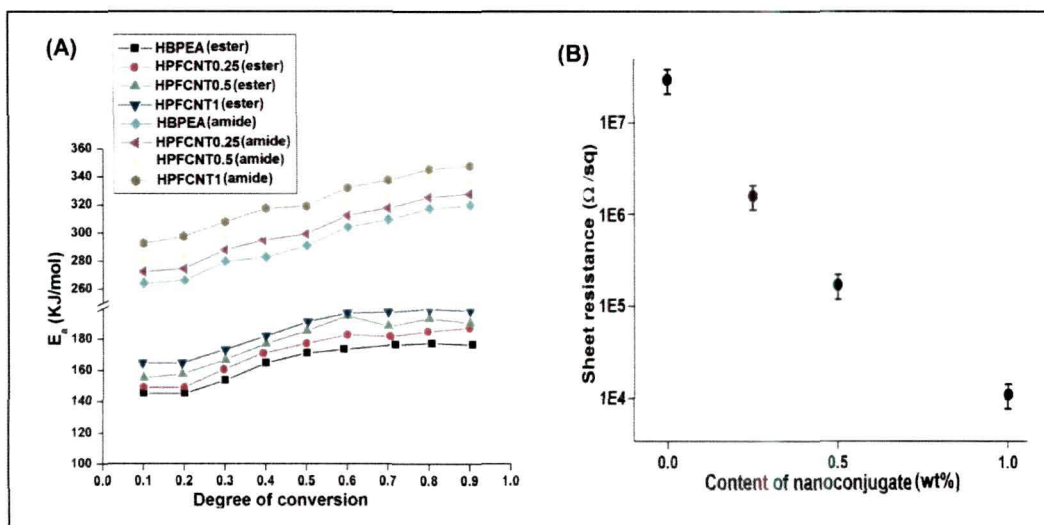


Fig. 5B.9 (A) Plots of E_a versus ' α ' for first and second decomposition steps; and (B) sheet resistance of HBPEA and noncovalent functionalized MWCNT/HBPEA nanocomposites

5B.4. Conclusion

The subchapter 5B presents the concomitant use of DEFA and green chemistry tool of sonication for noncovalent functionalization of MWCNT. The anchorage of amide moiety onto the surface of the nanotubes and the preparation of HBPEA nanocomposites was done by tailoring of carbonyl amide chemistry. The formation of Y-shaped junctions of the nanotubes in HBPEA matrix augmented in parallel lines with the antistatic property and thermal stability of the nanocomposites. The presence of the nanotubes in the nanocomposites was further confirmed by their pronounced antibacterial activity against Gram positive bacterial strains. We thus envision that these multifunctional nanocomposites would serve as an effective and economical material in advanced textiles in the consumer market.

References

1. Iijima, S. *Nature* **354**, 56--58, 1991.
2. Wang, S., et al. *Nanotechnology* **19** (8), 085710, 2008.
3. Spitalskya, Z., et al. *Prog. Polym. Sci.* **35** (3), 357--401, 2010.
4. Ma, P.C., et al. *Compos. Part A-Appl. S* **41** (10), 1345--1367, 2010.
5. Balasubramanian, K., & Burghard, M. *Small* **1** (2), 180--192, 2005.
6. Crescenzo, A.D., et al. *Eur. J. Org. Chem.* **2011** (28), 5641--5648, 2011.
7. Huang, J., & Kaner, R.B. *J. Am. Chem. Soc.* **126** (3), 851--855, 2004.
8. Gizdavic M.R.N., et al. *Acta Biomater.* **7** (12), 4204--4209, 2011.
9. Kang, S., et al. *Langmuir* **24** (13), 6409--6413, 2008.
10. Brunetti, F.G., et al. *J. Am. Chem. Soc.* **130** (25), 8094--8100, 2008.
11. Gizdavic-Nikolaidis, M.R., et al. *Macromol. Rapid Comm.* **31** (7), 657--661, 2010.
12. Das, B., et al. *Macromol. Biosci.* **13** (1), 126--139, 2013.
13. Andrews, J.M. *J. Antimicrob. Chemoth.* **56** (1), 60--76, 2005.
14. Fernandes, S.C.M., et al. *ACS Appl. Mater. Inter.* **5** (8), 3290--3297, 2013.
15. Bradford, M.M., et al. *Anal. Biochem.* **72** (1-2), 248--254, 1976.
16. Vissers, M.C.M., et al. *J. Immunol. Methods* **110** (2), 203--207, 1988.
17. Niu, Q., et al. *J Immunol Methods* **251** (1-2), 11--19, 2001
18. Benzie, I.F.F., & Strain, J.J. *Anal. Biochem.* **239** (1), 70--76, 1996.
19. Wang, S., et al. *Carbon* **45** (15), 3042--3059, 2007.
20. Vazquez, E., & Prato, M. *ACS Nano* **3** (12), 3819--3824, 2009.
21. Guo, G., et al. *Macromolecules* **39** (26), 9035--9040, 2006.
22. Watts, P.C.P., et al. *J. Mater. Chem.* **13**, 491--495, 2003.
23. Homenick, C.M., et al. *Polym. Rev.* **47** (2), 265--290, 2007.
24. Banerjee, S., et al. *Sensor Actuat. B-Chem.* **171-172**, 924--931, 2012.
25. Jayakannan, M., et al. *J. Polym. Sci. Polym. Phys.* **43** (11), 1321--1331, 2005.
26. Gajendran, P., & Saraswathi, R. *Pure Appl. Chem.* **80** (11), 2377--2395, 2008.
27. Li, W., et al. *J. Phys. Chem. B* **107** (26), 6292--6299, 2003.
28. Banerjee, S., et al. *Nanotechnology* **21** (4), 045101, 2010.
29. Antunes, E.F., et al. *Carbon* **44** (11), 2202--2211, 2006.
30. Liu, B., et al. *J. Mater. Sci. Technol.* **26** (1), 39--44, 2010.
31. Konwarh, R., et al. *Ultrason. Sonochem.* **19** (2), 292--299, 2012.
32. Hu, H., et al. *Carbon* **50** (2), 3267--3273, 2012.

33. de Keijser, Th.H., et al. *J. Appl. Cryst.* **15** (3), 308--314, 1982.
34. Konwarh, R., et al. *Appl. Microbiol. Biotechnol.* **87** (6), 1983--1992, 2010.
35. Liu, S., et al. *ACS Nano* **3** (12), 3891--3902, 2009.
36. Shvedova, A.A., et al. *Pharmacol. Therapeut.* **121** (2), 194--204, 2009.
37. Fernandes, E.G.R., et al. *J. Macromol. Sci. A* **47** (12), 1203--1207, 2010.
38. Hofmanna, S., et al. *Biomaterials* **28** (6), 1152--1162, 2007.
39. Rajaraman, R., et al. *Exp. Cell Res.* **107** (1), 179--190, 1977.
40. Liu, Z., et al. *J. Biomed. Mater. Res. A* **102** (3), 665--673, 2014.
41. Jacobsen, N.R., et al. *Environ. Mol. Mutagen.* **49** (6), 476--487, 2008.
42. Brzozowski, A.M., et al. *Nature* **351**, 491--494, 1991.
43. Kagan, V.E., et al. *Nat. Nanotechnol.* **5**, 354--359, 2010.
44. O'Connell, M.J., et al. *Chem. Phys. Lett.* **342** (3-4), 265--271, 2001.
45. Gotovac, S., et al. *Nano Lett* **7** (3), 583--587, 2007.
46. Ozawa, T. *Bulletin of The Chemical Society of Japan* **38** (11), 1881--1886, 1965.
47. Flynn, J.H., & Wall, L.A. *Journal of Research of the National Bureau of Standards* **70A** (6), 487--523, 1966.
48. Strano, M.S., et al. *Journal of Nanoscience and Nanotechnology* **3** (1-2), 81--86, 2003.
49. Pan, B., & Xing, B. *Environ. Sci. Technol.* **42** (24), 9005--9013, 2008.
50. Szleifer, I., & Rozen, R.Y. *Polymer* **46** (19), 7803--7818, 2005.
51. Baskaran, D., et al. *Chem. Mater.* **17** (13), 3389--3397, 2005.
52. Star, A., & Stoddart, J.F. *Macromolecules* **35** (19), 7516--7520, 2002.
53. Vaisman, L., et al. *Adv. Colloid Interfac.* **128-130**, 37--46, 2006.
54. Amelinckx, S., et al. *Science* **265**, 635--639, 1994.
55. Bazilevsky, A.V., et al. *Langmuir* **23** (14), 7451--7455, 2007.
56. Rezakhaniha, R., et al. *Biomechanics and Modeling in Mechanobiology* **11** (3-4), 461--473, 2012.
57. Kim, P., et al. *Phys. Rev. Lett.* **87** (21), 215502, 2001.
58. Colon, M.L., et al. *ACS Appl. Mater. Inter.* **2** (3), 669--676, 2010.
59. Ando, T. *NPG Asia Mater.* **1**, 17-21, 2009.
60. Li, C., et al. *Compos. Sci. Technol.* **64** (13-14), 2089--2096, 2004.

Chapter 6

Hyperbranched poly(ester amide)/silver nanoparticles decorated multi-walled carbon nanotube nanocomposites

Highlights

The ‘contact sport’ between zero- and one-dimensional nanomaterials amalgamating the novel properties of both continues to make advancements in carving out endless utilities across the globe. In this context, coalescing the unique properties of MWCNT and silver (Ag) nanoparticles have sparked the hopes of game-changing applications across the domains as a potent antistatic, antibacterial and thermostable material. The ultrasonication assisted and DEFA mediated bio-reduction of Ag acetate in the presence of MWCNT by a facile and environmentally benign ‘single step one pot approach’ is documented. DEFA was used to impart ‘green capping’ attribute to Ag nanoparticles, apart from noncovalent functionalization of the nanotubes. The probable complexation of Ag ions with DEFA and the bio-reductive potency of the latter were analyzed using spectroscopic tools. The subsequent polymerization of DEFA functionalized ‘Ag nanoparticles decorated MWCNT’ with dibasic acids/anhydrides was explored to ameliorate over the previously reported HBPEA/noncovalently functionalized MWCNT nanocomposites. The wider aspects of antibacterial activity against both Gram positive and Gram negative bacteria were the overwhelming asset as compared to HBPEA nanocomposites stated earlier in previous chapters. The significant antibacterial activity, pronounced sheet resistance of the order of $10^6 \Omega/\text{sq}$, good mechanical performance and thermal stability upto 325°C of these thermosetting nanocomposites forwarded them as potent antibacterial, thermostable and antistatic sustainable materials for different advanced applications including coatings, textiles, biomedical electronics and so on.

6.1. Introduction

Inspired by the potent features of DEFA in the noncovalent functionalization of MWCNT (to explore its unique properties as mentioned in section 5A.1. of subchapter 5A) and using the same for *in-situ* preparation of HBPEA nanocomposites, we intend to exploit the same template for integrating the intriguing aspects of the zero-dimensional nanomaterials with that of the nanotubes. Further the comparatively low TS and selective antibacterial efficacy against Gram positive bacteria creates the hurdles in the applicability of the nanocomposites in diversified horizons. Considering the remarkable properties of both the nanotubes and silver (Ag) nanoparticles, it is reasonable to coalesce both in a single matrix for an attempt to address the aforementioned twin problems.

As noted in section 1.3.1.2. of Chapter 1, the phenomenal properties of Ag nanoparticles primarily attributed to their quantum confinement effect have conferred them special niche in the domains, ranging from biomedical to coating industries since last two decades. It is worth noting that these nanoparticles exhibit remarkable and unique properties when their dimensions are reduced to the order of that of the Fermi wavelength of an electron wherein their properties are dictated by the quantum mechanical rules.¹ In view of present desires, the fabrication of ‘Ag nanoparticles decorated MWCNT’ (AgCNT) using the same templating attributes of DEFA is an important proposition. In lines with our previous work discussed in subchapter 5B, DEFA functionalized AgCNT can be used as one of the reactive precursors for the preparation of HBPEA nanocomposites. Nevertheless, *in-situ* preparation of such ternary HBPEA nanocomposites in a single pot has not been reported till date. Thus the harboring of the unique properties of AgCNT in bio-based HBPEA nanocomposites enrolls them as high-value added materials for coatings, textiles, biomedical electronics and so on.

Thus in continuation of our previous work documented in subchapter 5B, the bio-reductive efficacy of DEFA in the preparation of Ag nanoparticles and their decoration onto the surface of the nanotubes was delved into. A plausible mechanistic approach for the formation of DEFA functionalized AgCNT was elaborated. The prime focus remained on the use of DEFA functionalized AgCNT as a precursor for *in-situ* preparation of bio-based HBPEA nanocomposites. Furthermore, the antibacterial activity against a spectrum of Gram positive and Gram negative bacterial species was scrutinized together with evaluation of antistatic property of the nanocomposites for forwarding them in their potential advanced applications.

6.2. Experimental

6.2.1. Materials

6.2.1.1. Chemicals

The materials utilized in the preparation of HBPEA including such as castor oil, DiEA, MAn, PhAn, IPhA, epoxy resin and poly(amido amine) were of same specification as described in section 2.2.1.1. of Chapter 2. Silver acetate with 166.91 g/mol and density 3.26 g/cm³ was purchased from Merck, India. MWCNT used was of same specification as mentioned in section 5A.2.1.1. of subchapter 5A.

6.2.1.2. Microbial strains

The bacterial strains such as *Escherichia coli* (DH5 α) and *Klebsiella pneumonia* (MTCC618), *Bacillus subtilis* (MTCC441) and *Staphylococcus aureus* (MTCC373) *Mycobacterium smegmatis* (ATCC14468) were obtained from the Department of Molecular Biology and Biotechnology, Tezpur University, India. The reagents used in this study were the same as mentioned in section 5B.2.1.2. of subchapter 5B.

6.2.2. Methods

6.2.2.1. Preparation of silver nanoparticles decorated MWCNT

DEFA was prepared by the same process as discussed in section 2.2.2.3. of Chapter 2. Ag nanoparticles were prepared by *in-situ* reduction of CH₃COOAg (in varying wt% of 0.25, 0.5 and 1) as the metal precursor in presence of MWCNT (0.25 wt% with respect to DEFA) as the template and DEFA as the reducing and stabilizing agent with the aid of a sonication.

6.2.2.2. Preparation of nanocomposites

DEFA functionalized AgCNT were used as one of the reactive components in the polycondensation reaction under similar conditions as mentioned in section 5B.2.2.2. of subchapter 5B. The nanocomposites prepared with 0.25, 0.5 and 1wt% of DEFA functionalized AgCNT, separately were encoded as HPAgNT0.25, HPAgNT0.5 and HPAgNT1 respectively. The curing of the nanocomposites was done in the similar manner as mentioned in section 3.2.2.2. of Chapter 3.

6.2.3. Instrumentation

FTIR, UV-visible, TG, sheet resistance and HRTEM analyses together with X-ray diffractograms were carried out using the same instruments as described in section 5A.2.3. of subchapter 5A. The elemental detection of Ag in the nanocomposites was investigated using electron dispersive X-ray (EDX) JSM-6390LV. The curing time, percent gel fraction, scratch

hardness, impact resistance, gloss, TS and EB were evaluated as per as the standard methods mentioned in section 2.2.3. of Chapter 2.

6.2.4. Antimicrobial activity

The antibacterial activity of the prepared nanocomposites was determined using the same method as described in section 5A.2.4. of subchapter 5A. The death rate of the bacteria² was calculated using the following equation 6.1.

$$\text{Death rate (\%)} = \frac{[(\text{counts in the control}) - (\text{counts upon incubated with the nanocomposites})]}{(\text{counts in the control})} \quad \text{----- (6.1)}$$

6.3. Results and discussion

6.3.1. Preparation of silver nanoparticles decorated MWCNT

The adsorption, complexation and bio-reduction of Ag salt and noncovalent functionalization of the nanotubes were exploited using the same template of DEFA in a single pot without using any external reducing or stabilizing agent. The rationale behind the choice of DEFA relies on the fact that it possesses both reducing and templating attributes for *in-situ* preparation of DEFA functionalized AgCNT. DEFA adsorbed onto Ag salt (owing to secondary electrostatic interactions)^{3,4} formed nanoscopic domains/nanocavities with hydrophobic interiors which helped them to adhere onto the nanotubes. In other words the presence of suitable microenvironment of DEFA facilitated both complexation of Ag salt and noncovalent functionalization of the nanotubes. The long hydrocarbon chain and amide functional groups of DEFA formed reactive sites for the surface functionalization of the nanotubes and reduction of Ag salt respectively.³ The –OH groups of the same conferred steric stabilization to the nanomaterials against aggregation. Such individual interactions are weak, but the integral interactions resulted in high adsorption forces. Further the bio-reduction of Ag acetate using DEFA is based on supramolecular complexation of Ag ions with amide groups⁴ of DEFA which acts as an interacting ligand with lone pair on N-atom as a hard base. In the light of hard-soft acid base (HSAB) principle, a competition between the two *viz.*, N-atom of DEFA (hard base) which is stronger than the acetate ion (soft base) sets up, wherein the former replaces the latter and effectively coordinates with Ag ions. The accessibility of the lone pair of tertiary N-atom of DEFA renders stability to Ag ions through electrostatic attractions between the two. Moreover the coordination of carbonyl amide O-atom with Ag ions⁵ by electron-transfer mechanism (as supported by FTIR study in section

6.3.3.) rendered capping of Ag nanoparticles. A similar study by Zamiri et al.⁶ validated the stabilizing mechanism of Ag nanoparticles by O-atom of the carbonyl amide. In essence, the encapsulation by DEFA creates a diffusion barrier to the growing Ag nuclei, and predominantly stabilizes Ag nanoparticles by electrostatic interaction.⁴⁻⁶ Further the hydrophobic alkyl chain of DEFA adheres onto the nanotubes (*via* CH- π interactions) and provides a locale for Ag nanoparticles to anchor using its amide groups as linker. This was supported by one of such representative works reported by Zamudio and his coworkers⁷ wherein Ag nanoparticles (having diameter within 2-10 nm) anchored onto N-doped MWCNT without prior functionalization of the nanotubes.

In addition to the above interactions, the comprehending role of ultrasonication is indispensable in context of preparation of DEFA functionalized AgCNT. The implosion of small cavitation bubbles and dissipation of energy by microstreaming during compression and rarefaction acoustic cycles of sonication⁸ are also instrumental in driving both the reduction of Ag salt and exfoliation of the nanotubes.

6.3.2. Preparation of nanocomposites

DEFA functionalized AgCNT possessing high esterification rate towards the dibasic acids/anhydrides was used as a precursor for *in-situ* polycondensation reaction to yield AgCNT/HBPEA nanocomposites. DEFA acted as a reactive diluent to aid in the degree of dispersion of the nanotubes in the polymeric matrix. The formation of polymeric chains impeded the Brownian motion of the nanomaterials and thereby aiding their stabilization. The narrow size window of Ag nanoparticles and good dispersion of the same in HBPEA matrix (evident from HRTEM study discussed in section 6.3.4.) is primarily attributed to the steric stabilization.⁶ The decrease in the entropy or possible orientations of HBPEA chains adsorbed onto AgCNT resulting in the volume restriction forms the basis of the steric stabilization process. In other words, the architectural features of HBPEA served as nanocavities with ligand sites for stabilization and pre-organization of AgCNT, which was validated using FTIR tool. Scheme 6.1 presents the preparative protocol of DEFA functionalized AgCNT/HBPEA nanocomposite.

6.3.3. FTIR study

FTIR spectra of DEFA functionalized AgCNT (containing 0.25 % Ag) (both immediately after mixing and after sonication), HPAgNT0.25, HPAgNT0.5 and HPAgNT1 are shown in Fig. 6.1. Attempts were made to ascertain the formation of the above-mentioned coordination

complex of Ag salt with DEFA using FTIR. As noted in section 2.3.3. of Chapter 2, the amide stretching, -CH=CH- bending and C-N vibrations of DEFA appeared at around 1620, 772 and 1380 cm^{-1} respectively. FTIR spectrum of DEFA immediately after mixing of Ag salt and the nanotubes showed shifting in -C=O carbonyl amide and bond. The absorption peak fundamental to the stretching vibrations of the carbonyl amide ester and C-N bond of DEFA shifted to 1629 and 1400 cm^{-1} respectively owing to the interaction of Ag ions and the nanotubes with DEFA. The coordination of Ag ion with the ester and N-atom lone pair of the carbonyl amide functional group resulted in the shifting of their bond vibrations.^{5,6} However upon sonication (formation of Ag^0 nanoparticles), DEFA functionalized AgCNT showed that the carbonyl amide bond vibrations restarted back to their original wavenumber (same as DEFA) but C-N bond vibration remained at 1400 cm^{-1} . This observation justified the formation of coordination complex of Ag salt using both O-atom and N-atom of carbonyl amide bond of DEFA, with subsequent stabilization of Ag nanoparticles so formed by association with N-atom of the same. Unlike other reported protocols^{9,10} wherein hydroxyl groups take part in the reduction process, the carbonyl amide is the key player in this case of bio-reduction. This assumption is supported by the absorption peak of -OH which remains intact without shifting (in case of DEFA and DEFA functionalized AgCNT). Further the appearance of absorption band at around 1726 cm^{-1} confirmed the formation of ester groups along with the carbonyl amide in the backbone of HBPEA. As mentioned in section 5B.3.3. of subchapter 5B, the C-H bending peak of HBPEA appears at 1441 cm^{-1} , whose interaction with the nanotubes was attested by the broadening of C-H bending bands.

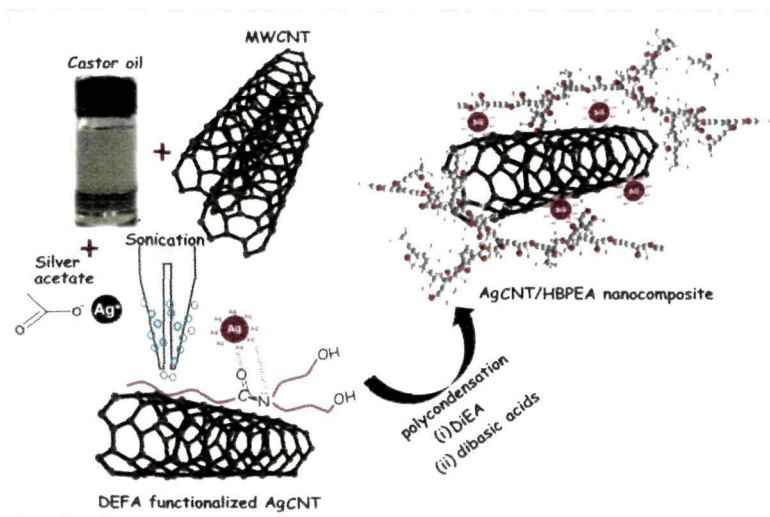
6.3.4. HRTEM study

HRTEM micrographs at different scale bar of 100 and 50 nm (Fig. 6.2 (A) and (B)), and SAED of HPAgCNT1 provide an insight into its microstructure and crystallinity. The crystallinity of HPAgCNT1 is evident from SAED pattern (Fig. 6.2 (C)). It was apparent from the particle size histograms (Fig. 6.2 (D)) of the nanocomposites that Ag nanoparticles within the control size range of 2-10 nm remained well dispersed in the polymeric matrix. It is noteworthy that the highest fraction of Ag nanoparticles lies in the diameter range of 5-7 nm. Further the disentanglement and well-dispersion of the nanotubes reflected from HRTEM micrograph is supportive of the noncovalent functionalization of the same.

6.3.5. UV-visible study

UV-visible spectra of DEFA functionalized AgCNT (with 0.25 % Ag), HPFCNT0.25 (as

mentioned in section 5B.2.2.3 of subchapter 5B) and HPAgCNT1 are shown in Fig. 6.3. UV-visible absorption band of DEFA functionalized AgCNT (with 0.25 % Ag acetate) contained the characteristic one-dimensional van Hove singularities of the nanotubes¹¹ at around 264 nm. The absence of the plasmon absorption of Ag nanoparticles is attributed to its quantum size effect. This observation is consistent with the reports of Zheng et al.¹² according to which metal nanoparticles (having diameter <10 nm) including nanoclusters are too small to possess the continuous density of states to support the plasmon characteristics of



Scheme 6.1 Plausible mechanism of the formation of DEFA functionalized AgCNT and its polymerization to yield nanocomposite

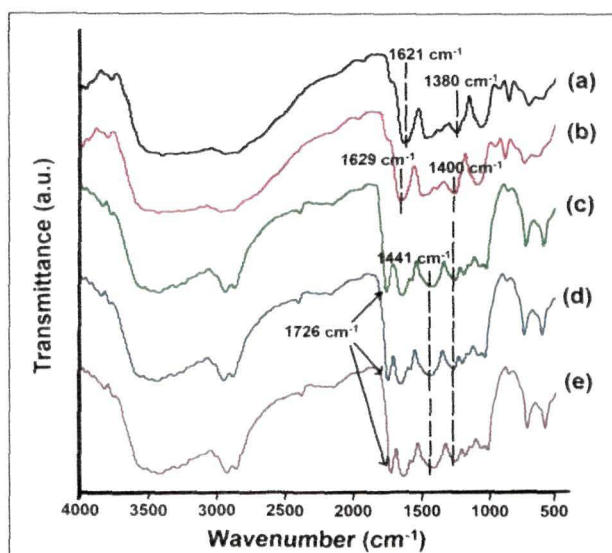


Fig. 6.1 FTIR spectra of DEFA functionalized AgCNT: immediately after mixing (a), and after sonication (b), HPAgCNT0.25 (c), HPAgCNT0.5 (d) and HPAgCNT1 (e)

comparatively larger metal nanoparticles. The appearance of absorption band of HPAgCNT1 at around 283 nm is attributed to the formation of carbonyl ester group in the backbone of HBPEA.

6.3.6. XRD study

Fig. 6.3 (B) shows X-ray diffractograms of the nanocomposites. As noted in section 5A.3.1.2. of subchapter 5A, the characteristic (002) Bragg's peak of pristine nanotubes appears at around 26.2° . The peaks centered at around 38° , 44.5° , 64.5° signifies the (111), (200) and (220) planes of fcc structured Ag nanoparticles.⁹ A broad halo (at around 20°) was observed for HBPEA owing to its amorphousness, as discussed in section 3.3.6 of Chapter 3. The appearance of XRD peaks at around 26° , 38.2° , 44° and 64.3° in the nanocomposites is ascribed to the presence of Ag nanoparticles and the nanotubes in HBPEA matrix. However the low intensity of the above mentioned peaks of the nanocomposites is due to their low content as compared to the polymeric matrix (maximum 1%).

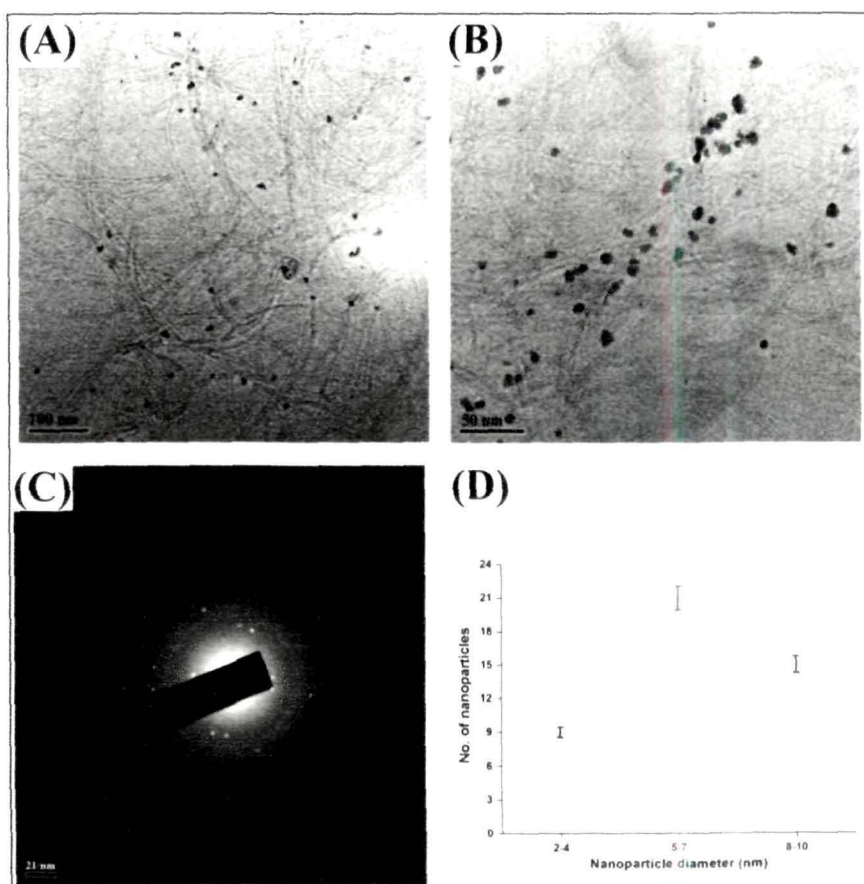


Fig. 6.2 HRTEM micrographs of HPAgCNT1 at magnification scale of (A) 100 nm; (B) 50 nm; (C) SAED pattern; and (D) silver nanoparticles size distribution histogram

6.3.7. EDX study

EDX spectrum of HPAgCNT0.25 (Fig. 6.3 (C)) confirmed the presence of elemental Ag in the same. The peaks observed at 0.25, 0.39 and 3.2 keV are attributed to the binding energies of carbon (CK_{α}), nitrogen (NK_{α}) and silver (AgL_{β}), respectively.¹³

6.3.8. Physico-mechanical performance study

The epoxy-poly(amido amine) cured thermosetting DEFA functionalized AgCNT/HBPEA nanocomposites exhibited pronounced increment in their performance as compared to HBPEA (Table 6.1). The curing time of the nanocomposites (baked at 150 °C) effectively decreased with an increase in AgCNT content. This is attributed to the presence of AgCNT which aids in crosslinking reaction by acting as a pseudo organometallic catalyst. In other words, the vacant orbitals of Ag and defect sites of the nanotubes of AgCNT are envisaged to coordinate with the lone pair of O-atom of oxirane ring of epoxy and N-atom of HBPEA and poly(amido amine), and thereby aid in bringing the components in the close proximity and hence facilitating the crosslinking reaction.¹⁴ The crosslinking of HBPEA and its nanocomposites with 0.25 wt% MWCNT and 1 wt% Ag nanoparticles, separately under the curing conditions took 10, 3.2 and 3 h respectively. Thus AgCNT forms the key player in the curing process of the nanocomposites by synergistically combining the attributes of both Ag nanoparticles and the nanotubes.

The gloss and scratch hardness increased with AgCNT content in the nanocomposites. The obtained findings are in accord with the presence of profound interfacial interactions of AgCNT with HBPEA matrix (as evident from FTIR study discussed in section 6.3.3) which are instrumental in imparting significant dimensional stability and surface texture to the cured thermosetting nanocomposites. The rigidity in the structure (optimum gel fraction) along with the flexibility of the fatty acid chains account for their high impact resistance. The compatibility, interfacial interactions and nano-reinforcement effect of AgCNT with the polymeric matrix resulted in the increment in TS of the nanocomposites from 9.5 to 15.2 MPa. The decrement in EB is attributed to the restriction of the movement of the polymeric chains at the interface between AgCNT and HBPEA.

6.3.9. Thermal study

It is observed from Fig. 6.3 (D) that the inclusion of DEFA functionalized AgCNT in the preparation of HBPEA nanocomposites imparted dose-dependent thermostability to the system. As noted in section 2.3.8. of Chapter 2, HBPEA exhibits two-step degradation owing

to the degradation of ester and amide functional groups at 277 and 521 °C respectively. The increment of DEFA functionalized AgCNT content from 0.25 to 1 wt % in the nanocomposites increased the thermal stability from 293 to 324 °C. The interfacial interactions of AgCNT with HBPEA matrix (as evident from FTIR study discussed in section 6.3.3.) and catalytic action in the crosslinking process with epoxy and poly(amido amine) by behaving as a pseudo-organometallic catalyst account for the above findings. Further the restriction in the movement of HBPEA chains owing to the presence of AgCNT resulted in the improvement of the thermostability of the nanocomposites as compared to HBPEA.

Table 6.1 *Physico-mechanical performance of thermosetting AgCNT/HBPEA nanocomposites*

Physico-mechanical property	HBPEA	HPAgCNT0.25	HPAgCNT0.5	HPAgCNT1
Curing time (h)	10±0.02	2.9±0.01	2.6±0.01	2±0.01
Gel fraction (%)	77±0.5	77.4±0.2	76.6±0.4	76.1±0.1
Scratch hardness (kg)	8.5±0.2	9.5±0.3	10	10
Impact resistance (cm)	100	100	100	100
Gloss at 60°	90±0.5	92.3±0.4	93.7±0.5	94.2±0.5
TS (MPa)	7.3±0.5	9.5±0.3	11.7±0.2	15.2±0.4
EB (%)	88.1±0.8	84.3±0.6	83.4±0.5	80.7±0.6

*Maximum limit of the instrument is 100 cm

6.3.10. Antistatic property

Fig. 6.4 (A) shows the variation of the sheet resistance values of the nanocomposites with DEFA functionalized AgCNT content. As mentioned in section 5B.3.9 of subchapter 5, HBPEA exhibits sheet resistance of the order of 10^7 , which dropped to the order of 10^6 upon incorporation of 0.25 wt% nanotubes in HBPEA matrix. However the incorporation of 1 wt% DEFA functionalized AgCNT decreased the sheet resistance to the order of 10^5 owing to efficient dissipation of the static electric charges. This sheet resistance value is found to be adequate for many applications as mentioned above in section 6.1.

6.3.11. Antibacterial activity

It was observed from the enumeration of bacterial death rate (Fig. 6.4 (B)) that DEFA functionalized AgCNT/HBPEA nanocomposites exhibited potent antibacterial activity against acid fast, Gram positive and Gram negative bacterial strains as compared to the

experimental control. These observations are in contrary to our earlier finding wherein HBPEA and HPFCNT0.25 (discussed in sections 5B.3.7. of subchapter 5B) showed selective antibacterial activity against Gram positive bacterial species. The incorporation of Ag nanoparticles thus, plays a key role in widening the antibacterial attributes of DEFA functionalized AgCNT/HBPEA nanocomposites against broad spectrum of bacterial species. The electrostatic interactions between Ag and the negative charges of lipopolysaccharides (key component of outer membrane of Gram negative bacteria) subsequently led to their

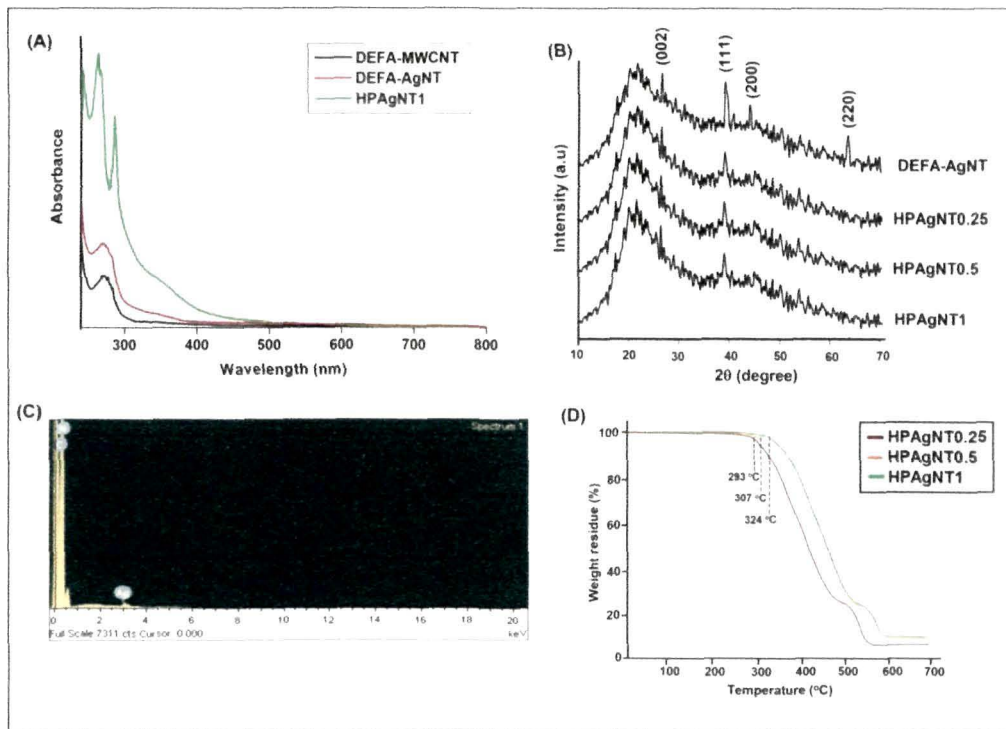


Fig. 6.3 (A) UV-visible spectra; (B) XRD patterns; (C) EDX of HPAgCNT0.25; and (D) TG thermograms of thermosetting HBPEA and AgCNT/HBPEA nanocomposites

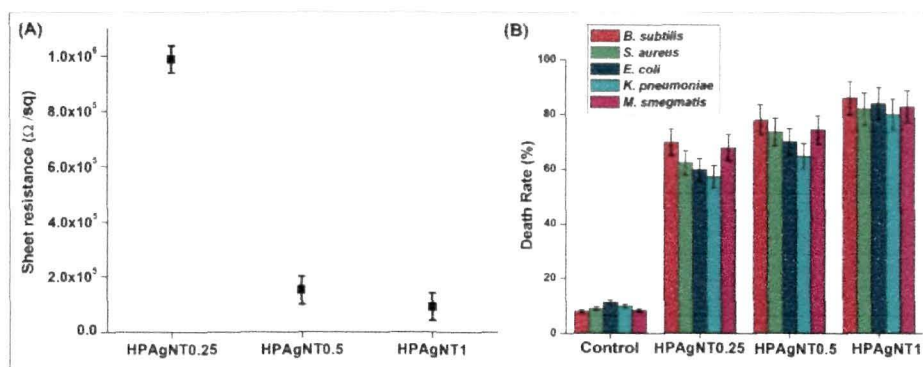


Fig. 6.4 (A) Sheet resistance; and (B) antibacterial activity of HBPEA and AgCNT/HBPEA nanocomposites

cellular distortion by different mechanisms (including denaturation of DNA and RNA, generation of reactive oxygen species and so on) and loss of bacterial replication and viability.¹⁵ Thus the high surface activity of Ag nanoparticles and MWCNT entities is imperative in imparting significant antibacterial activity.

6.4. Conclusion

The present chapter demonstrated a facile one-pot preparation of DEFA functionalized AgCNT without using any solvent or stabilizing agent. Exploiting the concomitant use of green tool of sonication and bioresource, reactive sites of the nanotubes are generated for adsorption of Ag nanoparticles and anchoring of DEFA at shorter reaction time period of 15 min. FTIR, UV-visible, EDX and HRTEM tools coupled with thermogravimetric analyses supported the formation of the DEFA functionalized AgCNT/HBPEA nanocomposites. Coalescing the multifaceted attributes of the prepared nanocomposites such as antistatic, thermostable and wider antibacterial property open new opportunities for advanced sustainable applications in the realm of textiles, biomedical electronics and coatings.

References

1. Lindberg, V., & Hellsing, B. *J. Phys.-Condens. Mat.* **17** (13), S1075--S1094, 2005.
2. Liu, S., et al. *ACS Nano* **3** (12), 3891--3902, 2009.
3. Kang, S., et al. *J. Polym. Sci. Pol. Phys.* **42** (18), 3344--3350, 2004.
4. Hakimi, M., et al. *Journal of the Korean Chemical Society*, **57** (3), 352, 2013.
5. Qiu, L., et al. *Langmuir*, **22** (10), 4480--4482, 2006.
6. Zamiri, R., et al. *Int. J. Mol. Sci.* **11** (11), 4764--4770, 2010.
7. Zamudio, A., et al. *Small* **2** (3), 346--350, 2006.
8. Konwarh, R., et al. *Ultrason. Sonochem.* **19** (2), 292--299, 2012.
9. Barua, S., et al. *Colloid Surface B* **105**, 37--42, 2013.
10. Sharma, V. K., et al. *Adv. Colloid Interfac.* **145** (1-2), 83--96, 2009.
11. Ponnamma, D., et al. *Eur. Polym. J.* **53**, 147-159, 2014.
12. Zheng, J., et al. *Phy. Rev. Lett.* **93** (7), 077402, 2004.
13. Khan, M. A. M., et al. *Nanoscale Res. Lett.* **6** (1), 434, 2011.
14. Dong, Y. B., et al. *Organometallics* **25** (2), 447--462, 2006.
15. Prabhu, S., & Poulouse, E. K. *International Nano Letters* **2**, 32, 2012.

Chapter 7

Conclusions and future scopes

Highlights

This concluding chapter of the thesis makes an effort to coalesce the conclusions drawn from each chapter, in addition to re-scrutinizing the current interests on the use of innovative technologies for the preparation of advanced materials with multifunctional properties. The challenges and possible future scopes of advancing HBPEA and its nanocomposites from laboratories to high-volume applications in commercial markets have also been focused upon. In a nut-shell, the major achievements of the compiled works, limitations and challenges that remained together with the scopes to be explored are presented.

7.1. Concluding remarks and outlook

The main objective of the proposed research work was to fabricate bio-based HBPEA nanocomposites for multimodal applications. In this context, the thesis comprised of seven chapters.

The first chapter presented a comprehensive introductory glimpse on HBPEA and their nanocomposites. The technological progress in the synthesis of HBPEA was surveyed over the past few decades with emphasis on the hunt for appropriate raw materials. HBPEA nanocomposites were highlighted in context of achieving material's property for advanced engineering applications. Starting off with the study of different nanomaterials, the chapter explored the suitable preparative protocols for the fabrication of HBPEA nanocomposites. The chapter moved ahead with the characterization tools and testing methods to comprehend the bio-physico-chemical attributes of HBPEAs and their nanocomposites. The properties of the same were critically discussed for leveraging their ample potential in diversified domains of material and biomedical sciences. An archive of the multihued diorama of these advanced materials is presented together with pointing out the scopes, which formed the basis of the objectives for the present research work.

The utility of the biodegradable hyperbranched polymers as thin film materials for disposable packaging, lamination and surface coatings is in vogue in the contemporary times owing to the concerns over sustainability. Towards this end, the second chapter dealt with the use of the castor oil as the biorenewable for the synthesis of HBPEA resin *via* an $A_2+B_2+A'A_2$ approach. This was an attempt to coalesce the innate advantages of using bioresource and hyperbranched architecture bequeathed with multiple number of functionality for new perspectives and opportunities in the domain of advanced surface coating materials. DEFA was obtained in quantitative yield for the first time. The influence of the varying wt% of the trifunctional $A'A_2$ monomer (DiEA) on the degree of branching, rheological behavior, performance and microbial and lipolytic degradation of the synthesized resin was scrutinized. The varied performance of the same was probed into and compared with its linear analog. The study attested the best performance of 10 wt% DiEA containing HBPEA and forwarded it as a biodegradable thin film material, and as the matrix for further studies for the preparation of different nanocomposites.

Tasked with improvement and attainment of some special properties of the pristine polymer, a concert of the same and nanotechnology seemed to be promising in revolutionizing the arena of bio-based HBPEA in pursuit of advanced engineering applications. Prompted by the above

fact, different nanomaterials and their combinations were explored in rest of the chapters to confer new and modulate the bio-physico interfacial properties to the pristine HBPEA which can wheel different realms ranging from material to biomedical sciences.

Starting on with the one dimensional nanomaterial *viz.*, PANi nanofiber which can control the build-up of static electric charges that are creating electrostatic ignition hazards to both industries and mankind over the years, the third chapter delved into the *ex-situ* preparation of HBPEA/PAni nanofiber nanocomposites. The changes in the structural attributes of PANi nanofibers as a function of solubility parameters of the organic solvent used in the interfacial polymerization was probed into to precisely control the degree of conjugation of the same. PANi nanofiber prepared using chloroform exhibited the best performance amongst all others and was used in the preparation of HBPEA nanocomposites. The efficacy of sonication was exploited in modulating the interfacial interactions of benzenoid-quinoid moieties of PANi with HBPEA, which resulted in improved mechanical and antistatic properties together with thermostability as compared to the pristine polymer to forward the same as potent antistatic materials.

Extending the concept of the amalgamation of the remarkable properties of one- and two- dimensional nanomaterials, the fourth chapter highlighted the modification of MMT using PANi nanofiber as the organo-modifier without any pillaring agent. Further the chapter provided avenues in addressing the emerging problems of microbial infection and contamination using nano-biotechnology. Towards this end, fabrication of HBPEA/PAni nanofiber modified MMT nanocomposites possessing potent antimicrobial efficacy was a contribution to stride out towards greener technology to embrace diverse domains across the globe including biomedical sciences. The prepared nanocomposites exhibited potent antibacterial efficacy against Gram positive bacteria as compared to the Gram negative ones. The nanocomposites showed significant antifungal activity and antialgal activity against algal consortium. The formation of thermosetting nanocomposites resulted in the acceptable improvement of desired physico-chemical and mechanical properties including thermostability. The pronounced antimicrobial activity of the nanocomposites against a spectrum of bacterial and fungal strains as well as a consortium of algal species along with their desired performance vouched them as potent antimicrobial materials in the realm of health and biomedical industry.

Inspired by the extraordinary and unique properties exhibited by MWCNT, the fifth chapter (consisting of two subchapters) focused on their emerging technological advancements

in the exploration of functionalization strategies to endow these nanotubes into new ventures with multifunctional applications. In context of exploiting greener tools, the power of the microwave irradiation and ultrasonication are being tamed for the functionalization of the nanotubes. In this vein, subchapter 5A dealt with the use of microwave irradiation in the functionalization of the nanotubes through a single pot covalent-noncovalent approach. The *ex-situ* prepared HBPEA nanocomposites using these functionalized nanotubes were found to be antibacterial, biocompatible and biodegradable materials for use in biomedical domain. The second part of the chapter (subchapter 5B) relied on the concept of exploiting the noncovalent functionalization of the nanotubes using DEFA and green chemistry tool of ultrasonication. The use of DEFA functionalized nanotubes as a reactive component for the *in-situ* polycondensation reaction to form HBPEA nanocomposites was explored in the subchapter 5B. These nanocomposites possess potent antibacterial activity, thermostability and antistatic properties to find utility in textile industries.

Delving into the colossal properties of zero- and one- dimensional nanomaterials and their utilities in diverse domains continue to remain the focal point of research works. In this regard, the sixth chapter attempted to combine the phenomenal properties of MWCNT and Ag nanoparticles for various applications across the domains as a potent antistatic, antibacterial and thermostable material. The ultrasonication assisted DEFA mediated bio-reduction of Ag acetate in presence of MWCNT by a facile and environmentally benign 'single step one pot approach' was documented in this chapter. DEFA was used to impart 'green capping' attribute to Ag nanoparticles and noncovalent functionalization of MWCNT. DEFA functionalized silver nanoparticles decorated MWCNT was used as a reactive component for the *in-situ* preparation of sustainable HBPEA nanocomposites. The study provided a probable mechanistic insight for complexation of Ag ions with DEFA and its reductive potency using different analytical tools. The significant bactericidal activity against a spectrum of Gram positive, Gram negative acid fast bacterial strains, pronounced sheet resistance and performance, and significant thermal stability of the nanocomposites forwarded them as potent antibacterial and thermostable antistatic materials for different advanced applications including coatings, textiles, biomedical electronics and so on.

The seventh chapter is the last chapter of the thesis which discussed the concluding remarks drawn from the experimental works with emphasis to the research contributions and its major findings together with pointing out the challenges and directions of possible future scopes which are yet to be explored.

The major findings of the thesis are given underneath:

- Quantative yield of DEFA was achieved over all others reported earlier.
- Castor oil based biodegradable HBPEA *via* an $A_2+B_2+A'A_2$ approach was synthesized and its superiority over the linear analog was proven.
- The organic solvents of varying solubility parameters used in the interfacial polymerization were found to modulate the structure and properties of PANi nanofiber.
- PANi nanofiber achieved to unveil its significant impact on the mechanical, thermal and antistatic properties of HBPEA/PAni nanofiber nanocomposites.
- HBPEA/PAni nanofiber modified MMT nanocomposites exhibited potent antimicrobial properties against a spectrum of bacterial and fungal strains as well as a consortium of algal species, and added facet of desirable physico-mechanical properties and thermal stability.
- The greener tool of microwave irradiation was effectively exploited for the functionalization of MWCNT through a single pot 'covalent-noncovalent approach' using glycidyl methacrylate and PANi nanofibers.
- The pronounced and selective antibacterial efficacies towards Gram positive and acid fast bacterial strains, biocompatibility with PBMC and biodegradation under simulated body fluid were observed for the covalent-noncovalent functionalized MWCNT/HBPEA nanocomposites. This enlisted the potent of the nanocomposites for use as dressing material for infected burn wounds.
- Ultrasonication assisted DEFA mediated noncovalent functionalized MWCNT formed a stable and uniform dispersion in different organic solvents and a potent precursor for the *in-situ* preparation of HBPEA nanocomposites.
- The noncovalent functionalized MWCNT/HBPEA nanocomposites showed promising antistatic property at low loading of the nanotubes (1 wt%).
- 'Silver nanoparticles decorated MWCNT' (AgCNT) was prepared *in-situ* by exploiting the templating attributes and reducing ability of DEFA.
- DEFA functionalized AgCNT/HBPEA nanocomposites exhibited wider antibacterial efficacy against a spectrum of Gram positive, Gram negative and acid fast bacterial strains, along with significant antistatic property and thermostability.

Thus the investigation on HBPEA nanocomposites using different nanomaterials compiled in the current thesis forwards the multifaceted sustainable DEFA functionalized

AgCNT/castor oil based HBPEA as one of the possible choices for different advanced applications including coatings, textiles, biomedical electronics and so on.

7.2. Future scopes

The present investigation documented a systematic and comprehensive study on castor oil based HBPEA and its different nanocomposites using Ag nanoparticles, PANi nanofiber, MWCNT and MMT. Although we have touched on several possibilities in this regard, but there remains still much room for future studies in this domain. The following attempts may be made as endeavors for future works.

- The effect of different non-edible vegetable oils with varying composition and structure as well as their amount needs further investigation.
- The influence of nature and amount of the branch generating units on the performance of such polymer could be proved into.
- The impact of different nanomaterials like graphene, carbon dots, polyhedral oligomeric silsesquioxane (POSS) and their combinations on the performance of HBPEA can be scrutinized to enable new contributions in the different realms including superhydrophobic materials.
- A theoretical investigation can be attempted to understand the interfacial attributes of the matrix and the nanomaterials in modulating the performance of HBPEA nanocomposites.
- Comprehensive *in-vitro* and *in-vivo* studies of such nanocomposites for application in the domain of biomedical sciences need to be speculated before clinical research are carried out in practical fields.

List of Publications

In journal

From thesis

1. Pramanik, S., Karak, N., Banerjee, S., & Kumar, A. Effects of solvent interactions on the structure and properties of prepared PANi nanofibers, *J. Appl. Polym. Sci.* **126** (3), 830--836, 2012.
2. Pramanik, S., Sagar, K., Konwar, B.K., & Karak, N. Synthesis, characterization and properties of a castor oil modified biodegradable poly(ester amide) resin, *Prog. Org. Coat.* **75** (4), 569--578, 2012.
3. Pramanik, S., Konwarh, R., Sagar, K., Konwar, B.K., & Karak, N. Bio-degradable vegetable oil based hyperbranched poly(ester amide) as an advanced surface coating material, *Prog. Org. Coat.* **76** (4), 689--697, 2013.
4. Pramanik, S., Konwarh, R., Deka, R.C., Aidew, L., Barua, N., Buragohain, A.K., Mohanta, D., & Karak, N. Microwave-assisted poly(glycidyl methacrylate)-functionalized multiwall carbon nanotubes with a 'tendrillar' nanofibrous polyaniline wrapping and their interaction at bio-interface, *Carbon* **55**, 34--43, 2013.
5. Pramanik, S., Hazarika, J., Kumar, A., & Karak, N. Castor oil based hyperbranched poly(ester amide)/polyaniline nanofiber nanocomposites as antistatic materials, *Ind. Eng. Chem. Res.* **52** (16), 5700--5707, 2013.
6. Pramanik, S., Das, G., & Karak, N. Facile preparation of polyaniline nanofibers modified bentonite nanohybrid for gas sensor application, *RSC Adv.* **3** (14), 4574--4581, 2013.
7. Pramanik, S., Barua, N., Buragohain, A.K., Hazarika, J., Kumar, A., & Karak, N. Biofunctionalized multiwalled carbon nanotube: A reactive component for the in situ polymerization of hyperbranched poly(ester amide) and its biophysico interfacial properties, *J. Phys. Chem. C* **117** (47), 25097--25107, 2013.
8. Pramanik, S., Konwarh, R., Barua, N., Buragohain, A.K., & Karak, N. Bio-based hyperbranched poly(ester amide)-MWCNT nanocomposites: Multimodalities at the biointerface, *Biomaterials Science* **2** (2), 192--202, 2014.

9. Pramanik, S., Bharali, P., Konwar, B.K., & Karak, N. Antimicrobial hyperbranched poly(ester amide)/polyaniline nanofiber modified montmorillonite nanocomposites, *Mat. Sci. Eng. C-Mater.* **35**, 61--69, 2014.
10. Pramanik, S., Hazarika, J., Kumar, A., Aidew, L., Buragohain, A.K., & Karak, N. Green silver nanoparticles decorated multiwalled carbon nanotube- A precursor for fabrication of multifunctional biobased sustainable nanocomposites, *ACS Sustainable Chemistry & Engineering* (revision submitted).

Other related publications

1. Konwarh, R., Pramanik, S., Devi, K.S.P., Saikia, N., Boruah, R., Maiti, T.K., & Karak, N. Lycopene coupled 'trifoliolate' polyaniline nanofibers as multi-functional biomaterial, *J. Mater. Chem.* **22** (30), 15062--15070, 2012.
2. Konwarh, R., Pramanik, S., Kalita, D., Mahanta, C.L., Karak, N. Ultrasonication—a complementary 'green chemistry' tool to biocatalysis: A laboratory-scale study of lycopene extraction, *Ultrason. Sonochem.* **19** (2), 292--299, 2012.

In conference/seminar/workshop proceeding

1. Pramanik, S. & Karak, N. Antibacterial, antistatic and thermostable bio-based hyperbranched poly(ester amide)/MWCNT nanocomposites for advanced textile coatings, in APA International Congress on Polymers: Vision & Innovations (APA' 14), New Delhi, India, 164.
2. Pramanik, S. & Karak, N. Hyperbranched poly(ester amide)/MWCNT nanocomposites as antimicrobial dressing materials, in International Conference on Harnessing Natural Resources for Sustainable Development: Global Trends (ICHNRSD' 14), Destiny Printing Press, Guwahati, Assam, 222.
3. Pramanik, S., Sagar, K., Konwar, B.K. & Karak, N. Prospect and synthesis of castor oil modified highly branched poly(ester amide) resins, in National Conference on "Chemistry, Chemical Technology and Society" (NCCCTS' 11), Kashi Block Industry Press, Tezpur, Assam, 44.